Universitetet
i Stavanger

FACULTY OF SCIENCE AND TECHNOLOGY

MASTER'S THESIS

Study programme/specialisation: Petroleum Engineering / Natural Gas Engineering	Spring semester, 2017 Open
Author: Ole Morten R. Isdahl	…… (signature of author)

Programme coordinator and supervisor: Prof. Aly Anis Hamouda
Co-supervisor: Nikhil Bagalkot

Title of master's thesis:

Influence of Silica Based Nanofluid on the Physical Properties, IFT, and CO_2 Diffusion in a Carbonated Water - *n*-decane system: An Experimental and Numerical Study

Credits: 30

Keywords: Interfacial tension Diffusion Coefficient Silica Nanofluid Carbonated water Pendant drop Decane n-Decane	Number of pages: 194 + supplemental material/other: 56 Stavanger,15/06/2017 date/year

University of Stavanger

Master thesis

Influence of Silica Based Nanofluid on the Physical Properties, IFT, and CO_2 Diffusion in a Carbonated Water - *n*-decane system: An Experimental and Numerical Study

Ole Morten R. Isdahl

supervised by
Prof. Aly A. Hamouda

co-supervised by
Nikhil Bagalkot

June 15, 2017

Acknowledgements

I would first and foremost offer my sincere gratitude to my supervisor, Professor Aly Anis Hamouda, at the University of Stavanger. His passion, wisdom and insight have resulted in countless advice, discussions and lessons. Prof. Hamouda have been an active part of my educational path for the past one and a half year, and responsible for shaping the way a look upon science, the industry and petroleum technology in general. I am grateful for the opportunities he have given me, and I owe a lot of my knowledge and understanding to him.

I have been working close with Ph.D. candidate Nikhil Bagalkot, to whom I am sincerely grateful. He has been co-supervising me during the work with this thesis, and devoted numerous hours to helping, guiding and advice me. He has also provided the numerical model for diffusion coefficients used.

Countless hours of this study have been in the laboratory, where laboratory technician, Krzysztof Nowicki has offered his skills and time to help in safely operate, modify and build experimental set-ups. I am truly thankful for his assistance.

There are several students supervised by Prof. Hamouda working on nanotechnology, which have resulted in a great forum for discussions. I thank Mr. Amr Ayoup, Mr. Ivan Murzin and Ph.D. candidate Rockey Abhishek for a great semester, and rewarding conversations.

I am truly gratefull of my parents, Elisabeth R. isdahl & Lars Sverre Isdahl, who have believed in me, supported me, and provided a home for early educational exploration.

My fiancé, Tonje Markset Lia deserves huge acknowledgement for her patiance and understanding during the work whit this thesis. Her kindness and support have been invaluable.

Finally, I thank the University of Stavanger, and the Department of Petroleum Engineering for ultimately making this thesis possible.

Abstract

Carbonated water injection (CWI) for enhanced oil recovery (EOR) overcomes mobility issues, macroscopic bypassing and sweep efficiency limitation of conventional CO_2 injection. It might also lead to reconnection of trapped or water blocked residual oil due to oil swelling. Molecular diffusion is a crucial and consequential process during CWI and carbon storage in subsurface geological structures. EOR, utilising nanotechnology have a potential for altering oil reservoirs to more water-wet, but it is also a high possibility that the combination of nano-EOR and CWI may increase the mass transfer rate (diffusion) of CO_2 into residual oils. Diffusion experiments have been carried out by the pendant-drop method together with numerical modelling to investigate the influence of silica nanofluid (NF) in a CW-n-decane system. Experiments have been carried out at 25°C and 45°C, 10-90 bar, for three concentrations (0.05, 0.5 and 1.0 g/l) of water-based silica NF, and one concentration (1 g/l) of synthetic sea water-based NF. P-T regions of gaseous, liquid and supercritical CO_2 have shown to be important to understand, where unexpected results of increased interfacial tension (IFT) and decreased diffusion coefficient (D) with an increase in pressure have been validated by two methods. Transition from gaseous to both supercritical and liquid state reverse this trend for D. Transition from gaseous to liquid reverse it dramatically for IFT, and it is found that density difference of the phase is predominantly affecting this property. The viscosity of the drop is counterintuitively shown to increase with temperature because of the CO_2 mass-transport into the n-decane, where the effect of increased solubility of CO_2 in the water with lower temperature is dominant to the direct effect of temperature on viscosity. Carbonated NF showed to improve swelling relative to CW. A possible optimum concentration for improving EOR properties in the CWI-process is found with 0.5 g/l water-based NF, suggested to be caused by solubility improvement of CO_2 in water, and generating a greater concentration gradient. The findings might indicate that coupling of nano-EOR and CW-EOR could enhance both oil recovery and CO_2 storage.

Contents

List of Figures

List of Tables

List of Abbreviations

ABS	Absorbance
CG	Concentration gradient
CNF	Carbonated nanofluid
CNFI	Carbonated nanofluid injection
CWI	Carbonated water injection
DIW	De-ionised water
DIW-CNF	Carbonated nanofluid with DIW as basefluid
DIW-NF	Nanofluid with DIW as basefluid
EOR	Enhanced oil recovery
EoS	Equation of State
HC	Hydrocarbon
HPHT	Highh pressure, high temperature
IFT	Interfacial tension
JIP	Joint Industry Project
MF	Mole fraction
MW	Molecular weight
nano-EOR	EOR utilising nanotechnology
NF	Nanofluid
NIST	National Institute of Standard and Technology
NP	Nanoparticle
PD	Pendant drop
PDD	Pendant drop diffusion
RF	Recovery factor
SD	Standard deviation
SF	Swelling factor
sol	Solubility
SRK-P	Soave-Redlich-Kwong-Peneloux
SSW	Synthetic sea water
SSW-CNF	carbonated nanofluid with SSW as basefluid
SSW-NF	Nanofluid with SSW as basefluid
SWAG	Simultaneous water alternating gas
UV	Ultra-violet light
VF	Volume fraction
WAG	Water alternating gas
WI	Water injection
wt%	Weight percent

List of Symbols

C	Concentration
D	Diffusion coefficient
δ	Distance between centre of nanoparticles
d_f	equivelent diameter of basefluid
d_p	nanoparticle diameter
F	Molecular flux
ϕ	nanoparticle volume fraction
h	Distance between centre nanoparticles
I	Light intensity
m	Mass
μ	Viscosity
μ_{app}	Appearant viscosity
μ_{eff}	Effective viscosity
N_{av}	Avogadro's Number
P	Pressure
P_c	Critical pressure
P_{cri}	Cricondenbar
ρ	Density
t	Time
T	Temperature
T_c	Critical temperature
$Tcri$	Cricondenterm
τ	Transmittance
V	Volume
x	Mole fraction
E	Objective function

Chapter 1

Introduction

1.1 Background

The Paris Agreement entered into force in November 2016, and has been ratified by 147 of 197 parties as of early June 2017. The agreement has a central aim of a global response to the threat of climate change. As stated in the agreement, "Recognizing the need for an effective and progressive response to the urgent threat of climate change on the basis of the best available scientific knowledge." [5]. The International Panel on Climate Change states also that substantial reductions in greenhouse gas emission are required to avoid further warming and increase in likelihood of "..severe, pervasive and irreversible impacts for people and ecosystems" [6]
Counterproductively, the population and demand for energy are increasing. According to British Petroleum's Energy Outlook for 2016, the energy demand will have increased by 34% in 2035 relative to 2014, with an expected population of almost 9 billion people. Even though fossil fuels are expected to have a decline in the normalised fuel mix, the total amount are increasing, occupying 60% of the added demand. Renewable energy are expected to account for 9% of primary energy need [7]
With a high forecasted energy demand - not sustained by supply of renewable energy, and a consensus of unsustainable climate with continued energy trends, the necessity for creative utilisation and energy solutions are evident.
Carbon dioxide injection has been a successful enhanced oil recovery method, and has been applied in various ways for decades [8]. It is usually applied as a secondary or tertiary recovery method, and are the most common injection fluid after water [9]. Atlantic Refining Co and Whorton et al. patented a method for miscible flooding with carbon dioxide as early as in 1952 [10]. In 1974, Holm and Josendal [11] stated that the benefits of CO2 injection is many, whereas the CO2 is soluble in oil, which initiates swelling of the oil, reduces viscosity and increasing density. It is also soluble in water. Diffusion of oil into the water reduces its density. Reduced weight differences between water and oil reduces gravity segregation. CO2 can also have acidic effects on the reservoir rock [11]. Water and CO2 forms carbonic acid, which carbon dioxide do also have the property of vaporising and carry oil components through the reservoir [11]. Due to the swelling of oil, the oil saturation in the reservoir is changed. This results in improved relative permeability. The increased relative permeability combined with the reduction in viscosity ultimately increases the oils mobility [12]. However, a problem with gas injection is the high mobility of the injected gas, even though

CO2 have a positive effect on the reservoir fluid's mobility, the mobility ratio is disfavourable, and the displacing fluid has much greater mobility than the displaced [13].

Immiscible Flooding When CO2 is used as an immiscible displacing phase, the relative permeability and mobility of the reservoir fluid decreases compared to a miscible flood. This is because of the existence of more phases in the pore structure. Wettability issues could also cause the reservoir fluid to be chemically or physically trapped. Due to the existing surface tension between the displacing and displaced fluid, the displacing front can bypass the oil. However gas injection in general have a tendency to have favourable microscopic displacement. The difference in mobility, for both miscible and immiscible floods can cause low macroscopic displacement. [13].

Miscible flooding Miscibility differs from solubility in that the interfacial tension between the miscible species are reduced to zero, and the fluids are able to form a homogenous mixture in all possible proportions. One advantage of a miscible flood is that the displacing fluid mixes with the displaced fluid, and the velocities become equal. This results in minimal residual oil in the swept zone [14], and reduced physical or chemical trapping [15]. A problem with miscible injection is, however, the large difference in mobility in swept and unswept regions. This ultimately leads to a lower macroscopic displacement compared to e.g. conventional water drive, but a better microscopic displacement [14]. Mobility issues cannot be neglected, and can be solved with various injection techniques such as water- alternating gas-injection (WAG) simultaneous WAG-injection (SWAG), or also the method focused on in this study, carbonated water injection (CWI).

Carbonated Water Injection A well known enhanced oil recovery (EOR) method is the commonly used, well understood waterflooding. A waterflood acts as pressure support and are meant to drive the reservoir fluid from the injectors to the producers, waterflooding is however largely dependent on mobility differences, and the rocks wettability. Sohrabi *et al.*,2015 [16] argues that an enhanced water flood should at least either reduce the oils viscosity, increase the waters viscosity, promote swelling of oil, favourably alter rock wettability, reduce interfacial tension between oil and water or improve injectivity near wellbore. Interstingly, all these alterations are taking place during carbonated water injection (CWI) [16]. Carbonated water injection or CO2 enriched water injection is a technique in which the water is enriched with CO2 prior to injection. During CWI, CO2 does not exists as a free gas phase, the CO2 is dissolved in the water and injected immiscibly with the reservoir fluid. This is a major difference from for instance CO2-WAG or CO2-SWAG [16]. In 1973, the Atlantic Richfield company, situated in New York and the inventor Loyd R. Kern patented what they called *High Pressure Gas-Carbonated Water Miscible Displacement* [17], which took advantage of the diffusion of CO2 from carbonated water into oil. The patent states the idea of creating a uniform distribution of carbonated reservoir fluid, which due to the CO2 has lowered the minimum miscibility pressure. Then a gas would be injected at a pressure at which it would have been immiscible with the reservoir fluid, but due to the prior carbonated water injection now has the possibility of gaining miscibility [17]. Mobil Oil Company and inventor Winston R. Shu patented a method in 1982

where the aim was to lower the viscosity of heavy oil by carbonated water. In addition to CO2 diffusing directly from water to oil, this method takes advantage of solubility promoters and demoters in the water. Where first water containing high amounts of CO2 and solubility promoters are injected at a pressure in which the flooding front are supposed to be oversaturated with CO2 at a distance from the injection well. This is due to a pressure gradient from the injector. CO2 would then come out of solution and form a free phase that dissolves in the oil, additionally a slug is injected subsequently that contains CO2 solubility demoters that further increases the amount of free CO2 that can dissolve in the oil. [18] Sohrabi *et al.* is currently part of a joint industry project at Heriot-Watt University, sponsored by ADCO, BG Group, Eni, Galp Energia, Oil India and the UK DECC. This project aims at understanding the mechanisms and parameters that are affecting CWI for EOR, and have had a large number of publication on the subject. This might suggest a relatively large interest in the technique from the industry. In 2015, they categorized the mechanisms that affect EOR by CWI into three main groups. One being the dissolution of CO2 in oil, which cause the oil to swell and reduces the viscosity. The swelling improves the relative permeability of the oil and may also reconnect trapped oil in dead end pores. When the oil swells, the oil saturation is increased and blocks more of the pathways. This phenomenon causes the injected carbonated water to face a greater obstruction and diversion of the flow, and on a microscale causes improved sweep efficiency. Sohrabi *et al., 2015* [16] observed this effect in a micromodel, carried out at reservoir conditions, where they also observed what they classify as the second EOR contributing mechanism from CWI. This is the nucleation and formation of a free gas phase within the oil as a result of dissolution of CO2, which substantially increases swelling. They observed this phenomenon to a much larger extend in live oils than dead oils, and in the live oil experiment contribute more than two thirds of the swelling to the formation of the new phase. This mechanism has a similar effect on the oil as the normal swelling, but to a much larger extent [16]. Since live oil contains significantly more light and intermediate components than dead oil, a logical assumptions would be that this specific mechanism is also contributing to increased recovery on a larger scale with lighter reservoir fluids than heavier. Benefits of CWI on heavy oil. The final category is the wettability alteration of an oil/brine/rock system, where CO2 reduces the pH of the water phase, which then again change the charges on the different interfaces. Overall this changes the wettability of the system [16]. This summarises some of the effects CWI has for EOR and further understanding of how the mechanisms physically and chemically behave and interacts of interest in this literature study.
Seyyedi *et al.* [19], also affiliated with the aforementioned project at Heriot-Watt University, conducted a series of contact angle measurements in 2015 to investigate the wettability alteration during CWI. Synthetic sea water (SSW) where used, with relatively high salt content (54597 ppm). They used crude oil for the experiments and investigated on mica, calcite and quartz minerals. This was done for both aged and unaged rock in a PVT cell, where pressure and temperature can be controlled. A conclusion reached experimentally was that carbonated water has significant effect on wettability in general. For unaged quartz it is concluded that the lower pH of the brine, as a result of dissolution of CO2, shifts the wettability towards neutral. In mica the exchange of ions, also as a result of dissolved CO2 and higher concentration of H+-ions, causes the shift in wettability towards more water-wet. Unaged calcite

also shifted towards more water-wet. Aged calcite experienced the largest wettability alteration, which is suggested to be caused by dissolution of calcite because of the acidic environment. Also it is believed that the pH is causing desorption of adsorbed oil layers. They also conclude that the effect on wettability alterations is higher for aged minerals, which would be the case in oil reservoirs. Reservoirs usually has a combination of different wettability, and the impact on recovery factor from wettability alteration on recovery might be significant. [19].
Mosavat and Torabi, 2014 [20] did an experimental study on the performance of CWI at different conditions, where the solubility of carbon dioxide in CO_2-H_2O-NaCl systems were studied with respect to pressure at two temperatures, 25°C and 45°C. They observed a greater solubility for lower temperature and higher pressure, with the solubility's sensitivity to pressure change decline with higher pressure. This study is in good agreement with an empirical model based on an equation of state (EoS) developed by Duan et al., 2006 [21]. This model is well known and used extensively for solubility calculations in this present study. The model will therefore be discussed in great detail. Further, Mosavat and Torabi conducted coreflood experiments with carbonated brine, and compares solubility and recovery factor (RF) versus pressure. It is observed that the RF largely follows the same trend as solubility, which the authors attribute to the diffusion of CO2 in the oil, which swells the oil and reduces the viscosity. The comparison is done at 25°C, where the pressure effect on solubility is small above 60 bar, the pressure effect on RF is also miniscule around this point. They also observed a lower recovery for the same pressure when the temperature was increased, this is consistent with attributing and increased RF to solubility oif CO_2. [20]. In the same study, CWI were compared as secondary and as tertiary EOR-method. It was observed that utilising CWI as a secondary recovery method is superior to tertiary with respect to RF. This is attributed to CW following the previously flooded areas of water during secondary water injection, and therefore contacting less oil than it will using CWI as secondary recovery method. When the CWI comes in contact with less oil, CO_2 has a smaller surface area for diffusion between the water and oil phase. In terms of recovery, this study concludes that CWI is best applied as secondary recovery method, and that the operating pressure has a large effect up until around 56 bar (T = 25°C). [20]
Dong *et al.*, 2011 [22], performed coreflood experiments on CWI as tertiary recovery method and concludes that the method has the ability remobilise oil ganglia, it is also found that CWI as secondary method outperforms waterflooding [22].
Shu *et al.*, 2014 [23], studied the problem of water blocking of oil during CO_2 flood as tertiary recovery method. When a water flood is applied as secondary method, especially in water wet reservoirs, oil may be trapped and water blocked in the sense that a tertiary CO_2 flood do not come in contact with that oil. Shu *et al.* investigated the effect of pre-flushing with active carbonated water (ACWI) between secondary and tertiary method for recovery. The reason for this is to use the CW, which is miscible with the water in the reservoir to deliver CO_2 to the oil through mass transfer (diffusion). The reason for ACW is that when surfactants is added, the interfacial tension between oil and water can be reduced and mass transfer promoted. By applying this pre-flush, the redistribution of trapped oil is promoted. The authors did 10 coreflood tests and reached 5 conclusions; 1) The effect on recovery by performing the pre-flush is firstly evident when the tertiary CO_2 -flood is applied, this do however *"greatly en-*

hance" the recovery. 2) ACWI + CO_2-flood, combined with an extended waterflood is better than CWI for enhancing the tertiary recovery. 3) Reducing IFT by ACWI causes the mass transfer of CO_2 to improve the tertiary recovery. 4) An optimum slug size of 0.6 PV of ACWI is found under the test conditions. 5) Longer cores do not affect the RF, which suggests adsorption of surfactants was not significant during the study [23].

Alizadeh *et al.*, 2014 [24], performed an extensive multi-scale experimental study of CWI, with subsequently free CO_2-phase due to pressure depletion and studied the physical aspects of the system. This study was conducted at relatively low pressure and temperature to also be able investigate the application for environmental engineering and sequestration of CO_2. Experiments utilising a long Barea sandstone core together with macro-CT, and a smaller Barea sandstone core together with micro-CT was used for the different scales. They observed an additional recovery of 34.6% on the macro-scale with immiscible CWI after WI. On the microscale, an additional recovery of 40.7% was observed. The CT on a pore level, showed that CO_2 were coming out of solution, that an internal gas drive occurred, that water blocked oil were remobilised and an overall reduction in the residual oil saturation from the primary water flooding. It was observed that oil accumulated in big layers between free gas and the brine, and that oil was reconnected in the early stages of CWI due to this layer formation. [24]

Yang *et al.*, 2013 [25] developed a three-component model to compare CWI to WI, where viscosity reduction, volume change and IFT were the analysed parameters. The model applies constant pressure boundaries, and concludes that any increased recovery from CWI is mainly due to the viscosity reduction caused by diffusion of CO_2 in the oil phase. They do however conclude that a major increase in recovery would occur if the IFT could be reduced to a lower region than what can be achieved by normal CWI alone. [25].

In 2011, Sohrabi *et al.* [26] performed various CWI coreflood experiments to investigate the potential for increased recovery and CO_2 sequestration. The experiments were conducted with both light oil (*n*-decane), refined viscous oil and stock tank oil. Multiple types of cores were also tested, such as a North Sea sandstone reservoir rock and Clashack sandstone cores. The tests were conducted at 38°Cand 137.9 bar, at which decane is miscible with CO_2, but the refined and stock tank oil are not. [26]. CWI proved to yield higher recovery compared to WI in all cases, both as secondary and tertiary recovery method. Using CWI as secondary recovery method was better than tertiary, and attributed to more difficulties in contacting and reaching water blocked residual oil in tertiary mode [26]. This is consistent with observations made by Mosavat and Torabi, 2014 [20]. CWI during miscible conditions has the same property as conventional CO_2-injection of causing extensive swelling of the oil, and the sweep efficiency is significantly improved. The amount of CO_2 needed in miscible CWI is miniscule compared to conventional CO_2 injection. Both wettability and viscosity were observed to affect the recovery by CWI, where it was observed that the lighter oils yielded the highest recovery, attributed to less fingering and a more piston-like displacement front. It is however noted that the improvement over waterflooding for both lighter and viscous oils was similar, indicating additional mechanisms, like viscosity reduction can compensate for the fingering effect in viscous oils. It is also noted that CO_2 moved a head of the displacement front, suggesting good mass trans-

fer and delivery of CO_2 to the oil. Additionally, at the end of the experiments 40% to 50% of the CO_2 remained trapped in the core, suggesting good possibilities for combining CWI for EOR and carbon storage [26]. The same authors presented results of corefloods conducted on Clashack sandstone cores saturated with crude oil, using synthetic sea water (SSW) for CWI at the *International Symposium of the Society of Core Analysts* [27]. They conclude that both secondary and tertiary CWI has great potential, and that it was in this case observed a larger recovery factor by using CWI as tertiary method. However, in tertiary mode the increase happened over a much longer time than in secondary mode, and happened more gradually. A conclusion reached is the important feature of better injectivity for CW than water, despite the slightly higher viscosity [27].
Several studies performed by the CWI JIP at Heriot-Watt University have been published from 2008 up until today, including mathematical modelling, coreflood experiments utilising different cores, bines, light oil, and viscous oil. A HPHT micro-model with a pore structure made from etched glass has also been used to investigate underlying physical aspects and visualise the flow patterns occurring during CWI. In 2008, a study [28] using both the micro-model and core flooding finds that CWI improves recovery relative to waterflooding, both when used as secondary and tertiary recovery method, this conclusion is verified several times in the following studies. A greater swelling has been observed for *n-decane* than for viscous oils, but CWI still enhances the recovery relative to waterflooding due to the reduction in viscosity [28]. The authors conclude that the main mechanisms for improved recovery is the improved sweep efficiency. This efficiency is a result of the swelling, which again is a result of CO_2 diffusion. The swelling and coalescence remobilises water blocked oil. The viscosity alterations of both phases are also concluded to be favourable for improved oil recovery. When the experiments were conducted at 138 bar and 38°Cthe swelling of n-decane was estimated to 23%, where the rate of swelling is greatest in the beginning and gradually decreases towards equilibrium [28]. Another study [29] done in 2008 focusing on both CWI for EOR and for CO_2 storage with the use of the aforementioned micromodel together with a 1-dimensional mathematical model also concludes that CWI increases the recovery used as both secondary and tertiary recovery method, where the most recovered oil was seen when the method was used as secondary. The displacement was observed to be piston-like and film flow depending on the location in the micromodel. A 2009 study by Riazi *et al.* [30], using the micromodel results in a 16% additional recovery compared to plain water flooding. A mathematical model is used to simulate the swelling and shrinking of oil in an alternating WI-CWI procedure, where it was observed an initial higher rate of shrinking post CWI, but at a later stage the rate of swelling surpassed shrinking [30]. Another 2009 study performed by Sohrabi *et al.* [31] reports and increase if recovery for tertiary CWI of 32.7% for light oil, and 11.82% for viscous oil, and attribute the difference to greater swelling of the light oil. The swelling was 105% for n-decane and 23% for viscous oil [31]. Tertiary oil recovery was studied by Kechut *et al.* [32] in 2010, where micromodel, core floods and mathematical modelling was used to study recovery and sequestration. The corefloods proved a higher recovery by means of CWI compared to water flood, and 45% stored CO_2 at abandonment [32]. An investigation of the pore-scale mechanisms conducted in 2010 by Riazi *et al.* [33], observed that the swelling of oil can cause partially and completely blocked pores locally, which obstruct flow and causes redistribution of the

displacing fluid. This increases the displacement efficiency and can cause increased recovery. It is also stated that CWI re-energises the mature or depleted reservoirs when CO_2 is dissolved. This can lead to additional recovery when pressure blow-down is performed [33]. Coreflooding and numerical modelling was performed by Kechut *et al.* 2011 [34], for secondary and tertiary recovery and the possibilities of carbon storage. The recovery was higher for CWI than waterflood in both scenarios, and the storage after the finished experiments was 46% for secondary and 51% for tertiary. Another important conclusion was the observation of good delivery of CO_2 to the displacing fron. I.e. C_2 is supplied by diffusion to the front simultaneously as the CO_2 front is ahead of the CW-front, diffusing into the oil [34]. Kechut *et al.* 2011 [35] conducted numerical simulation and experimental CWI using reservoir cores, stock tank crude oil and SSW. Compared to water injection CWI performed better for both secondary and tertiary recovery, with a storage of 46% to 51%. It is noted that the increase in recovery occurs at an earlier stage when CWI is used for secondary recovery instead of tertiary. Diffusion and convection of CO_2 and CW are important mechanisms, that play a larger role in tertiary recovery than secondary [35]. Sohrabi *et al.* 2011 [36], conducted micromodel and coreflood experiments, where 16% adiitional recovery was observed in the micromodel due to CWI, a core flood experiment using crude oil and SSW obtained an additional 9%. After tertiary recovery, about 50% CO_2 was stored in the core, which is higher than conventional CO_2 flooding [36]. Riazi *et al.* 2011 [37] have also developed a mathematical model to simulate the swelling of oil by CO_2 diffusion, this was modelled both when the oil was in direct contact with the source, e.g. CW, and when a water layer separated the oil and the CO_2 source. The model was verified by replicating literature data with.

Diffusion Mohammad R. Riazi developed a method for experimental measuring of diffusivity in reservoir fluids in 1994 [38]. The method uses a PVT cell to determine diffusion coefficients of dens gases in liquids, based on the change in pressure or liquid volume. Zhang *et al.*, 1999 [39], published a simple method for measuring and calculating the diffusion coefficient also with the use of pressure-decay, but then couple the diffusion equation with material balance, and use the diffusion coefficient as a variable to history match experimental and theoretical absorption, by this method the diffusion coefficient can be found. Upreti *et al*, 2002 [40], reported on the diffusion coefficients of carbon dioxide, methane, ethane and nitrogen into Athabasca Bitumen for 40 and 80 bar, at 25°C and 45°C using a pressure-decay method, and states an increased in diffusion coefficients with pressure when the gases diffuses into bitumen. Yang and Gu, 2003 [41] developed a new method for measuring diffusivity of a solvent into heavy oil by *dynamic pendant drop shape analysis*. Experimentally, the dynamic volume of the drop is recorded as mass-transfer occurs, with constant supply of the gas, a mathematical model is applied to calculate the diffusion coefficient. Yang and Gu determined by this method that the diffusion coefficient of CO_2 into brine is $1.086 \cdot 10^{-7}$ m^2/min at 25°C and 36 bar. They did also find the diffusion coefficient from CO_2 into heavy oil to be $0.684 \cdot 10^{-7}$ m^2/min at 25°C and 29 bar. Yang *et al.*, 2006 [42] did also develop a similar method, where the dynamic interfacial tension, rahter than the volume change is applied to calcualte the diffusion coefficients. In this work, the interfacial tension and diffusion coefficients of CO_2 into reservoir brine

is presented from ≈ 1 bar to ≈ 60 bar at 27°C. The equilibrium IFT is reported to decrease with pressure, and the diffusion coefficient to increase with pressure. Yang and Gu have done extensive work in this area and also in 2006 [42] reported on the diffusion coefficients of carbon dioxide, methane, ethane and mixes of them into heavy oil. Bagalkot and Hamouda, 2017 [43] published a modified method of the *dynamic pendant drop shape analysis*, where diffusion coefficients of carbon dioxide into light hydrocarbons were reported for 25-45 °C and 25-65 bar. This method is the same as applied in this thesis and is therefore thoroughly discussed in the methodology, the mathematical model is discussed in the *Mathematical Mass-Transfer Model*-chapter. Bagalkot and Hamouda concludes that in the system of CO_2/HC where CO_2 is the surrounding gas-phase and CO_2 + HC is the drop-phase, the IFT relation with temperature is a function of $\Delta\rho$ between the phases. They also report that the IFT initially decreases with pressure, and later increase as the pressure is increased.

Nanoparticles and Nanofluids Nanoparticles are small particles with a diameter in the range of 1 to 1000 nanometres, nanofluids are fluids consisting of a base-fluid (e.g. water, surfactant fluids, mixtures, oils and ethylene glycol [44]), with suspended, dispersed nanoparticles in it. Nanoparticles and nanofluids have in the recent decades been increasingly popular for industrial use, and spans across a wide range of industries. It is used in medical, biological, and pharmaceutical applications. It is used for pollution cleaning, in processes and for chemical applications such as lubrication, surfactants, and material coatings. The most widespread use for nanofluids are maybe utilising its good thermal conductivity for heat transfer applications in case of cooling or heating. This is applied for drilling, welding, housing, cooling of engines and nuclear plants, solar heating and much more. Thermal conductivity of nanofluids is increased with nanoparticle concentration. Nanoparticles and fluids are also used in biomedicine, material technology and electronics. Nano technology has also implemented itself in the field of petroleum technology, where it exists great potential for EOR applications [45], [46]. Bennetzen and Mogesen [45] at the Maersk Oil Research and Technology Centre generalises nanoparticles to usually consist of a core with a chemically modified surface. Nanoparticles do also have an extremely large surface to volume ratio, which means that combinations of cores and surface modifications (e.g. molecules of other substances) can be applied in a diverse manner. This leads to the ability of precisely attributing specific properties to the particles such as high mechanical strength, high electrical conductivity, give them catalytic properties, adsorption properties and thermal properties [45]. The use of nanofluids and particles for enhanced oil recovery have gained

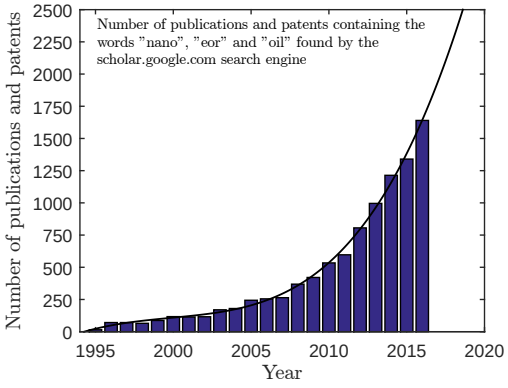

Figure 1.1: Number of publications and papents on EOR utilizing nanotechnology

increasingly interest, and several studies have been conducted lately. Figure 1.1 illustrates the increasing interest in this area. Google Scholar's search engine were used in order to get an overview, where the three key-words; "nano", "EOR" and "oil", were used as terms that had to be present to show a result. Citations containing those words were excluded from the search criterea. This method is obviously not representable for the actual number of peer-reviewed publications, but is assumed to show the signficant increase of interest, which in that case has increased with approximatly 1300% from 2000 to 2016. Nanoparticles is also small enough to flow through porous media, which make them applicable for altering both formation and fluid properties in reservoir rocks. They can be used to change the wettability, reduce oil viscosity, reduce interfacial tension, and stabilise foam and emulsions [45].

Numerous studies that proves the possibility of enhanced oil recovery utilising nano-EOR have been published, and many of them are carried out to investigate nanoparticles ability to alter the wettability of the reservoirs rock. Ju *et al.* 2006 [47], 2009 [48] have studied the effect of lipophobic, hydrophilic polysilicon nanoparticles, where also a mathematical model is developed to describe the transport and adsorption of nanoparticles. The resulting effects of it, such as alteration of wettability, were studied. Numerical modelling found that permeability and porosity may be reduced, but that a volume percentage of nanoparticles of 2-3% still offer possibilities of improving the oil recovery 2006 [47]. It is also found that these nanoparticles can alter the wettability from oil-wet to water-wet in sandstone reservoir. Hendraningrat and Torsæter, 2010 [49], Hendraningrat *et al.* 2013 [50], studied the effect of wettability, and the potential for flooding with silica nanofluid for EOR-purposes through a series of coreflooding experiments utilising nano-EOR (waterflood with nanoparticles) to displace crude oil, with the pre-flood wettabilities covering water-wet, intermediate, and oil-wet. They investigated both crude oil/SSW and crude oil /nanofluid systems, and found that nanoparticles improve the displacement efficiency compared to waterflooding, the best results were achieved with intermediate-wet cores. 0.05 wt % of silica nanoparticles were capable of altering the wettability in between 15 and 33 %, and wettability alteration is attributed to be the dominant factor in improving the displacement of crude oil. Li *et al.* 2016 [51] studied the effect of wettability alteration by silica nanoparticles in a micromodel experiment. Silica nanoparticles were found to alter the oil-bearing pore-wall from strong water-wet to neutral, and that 0.1 wt % silica nanoparticles reduced the residual oil saturation from about 50% to 20%. Al-Anssari *et al.* 2016 [52] studied the effect of wettability alteration of oil-wet limestone using silica nanoparticles. The nanoparticles altered the wetting-phase to strongly water-wet. They also found that the adsorption of the silica nanoparticles were mainly irreversible. The wettability alteration were studied at different salinity levels, where a 3-8 % NaCl content were found to be the most efficient. Metin *et al.* 2012 [53], performed contact angle measurements on a resting sessile *n*-decane drop surrounded by water with the presence of silica nanoparticles, where it was concluded that unmodified silica nanoparticles does not show any significant effect on the interfacial tension (IFT) between water and *n*-decane. However, when the silica nanoparticles are coated with polyethylene glycol (PEG), the IFT is greatly reduced. [53] Suleimanov *et al.* 2010 [54] , found that non-ferrous metal nanoparticles and anionic surface-active agents reduced the IFT of an oil/water interface with 70-90% relative to the same aqueous solution without the nanoparticles,

Taborda *et al.* 2017 [55] have studied the rheology of heavy oils when silica nanoparticles are introduced, which resulted in a reduced viscosity of the heavy oil. Corcione, 2011 [56], have established empirical equations for calculating the dynamic viscosity of nanofluids. These equation are utilised in this present study in order to establish the viscosity of carbonated nanofluid and therefore discussed in the respective chapter (3.4) Haghtalab *et al.* 2015 [57] investigated the absorption (solubility) of CO_2 in both silica and zinc oxide (ZnO) nanofluid at multiple pressures (1-36 bar), temperatures (2, 5, 8, 15, 25 and 40°C) and concentrations. The experiments were carried out in a high-pressure cell containing a stirrer. They found that 0.1 wt% ZnO-nanoparticles offered the greatest solubility increase compared to pure water of 14%, while silica nanoparticles improved the solubility of CO_2 in water by 7%. This study is discussed further in chapter 3.2, as the information is used for establishing density of carbonated nanofluid.

Combining carbonated water injection with nano-EOR, into carbonated nanofluid injection (CNFI) might seem like a natural next step with regards to both EOR and CCS, taking advantage of their synergy for both purposes. Nanoparticles do for instance have the ability to improve the CO_2 solubility in water, and maybe also alter liquid/liquid interfaces, which might improve the carbonated water injection (CWI). Additionally, nanoparticles can favourably alter the reservoir properties. Fathollahi and Rostami at the University of Tehran [58] have carried out CNFI out in a coreflood study, where silica nanoparticle did enhance the oil recovery compared to pure CWI.

1.2 Research Objective

The research objective of this thesis is to:

Investigate the influence of silica based nanofluid in a carbonated water-n-decane system in order to enhance the understanding of mechanisms related to carbonated water injection, and the possibilities of improving the process with utilisation of nanotechnology.

This study utilises pendant drop diffusion experiments (primary experiments) coupled with a mathematical mass-transfer model (Bagalkot and Hamouda [43]) to quantitatively investigate mass-transfer of carbon dioxide from CNF into *n*-decane. Extensive laboratory and numerical work have been carried out, and several properties are obtained, analysed and discussed. Auxiliary experiments have also been carried out to qualitatively or quantitatively ontain knowledge about properties needed in the analysis. Properties investigated are;

Primary experiment and numerical investigation

- Dynamic and equilibrium volume change
- Swelling factors
- Diffusion coefficients

- Dynamic and equilibrium interfacial tension
- Dynamic and equilibrium drop density
- Dynamic and equilibrium drop viscosity

Auxiliary investigation

- CO_2 solubility in nanofluid
- Nanofluid density (non-carbonated and carbonated)
- Nanofluid viscosity (non-carbonated and carbonated)
- Nanoparticle transport across nf/n-decane interface

All the aforementioned properties are investigated for three different concentrations of water-based silica nanofluids (0.05 g/l, 0.5 g/l and 1 g/l) at nine pressures (10-90 bar $\Delta P = 10$) and two temperatures (25°C and 45°C). Additionally, the investigation is conducted with 1 g/l silica nanofluid based on synthetic sea water (SSW). These experiments are carried out at 45°C for five pressures (10 to 90 bar $\Delta P = 20$). Two schemes for saturating the nanofluid with CO_2 is investigated, one where the nanofluid is saturated before an oil drop is introduced to the system, the other where the nanofluid is gradually saturated with the presence of the drop in the system. The experiments carried out with the former scheme is, additionally, carried out twice. This constitutes a total of 188 primary pendant drop diffusion experiments.

In this work, many auxilary investigations had to be carried out in order to obtain properties needed in further analysis of the primary experiments. As this work is large in itself, it is organised in a separate chapter preceeding the methodology of the primary epxperiments. In that chapter, methods, discussion and results are discussed in-situ, and may be viewed independantly.

Chapter 2

Theoretical Section

2.1 Diffusion

Diffusion is the phenomenon of a species being transported through a system based on a difference in concentrations of said species. This phenomenon results from random molecular movement, where individual molecules have no preferred direction of motion. Probability of collision with other molecules is however greater in the direction of higher concentration, and the net movement of the species becomes inclined towards the lesser concentrated areas [59].

Adolf Fick recognized the analogies between conductive heat transfer and molecular diffusion in 1855, and adopted Fourier's mathematical relationship (1822) for the latter phenomenon in what is called Fick's first law of diffusion, expressed in equation 2.1 [59].

$$F = -D \cdot \frac{\partial C}{\partial x} \tag{2.1}$$

This law states that the molecular flux (F) during a steady-state diffusion process is proportional to the diffusion coefficient (D) multiplied by the concentration gradient, where C is concentration and x is the distance from the boundary. Note that the negative sign originates from the concentration going from higher to lower levels, thus ∂C becomes negative [60].

Considering a cube element with the infinitesimally small sides of lengths dx, dy and dz, it can be stated that the rate of mass transfer of the diffusing species into, and out of, the element in x direction is given by $dydz(F_x - \frac{\partial F_x}{\partial x}dx)$ and $dydz(F_x + \frac{\partial F_x}{\partial x}dx)$, respectively. Contribution to accumulation of the diffusing species in the element is then expressed by subtracting the latter from the former, giving $-2dxdydz\frac{\partial F_x}{\partial x}$. This is true in all three directions [59].

Since the rate of accumulation is also given by $2dxdydz\frac{\partial C}{\partial t}$, equation 2.2 can be obtained [59].

$$\frac{\partial C}{\partial t} + \frac{\partial F_x}{\partial x} + \frac{\partial F_y}{\partial y} + \frac{\partial F_z}{\partial z} = 0 \tag{2.2}$$

What is known as Fick's second law of diffusion is obtained by substituting the first law into equation 2.2, assuming a constant diffusion coefficient. This gives

$$\frac{\partial C}{\partial t} = D\left[\frac{\partial^2 C}{\partial x^2} + \frac{\partial^2 C}{\partial y^2} + \frac{\partial^2 C}{\partial z^2}\right]. \tag{2.3}$$

2.2 Behaviour of Pure Carbon Dioxide

This section serves as an overview of the general properties of carbon dioxide as a pure substance, with special emphasis on the conditions relevant for this study.

2.2.1 Phase Behaviour

Figure 2.1 shows the phase behaviour of CO_2. The sublimation- and saturation lines are calculated with the Soave-Redlich-Kwong-Peneloux Equation of State (SRK-P EOS) using PVTSim Nova 2.00, The triple point is obtained from Angus *et al.*, 1976 [1]. The critical point is obtained by a combination of Suehiro *et al.*, 1996 [61] (T) and Angus *et al.*, 1976 [1] (P), where the former is the latest addition in NIST's overview, and the latter is the NIST-P_c entry with the least assigned uncertainty.

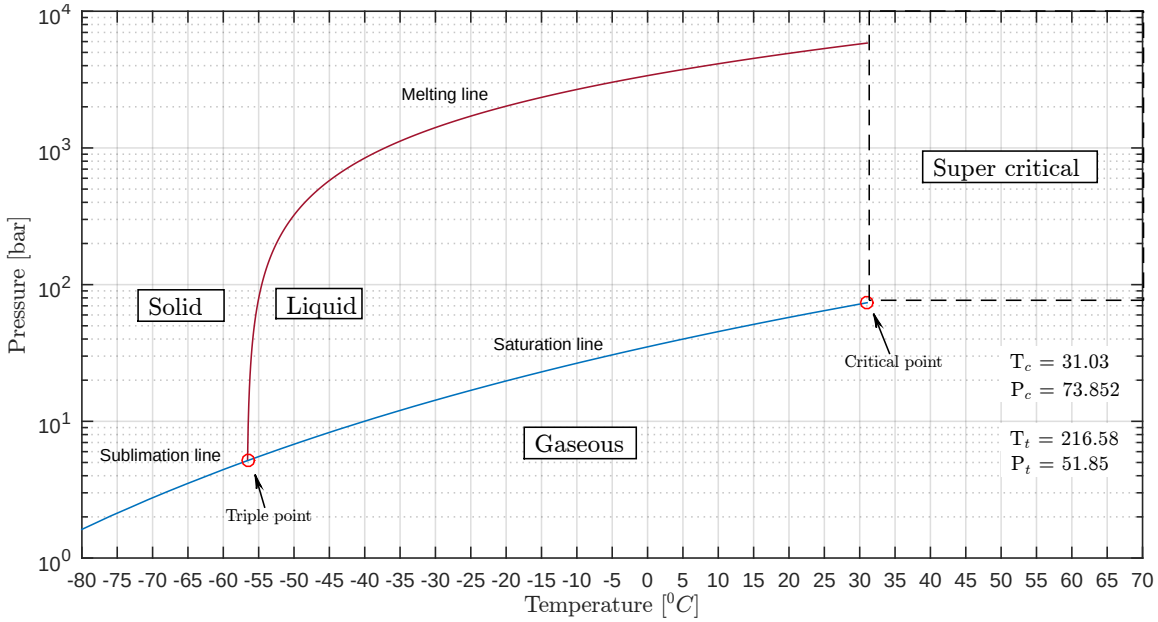

Figure 2.1: Phase behaviour of pure carbon dioxide [1], [2].

The melting line is calculated using the empirical relationship from Span *et al.*, 1996 [2]. Note that the ordenate direction is presented on a logarithmic scale, and that the gas/liquid saturation pressure exponentially increases with temperature. The empirical equation for the melting line has critical pressure and temperature as input,

which is slightly altered, 0.11% and -0.005%, respectively, from the original publication. This is done to match the tripple point data provided by Angus *et al.,* 1976 [1], which is the value suggested by NIST.

Figure 2.2 shows the zoomed in version of figure 2.1. The two temperatures studied in this work is marked with arrows (A and B), where it is observed that carbon dioxide experiences a phase change from gaseous to liquid phase at 25°C and 64 bar, wheras for 45°C it experiences a transition from gaseous phase to super critical phase at 73.9 bar.

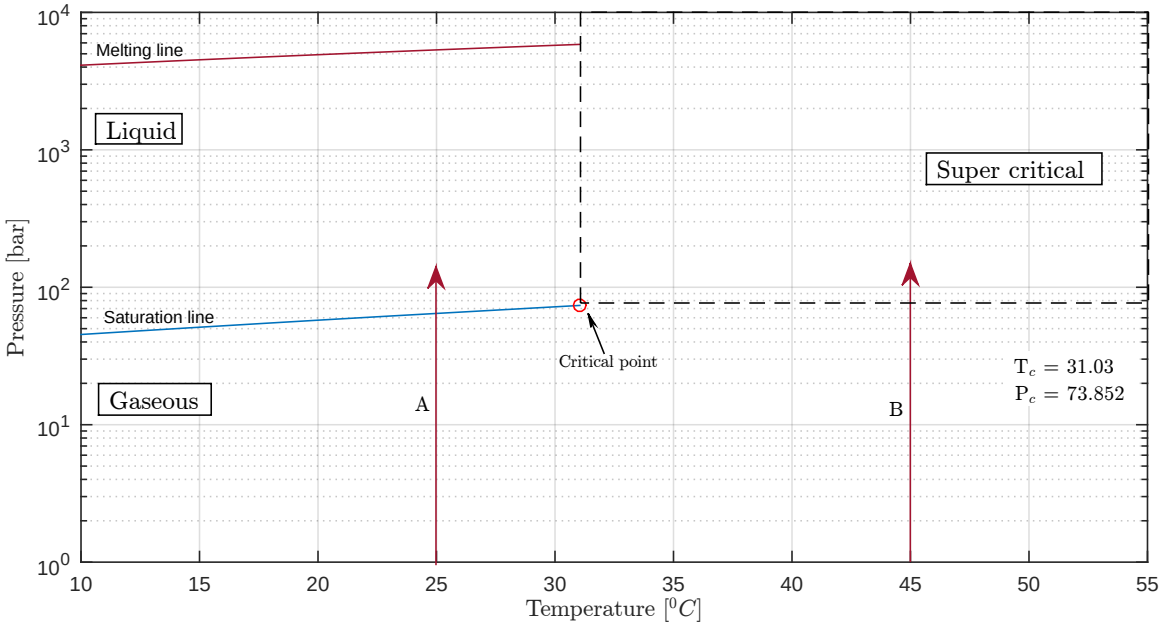

Figure 2.2: Zoomed in phase behaviour of pure carbon dioxide [1], [2].

2.2.2 Viscosity and Density

The phase change from gaseous to liquid state do affect both the density and viscosity substantially, which can be observed in figure 2.3 and 2.5, respectively. Contrary to the phase change over the gaseous/super critical boundary (Figure 2.4 and 2.6) the gaseous/liquid phase change experiences a sudden jump. More over, after the phase change, the rate of change of the latter slowes down, while the former increases. The magnitude of the two proerties is, however, significantly lower for the higher temperature.

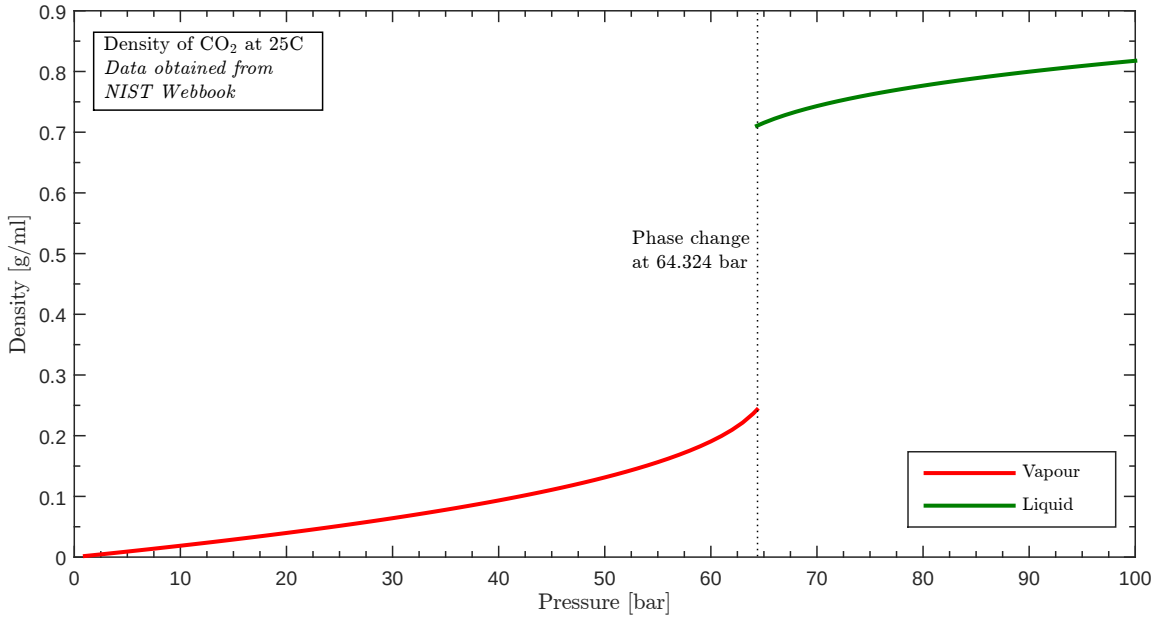

Figure 2.3: Density of pure carbon dioxide at 25°C.

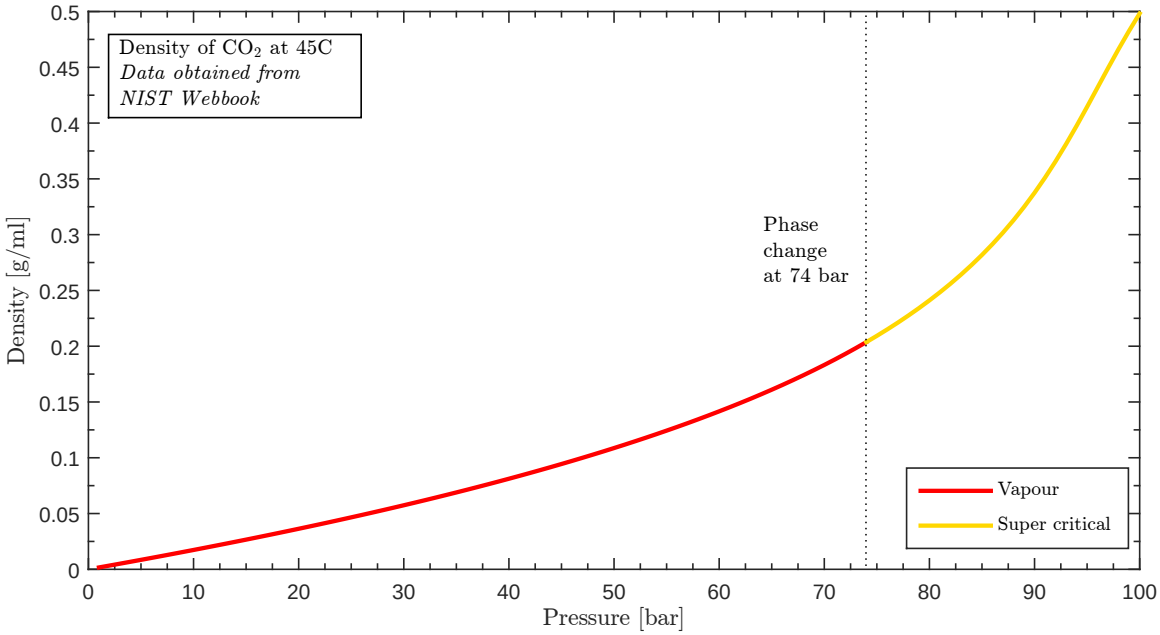

Figure 2.4: Density of pure carbon dioxide at 45°C.

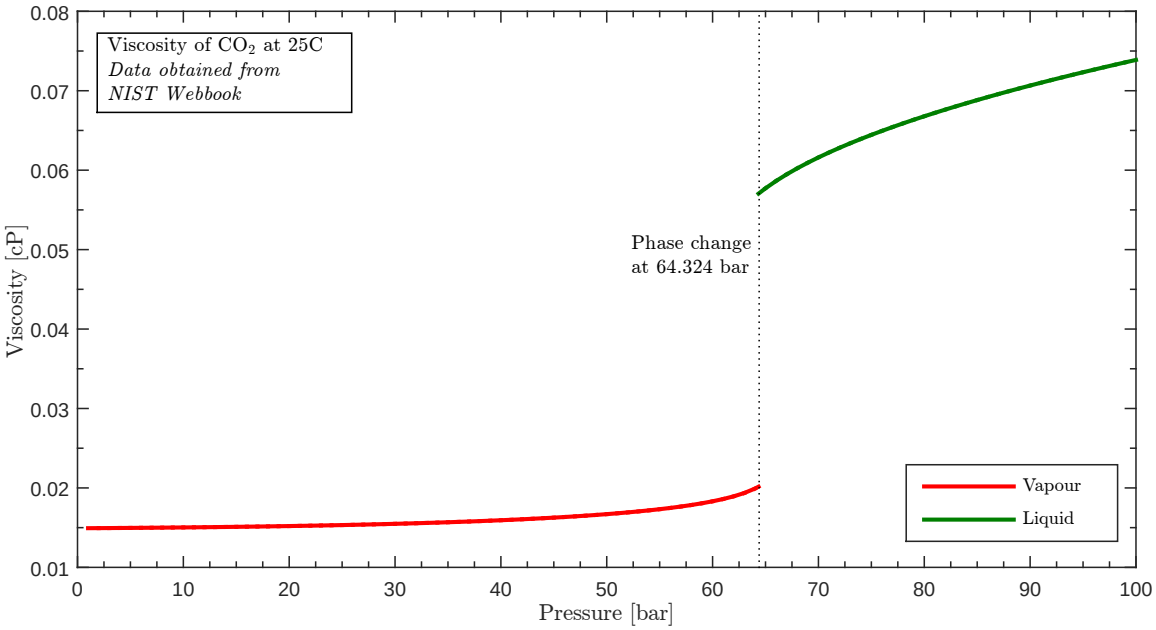

Figure 2.5: Viscosity of pure carbon dioxide at 25°C.

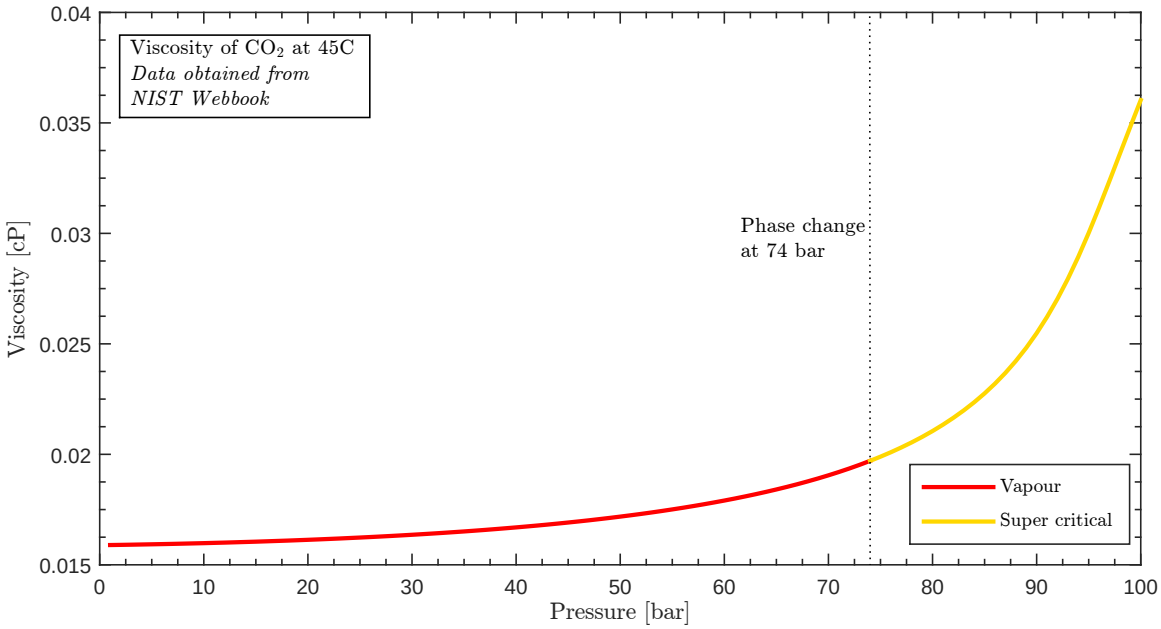

Figure 2.6: Viscosity of pure carbon dioxide at 45°C.

2.2.3 Property Tables

TABLE 2.1: Isothermal thermodynamic properties of carbon dioxide for 25°C. [3]

P [bar]	Density [g/ml]	Viscosity [cP]	U [kJ/mol]	H [kJ/mol]	S [kJ/mol]	C_v [$J/molK$]	C_p [$J/molK$]	Phase
1	0.00178	0.01493	19.796	22.263	120.56	28.935	37.442	vapour
5	0.00911	0.01497	19.680	22.096	106.78	29.380	38.723	vapour
10	0.01872	0.01503	19.527	21.879	100.50	29.970	40.528	vapour
15	0.02891	0.01510	19.367	21.651	96.583	30.603	42.615	vapour
20	0.03977	0.01520	19.196	21.409	93.603	31.291	45.067	vapour
25	0.05145	0.01532	19.014	21.153	91.113	32.047	48.005	vapour
30	0.06409	0.01548	18.818	20.878	88.908	32.889	51.608	vapour
35	0.07795	0.01568	18.605	20.581	86.867	33.847	56.161	vapour
40	0.09335	0.01593	18.370	20.256	84.910	34.961	62.145	vapour
45	0.11083	0.01626	18.106	19.893	82.966	36.300	70.447	vapour
50	0.13127	0.01670	17.800	19.476	80.956	37.992	82.938	vapour
55	0.15642	0.01732	17.429	18.976	78.762	40.306	104.44	vapour
60	0.19061	0.01832	16.932	18.317	76.123	44.010	153.28	vapour
65	0.71550	0.05772	11.653	12.053	54.798	46.584	266.59	liquid
70	0.74303	0.06160	11.421	11.835	53.965	44.553	200.08	liquid
75	0.76187	0.06444	11.256	11.689	53.377	43.558	172.52	liquid
80	0.77664	0.06679	11.124	11.577	52.906	42.904	156.41	liquid
85	0.78898	0.06882	11.012	11.486	52.505	42.432	145.50	liquid
90	0.79965	0.07065	10.913	11.409	52.153	42.075	137.46	liquid
95	0.80911	0.07233	10.825	11.342	51.838	41.796	131.23	liquid
100	0.81763	0.07388	10.745	11.283	51.550	41.573	126.22	liquid

TABLE 2.2: Isothermal thermodynamic properties of carbon dioxide for 45°C. [3]

P [bar]	Density [g/ml]	Viscosity [cP]	U [kJ/mol]	H [kJ/mol]	S [kJ/mol]	C_v [$J/molK$]	C_p [$J/molK$]	Phase
1	0.00167	0.01590	20.385	23.020	123.02	29.807	38.279	vapour
5	0.00849	0.01593	20.284	22.876	109.31	30.140	39.281	vapour
10	0.01735	0.01598	20.154	22.690	103.14	30.573	40.656	vapour
15	0.02662	0.01605	20.018	22.498	99.333	31.028	42.188	vapour
20	0.03634	0.01613	19.876	22.298	96.487	31.507	43.909	vapour
25	0.04658	0.01623	19.727	22.089	94.153	32.013	45.857	vapour
30	0.05741	0.01636	19.571	21.871	92.131	32.551	48.086	vapour
35	0.06891	0.01651	19.407	21.642	90.312	33.125	50.664	vapour
40	0.08120	0.01669	19.233	21.401	88.630	33.741	53.683	vapour
45	0.09440	0.01691	19.048	21.146	87.037	34.409	57.273	vapour
50	0.10869	0.01718	18.849	20.874	85.499	35.137	61.618	vapour
55	0.12432	0.01751	18.635	20.582	83.986	35.940	66.993	vapour
60	0.14161	0.01791	18.401	20.265	82.471	36.836	73.817	vapour
65	0.16100	0.01841	18.142	19.919	80.924	37.850	82.771	vapour
70	0.18320	0.01905	17.853	19.534	79.311	39.016	95.018	vapour
75	0.20928	0.01989	17.520	19.097	77.584	40.381	112.690	sc
80	0.24105	0.02105	17.126	18.587	75.672	41.999	140.010	sc
85	0.28181	0.02276	16.642	17.969	73.464	43.910	185.720	sc
90	0.33751	0.02548	16.018	17.191	70.794	45.993	264.390	sc
95	0.41456	0.03002	15.226	16.235	67.601	47.426	363.950	sc
100	0.49825	0.03603	14.443	15.326	64.595	46.891	355.660	sc

Chapter 3

Auxiliary experiments and Fundamental Properties of the Nanofluid and the *n*-decane

3.1 Density of nanofluid (SSW and DIW) without CO_2

When calculating interfacial tension (IFT), the density of both environmental phase and drop phase are required. In the case of experiments carried out with addition of nanofluid, the environmental phase will consist of CO_2 dissolved in water with varying concentration of nanofluid. Once the density of nanofluid + water is known, from now on just called nanofluid with the respective concentration, the CO_2+nanofluid density can be calculated by knowing the fraction of CO_2 dissolved. To obtain the density of nanofluid, a series of experiments were conducted. The density is needed for all temperatures and pressures. The experiments were carried out as a combination of a densiometer and a piston cylinder experiment. The reason for the piston cylinder is the density meters limitation of a maximum pressure of 10 bar. Its temperature range is sufficient for the needed interval of 25-45 °C.

The reason for not only using the piston cylinder set-up, and include two independent different experiments is an assumption of an initial error in the piston cylinder experiments. The principal idea is to obtain the higher pressure densities in the piston cylinder, and calibrate against the low pressure results from the densiometer. These assumptions are later explained in detail. The densiometer used is Anton Paar DM4500. Figure 3.3 and 3.4 shows a schematic of the piston cylinder experiments at both temperatures. For 25°C, the room temperature is just raised accordingly, for 45°C, the temperature is adjusted with the aid of a heat circulator. This is explained further.

Atmospheric Densiometer Experiment The density of DIW at 25°C and 45°C were measured in the densiometer and compared to literature for calibration of nanofluid experiments. All experiments were repeated a minimum of three times to ensure

repetability. There were also conducted experiments on decane to ensure the method of calibration. Table 3.1 shows the result of the DIW experiments. The densiometer was cleaned with acetone between different types of fluid.

TABLE 3.1: Density [g/ml] of DIW at 25°C and 45°C at atmospheric pressure, from densiometer

Exp. no	**Density at 25°C**	**Density at 45°C**
1	1.02340	1.01516
2	1.02309	1.01492
3	1.02321	1.01481
4	-	1.00960
5	-	1.00645
6	-	1.00930
Avg.	1.02323	1.011707
SD	0.00013	0.00341
NIST Webbook	0.99705	0.99021
Diff.	0.02618	0.02150

Table 3.2 shows the density of decane at 25°C and 45°C . This density is measured only to discuss the calibration of the instrument. Decane is suitable for that purpose in the sense that it has significant different density from water, and reliable values for the density is available in the literature.

TABLE 3.2: Density [g/ml] of decane at 25°C and 45°C at atmospheric pressure, from densiometer

Exp. no.	**Density at 25°C**	**Density at 45°C**
1	0.76320	0.75103
2	0.76280	0.74995
3	0.76264	0.74906
4	0.76280	-
Avg.	0.76286	0.75001
SD	0.00021	0.00081
NIST Webbook	0.72653	0.71097
Diff.	0.036338	0.03904

The standard deviation of the experiments are suffiently small, this is also true for the nanofluids. The deviation from literature values are suggested to increase with lower density. Comparing water and decane at two temperatures is consistant with this, except for water at 45°C , which has a slightly lower difference than water at 25°C . However, the DIW 45°C experiment has also the largest SD, which might be a reason for this irregularity. Additionally, atmospheric nanofluid density measured in the densiometer are very close to water density. For nanofluids, it is therefore considered valid to calibrate the results from the densiometer directly against water with the argument of a similar density range. Two additional arguments for this is the low SD, and the logical outcome of the measurements relative to each other. I.e.

$\rho_{DIW} < \rho_{C_1} < \rho_{C_2} < \rho_{C_3}$, where C is concentration and $C_1 < C_2 < C_3$. Table 3.5 summarises the nanofluid density experiments at atmospheric conditions. Figure 3.1 shows the final calibrated atmospheric densities at 25°C and 45°C .

TABLE 3.3: Density [g/ml] of nanofluids at 25°C and 45°C at atmospheric pressure, from densiometer. 6 consecutive experiments

Temp.	**25°C**	**25°C**	**25°C**	**45°C**	**45°C**	**45°C**
Conc.	0.05 g/l	0.5 g/l	1 g/l	0.05 g/l	0.5 g/l	1 g/l
1	1.02355	1.02382	1.02409	1.01794	1.01811	1.01690
2	1.02356	1.02381	1.02410	1.01652	1.01760	1.01731
3	1.02357	1.02376	1.02410	1.01717	1.01811	1.01674
4	-	-	-	1.00768	1.01522	1.01794
5	-	-	-	1.00805	1.01567	1.01778
6	-	-	-	1.00508	1.01542	1.01777
Average	1.02356	1.02380	1.02410	1.01207	1.01669	1.01741
SD	$8 \cdot 10^{-6}$	$26 \cdot 10^{-6}$	$5 \cdot 10^{-6}$	$5.23 \cdot 10^{-3}$	$1.27 \cdot 10^{-3}$	$0.45 \cdot 10^{-3}$
Corrected	0.99738	0.99761	0.99791	0.99057	0.99591	0.99591

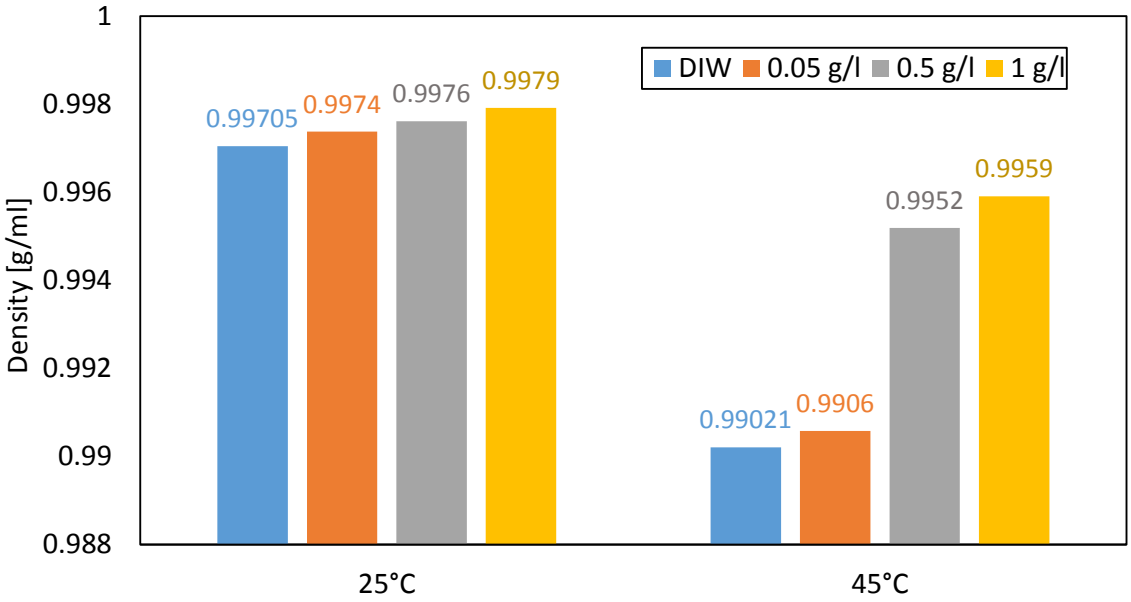

Figure 3.1: Density [g/ml] of nanofluids at 25°C and 45°C at atmospheric pressure, from densiometer

The same prosedure is followed for nanofluid with synthetic sea water (SSW) as basefluid. Hamouda and Maevskiy, 2014 [62], did a study on recovery mechanisms and the low salinity brines interaction with chalk. In this study, the density of SSW with the exact same composition as the one used in this study are reported for three temperatures. These densities are used for calibrating the results form the densiometer. A second order polynomial equation is fitted to these three densities with $R^2 = 1$, and used for interpolating the correct density at the wanted temperatures. The equation an its parameters are shown in equation 3.1 and table 3.4.

$$\rho_{SSW}(t) = m_1 t^2 + m_2 t + b \tag{3.1}$$

TABLE 3.4: Parameters for eq. 3.1

m_1	-0.00000200000000000373
m_2	0.000832600000002516
b	1.00000000006422

Figure 3.2 displays the nanofluid density with SSW as basefluid, and the density of SSW + 1g/l nanofluid. Table 3.5 summarises the experiment.

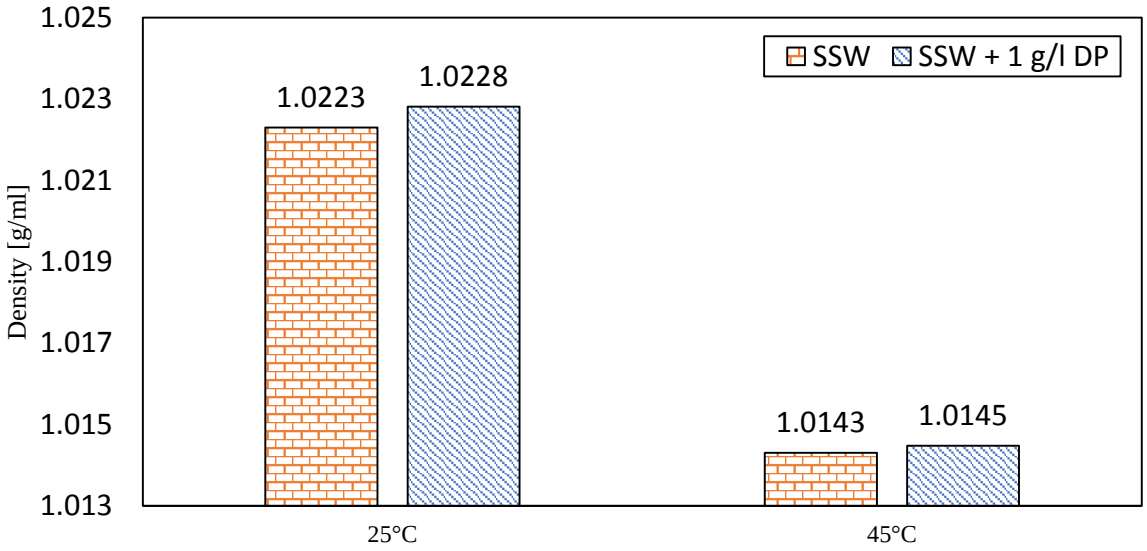

Figure 3.2: Density [g/ml] of SSW + 1 g/l nanofluid at 25°C and 45°C at atmospheric pressure, from densiometer

TABLE 3.5: Density [g/ml] of SSW + nanofluids at 25°C and 45°C at atmospheric pressure, from densiometer. 3 consecutive experiments

Temp.	**25°C**	**25°C**	**45°C**	**45°C**
Conc.	0 g/l	1 g/ll	0 g/l	1 g/l
1	1.04881	1.04933	1.04171	1.04108
2	1.04882	1.04933	1.04139	1.04196
3	1.04882	1.04934	1.04139	1.04198
Average	1.04882	1.04933	1.04150	1.04167
SD	0.000005	0.000005	0.000151	0.000420
Corrected	1.02230	1.02282	1.01430	1.01448

Piston-Cylinder Experiment The set-up utilises parts of the EUROTECHNICA equipment described for the diffusion experiments 4.1. Refering to figure 3.3, prior to any test, valve 1 was kept open, while valve 2 was kept closed, the piston was then moved dead-end. Water was poured into the liquid container and the water sucked in

by moving the piston backwards. Valve 1 was then closed while valve 2 was opened. The piston were driven in again to let some water pass through the lining before the pressure gauge was mounted. This was done to try to get rid of any air in the system. Experiments are conducted by firstly moving the piston from zero volume to full volume, while valve 1 is open and 2 closed. Valve 1 is then closed, and valve 2 is opened. The wheel is turned until wanted pressure is obtained. By knowing the revolutions of the wheel, the new volume can be calculated based on volume change per degree and knowledge of the initial volume. The new volume is used to calculate the density based on mass conservation. At elevated temperature, in this case 45°C, the fluid was pre-heated to one or two degrees above 45°C, the cylinder was coiled with a rubber hose in which water at 70°C was circulated through with the aid a of heat circulator (Julabo ME-4). The inside temperature of the cylinder was known by keeping stationary water inside and regularly take it out and measure its temperature. When the experiments were conducted, the temperature of the test fluid was measured before and after, and was in the range of 45°C $\pm$ 2°C.

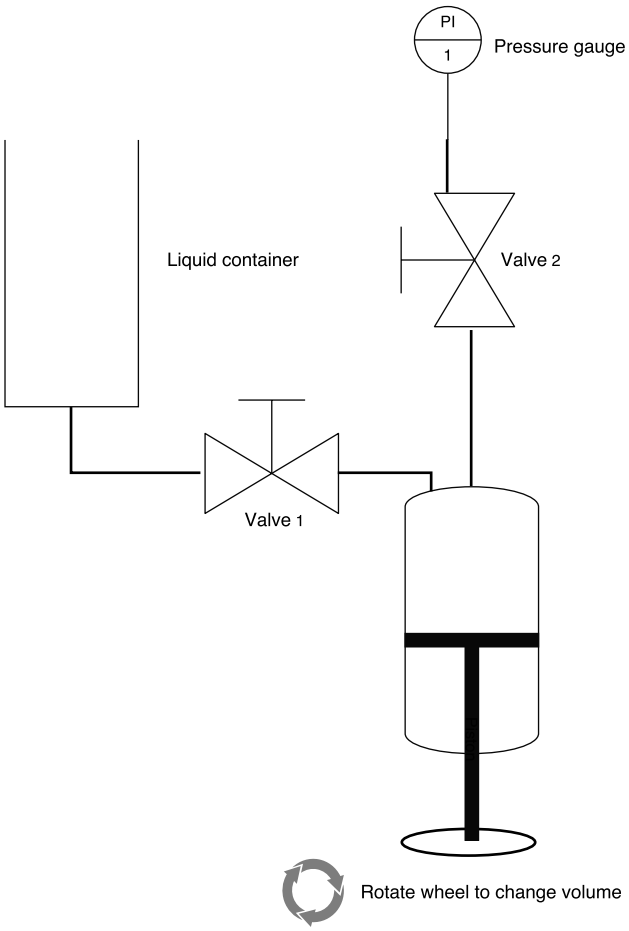

Figure 3.3: Schematic of the piston cylinder density experiment at 25 °C

Four parameters are required; 1) Initial volume of the test fluid. This is easily obtained by filling the cylinder with a known volume. 2) Volume change with movement of the piston. This is obtained by knowing the number of revolutions required to run the piston from dead-end to maximum volume. 3) Density of the fluid at atmospheric

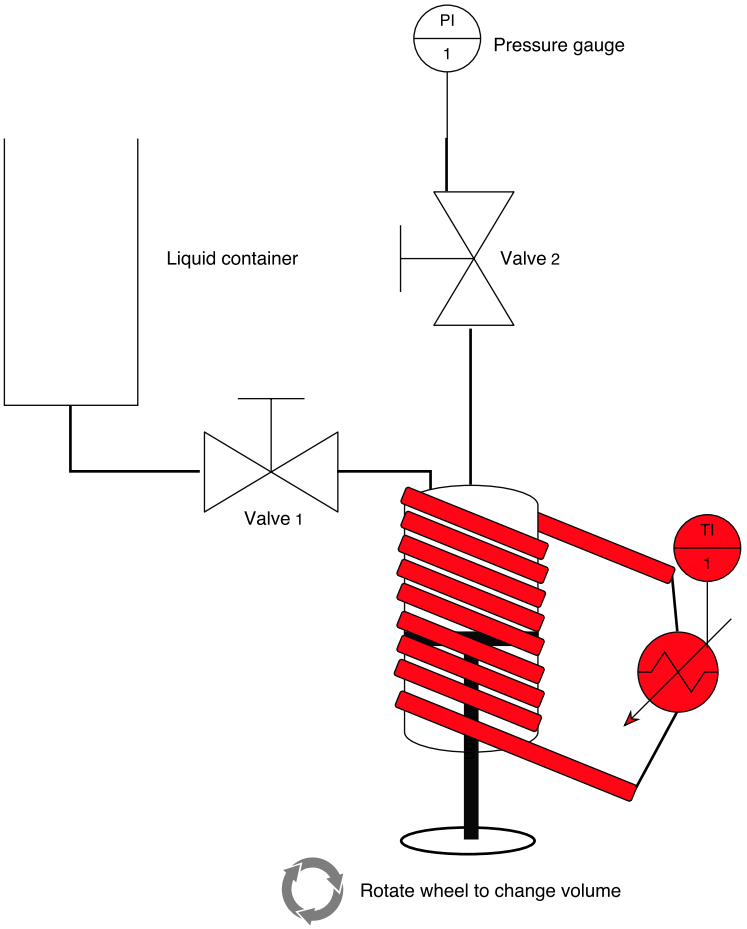

Figure 3.4: Schematic of the piston cylinder density experiment at 45 °C

pressure at given temperature. This is obtained from the densiometer. Total mass into the system can then be calculated.

Some assumptions are made; 1) The extra volume in the piping between the cylinder and valve 1, and between the cylinder and the gauge are negligible. 2) The threads for rotating the piston is uniform. 3) Mass is conserved. 4) Any error caused by potentially small amount of air in the system is negligible. 5) Initial mechanical lag of rotations is absorbed by the first pressurising from 1 to 10 bar, and that the readings from that point is correct relative to each other. 6) The density of nanofluid follows a linear trend with pressure, similar to water, this is justified by the small amounts of nanoparticles dispersed in the weater base. Assumption 5 and 6 seems reasonable by studying figure 3.5 and 3.6 that shows the results of a water density experiment. A trendline is fitted through the points, neglecting the first reading, which is substantially lower than the others.

Since the argument of mass conservation is believed to be certain, and that density is a function of mass and volume, taking into consideration assumption number 5, it is logical to conclude that an error is present due to volume. Since the density is calculated by $density = mass/(intitialvolume - deg.rev. \cdot vol/deg)$, an initial error would carry in all the following absolute density values. A trendline was therefor generated, excluding the initial value, and the intersection at 1 bar obtained. The

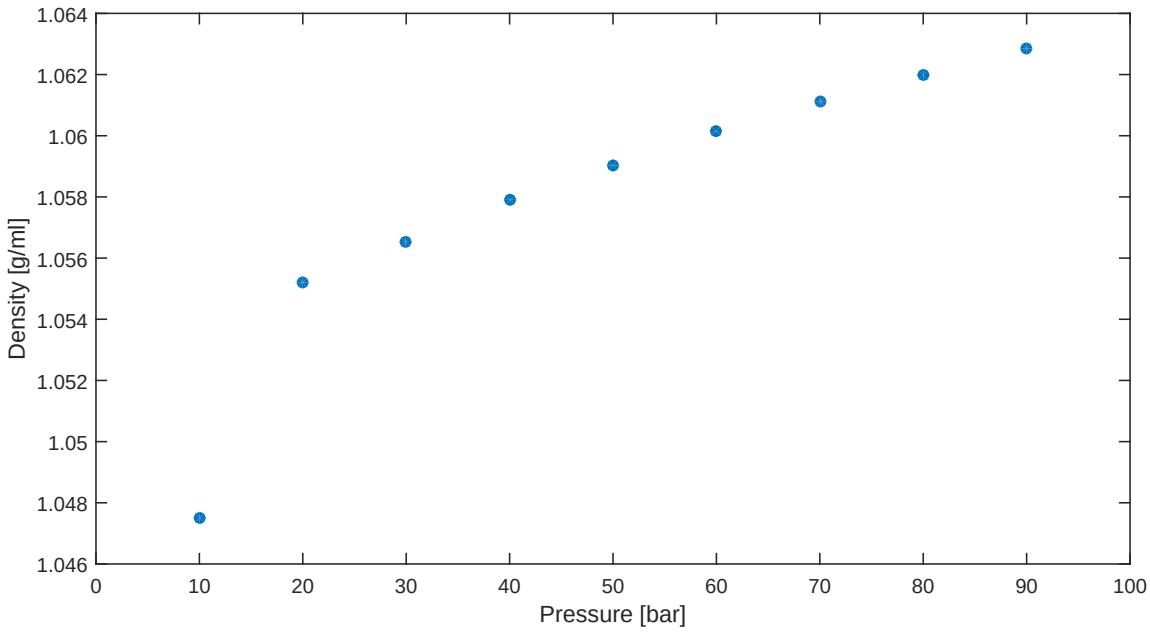

Figure 3.5: Measured density of water

difference between this value, and the value obtained in the densiometer was used as correction for all succeeding points. This is to lower the absolute values, but preserve their relative increase with pressure. To test the validity of this procedure, it was conducted three experiments with water, both at 25 and 45°C, and then compared to thermodynamical water data from NIST Webbook [3]. The test was done three times, with a total reset of the set-up every time to check for consistency. For 25°C, the tests proved highly consistent, with the standard deviation being in the range from 0.0003 g/ml to 0.003 g/ml, depending on the pressure. The average corrected results proved a maximum error less than 0.6% from NIST webbook values, with the average beeing 0.33%. Figure 3.7 shows the results of that experiment. It can be observed that the experimental values have to some extent a steeper slope than the analytical NIST data. The experiments for 45°C proved equaly consistent in terms of standard deviation, but had a slightly higher maximum error from NIST values, with the maximum beeing 1.5% and the average 0.9%. These results are provided in figure 3.8. The deviation of point "A" (Fig. 3.8) can be attributed to inaccuracies in reading wheel angles, and be explained by the large sensitivity to degrees turned. It is also observed that this error is carried on further. The percentage error is, however, still fairly small, and the average between three consecutive separate experiments may still give a fair representation.

TABLE 3.6: Standard deviation [g/ml] of nanofluid density experiments

Concentration [g/l]	25°C	45°C
0.05	0.00017	0.00017
0.50	0.00010	0.00029
1.00	0.00011	0.00046

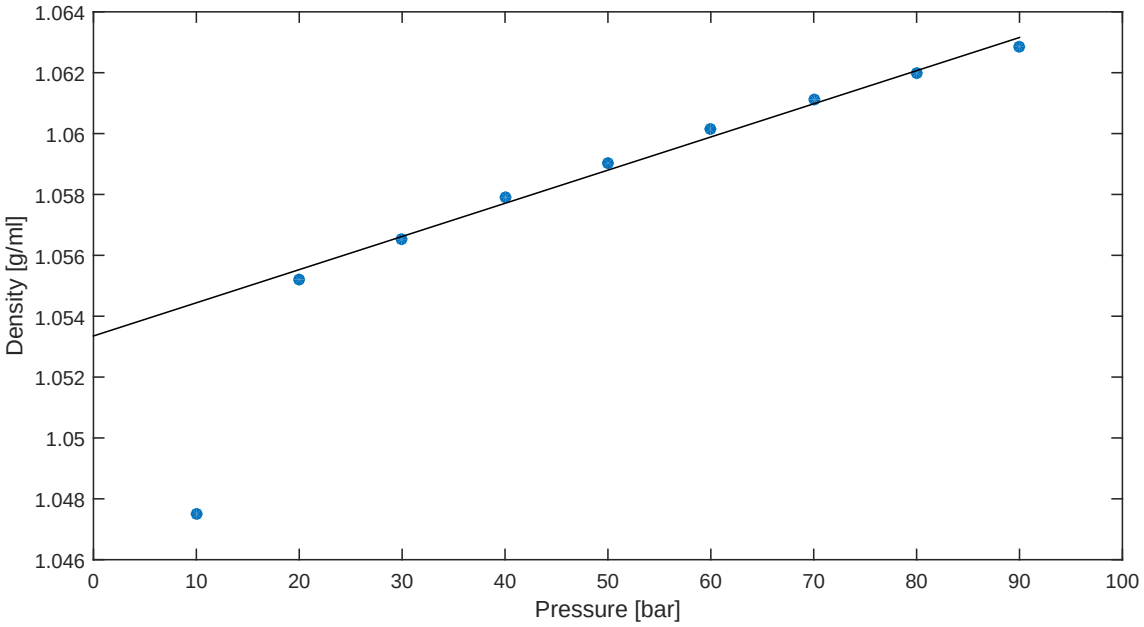

Figure 3.6: Measured density of water with trend line exluding the first point

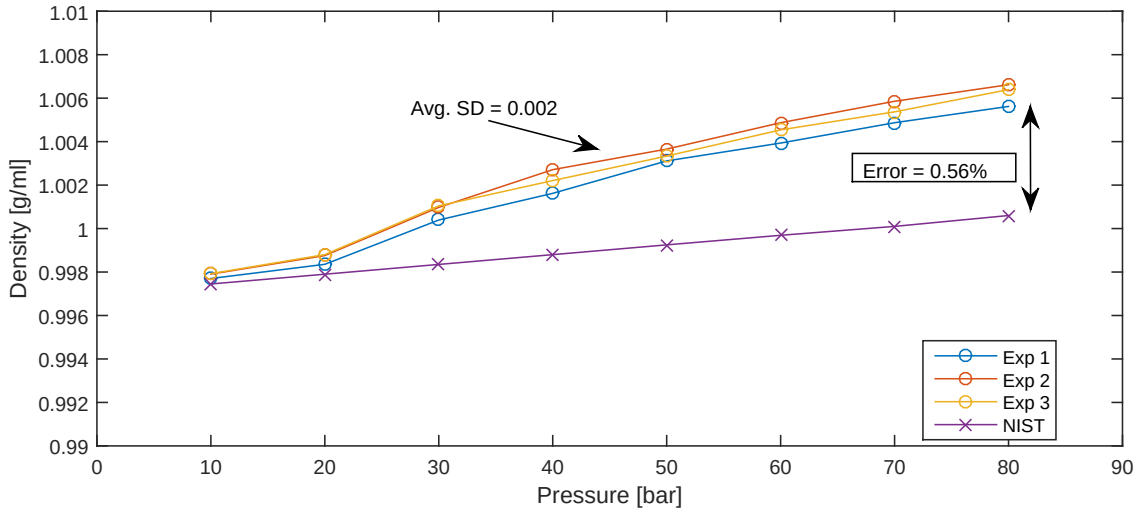

Figure 3.7: Measured density of water at 25°C

Due to the high repeatability of the experiments, water's deviation from NIST values are quite confidently attributed to unknown consistent mechanical features of the system, i.e. experimental errors such as small amounts of arbitrary air in the system is believed to not provide such consistency. The nanofluid also experience similar trends as water, and repeatability of the nanofluid experiments are also remarkable, which is believed to justify using the experimentally obtained water values as a calibration line against know water density, effectively finding the specific gravity, experimentally for the whole pressure and temperature range (10-90 bar, 25°C and 45°C). Table 3.6 shows an overview of the consitency in the nanofluid experiments.

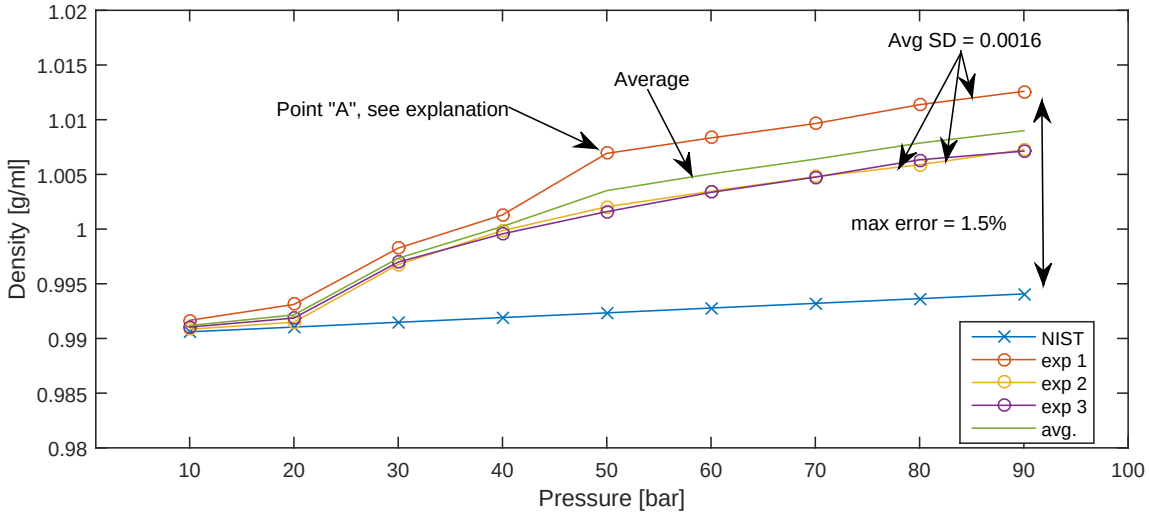

Figure 3.8: Measured density of water at 45°C

Figure 3.9 shows all the results of the nanofluid density experiments, the graph's magnitude are corrected against densiometer results at 1 bar, but not calibrated. It can be observed that the deviation from analytical water values are increased with higher temperature. A reason for this might be enhancing of mechanical errors, such as expansion of metal, gauge accuracy and human error due to necessity of completing the experiments faster to maintain the temperature. The consistency of the deviation is however still sufficient, and the complete picture strengthens the assumption of the validity of using the experimental water line as a calibration line and obtain the specific gravity.

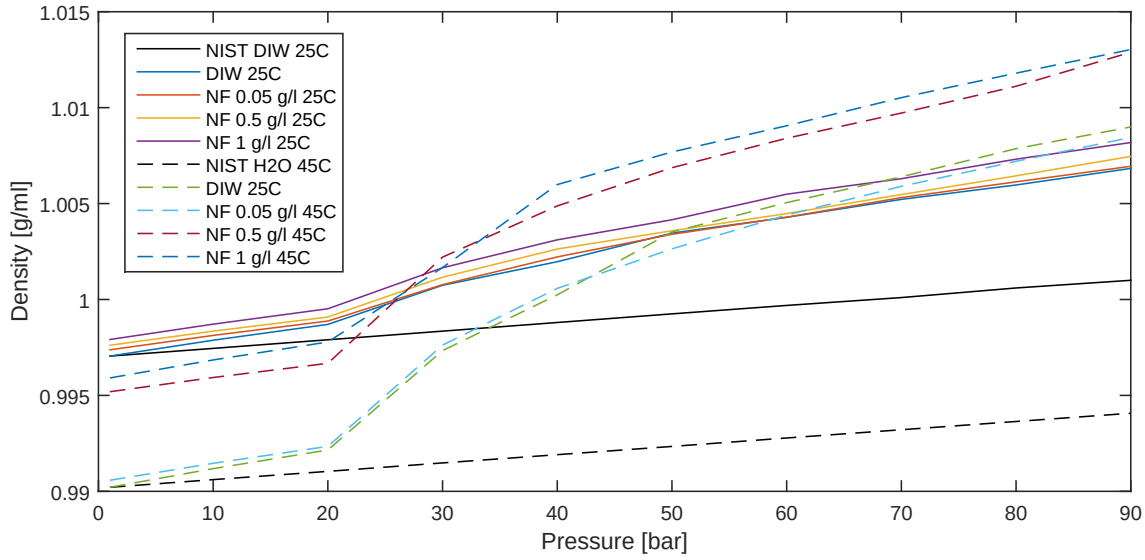

Figure 3.9: All density results before calibration

Using the experimental water density as calibration is achieved by calculating the experimental specific gravity of the nanofluid, and multiplying by analytical water density. To further investigate the experimental method and its assumptions, it is compared to a relatively simple analytical way of finding the density of the nanofluid.

This analytical method assumes no change in the volume of the water when mixing in the nanofluid, this is due to the minuscule addition of high concentrated nanofluid to large amounts of water. The nanoparticles in the nanofluid is then assumed to have no unexpected effects on waters density with pressure and temperature. Density is calculated by accounting for the addition of mass caused by the particles. Equation 3.2 to 3.5 explains this analytical method mathematically. Figure 3.10 shows the comparison of experimentally and analytically obtained density for 25°C, which coincides well, especially considering the small scale.

$$\rho_{NF} = \frac{m_{H_2O} + m_{NP}}{V_{H_2O} + V_{NP}} \tag{3.2}$$

$$\rho_{NF} = \frac{m_{H_2O}}{V_{H_2O} + V_{NP}} + \frac{m_{NP}}{V_{H_2O} + V_{NP}} \tag{3.3}$$

$$\rho_{NF} = \frac{\rho_{H_2O} V_{H_2O}}{V_{H_2O} + V_{NP}} + \frac{m_{NP}}{V_{H_2O} + V_{NP}} \tag{3.4}$$

$$V_{NP} << V_{H_2O}$$

$$\rho_{NF}(p, t, C) \approx (\rho_{H_2O})_{p,t} + C_{NP} \tag{3.5}$$

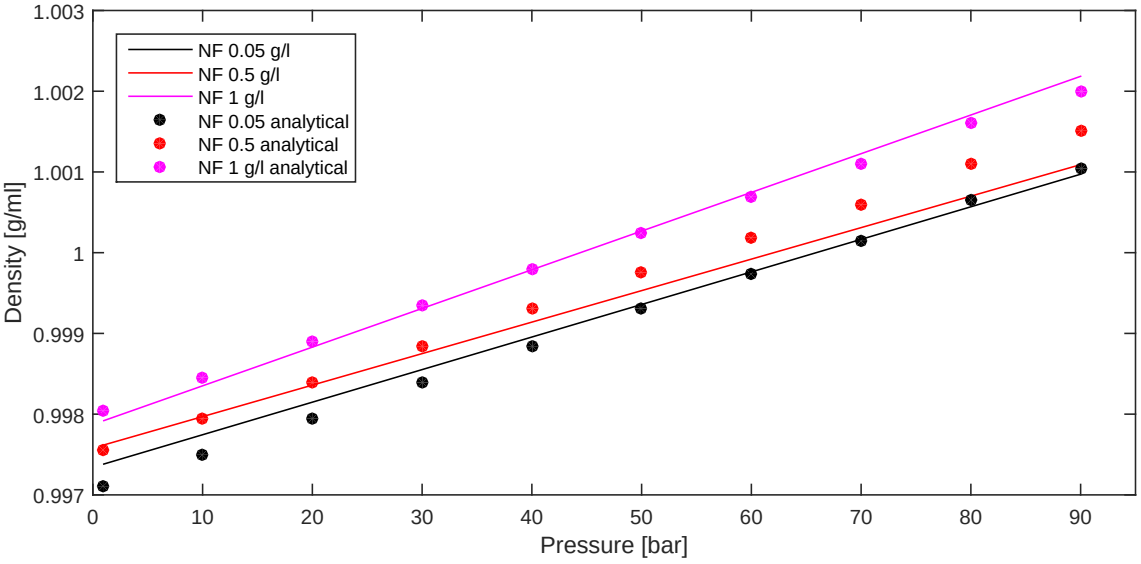

Figure 3.10: Experimental and analytical comparison (25°C)

Figure 3.11 shows the same comparison of analytically and experimentally obtained density for the nanofluid at 45°C, it can be observed that the values are not matching as good as for 25 °C. The maximum difference is 0.47%. Comparing equation 3.5 and experimental values at both 25°C and 45°C, reveals that the higher temperature always has lower density than the lower temperature, independent of analytical or experimental. This seems reasonable and might justify the discrepancy as minuscule. Figure 3.12 shows that comparison. For further analysis, especially with regards to IFT, the nanofluid density when CO_2 is dissolved in it is of interest, sensitivity is therefore done, especially focusing on 45°C to determine the effect of the

discrepancy on the carbonated nanofluid density.

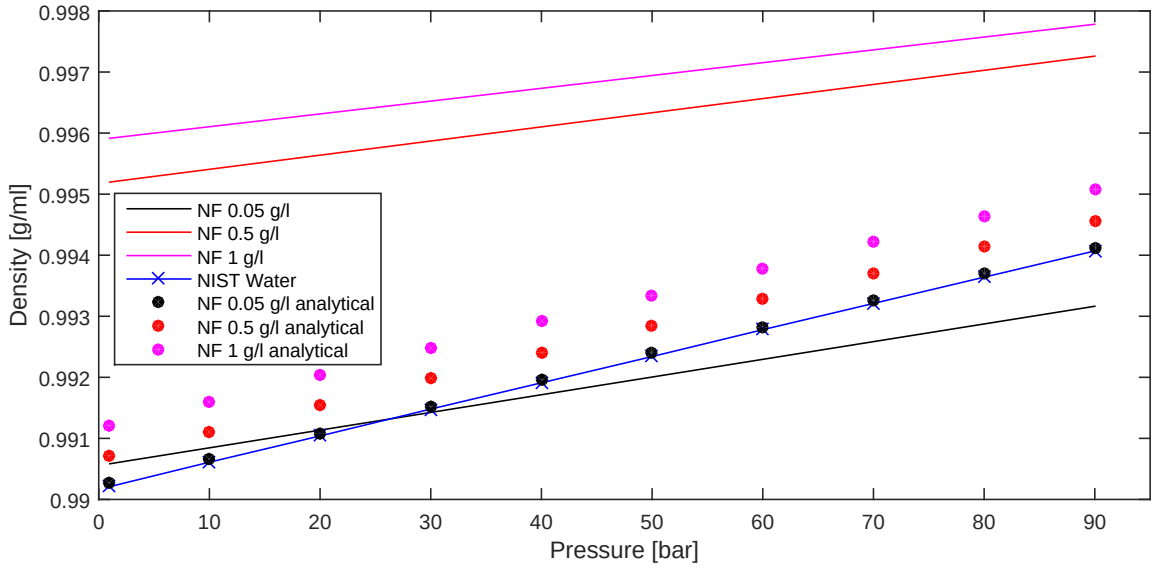

Figure 3.11: Experimental and analytical comparison (45°C)

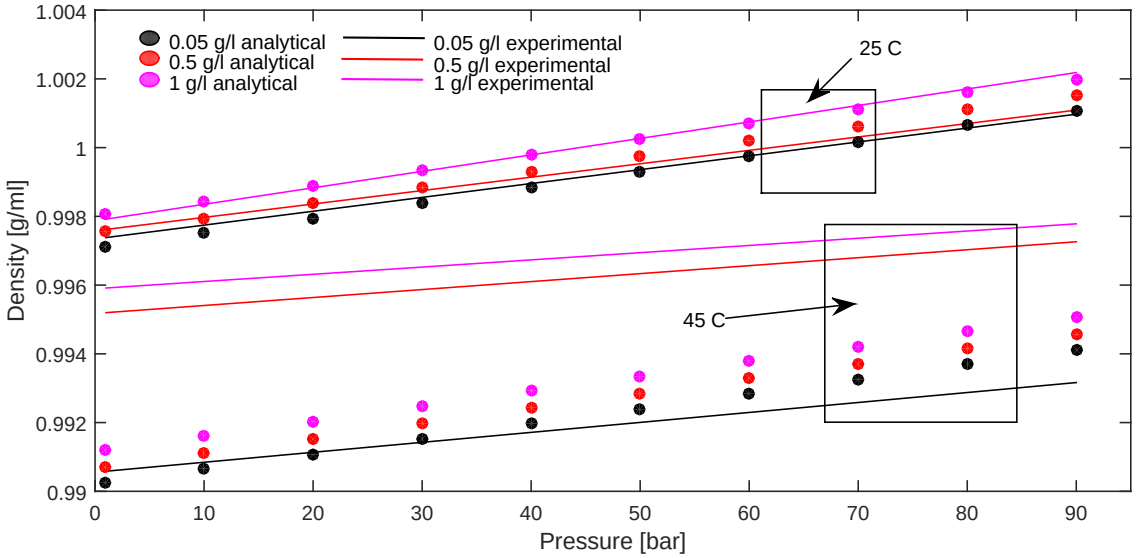

Figure 3.12: Experimental and analytical comparison (45°C)

Table 3.7, shows the analytical and experimental results for water density at 25°C and 45°C

TABLE 3.7: Experimental and analytical density of uncarbonated nanofluid

Analytical	25°C	25°C	25°C	45°C	45°C	45°C
P [bar]	1 g/l	0.5 g/l	0.05 g/l	1 g/l	0.5 g/l	0.05 g/l
10	0.99845	0.99795	0.99750	0.99161	0.99111	0.99066
20	0.99890	0.99840	0.99795	0.99204	0.99154	0.99109
30	0.99935	0.99885	0.99840	0.99248	0.99198	0.99153
40	0.99980	0.99930	0.99885	0.99291	0.99241	0.99196
50	1.00025	0.99975	0.99930	0.99334	0.99284	0.99239
60	1.00069	1.00019	0.99974	0.99378	0.99328	0.99283
70	1.00110	1.00060	1.00015	0.99421	0.99371	.088215
80	1.00160	1.00110	1.00065	0.99464	0.99414	0.99369
90	1.00200	1.00150	1.00105	0.99507	0.99457	0.99412
Exp	25°C	25°C	25°C	45°C	45°C	45°C
P [bar]	1 g/l	0.5 g/l	0.05 g/l	1 g/l	0.5 g/l	0.05 g/l
10	0.99835	0.99797	0.99774	0.99610	0.99541	0.99085
20	0.99883	0.99836	0.99815	0.99631	0.99564	0.99114
30	0.99931	0.99875	0.99855	0.99652	0.99587	0.99142
40	0.99979	0.99914	0.99896	0.99673	0.99610	0.99171
50	1.00027	0.99953	0.99936	0.99694	0.99633	0.99200
60	1.00075	0.99992	0.99976	0.99715	0.99657	0.99229
70	1.00123	1.00031	1.00017	0.99736	0.99680	0.99258
80	1.00171	1.00070	1.00057	0.99757	0.99703	0.99287
90	1.00218	1.00109	1.00097	0.99778	0.99726	0.99316

The experimentally obtained density is used in further analysis, as the analytical method is believed to be too simplistic. Further, the experiments proved good repitability. The density for pressurised SSW + NF is estimated by using the relative difference of SSW +NF and DIW + NF at atmospheric pressure. This is described by equation 3.6 and the results are shown in table 3.8.

$$\rho_{SSW,nf}(p,t) = \rho_{DIW,nf}(p,t)\frac{(\rho_{SSW,nf})_{P_{atm},t}}{(\rho_{DIW,nf})_{P_{atm},t}} \tag{3.6}$$

TABLE 3.8: Density of SSW + NF at 25°C and 45°C

	25°C	45°C
P [bar]	1 g/l	1 g/l
10	1.02327	1.01467
20	1.02376	1.01488
30	1.02425	1.01510
40	1.02475	1.01531
50	1.02524	1.01553
60	1.02573	1.01574
70	1.02622	1.01595
80	1.02671	1.01617
90	1.02720	1.01638

3.2 CO_2 Solubility in Nanofluid, DIW and SSW

The solubility of CO_2 in the nanofluid is important to obtain in order to calculate the density of carbonated nanofluids, and also to understand the diffusion proccess from nanofluids into hydrocarbon. Duan *et al.* developed a model in 2003 [63], for calculating solubility of CO_2 in aqueous solutions containg NaCl, the model was improved at lower pressures in 2006 [64], and also developed to account for Na^+, K^+,Ca^{2+}, Mg^{2+}, Cl^- and SO_4^{2-}. To investigate CO_2 solubility of pure water and SSW, a MATLAB-script of the model was written. This model can be found in appendix C. Figure 3.13 shows the solubility vs. pressure of both De-ionized water and SSW at the two temperatures for diffusion experiments. Figure 3.14 shows a 3D-grid plot for the whole range of the diffusion experiments (10-90 bar, 25°C - 45°C).It can be observed that the solubility is greater for pure water than SSW, and that solubility decreases with temperature.

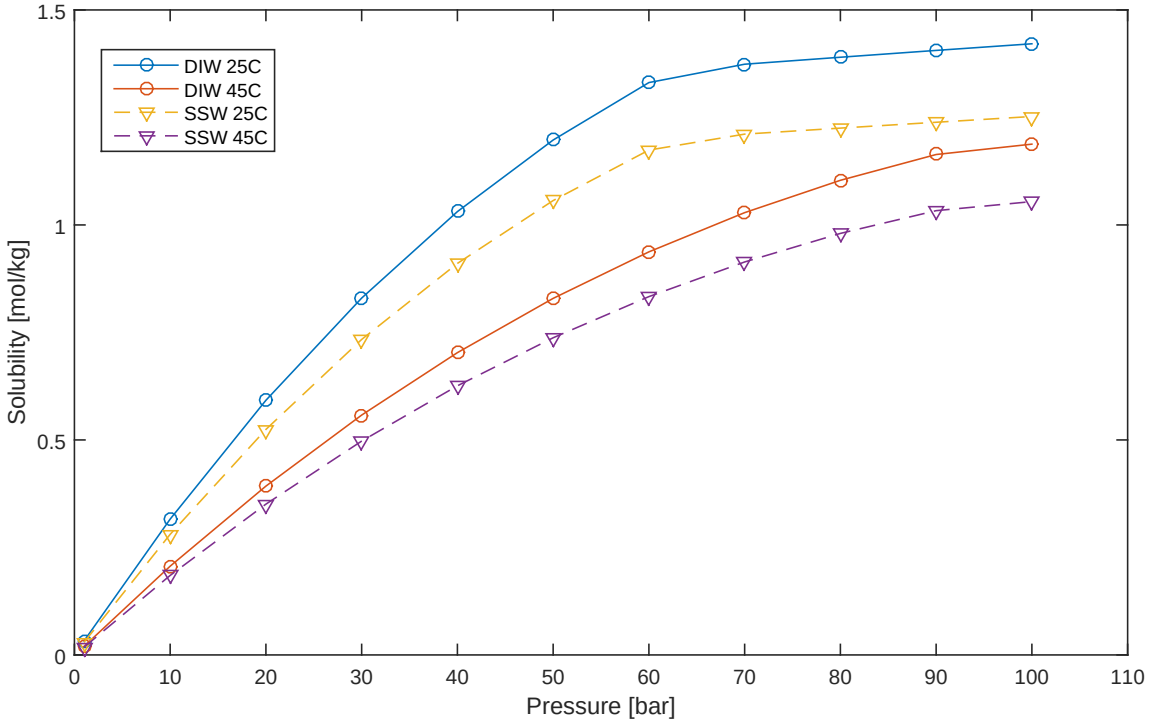

Figure 3.13: Duan *et al.* model for solubility

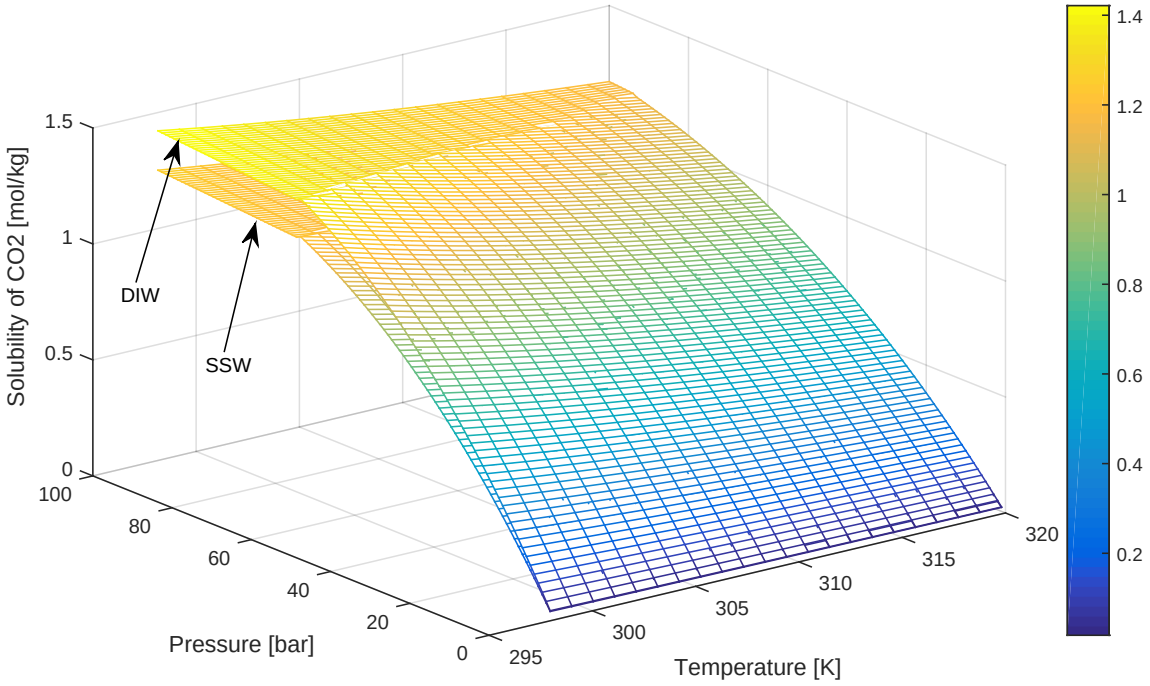

Figure 3.14: Duan *et al.* model for solubility (range of present experiments)

TABLE 3.9: Solubility [mol/kg] of DIW and SSW at 25 and 45°C

P [bar]	DIW 25°C	DIW 45°C	SSW 25°C	SSW 45°C
1	0.0325	0.0198	0.0292	0.0179
10	0.3159	0.2064	0.2805	0.1849
20	0.5922	0.3926	0.5244	0.3507
30	0.8299	0.5578	0.7337	0.4973
40	1.0310	0.7030	0.9105	0.6259
50	1.1975	0.8292	1.0567	0.7376
60	1.3311	0.9374	1.1741	0.8333
70	1.3738	1.0286	1.2112	0.9139
80	1.3900	1.1038	1.2252	0.9803
90	1.4059	1.1638	1.2388	1.0332
100	1.4213	1.1879	1.2522	1.0543

Haghtalab *et al.*, 2015 [57] studied the effect of ZnO and SiO_2 nanoparticles on the solubility of water. The greatest increase for SiO_2 where observed with 0.1wt%, which increased the solubility at an average of 7% relative to pure water. In order to calculate the solubility, the model of Duan *et al.* is applied for DIW and SSW, and three methods for estimating the additional solubility for nanofluid is discussed, sensitivity with reagard to density is carried out using these three methods.

Method 1 Experimentally obtained increase in solubility of 7% is reported by Haghtalab *et al.*, for 0.1wt% of SiO_2 NP in water. This is the same concentration as the highest concentration investigated in this work and the increase added to Duan *et al.*'s model can be taken directly from Haghtalab *et al.* However, to obtain the increase in solubility for the lower concentrations, a simple straight line interpolation between DIW solubility from Duan *et al.* and Duan *et al.* +7% is carried out. The assumption made for application of this method is a linear relationship between increased solubility and concentration of nanoparticles.

Method 2 This method follows the same logic as *Method 1*, but with a different assumption for the interpolation. The solubility is assumed to be proportional to the relative change in density with concentration. This would be exactly the same as *Method 1* if the density had a linear relation with concentration.

Method 3 The nanofluids solubility is calculated based on the relative change in density from pure DIW, this method follows the same assumption as *Method 2*, but do not take the experimental data form literature into account.

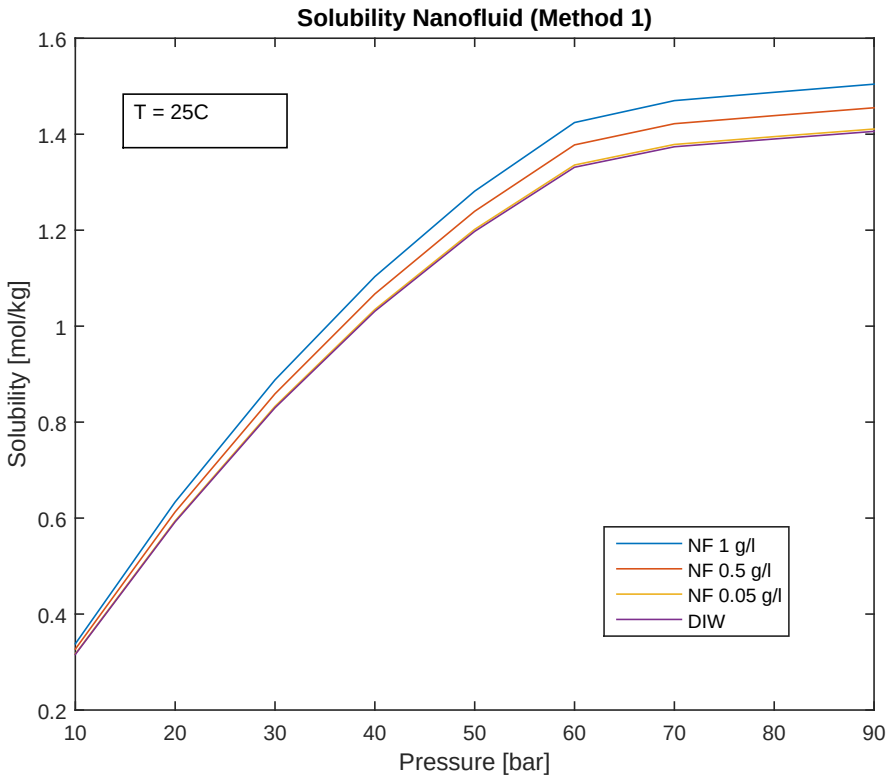

Figure 3.15: Solubility of Nanofluid (1 g/l, 0.5 g/l, 0.05 g/l) at 25 °C using *method 1*

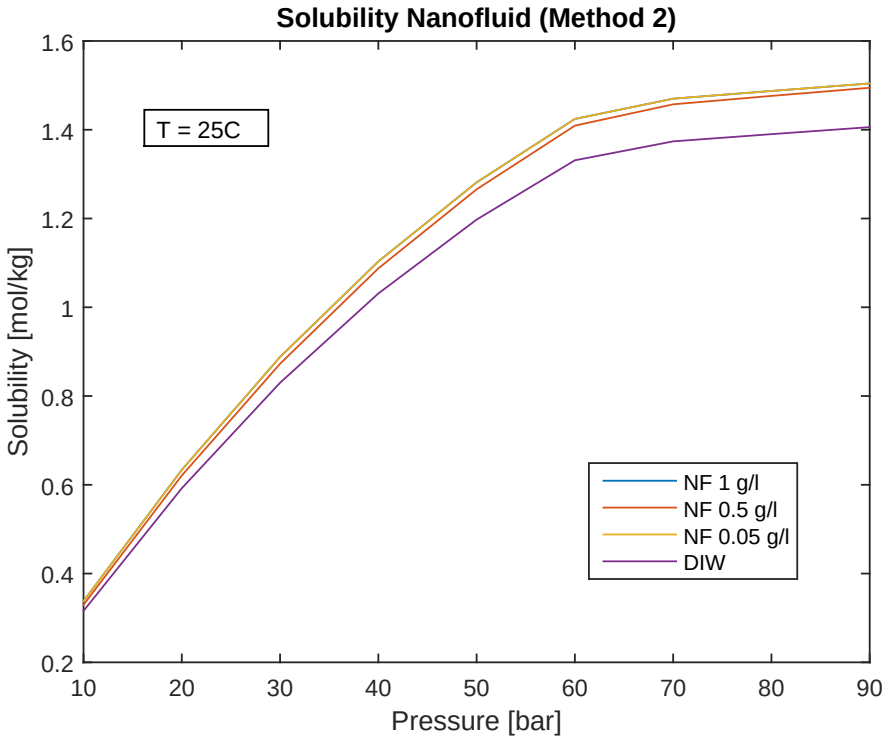

Figure 3.16: Solubility of Nanofluid (1 g/l, 0.5 g/l, 0.05 g/l) at 25 °C using *method 2*

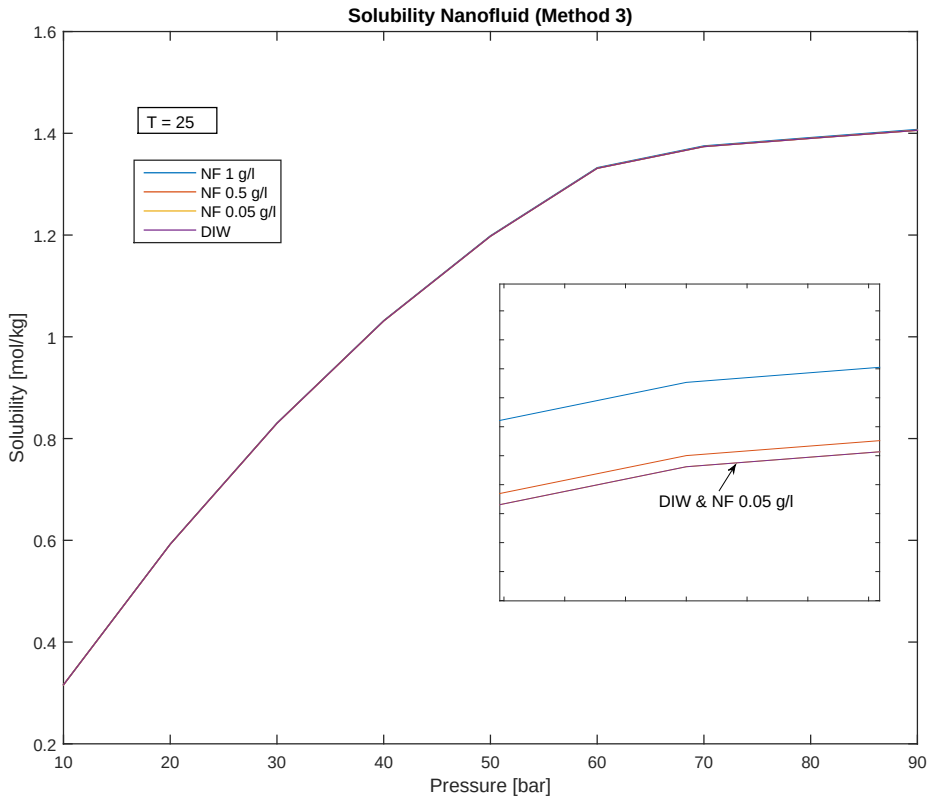

Figure 3.17: Solubility of Nanofluid (1 g/l, 0.5 g/l, 0.05 g/l) at 25 °C using *method 3*

TABLE 3.10: Method 1: Solubility [mol/kg] of nanofluid at 25 and 45°C

P [bar]	25°C 1 g/l	25°C 0.5 g/l	25°C 0.05 g/l	45°C 1 g/l	45°C 0.5 g/l	45°C 0.05 g/l
10	0.3380	0.3269	0.3170	0.2208	0.2136	0.2071
20	0.6336	0.6129	0.5943	0.4201	0.4064	0.3940
30	0.8880	0.8590	0.8328	0.5968	0.5773	0.5598
40	1.1032	1.0671	1.0347	0.7522	0.7276	0.7054
50	1.2813	1.2394	1.2017	0.8872	0.8582	0.8321
60	1.4243	1.3777	1.3358	1.0030	0.9702	0.9407
70	1.4700	1.4219	1.3786	1.1006	1.0646	1.0322
80	1.4873	1.4387	1.3949	1.1810	1.1424	1.1076
90	1.5043	1.4551	1.4108	1.2453	1.2046	1.1679

TABLE 3.11: Method 2: Solubility [mol/kg] of nanofluid at 25 and 45°C

P [bar]	25°C 1 g/l	25°C 0.5 g/l	25°C 0.05 g/l	45°C 1 g/l	45°C 0.5 g/l	45°C 0.05 g/l
10	0.3380	0.3287	0.3230	0.2208	0.2190	0.2070
20	0.6336	0.6127	0.6033	0.4201	0.4166	0.3931
30	0.8880	0.8541	0.8420	0.5968	0.5918	0.5573
40	1.1032	1.0558	1.0427	0.7522	0.7457	0.7009
50	1.2813	1.2205	1.2065	0.8872	0.8795	0.8249
60	1.4243	1.3513	1.3373	1.0030	0.9943	0.9300
70	1.4700	1.3917	1.3798	1.1006	1.0909	1.0177
80	1.4873	1.3988	1.3874	1.1810	1.1704	1.0886
90	1.5043	1.4134	1.4034	1.2453	1.2339	1.1438

TABLE 3.12: Method 3: Solubility [mol/kg] of nanofluid at 25 and 45°C

P [bar]	25°C 1 g/l	25°C 0.5 g/l	25°C 0.05 g/l	45°C 1 g/l	45°C 0.5 g/l	45°C 0.05 g/l
10	0.3162	0.3160	0.3160	0.2080	0.2079	0.2078
20	0.5911	0.5907	0.5880	0.3946	0.3944	0.3926
30	0.8303	0.8299	0.8298	0.5619	0.5617	0.5616
40	1.0285	1.0278	1.0231	0.7061	0.7056	0.7024
50	1.1976	1.1969	1.1967	0.8350	0.8345	0.8343
60	1.3269	1.3260	1.3201	0.9409	0.9403	0.9361
70	1.3734	1.3725	1.3722	1.0354	1.0347	1.0346
80	1.3847	1.3838	1.3777	1.1072	1.1065	1.1016
90	1.4048	1.4038	1.4036	1.1711	1.1702	1.1700

r A relatively simple experimental proceedure was developed to try to observe a potential increased solubility with nanoparticles present in DIW and SSW, and thereby establish confident in an increased solubility relative to pure water. An increased solubility do also indicate that nanoparticles have a possibility of enhancing carbon storage in subsurface structures. A PVT-cell containing the fluid of interest were pressurised quickly to 48 bar from a connected CO_2 cylinder. The valve connecting the two was then closed.The pressure decay was then observed. By knowing volume of the cell, volume of fluid, mass of fluid, temperature and the two pressures, the number

of moles of CO2 that went into the fluid were calculated. Volume increase of the fluid was neglected for this simple indicative experiment. A reasonable presentation of the observations could have been the pressure decrease. However, relative solubility is presented instead in order to account for the effect of CO_2 compressibility, and the different volume of fluid regarding SSW. Table 3.13 shows the raw data, and figure 3.18 visualises the results as relative solubility increase. The set-up inherent some

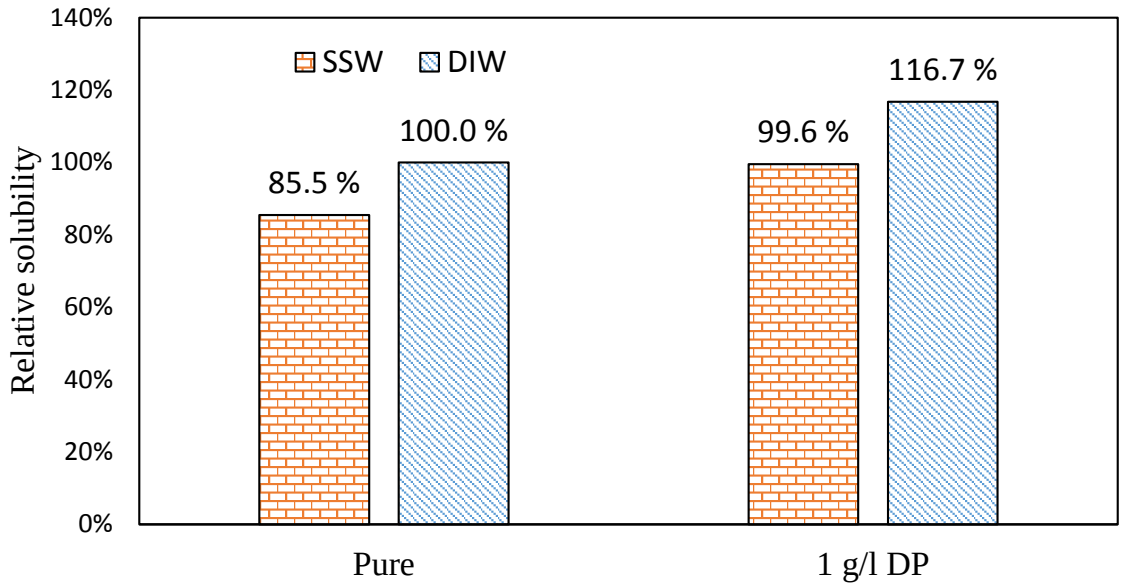

Figure 3.18: Solubility of SSW, SSW + 1 g/l NP, DIW and DIW + 1 g/l NP, at 45°C , obtained from pressure decay method starting at 48 bar. Pure De-ionised water is chosen as the reference

relatively large sources of error, such as pressure accuracy of $\pm 1bar$, unknown line volume, and $\pm 1ml$ accuracy for volume measurement. Even though this experiment is too simplistic, and some sort of stirring device would be preferable to obtain the maximum solubility, it is still indicative that the nanofluid do increase the solubility of both DIW and SSW. The experiment is also indicative of a similar relative solubility increase for DIW and SSW when adding 1 g/l NP. For further calculations and discussions, the literature data is used for solubility, where *method 2* is selected for calculation. This decision is based on the the fact that this method is a combination of the two others, and take both the experimentally found density and literature data into account. The main purpose of obtaining the solubility is for further calculation of density of carbonated nanofluid. Density of carbonated nanofluid with SSW as basefluid is calculated relative to nanofluid with DIW as basefluid by a factor calculated from the pure basefluids.

TABLE 3.13: Results from solubilitity experiment at 45°C

	DIW		SSW	
Concentration NP	0 g/l	1 g/l	0 g/l	1 g/l
Volume fluid [ml]	19	19	16.5	19
Mass fluid [g]	18.93	18.92	16.99	19.01
Volume CO_2 [ml]	6	6	8.5	6
P_i [bar]	48	49	48	48
P_f [bar]	36	35	3 9	36

Table 3.14, 3.15, and 3.16 is generated to compare the three different solubility methods in terms of density. It can be observed that method 1 and 2 differs very little, while method 3 is much lower the method 1 and 2. This can be explained by the fact that method 1 and 2 share the property of incorporating a relatively large solubility increase reported in the literature, while method 3 bases its calculations solely on the density increase caused by addition of nanofluid. This density alteration is relatively small in itself, and the solubility calculated only by this means do naturally result in this trend this trend.

TABLE 3.14: Sensitivity study on the effect of the different solubility methods on density [g/ml] of carbonated nanofluid, method 1

Solubility Method 1	25°C	25°C	25°C	45°C	45°C	45°C
P [bar]	1 g/l	0.5 g/l	0,05 g/l	1 g/l	0.5 g/l	0.05 g/l
10	1.00828	1.00757	1.00705	1.00215	1.00126	0.99650
20	1.01763	1.01653	1.01576	1.00790	1.00684	1.00195
30	1.02588	1.02441	1.02341	1.01309	1.01188	1.00687
40	1.03303	1.03124	1.03005	1.01771	1.01638	1.01127
50	1.03911	1.03703	1.03568	1.02181	1.02035	1.01518
60	1.04414	1.04181	1.04032	1.02538	1.02384	1.01860
70	1.04611	1.04362	1.04211	1.02845	1.02683	1.02155
80	1.04717	1.04457	1.04305	1.03103	1.02935	1.02405
90	1.04821	1.04551	1.04398	1.03316	1.03143	1.02612

TABLE 3.15: Sensitivity study on the effect of the different solubility methods on density [g/ml] of carbonated nanofluid, method 2

Solubility Method 2	25°C	25°C	25°C	45°C	45°C	45°C
P [bar]	1 g/l	0.5 g/l	0,05 g/l	1 g/l	0.5 g/l	0.05 g/l
10	1.00828	1.00763	1.00723	1.00215	1.00141	0.99650
20	1.01763	1.01652	1.01603	1.00790	1.00713	1.00193
30	1.02588	1.02427	1.02369	1.01309	1.01229	1.00680
40	1.03303	1.03089	1.03030	1.01771	1.01689	1.01115
50	1.03911	1.03644	1.03583	1.02181	1.02096	1.01497
60	1.04414	1.04097	1.04037	1.02538	1.02453	1.01829
70	1.04611	1.04266	1.04215	1.02845	1.02759	1.02113
80	1.04717	1.04330	1.04281	1.03103	1.03017	1.02350
90	1.04821	1.04418	1.04375	1.03316	1.03229	1.02542

TABLE 3.16: Sensitivity study on the effect of the different solubility methods on density [g/ml] of carbonated nanofluidm method 3

Solubility Method 3	25°C	25°C	25°C	45°C	45°C	45°C
P [bar]	1 g/l	0.5 g/l	0,05 g/l	1 g/l	0.5 g/l	0.05 g/l
10	1.00764	1.00725	1.00702	1.00180	1.00111	0.99652
20	1.01635	1.01586	1.01557	1.00719	1.00651	1.00191
30	1.02411	1.02353	1.02332	1.01210	1.01144	1.00692
40	1.03071	1.03002	1.02970	1.01640	1.01575	1.01119
50	1.03648	1.03570	1.03552	1.02031	1.01968	1.01524
60	1.04106	1.04017	1.03982	1.02358	1.02298	1.01847
70	1.04303	1.04205	1.04191	1.02655	1.02596	1.02162
80	1.04390	1.04283	1.04251	1.02887	1.02830	1.02388
90	1.04504	1.04388	1.04375	1.03098	1.03042	1.02619

3.3 Density of Carbonated Nanofluid

Duan *et al., 2008* [65], developed a liquid density model for CO_2-H_2O systems, based on a previously developed [66] virial equation of state (EoS) by the same authors, which were intendet for CH_4-CO_2-H_2O systems. The EoS results in equation 3.7 and 3.8, which calculates the total volume of the system, i.e. the volume of water + dissolved CO_2, constants for equation 3.8 are given in table 3.17. Further, the new density is calculated by equation 3.9, where V_ϕ is the appearant CO_2 volume calculated from equation 3.10.

$$V = V_1[1 + (A_1 + A2P)x_2] \tag{3.7}$$

Where $V1$ is the molar water volume, and x_2 is the mole fraction of CO_2 in solution.

$$A_i = A_{i1}T^2 + A_{i2}T + A_{i3} + A_{i4}T^{-1} + A_{i5}T^{-2} \tag{3.8}$$

TABLE 3.17: Constants for equation 3.8

j	A_{1j}	A_{2j}
1	$0.38384020 \cdot 10^{-3}$	$-0.57709332 \cdot 10^{-5}$
2	$-0.55953850 \cdot 10^{0}$	$0.82764653 \cdot 10^{-2}$
3	$0.30429268 \cdot 10^{3}$	$-0.43813556 \cdot 10^{1}$
4	$-0.72044305 \cdot 10^{5}$	$0.10144907 \cdot 10^{4}$
5	$0.63003388 \cdot 10^{7}$	$-0.86777045 \cdot 10^{5}$

$$\rho = \frac{x_1 Mw_1 + x_2 Mw_2}{x_1 Mw_1/\rho_1 + x_2 V_\phi} \tag{3.9}$$

Where x_1, Mw_1, Mw_2 and ρ_1 is mole fraction of water, molecular weight of water, molecular weight of CO_2 and density of water, respectively.

$$V_\phi = (V_1(1 + A_1 + A_2 P)) \tag{3.10}$$

In the case of carbonated nanofluid, this model by Duan *et al.* is applied, but with the assumption of volume conservation of H_2O and nanoparticles in the nanofluid, and that all water properties in the model by Duan is substituted with nanofluid properties. This results in a pseudo-molar volume, V1, represented by equation 3.11

$$V_1 = \frac{x_{H_2O} Mw_{H_2O} + x_{NP} Mw_{NP}}{(\rho_{NP})_{p,t}} \tag{3.11}$$

The density of the uncarbonated nanofluid is found experimentally, and molar fractions of the two species is known from the concentration of nanoparticles and individual densities at standard conditions. When calculating the molar volume of the nanofluid, the sum of water and nanoparticle molar fractions is equal to one, but when advancing in the calculations, CO_2 is present, and in equation 3.9, x_{H_2O} and x_{NP} is therefore considered to form x_1 combined. x_1 and x_2 is found from the solubility of CO_2 in the nanofluid.

Table 3.18 shows the density of carbonated DIW-NF for all pressures, temperatures and concentrations. Table 3.19 shows the density of SSW-NF for 1 g/l at all pressures and temperatures, and table 3.20 shows the density of DIW and SSW without nanoparticles for all pressures and temperatures. The relationship between carbonated DIW and carbonated SSW is used for calculating the carbonated SSW-NF density from carbonated DIW-NF. Interestingly, it can be observed in table 3.20 that density of carbonated SSW is less than density of carbonated DIW, even though SSW without CO_2 have greater density. The reason for this phenomenon is the increased density from adding CO_2 in combination with decreased solubility of CO_2 in water when salts are added.

TABLE 3.18: Density of carbonated DIW-NF

P [bar]	25°C 1 g/l	25°C 0.5 g/l	25°C 0.05 g/l	45°C 1 g/l	45°C 0.5 g/l	45°C 0.05 g/l
10	1.00822	1.00757	1.00717	1.00213	1.00139	0.99648
20	1.01741	1.01632	1.01583	1.00782	1.00704	1.00185
30	1.02545	1.02387	1.02331	1.01291	1.01211	1.00664
40	1.03236	1.03028	1.02971	1.01743	1.01661	1.01090
50	1.03820	1.03562	1.03503	1.02140	1.02057	1.01463
60	1.04301	1.03996	1.03937	1.02486	1.02403	1.01785
70	1.04490	1.04158	1.04109	1.02782	1.02698	1.02060
80	1.04593	1.04221	1.04174	1.03031	1.02946	1.02289
90	1.04694	1.04307	1.04265	1.03235	1.03150	1.02475

TABLE 3.19: Density of carbonated SSW-NF 1 g/l

P [bar]	25°C	45°C
10	1.00782	1.00193
20	1.01664	1.00742
30	1.02433	1.01232
40	1.03095	1.01668
50	1.03654	1.02051
60	1.04115	1.02384
70	1.04296	1.02669
80	1.04397	1.02909
90	1.04495	1.03105

TABLE 3.20: Density of carbonated SSW and DIW

P [bar]	CW 25°C	CW 45°C	SSW 25°C	SSW 45°C
10	1.00097	0.99635	1.00058	0.99615
20	1.00453	0.99855	1.00377	0.99815
30	1.00768	1.00055	1.00658	0.99998
40	1.01043	1.00238	1.00905	1.00165
50	1.01279	1.00404	1.01117	1.00316
60	1.01478	1.00552	1.01297	1.00452
70	1.01570	1.00686	1.01382	1.00575
80	1.01640	1.00803	1.01449	1.00684
90	1.01700	1.00908	1.01506	1.00781

3.4 Viscosity of Carbonated Nanofluid

For calculating the viscosity of the uncarbonated nanofluid, two models are compared. Corcione, 2011 [56] and Duangthongsuk & Wongwises, 2009 [67].

Duangthongsuk & Wongwises measured the viscosity of nanfluids with 0.2%, 0.6%, 1.0%, 1.5% and 2.0% volume fraction of TiO_2 nanoparticles at 15°C, 25°C, and 35°C. They further compared their results to values obtained from the models of Batchelor [68], Drew and Passman [69], Brinkman [70], and Wang *et al.* [71] described accordingly by equation 3.12 to 3.15, where μ_{nf},μ_w and ϕ are nanofluid viscosity,

basefluid (water) viscosity and nanoparticle volume concentration, respectively.

$$\frac{\mu_{nf}}{\mu_w} = (1 + 2.5\phi + 6.2\phi^2) \tag{3.12}$$

$$\frac{\mu_{nf}}{\mu_w} = (1 + 2.5\phi) \tag{3.13}$$

$$\frac{\mu_{nf}}{\mu_w} = \frac{1}{(1-\phi)^{2.5}} \tag{3.14}$$

$$\frac{\mu_{nf}}{\mu_w} = (1 + 7.3\phi + 123\phi^2) \tag{3.15}$$

Duangthongsuk & Wongwises then proposed a new equation for predicting the viscosity of TiO_2 nanofluids, described by equation 3.16 and table 3.21

$$\frac{\mu_{nf}}{\mu_w} = (a + b\phi + c\phi^2) \tag{3.16}$$

TABLE 3.21: Constants for equation 3.16

T [°C]	a	b	c	R^2
15	1.0226	0.0477	-0.0112	0.9885
25	1.013	0.092	-0.015	0.9767
35	1.018	0.112	-0.0177	0.9937

Corcione, 2011 [56] studied the effect on viscosity with nanoparticles on both ethane and water as a basefluid, and compared a large number of experimental data from the literature. Different nanoparticles were studied, such as alumina, titanium, copper and silica based. The volume fractions of the particles ranged from 0.0001 to 0.071, particle size between 25 and 200 nm, and a temperature between 20 and 50°C. Equation 3.17 shows a fitted correlation to all these data with a standard deviation of 1.84%. The equation incorporates the effect of nanoparticle size in addition to its volume fraction, and points out that earlier correlations such as the Brinkman equation (Equation 3.14) largely fails with regards to nanofluids, and that the error increases with decreasing particle size.

$$\frac{\mu_{nf}}{\mu_b f} = \left[1 - 34.87\left(\frac{d_p}{d_f}\right)^{-0.3}\phi^{1.03}\right]^{-1} \tag{3.17}$$

d_f is the equivalent diameter of the base fluid, calculated according to equation 3.18

$$d_f = 0.1\left(\frac{6MW}{N_{av}\pi\rho_{f0}}\right)^{1/3} \tag{3.18}$$

The correlation of Corcione [56] is chosen to be used further in this study based on four factors; 1) The range of data the correlation is fitted to lies within the range of this study, 2) The correlation is fitted to a large set of different data with good standard deviation, 3) Contrary to Duangthongsuk & Wongwises, 2009 [67], SiO_2, which is the material used in this study, is included when fitting the correlation.

Further, to calculate the viscosity of carbonated nanofluid, the Herning and Zipperer, 1936 [72] equation for viscosity of mixtures are used, where nanofluid is treated as one component, and CO_2 as the other. This is a similar aproach to how the density of carbonated nanofluid were calculated. Equation 3.19 and 3.20 describes this mathematically.

$$\mu = \frac{\sum_i^n x_i \mu_i \sqrt{MW_i}}{\sum_i^n x_i \sqrt{MW_i}} \tag{3.19}$$

$$\mu_{cnf} = \left(\frac{x_{CO_2} \mu_{CO_2} \sqrt{MW_{CO_2}} + x_{nf} \mu_{nf} \sqrt{MW_{nf}}}{x_{CO_2} \sqrt{MW_{CO_2}} + x_{nf} \sqrt{MW_{nf}}} \right)_{(p,t)} \tag{3.20}$$

Table 3.22 shows the estimated viscocity of the uncarbonated nanofluid used in this study.

TABLE 3.22: Viscosity [cP] of nanofluid at 25 and 45°C

P [bar]	25°C DIW	25°C 0.05 g/l	25°C 0.5 g/l	25°C 1 g/l]	45°C DIW	45°C 0.05 g/l	45°C 0.5 g/l	45°C 1 g/l
10	0.8899	0.8912	0.9039	0.9190	0.5962	0.5971	0.6056	0.6157
20	0.8896	0.8909	0.9037	0.9188	0.5963	0.5972	0.6057	0.6159
30	0.8894	0.8907	0.9035	0.9186	0.5965	0.5973	0.6059	0.6160
40	0.8892	0.8905	0.9032	0.9183	0.5966	0.5975	0.6060	0.6161
50	0.8890	0.8903	0.9030	0.9181	0.5967	0.5976	0.6062	0.6163
60	0.8888	0.8901	0.9028	0.9179	0.5969	0.5977	0.6063	0.6164
70	0.8886	0.8899	0.9026	0.9177	0.5970	0.5979	0.6064	0.6166
80	0.8884	0.8897	0.9024	0.9175	0.5972	0.5980	0.6066	0.6167
90	0.8882	0.8895	0.9022	0.9173	0.5973	0.5982	0.6067	0.6169

Table 3.23 shows the estimated viscocity of the carbonated nanofluid used in this study.

TABLE 3.23: Viscosity [cP] of carbonated nanofluid at 25 and 45°C

P [bar]	25°C 0.05 g/l	25°C 0.5 g/l	25°C 1 g/l	45°C 0.05 g/l	45°C 0.5 g/l	45°C 1 g/l
10	0.88330	0.89575	0.91048	0.59373	0.60199	0.61199
20	0.87627	0.88863	0.90296	0.59084	0.59886	0.60889
30	0.87043	0.88264	0.89656	0.58832	0.59624	0.60609
40	0.86555	0.87758	0.89110	0.58626	0.59388	0.60366
50	0.86160	0.87355	0.88670	0.58442	0.59196	0.60169
60	0.85846	0.87037	0.88320	0.58290	0.59027	0.59996
70	0.85892	0.87088	0.88366	0.58177	0.58889	0.59863
80	0.85876	0.87073	0.88329	0.58084	0.58791	0.59752
90	0.85837	0.87037	0.88288	0.58033	0.58718	0.59686

3.5 Mole- and Volume Fraction - Viscosity and Density of HC-drop

Mole fraction of CO_2 in the drop is calcualted by equation 3.21, based on the experimental volume change of the drop, the same is true for volume fraction. Viscosity and density is dependent on these properties, which is obtained from the primary pendant drop diffusion experiments. Therefore, this section serves as a theory for how it is calculated, while the results are present in the primary *Results and Discussion*-chapter (Ch. 5).

$$MF_{CO_2} = \frac{\frac{\Delta V \cdot \rho_{CO_2}(p,t)}{MW_{CO_2}}}{\frac{\Delta V \cdot \rho_{CO_2}(p,t)}{MW_{CO_2}} + \frac{V_0 \cdot \rho_{C10}(p,t)}{MW_{C_{10}}}}, \tag{3.21}$$

Volume fraction of CO_2 in the drop is calculated by equation 3.22

$$VF_{CO_2} = 1 - \frac{V_i}{V_f}, \tag{3.22}$$

where V_i and V_f is initial and final volume, respectively.

The viscosity of the drop is calculated with equation 3.23, the results of this calculations are presented in the *Results*-chapter. The mole and volume fractions needed in these calculations are calculated from volume change of the drop, which is also presented in the *Results*-chapter. The densities and viscosities calculated based on the volume change, are needed in interfacial tension calculations, related to the pendant drop in the primary experiments.

$$\mu_{chc} = \left(\frac{x_{CO_2}\mu_{CO_2}\sqrt{MW_{CO_2}} + x_{HC}\mu_{nf}\sqrt{MW_{HC}}}{x_{CO_2}\sqrt{MW_{CO_2}} + x_{HC}\sqrt{MW_{HC}}} \right)_{(p,t)} \tag{3.23}$$

TABLE 3.24: Viscosity [cP] of decane and CO_2 at 25 and 45°C

P [bar]	25°C *n*-C10	45°C *n*-C10	25°C CO_2	45°C CO_2
10	0.85734	0.65525	0.01503	0.01598
20	0.86764	0.66316	0.01520	0.01613
30	0.87797	0.67108	0.01548	0.01636
40	0.88835	0.67902	0.01593	0.01669
50	0.89877	0.68698	0.01670	0.01718
60	0.90923	0.69496	0.01832	0.01791
70	0.91974	0.70297	0.06160	0.01905
80	0.93028	0.71099	0.06679	0.02105
90	0.94087	0.71904	0.07065	0.02548

The density of the drop is calculated with equation 3.24

$$\rho_{drop} = (VF_{CO_2}\rho_{CO2} + VF_{HC}\rho_{HC})_{p,t} \tag{3.24}$$

TABLE 3.25: Density [g/ml] of decane and CO_2 at 25 and 45°C

P [bar]	25°C *n*-C10	45°C *n*-C10	25°C CO_2	45°C CO_2
10	0.72725	0.71180	0.01872	0.01735
20	0.72805	0.71270	0.03977	0.03634
30	0.72884	0.71359	0.06409	0.05741
40	0.72963	0.71447	0.09335	0.08120
50	0.73040	0.71533	0.13127	0.10869
60	0.73117	0.71619	0.19061	0.14161
70	0.73193	0.71704	0.74303	0.18320
80	0.73268	0.71788	0.77664	0.24105
90	0.73342	0.71871	0.79965	0.33751

3.5.1 Nanoparticle's Possible Effect on Decane Viscosity

To investigate the significance on viscosity of possible mass transfer of nanoparticles across the decane boundary from the nanofluid, two different analytical models were consulted. Both based on Brownian motion. From Graham, 1981 [73] we have equation 3.25, where the new viscosity, or the change in viscosity, can be estimated based on the viscosity of pure decane. It is important to stress that this preliminary analysis does not account for possible synergetic effects between CO_2 and nanoparticles.

$$\frac{\mu_{eff}}{\mu_{bf}} = 1 + 2.5\phi + 4.5\left[\frac{1}{\left(\frac{\delta}{d_p}\right)\left(2+\frac{\delta}{d_p}\right)\left(1+\frac{\delta}{d_p}\right)^2}\right] \tag{3.25}$$

In equation 3.25, ϕ denotes volume fraction of nanoparticles in the bulk fluid, h is the distance between the particles, asuming homgeneous distribution, and d_p is the diameter of the particle. For the purpose of this analytical investigation, it is assumed that the concentration of nanoparticles in the decane and nanofluid are the same, which would yield a concentration gradient of zero. Volume fraction are calculated from the density and concentration of the nanoparticles, assuming no change in the decane volume if masstransfer happens. This is considered valid since the maximum viscosity change is investigated, and an increase in the decane volume would yield a lower nanoparticle volume fraction, which in turn would decrease the change in viscosity. This assumption would also render the calculation independent of the initial volume of the pendant drop. Silicon dioxide nanoparticle density are assumed to have a specific gravity close to silicon dioxide of $2.4g/l$ [74].

The distance between centre of particles are calculated from equation 3.26, assuming homogeneous distribution and considering a cubicle element containing one nanoparticle and the basefluid, which in this case is decane [75]. The nominal particle diameter of the nanofluid is reported to be 20 nm [4], which is used in these calculations

$$\delta = d_p\left(\frac{\pi}{6\phi}\right)^{1/3} \tag{3.26}$$

Graham, 1981 [73] points out that this model have a lot of assumptions and limitations, but that the results are generally satisfactory when hydrodynamic forces is the

TABLE 3.26: Constants for equation 3.29

Constant	Value
c_1	-0.000001133
c_2	-0.000002771
c_3	0.00000009
c_4	-0.000000393

governing effect. Using this model to calculate the new viscosity of decane containing 1 gram per liter nanoparticles transfered from DP9711 nanofluid, constitutes an effect of 1.73 %.

Masoumi *et al.*, 2009 [75], have developed a new model for estimating the effective viscosity. The model is also based on Brownian motion, but in addition accounts for temperature and, includes a correction factor for simplifications made. The effective viscosity is calculated from equation 3.27, where the subscripts *eff*, *bf* and *app* stands for *effective*, *bulk fluid* and *appearant*, respectively.

$$\mu_{eff} = \mu_{bf} + \mu_{app} \tag{3.27}$$

$$\mu_{app} = \frac{\rho_p V_B d_p^2}{72 C \delta} \tag{3.28}$$

where ρ_p is density of the nanoparticle, V_B is its volume, d_p is the particle diameter, δ is the distance between particles and C is the correction factor, calculated from equation 3.29

$$C = \mu_{bf}^{-1}\left[(c_1 d_p + c_2)\phi + (c_3 d_p + c_4)\right] \tag{3.29}$$

Using this model, the maximum viscosity change from a zero consentration gradient between the nanofluid and decane is 4.7 % at 25 °Cand 5.1 % at 45 °C.

3.6 pH of fluids

The pH of the fluids used have been measured with a Mettler Toledo™ S220 SevenCompact™ pH/Ion Benchtop Meter. This meter has an accuracy of ± 0.002 (pH). Table 3.27 shows the pH of the substances. To avoid increased acidity from air exposure, and CO_2 solved in the fluids, the DIW measurement were taken imidiatly after withdrawal from the water purifyer, the different consentrations of nanofluid were made by dilution of the same sample.

TABLE 3.27: pH of the fluids

Species	pH	
DIW	6.31	
NF 0.05 g/l	6.17	
NF 0.5 g/l	6.03	
NF 1 g/l	5.86	
NF 30 wt%	3.00	[4]

3.7 Possible Mass-Transfer of Nanofluid

It is of interest to investigate if mass-transfer of nanoparticles/nanofluid occurs over the NF/*n*-decane boundary. It has therefore been conducted two different sets of experiments, HPHT pendant drop diffusion, and absorbance experiments with UV-spectrophotometry. UV double-beam absorption experiments have been conducted with the aid of the UV-1700 PharmaSpec UV-Vis Spectrophotometer from Shimadzu. In these experiments, absorbance of a sample is measured relative to a reference sample. A beam of ultra-violet light ($\lambda = 240$ nm) is alternated between the reference and the sample, and the difference in light let through forms the basis of measurement. The full principle is explained below. The aim of the experiments is to generate an absorbance line for the concentration of nanofluid, expose the same nanofluid to decane, and conduct the absorbance experiments again. If mass-transfer of nanofluid/nanoparticles occurs, the absorbance will be less, and the new concentration and total amount transferred can be calculated by tracing back on the calibration line.

3.7.1 Principles of Spectrophotometry

This section is written based on information from the manufacturer of the spectrophotometer used [76].

- Transmittance (τ) is calculated by equation 3.30, where I_t and I_0 is measured by shooting light through both a reference sample containing the pure solvent, and then through the solution. I_t is the intensity of the light passing through the pure solvent, while I_0 is the intensity of light passing through the sample.

$$\tau = \frac{I_t}{I_0} \tag{3.30}$$

- Absorbance is calculated from the transmittance as in equation 3.31. Lambert-Beer law states that there exists a linear relationship between absorbance and the concentration of a solution, which founds the basis for the experiments where a calibration line is used.

$$ABS = Log_{10}\Big(\frac{1}{T}\Big) \tag{3.31}$$

3.7.2 Results of Absorbance Experiments

Two kind of experiments have been carried out, A and B.

A) A calibration line was generated by measuring the absorbance of 3 concentrations of nanofluid (0.5 g/l, 1 g/l and 4 g/l), relative to DIW. The same nanofluid was carefully placed in a container with n-decane resting on top of it for 2-3 weeks, without disturbing it. This was also done for pure DIW and n-decane. The absorbance of the solution did actually slightly increase, and not decrease as expected. This is believed to be due to small amounts of n-decane going into the NF. As a sample of pure DIW with n-decane had been prepared, the relative difference in absorbance between the pure DIW and DIW exposed to n-decane wa measured. This value was subtracted from the nanofluid experiments with the assumption that amount of n-decane going into the nanofluid is independent of the nanofluids concentration. This assumptions is partly justified by experiment B. Figure 3.19 shows the result of experiment A, where the black dots are points measured to generate the calibration line, which is market with a dotted line. By definition, pure DIW should have zero absorbance when DIW is used as reference, therefore this point is accounted for in the trendline. The red crosses shows the absorbance after the nanofluid has been exposed to n-fluid. It can be concluded that at atmospheric conditions, no significant mass-transfer of nanofluid/nanoparticles occur over the n-decane border.

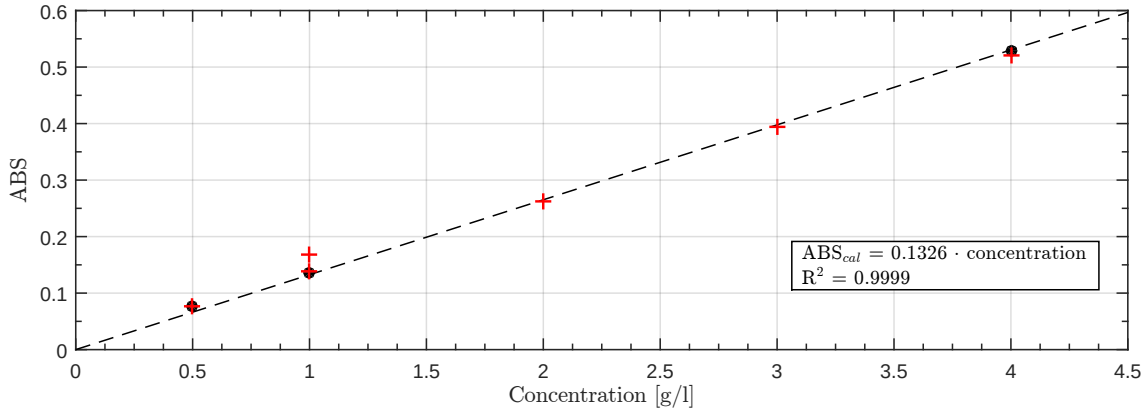

Figure 3.19: Concentration of nanofluid exposed to n-decane

B) In addition to doing the absorbance experiments with the n-decane exposed nanofluid relative to DIW, it was done relative to itself. I.e. the reference is the nanofluid *not* exposed to n-decane, and the sample is nanofluid exposed to n-decane. The aim of this experiment is to try to observe if a difference in mixing of n-decane is evident with the concentration of nanofluid, if so the absorbance should differ from concentration to concentration. This is done for 6 concentrations; 0 g/l (DIW), 0.5 g/l, 1 g/l, 2 g/l, 3 g/l and 4 g/l. Figure 3.21 shows the outcome, where a linear regressions between the point is added. It can be observed that the trend is almost horizontal, with a slight dip. It is believed that the dip is coincidental. If it is not coincidental, the decrease is so miniscule compared to the absolute absorbance that it would not make a significant difference for experimenent A. Figure 3.20 shows the same plot as 3.21, but with the y-axis adjusted to the same proportions as figure 3.19 from experiment A.

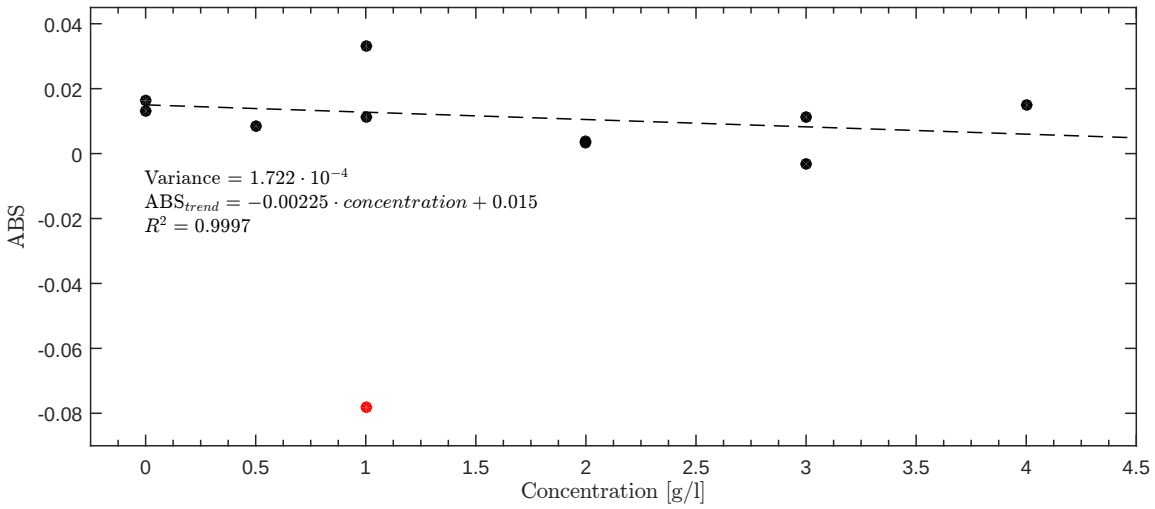

Figure 3.20: Concentration relative to itself

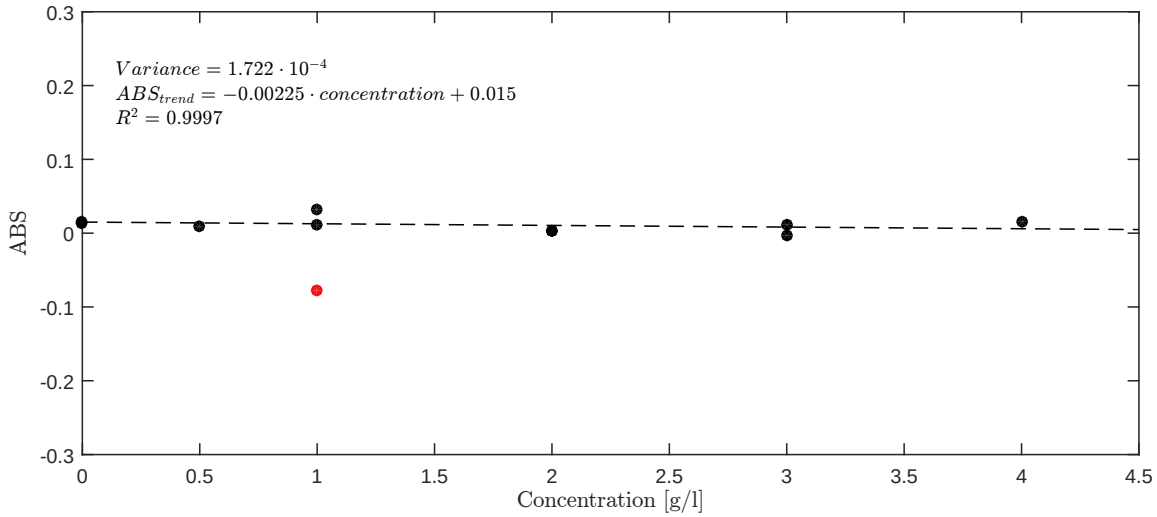

Figure 3.21: Concentration relative to itself at the same scale as experiment B

3.7.3 Pendant-Drop Diffusion Experiment without CO_2

To check for significant volume alterations as a result of mass-transfer of nanofluid/nanoparticles at higher pressures and temperatures, an isothermal pendant drop diffusion experiment with no CO_2 present was conducted in the equipment supplied by EUROTECHNIKA (Described in chapter 4.1), 1 g/l NF were introduced as the environment, and *n*-decane as the drop-phase . The experiment was carried out with a duration of 24 hours, where also pressure and temperature were recorded. The temperature was perfectly stable at 45°C, but the pressure experienced a decrease (Depicted in lower part of figure 3.22). The pressure was brought to approximately 80 bar, and the system was left. The drop shape and size were recorded. It is no pressure support in this set-up when CO_2 is not present, and the source of pressure decrease needs more investigation, but an hypothesis might be the compressibility of the fluids, and that the fluids take up slightly less space as it is exposed to high pressures for long a duration. However, it is observed a very slightly decrease of 2.13% in the volume over 24 hours. When CO_2 is present at the same conditions an increase of

more than 200% i observed. Additionally, if mass-transfer of nanofluid/nanoparticles occured, and was the only contribution to a change it volume, the volume should increase and not decrease. The decrease in n-decane volume is however consistant with the observations of n-decane entering the nanofluid in the spectrophotometry experiments.

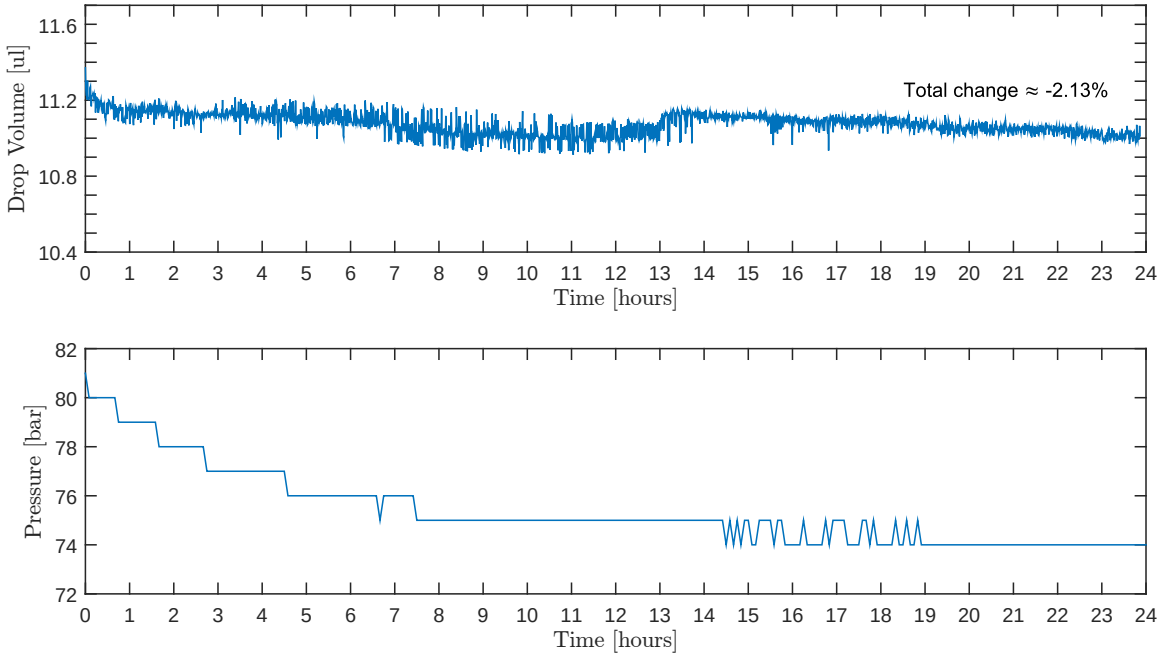

Figure 3.22: HPHT-Pendant-drop. Volume change with no CO_2 present

3.7.4 Concluding Remarks

- UV-spectrophotometry is conducted at atmospheric conditions, where it is not observed any evidence of mass-transfer of nanofluid/particles across the nanofluid/n-decane boundary.

- Long duration pendant-drop experiments have been carried out at high pressure and temperature where no significant volume change was observed, relative to what is obsrved in the presence of CO_2.

- Even though no significant volume alterations were observed in the HPHT-experiment, does it not eliminate the possibility of nanofluid entering without visibly altering the volume. It can however, be concluded that the nanofluid/-particles does not contribute significantly to the change in volume or density on its own.

- In cases where CO_2 is present, nanofluid/nanoparticles, if it enters the$n$-decane might alter other properties than volume, such as solubility of CO_2 in n-decane. however, in the case of CWI or pendant-drop diffusion experiments, the solubility of the nanofluid is the limiting factor. The synergy between nanofluid/-nanoparticles and CO_2 is important, and it is observed an effect relative to pure

CWI in the main diffusion experiments, which is discussed in the *Results and Discussion*.

- From the two types of experiments discussed in this seciton, absorbance at atmospheric conditions and HPHT-PD diffusion, it may be concluded that it is a low probability of nanofluid/nanoparticle transport across the NF/*n*-decane interface.

Chapter 4

Methodology

4.1 Experimental Method and Set-up for Diffusion Experiments

By exposing a drop of *n*-decane to carbonated water or carbonated nanofluid, mass-transfer of CO_2 will occure across the interface. This causes the volume of the drop to increase. The fundamental principal of these experiments is to record the change in volume and shape with time. The results of such an experiment, when the data is processed and analysed can reveal information on solubility behaviour, density, viscosity, interfacial tension and diffusion coefficient. The aim for this work is to use an experimental set-up like this to understand as much as possible of the diffusion process of CO_2 into *n*-decane from carbonated nanofluid, and to analyse the aformentioned properties. Similar work have previsously been concducted by Dr. Aly A. Hamouda and Nikhil Bagalkot for pure carbonated water, some of their results are made available to this study for comparison.

The outlining of the experimental method is to generate a pendant drop (drop phase) and surround it with carbonated nanofluid (environmental phase). This is done at various pressures and temperatures, as well as varying concentration of nanofluid in the environmental phase. Additionaly the experiments are also done at conditions where the nanofluid initially is not containing CO_2. In these cases, the nanofluid is exposed to CO_2 at the moment the experiment commences, CO_2 will in these types of experiments diffuse through the nanofluid, saturate it, while simultaneously diffusing into the *n*-decane drop. The two different cases of experiments will hereafter be called *saturated* experiments and *gradually saturated* experiments, and is explained furhter. Figure 4.1 serves as an illustration of how the experiment is recorded. In the figure, the same drop at the beginning and at the end of an experiment is depicted. In order to analyse the video recorded during the experiments, Krüss's software, DSA4, is utilised, which recognises the phases interface and contact angle, and are able to calculate both the volume and IFT at any particular timestep, as long as a distance-reference is given. The capillary tube is used as reference. In order for the software to calculate IFT, density and viscosity at that particular timestep is needed as input. As discussed in section 3.5, these values are obtained from the volume increase and calculated manually.

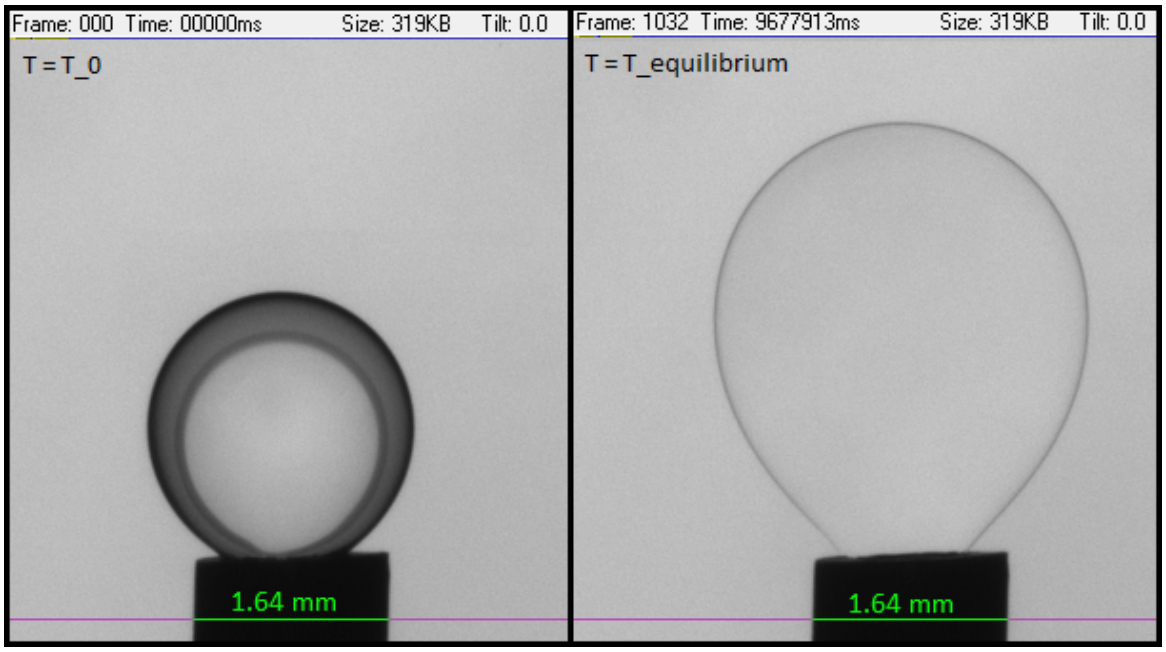

Figure 4.1: 60 bar, 25°C *saturated* experiment with *n*-decane drop surrounded by 0.5 g/l DIW-CNF. The left picture shows the drop when the first frame was recorded, while the right picture show the same drop when the volume change has reached equilibrium, i.e. the volume has stopped increasing.

4.1.1 Apparatus

The components of the apparatus consists of a high pressure corrosion free PVT cell, cylinders and pistons for introduction of the different phases into the cell, high resolution camera, light source, and a computer with analysis software (DSA4). The apparatus (PD-E170 LL-H) is deliver by EUROTECHNICA and KRUSS, with some on-site modifications for CO_2 supply. Figure 4.2 shows a schematic representation of the setup. A complete engineering flowchart may be found in Appendix A.

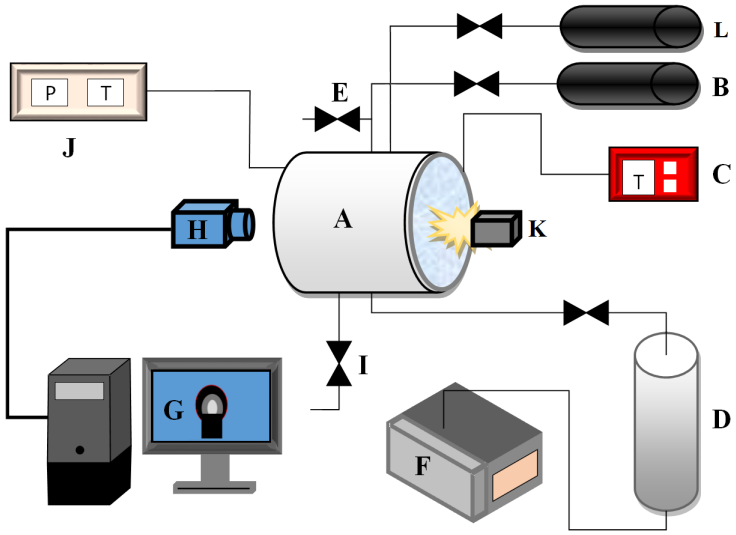

Figure 4.2: Schematic of the experimental setup

A	PVT Cell	G	Computer
B	Piston cylinder for drop generation	H	High resolution camera
C	Thermostat controller	I	Relief valve
D	CO_2 cylinder	J	Pressure and temperature indicator
E	Purge drop	K	Light source
F	Pump	L	Piston cylinder for water (nanofluid)

4.1.2 Procedure

For all experiments, the system will be properly cleaned based on which substances have been introduced to the system previously, the cleaning procedure can be found in section 4.1.3. CO_2 are introduced to the system from a cylinder (Fig. 4.2 D). At the beginning of any experiment, this cylinder is brought to the respective pressure, with aid of a pump (Fig. 4.2 F). This pump uses water as displacing fluid, and acts upon a piston inside the CO_2-cylinder. This cylinder do also have an adjacent twin which is used to supply the operating cylinder on occasions. The non-operating cylinder is filled to a maximum of 200 bar, which then is slowly decreased as the operating one needs refilling. When the prefered pressure in the operating cylinder is higher than the supply cylinder, their roles are switched, and the previous operating cylinder are pressurised with CO_2 to 200 bar. Before the refill, the cylinder is properly cleaned, and in that way, both cylinders gets cleaned on a cycle. The CO_2 is introduced to the PVT cell (Fig. 4.2 A) directly from the pressurised cylinder through a corrosion-free line.

Two piston cylinders (Fig. 4.2 B & L) exists inside the apparatus supplied by EUROTECHNICHA, one cylinder is used for introduction of drop phase, while the other is used for introduction of water or nanofluid, respectively. Both cylinders are manually operated and has a gauge. The exact order of operations of this pistons and cylinders depends on the particular experiment, and will be discussed seperately.

When a drop is generated, the high resolution camera (Fig. 4.2 H) captures the change in circumference, and calculates the change in volume based on a reference. This reference is set to be the diameter at the tip of the drop generating syringe, and are equal to 1.64 mm. The output from the analysis software is further used in the mathematical model discussed in section 4.2. The temperature of the cell are controlled by a thermostat (Fig. 4.2 C) and heating element.

A pendant oil drop are to be generated, and for this to be possible in an environment with higher density than the drop phase, the drop needs to be introduced from the bottom. In that case, the buoyancy (upward thrust) will work in favour of generating a pendant drop, and counteract gravity sufficiently. Before the drop is generated, nanofluid will be introduced to the PVT cell to occupy 80 - 90 % of the volume, CO_2 will then be introduced at preferred pressure from the top. For the CO_2 management, initially the cylinder containing CO_2 will be brought to the pressure which the respective experiment will be conducted at. This is done with the water pump building the pressure on the water side of the cylinder, when the pressure is reached, CO_2 will be introduced to the PVT cell. At this point, the proceedure differs among which environment is to be investigated. The two following paragraphs explain

the two different environments (*gradual saturation* and *saturated*), and how they are achieved.

Gradually Saturated - CO_2 into *n*-decane from unsaturated nanofluid Experiments which are carried out under these conditions are meant to represent a tertiary CO_2 gas injeciton in which a water/NF flood have been applied as secondary recovery method, or more specifically, CO_2 diffusing from free gas phase, through water/NF and into oil (in this case *n*-decane). Just after CO_2 have been introduced to the PVT cell, when the cell reach the desired pressure (It stabilises in the time-frame of seconds), an *n*-decane drop will be generated. CO_2 will then diffuse through, and into the water and make it carbonated, it will then diffuse into the *n*-decane. The volume change of the drop is then recorded and the system is left until equilibrium volume is reached. This means that the nanofluid CO_2 saturation will go from 0% saturated to $\approx$ 100% saturation (dissolution will take extremely long time near to fully saturated because of Le Chatelier's principle), i.e. two processes occur. Dissolution into the nanofluid under the applied pressure, and diffusions within the liquid phase (slow process, which gets slower and slower with time) and at the interface between the carbonated nanofluid and the drop. CO_2 diffuses into the water, then followed by diffusion into the drop. Hence, it will exist 3 concentration gradients (Illustrated in Fig. 4.3; 1) A horizontal 100% CO_2 *gradient* in the gas phase, 2) a dipping concentration gradient in the CO_2 + NF phase, which has it's highest point at the interface between nanofluid and free CO_2, because of IFT, the higest point will not be 100%. 3) A gradient in the oil phase, which has it higest point at the interface between itself and CO_2 + NF Practically. The free CO_2 will be in contact with the CO_2 source.

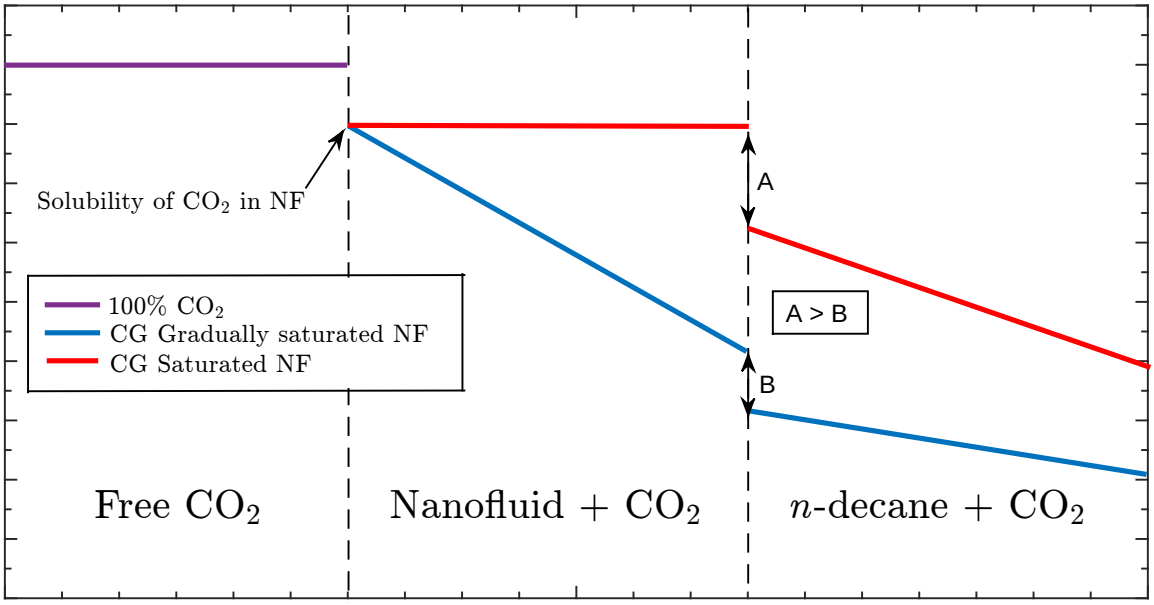

Figure 4.3: Illustration of consentration gradients at a particular time during *gradually saturated* and *saturated* nanofluid experiments

Saturated - CO_2 into *n*-decane from saturated nanofluid The procedure is identical to the the one in *variable saturation*, but the nanofluid will be saturated with CO_2 before the *n*-decane (*drop*) is introduced to the system. This is representation of the CWI, where the nanofluid is already saturated with CO_2 when it is injected and comes in contact with the oil. When the drop is introduced it will still exists three CO_2 concentration gradients, but two of them, namely free CO_2 and CO_2 + NF, will be horizontal and saturated. A concentration gradient will exist in the drop. The free CO_2 is still in contact with the CO_2 source, so any CO_2 taken from the environment by the oil will be replaced by the continous supply of CO_2. In order to ensure saturated nanofluid before the introduction of the drop-phase, the nanofluid is left exposed to CO_2 for a least 4 hours. In order to not waste those hours, the saturated experiments are done subsequently to the gradually saturation experiments, this is asusmed valid by the fact that it is $\approx$ 3500 times more nanofluid in the environment-phase than the volume of one released drop. Since the end-point of those experiments are after equilibrium, it can be fairly certain that the nanofluid is close to saturated with CO_2 before commencement of the *saturated* experiments. In this way the oil droplet from the previous experiment is just released from the capillary tube, and a new one is introduced, and the recording started.

Figure 4.4 shows an example of the behaviour of swelling with time for a *saturated* and *gradually saturated* environment.

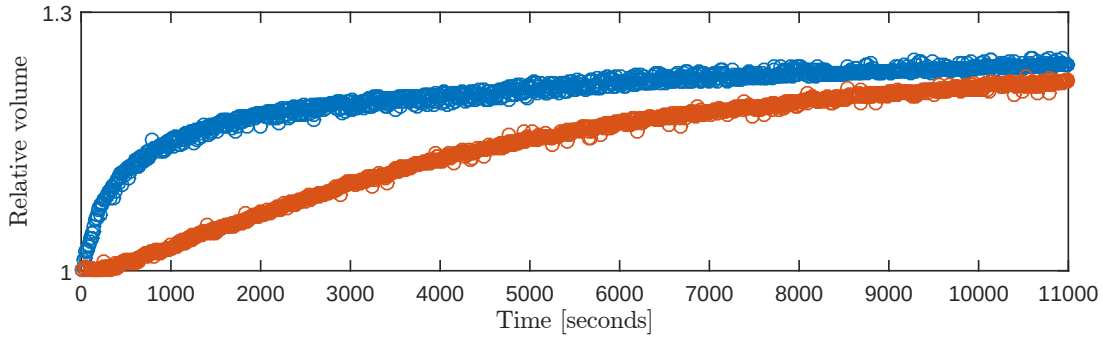

Figure 4.4: Example of behaviourn of swelling as a result of CO_2 diffusion in *gradually saturated* and *saturated* nanofluid experiments

Theoretically it will exist three phases in the system regardless of the experiment being a *gradual saturation* or *saturated* experiment. The reason for this is the pressure support from free CO_2 in both cases. In the *saturated* experiments, from the decane-drop's point of view it does only exist two phases, decane and CO_2-saturated nanofluid. This is because the drop is separeted from the supply gas, and the environment surrounding the drop is already saturated. The pressure support ensures the nanofluid to always be saturated, and the system to always be isobaric. A thermostat ensures the system is isothermal. Experiments are conducted at 25°C and 45°C. When preparing an experiment, it is not crucial to recognize the effects of temperature in the former, as the fluid is heated very quickly from room temperature to 25°C and expansion to the correct level occurs long before the experiment is physically possible to commence, but temperature effects needs to be acknowledged for the higher temperature. As the

nanofluid is introduced to the system as room temperature, it needs to be allowed to heat and expand, before the experiment is initiated. If this is not done properly it will be recognised in the pressure build-up. The pump and CO_2 will strive to keep the pressure at the wanted level, but cannot reduce it. This means that if preferred pressure is obtained before the fluid is properly heated, the fluid expansion will result in overshooting the pressure and be evident from the pressure indicator. However, the fluid is given enough time to expand before CO_2 is introduced to the system, and this is not a problem.

4.1.3 Cleaning

Proper cleaning of the equipment between experiments is important. Before any new experiment is initiated, the PVT cell is cleaned with acetone, after the acetone has evaporated, the cell is flushed with DIW and extensively dried with pressurised air. This is both to avoid diluting any introduced NF, but also to clear the system of as much dust as possible. The sapphire glasses, which is a part of the cell is taken out and cleaned with acetone, DIW and dried with pressurized air. If a new fluid is to be introduced to the system (e.g. a different concentration of nanofluid) the whole system is flushed with that fluid before any cleaning takes place, to ensure all lines contains the fluid for the next experiment. In the case of SSW introduced to the system, an additional pre-cleaning with water and tissue is included to dissolve preciptated salts and successfully eliminate them from the system.

4.1.4 Nanofluid

The nanofluid (DP9711) used are supplied from Nyacol® Nano Technologies, Inc. and are a colloidal silica surface modified fluid [4]. The spesific properties can be found in table 4.1. Nyacol® states that the fluid is stable over a wide pH range, but an arising concern was the potential interaction with dissolved CO_2 affect the stability of the fluid, either by a combination of pH decrease and molecular interaction, or one of them. Three preliminary experiments were conducted to dismiss or further investigate this concern.

TABLE 4.1: Nanofluid Properties, Nyacol Nano Technologies [4]

Silica, weight %	30
Nominal Particle Size, nm	20
pH @ 25°C	3
Viscosity @ 25°C, cP	5
Spesific Gravity	1.2

Test 1 A sample of 1 g/l DP9711 was prepared and the pH reduced to 3.38 by hydrochloric acid. The sample was kept at at 50°C for 24 hours and the transmisibility of the sample was compared to the transmissibility of a 1 g/l sample with no pH reduction or heating This was done in a Turbididy scanner. The test showed no significant difference, and the fluid was concluded to not be affected by the low pH.

This is assumed true for at least the timeframe of the main experiments, and also compares well with the statement of the manufacturer.

Test 2 A sample of 1 g/l DP9711 was prepared in cylinder, introduced to CO_2, pressurised to 35 bar and heated to 50°C. The sample was kept at these conditions for 2 hours. The transmissibility was measured and compared to pure 1 g/l nanofluid. A distinct reduction in transmissibility was confirmed. In order to investigate if the transmissibility reduction was due to unstable nanoparticles, a third test was conducted.

Test 3 The exact same procedure as for *test 2* was followed, but with pure DIW instead of DIW + nanofluid. The test showed simililar properties as the results from *test 2*.

The conclusion from the three tests is that the reduced transmissibiliy when CO_2 is added probably is due to dissolved CO_2 alone, and not interference and unstabilization of the nanoparticles, this is stated based on similarities of outcome woth and without nanoparticles. pH seems to have no affect on the particle's stability. The conclusion justifies further use of the spesific nanofluid in the main experiments. Table 4.2 shows the results of the three tests.

TABLE 4.2: Preliminary Test Results

Solution	pH	Transmissibility
DIW		90 %
DIW+DP		87 %
DIW+DP+HCl	3.38	87 %
DIW+CO_2		75 %
DIW+CO_2+DP		77 %

Preparation Procedure of Nanofluid 0.05, 05 and 1 g/l DIW-NF and 1 g/l SSW-NF is used in this work. These fluids were prepared by using the 30 wt% DP9711 silica based nanofluid provided from Nyacol Nano Technologies.

Equipment

- Beaker
- Volumetric flasks
- Scale (Metler^{TM} Toledo NewClassic MF MS1046 /01)
- Syringe
- Magnetic stirrer (VWR^{TM} VMS-C7)
- Glass bottles

Chemicals

- High concentrated nanofluid (30wt% DP9711 Nyacol^{TM} Nano Technologies)
- Water (Distilled + de-ionised, hereby referred to as DIW)
- Synthetic Sea Water (SSW)

Cleaning Process

- All flasks, beakers and containers were pre-washed with a dishwasher
- Flushed with DIW
- Dried in oven at 50°C
- Cooled to room temperature before use

1 g/l DIW-NF were prepared by measuring 3.2786 g of 30wt% NF in a small *beaker*, this fluid was then transferred to a 1000 ml *volumetric flask*, by filling the *beaker* with *DIW*, and then perform the transferring. The process of filling the *beaker* with *DIW* and then transfer was repeated several times to ensure all the NF was transferred. When confidence in the former was established, *DIW* was poured directly into the *volumetric flask* until the liquid level was just below the volume mark. A *syringe* with *DIW* was then used to rise the liquid level exactly to 1000 ml. A *magnetic stirrer* was applied to make a homogeneous mixture. The *nanofluid* was then transferred and capped in a laboratory *glass-bottle*.

0.5 g/l DIW-NF was prepared by using two *volumetric flasks* (500 ml and 1000 ml), The 500 ml was used to measure 1 g/l DIW-NF, which then was poured into the 1000 ml flask, *DIW* was then used to collect all rests of NF in the first flask and transfer to the latter. DIW was eventually used to fill the 1000 ml flask by the same principal as described for *1 g/l DIW-NF*.

0.05 g/l DIW-NF was prepared in a similar way as *0.5 g/l DIW-NF*, but with the use of a 100 ml *volumetric flask* filled with 0.5 g/l DIW-NF, rather than 500 ml filled with 1 g/l DIW-NF.

1 g/l SSW-NF was prepared similarly as for *1 g/l DIW-NF*, but with the use of *SSW* instead of *DIW*.

4.1.5 Data Processing

In the diffusion experiments a frame is recorded every tenth second. The record is then run through DSA4 from Krüss, which is an abbreviation for *Drop Shape Analyser*. The shape and profile of the drop is recognised, and since the drop is axisymetrix, the volume is calculated by information of the profile, baseline, and a reference for distance. Absolute volume with time is output from the software. Plotting these values shows a clear trend, but a bit of scattering occurs, this is due to the software recognising, seemingly randomly, the boarder slightly different from frame to frame.

With the light source opposing the camera, the greater the transmissibility difference between environment and drop-phase, the easier it is to recognise the profile. Because of this, the data tends to be a bit more scatter at later times because more CO_2 have diffused into the drop, and the drop is more transparrent. This can be observed in Figure 4.5, which is the same image as Fig. 4.1

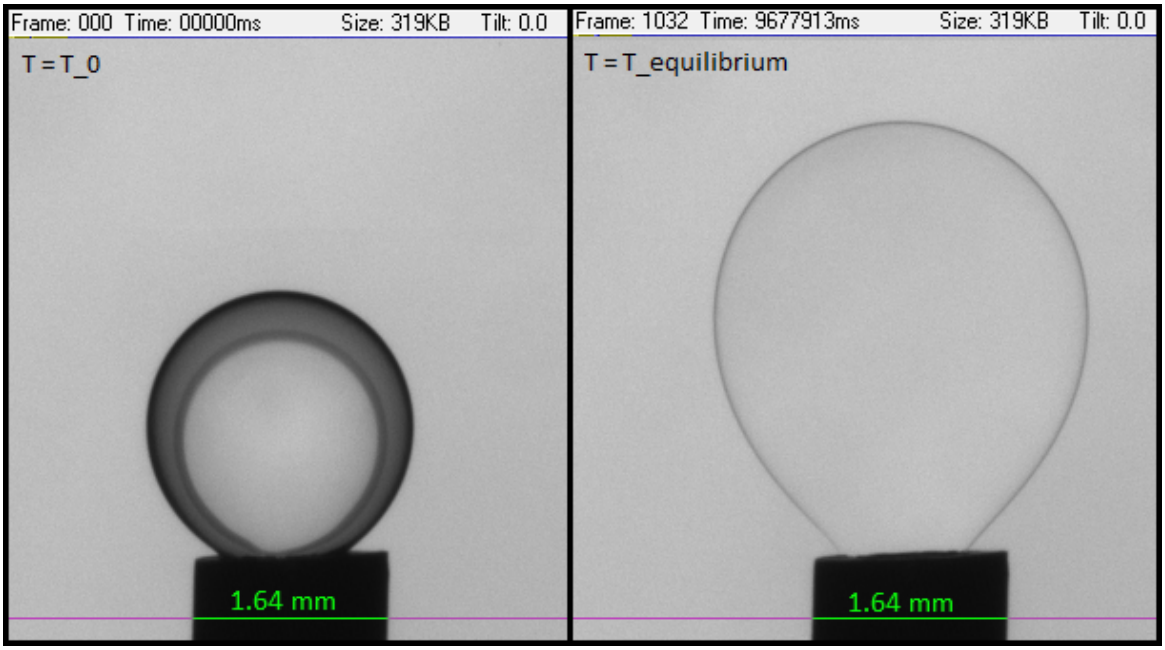

Figure 4.5: 60 bar, 25°C *saturated* experiment with *n*-decane drop surrounded by 0.5 g/l DIW-CNF. The left picture shows the drop when the first frame was recorded, while the right picture show the same drop when the volume change has reached equilibrium, i.e. the volume has stopped increasing.

For better representation of the data, but more importantly, to use this volume change data in the mathematical mass-transfer model for diffusion coefficient calculation, a value for every 5th minute needed to be extracted. This was done with a MATLAB script. In the work with this thesis, enormous amounts of data have been gathered, and an efficient MATLAB script needed to be generated. Approximately $0.43 \cdot 10^6$ data-pairs needed to be processed, this includes IFT calcualtion, which also need manual viscosity and density input for every individual case (177 cases). With this amount of data, the method for most efficiently and simultaneously accuratly process the data were well thought through. Initially it was made a complete script that processed all the data automatically, ready for use within 1 minute of computing time. Unfortunetly, this needed polynomial fitting with too high exponent and also resulted in minimal opportunity for quality checking. Instead, a semi-automatic script were made that made it easy to select which data to process, and then automatically plot this data waiting for user input. The user input is which points that shall represent every 5th minute for volume-data, and every 10th minute for IFT data. This was hand-selected with the aid of a grid, and the data points used in further analysis are actual values and not fitted or interpolated ones. The help of fitting curves were occationally used in cases with a lot of scattering, but real points were selected. It was also obvious that human interpretation was unavoidable, as fitting curves were

```
clear
clc
sheet = 1; %Which sheet in current excel file to read
position = 'm:n'; %Which columns to read

data = xlsread('data.xlsx',sheet,position);
a = data(:,1)./60;
b = data(:,2);
data = [a,b];

scatter(data(:,1),data(:,2))
drawnow
hold on
```

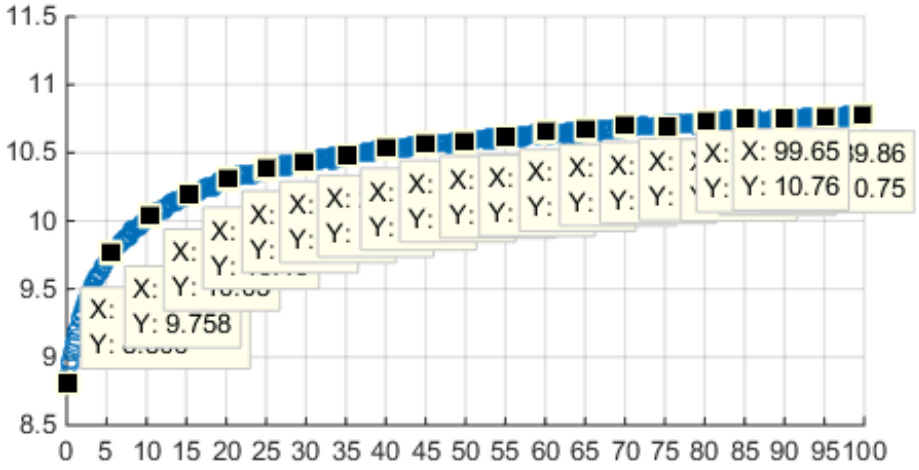


```
for i = 1:length(cursor_info)


c(i,:) = cursor_info(i).Position;


end

c = flipud(c);
c = c(:,2)
```

Published with MATLAB® R2014b

Figure 4.6: Data processing on 70 bar, 25°C, *saturated* SSW-CNF, snippet at 100 min for representation purposes

rarely sufiecient. This work constituted in approximatly 7 000 accuratly hand-selected data-pairs, with a roughly estimated work-time of 40-60 hours. Figure 4.6 shows a picture of the 3-step script.

Figure 4.7 shows the finished processed data of the experiment conducted at 25°C

for 0.05 g/l DIW-CNF as environment. The experiment is conducted at *gradually saturated* conditions, which generally had a moderate degree of scattering.

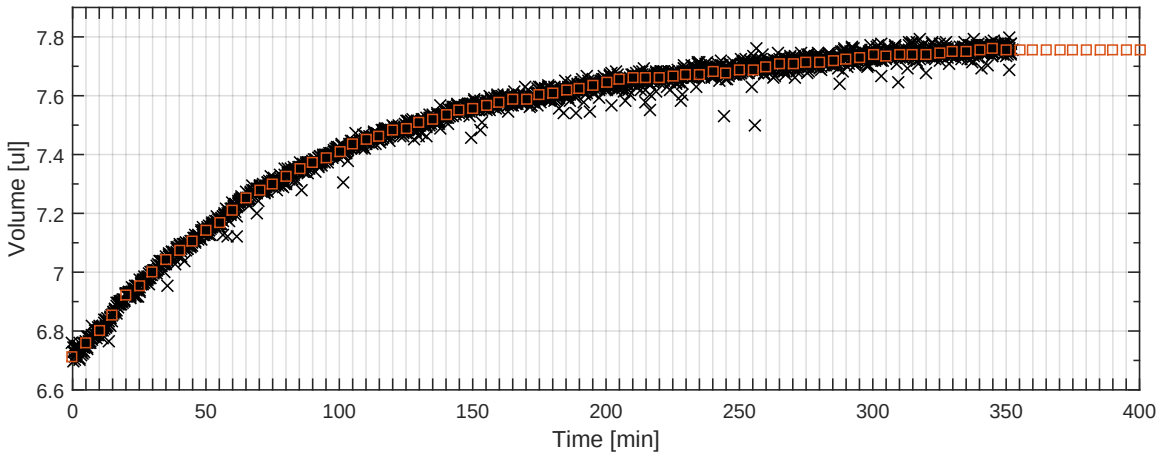

Figure 4.7: Processed volume data of *n*-decane volume at 25°C *gradually saturated*, 0.05 g/l DIW-CNF

Since IFT data were not going to be used as input for any model, the time interval at which data were selcted for representation could be increased, most of the analysis is concerned around equilibrium IFT, but behaviour with time is of course also important and discussed. Increasing the time interval from 5 to 10 minutes for IFT reduced the total number of hand-selected data-pairs with 25%, and saved approximatly 10 hours of work. Figure 4.8 and 4.9 shows two examples of IFT processing, where one shows a case with scattering and one shows a perfect example. The behaviour of these graphs are not to be discussed in this chapter.

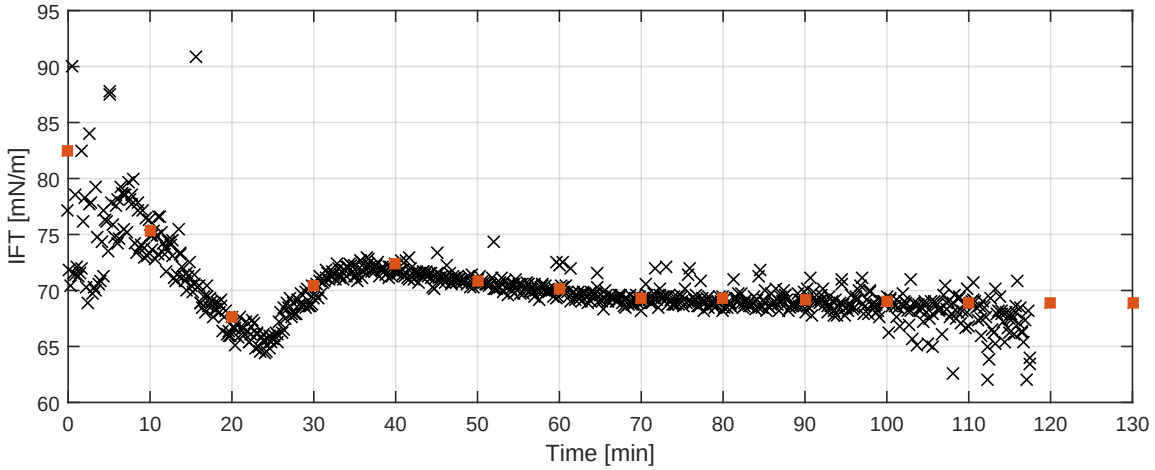

Figure 4.8: Processed IFT data of *n*-decane volume at 25°C *saturated*, 0.5 g/l DIW-CNF at 60 bar

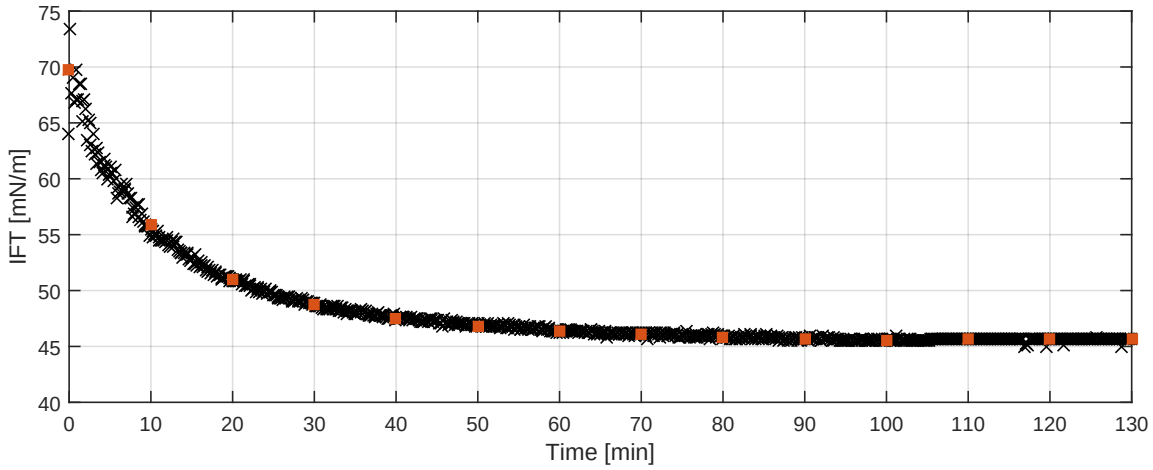

Figure 4.9: Processed IFT data of *n*-decane volume at 25°C *saturated*, 0.5 g/l DIW-CNF at 30 bar

4.1.6 Repetability and Error Analysis

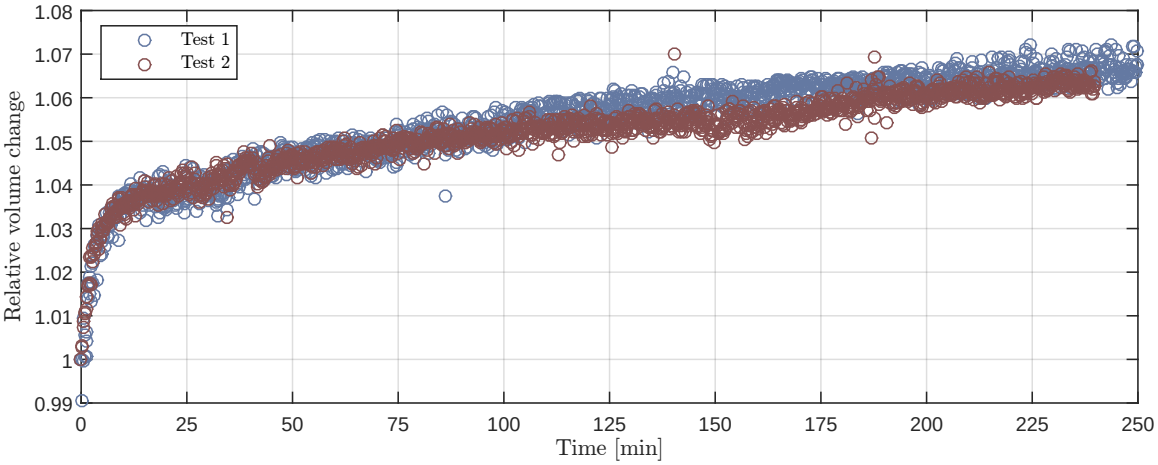

Figure 4.10: Repetability test: The same experiment carried out twice for the same constant pressure and temperature.

Figure 4.10 shows the same experiment carried out twice, the results are in good agreement with each other, and the repetability can be said to be good. All the recorded volumes for every tenth second up until 250 minutes is plotted against time.

To get a better understanding of the uncertainty of the scattering, a method for calcualting pseudo standard deviation was carried out. Since no point in time is recorded twice, there exists no proper standard deviation, but with the assumption that all frames (i.e. 6 frames) recorded within a minute is, for all intents and purposes, the same point in time (exception at the commencement of the experiment), some analysis might be done. If it is pretended that 6 adjecent frames are in fact the same point, the standard deviation for that point can be calculated. This is not an unreasonable assumption, in the sense that if deviations occur due to real physics during that time-period, it increases the precieved innacuracy, which means the error is over-estimated. Performing this analysis is elaborate work and it was therefore

decided to do the analysis on two full pressure-sets, and not 14. The two first experimental sets were chosen based on two reasons; 1) The pair contains 1 *saturated* and 1 *gradually saturated* set of experiments. 2) As they were the two first experimental sets carried out, it is asusmed that the greates uncertainty lies among these experiments.

The average percentage pseudo standard deviation from the mean of volume change with time was therefore calculated from equation 4.1

$$\frac{100\%}{n-5}\left[\sum_{1}^{n-5}\sqrt{\frac{1}{6}\sum_{m=k}^{k+5}(\bar{v}-v_i)^2}\Bigg|_{k=1}^{n-5}-1\right], \tag{4.1}$$

where n is the total number of data-points and k works as a counter for moving 1 frame at a time and calculate the standard deviation of 6 adjecent frames (1 minute). The results is found in table 4.3. As it may be seen, the error is quite small, and in further analysis it will be rounded up to be within 1%

TABLE 4.3: Average percentage pseudo standard deviation from the mean of volume change with time for 1 g/l DIW-CNF

P [bar]	10	20	30	40	50	60	70
SD *sat.*	0.1775	0.2995	0.3273	0.1477	0.6672	0.9571	0.9259
SD *g. sat.*	0.2652	0.2964	0.2141	0.2232	0.6159	0.7755	0.4519

4.1.7 Overview of Experiments

It has been carried out experiments for *n*-decane in DIW-based nanofluid, both *saturated* (x2) and *gradually saturated*, for 25°C and 45°C, for all three concentrations (0.05, 0.5 and 1 g/l). This is done for pressures from 10 to 90 bar, with the exception of 1 g/l DIW-NF, which is only from 10-70 bar. The pressure increment is 10 bar. For SSW-NF it has been carried out for both 2- and *gradually saturated* at 45°C, for 1 g/l NF concentration. The pressures in the SSW- experiments is 10, 30, 50, 70 and 90 bar. This results in 177 individual experiments ranging from 3 to 6 hours in duration. With the most modest estimation, this constitutes a total run-time of 531 hours, the true value is probably closer to 800 hours. Table 4.5 shows an overview of every diffusion experiment conducted. The experiments that is carried out twice is mentioned 2 times.

TABLE 4.4: Overview of all conducted diffusion experiments. The ones that do say SSW is SSW-based NF, the ones that do not say SSW is implied to be DIW-based nanofluid (10 - 50 bar)

P = 10 bar	P = 20 bar	P = 30 bar	P = 40 bar	P = 50 bar
2-p. 25°C 0.05 g/l	2-p. 25°C 0.05 g/l	2-p. 25°C 0.05 g/l	2-p. 25°C 0.05 g/l	2-p. 25°C 0.05 g/l
2-p. 25°C 0.5 g/l	2-p. 25°C 0.5 g/l	2-p. 25°C 0.5 g/l	2-p. 25°C 0.5 g/l	2-p. 25°C 0.5 g/l
2-p. 25°C 1 g/l	2-p. 25°C 1 g/l	2-p. 25°C 1 g/l	2-p. 25°C 1 g/l	2-p. 25°C 1 g/l
2-p. 45°C 0.05 g/l	2-p. 45°C 0.05 g/l	2-p. 45°C 0.05 g/l	2-p. 45°C 0.05 g/l	2-p. 45°C 0.05 g/l
2-p. 45°C 0.5 g/l	2-p. 45°C 0.5 g/l	2-p. 45°C 0.5 g/l	2-p. 45°C 0.5 g/l	2-p. 45°C 0.5 g/l
2-p. 45°C 1 g/l	2-p. 45°C 1 g/l	2-p. 45°C 1 g/l	2-p. 45°C 1 g/l	2-p. 45°C 1 g/l
2-p. 25°C 0.05 g/l	2-p. 25°C 0.05 g/l	2-p. 25°C 0.05 g/l	2-p. 25°C 0.05 g/l	2-p. 25°C 0.05 g/l
2-p. 25°C 0.5 g/l	2-p. 25°C 0.5 g/l	2-p. 25°C 0.5 g/l	2-p. 25°C 0.5 g/l	2-p. 25°C 0.5 g/l
2-p. 25°C 1 g/l	2-p. 25°C 1 g/l	2-p. 25°C 1 g/l	2-p. 25°C 1 g/l	2-p. 25°C 1 g/l
2-p. 45°C 0.05 g/l	2-p. 45°C 0.05 g/l	2-p. 45°C 0.05 g/l	2-p. 45°C 0.05 g/l	2-p. 45°C 0.05 g/l
2-p. 45°C 0.5 g/l	2-p. 45°C 0.5 g/l	2-p. 45°C 0.5 g/l	2-p. 45°C 0.5 g/l	2-p. 45°C 0.5 g/l
2-p. 45°C 1 g/l	2-p. 45°C 1 g/l	2-p. 45°C 1 g/l	2-p. 45°C 1 g/l	2-p. 45°C 1 g/l
3-p. 25°C 0.05 g/l	3-p. 25°C 0.05 g/l	3-p. 25°C 0.05 g/l	3-p. 25°C 0.05 g/l	3-p. 25°C 0.05 g/l
3-p. 25°C 0.5 g/l	3-p. 25°C 0.5 g/l	3-p. 25°C 0.5 g/l	3-p. 25°C 0.5 g/l	3-p. 25°C 0.5 g/l
3-p. 25°C 1 g/l	3-p. 25°C 1 g/l	3-p. 25°C 1 g/l	3-p. 25°C 1 g/l	3-p. 25°C 1 g/l
3-p. 45°C 0.05 g/l	3-p. 45°C 0.05 g/l	3-p. 45°C 0.05 g/l	3-p. 45°C 0.05 g/l	3-p. 45°C 0.05 g/l
3-p. 45°C 0.5 g/l	3-p. 45°C 0.5 g/l	3-p. 45°C 0.5 g/l	3-p. 45°C 0.5 g/l	3-p. 45°C 0.5 g/l
3-p. 45°C 1 g/l	3-p. 45°C 1 g/l	3-p. 45°C 1 g/l	3-p. 45°C 1 g/l	3-p. 45°C 1 g/l
2-p. 45°C 1 g/l SSW	-	2-p. 45°C 1 g/l SSW	-	2-p. 45°C 1 g/l SSW
2-p. 45°C 1 g/l SSW	-	2-p. 45°C 1 g/l SSW	-	2-p. 45°C 1 g/l SSW
3-p. 45°C 1 g/l SSW	-	3-p. 45°C 1 g/l SSW	-	3-p. 45°C 1 g/l SSW

TABLE 4.5: Overview of all conducted diffusion experiments. The ones that do say SSW is SSW-based NF, the ones that do not say SSW is implied to be DIW-based nanofluid (60 - 90 bar)

P = 60 bar	P = 70 bar	P = 80 bar	P = 90 bar
2-p. 25°C 0.05 g/l	2-p. 25°C 0.05 g/l	2-p. 25°C 0.05 g/l	2-p. 25°C 0.05 g/l
2-p. 25°C 0.5 g/l	2-p. 25°C 0.5 g/l	2-p. 25°C 0.5 g/l	2-p. 25°C 0.5 g/l
2-p. 25°C 1 g/l	2-p. 25°C 1 g/l	-	-
2-p. 45°C 0.05 g/l	2-p. 45°C 0.05 g/l	2-p. 45°C 0.05 g/l	2-p. 45°C 0.05 g/l
2-p. 45°C 0.5 g/l	2-p. 45°C 0.5 g/l	2-p. 45°C 0.5 g/l	2-p. 45°C 0.5 g/l
2-p. 45°C 1 g/l	2-p. 45°C 1 g/l	2-p. 45°C 1 g/l	2-p. 45°C 1 g/l
2-p. 25°C 0.05 g/l	2-p. 25°C 0.05 g/l	2-p. 25°C 0.05 g/l	2-p. 25°C 0.05 g/l
2-p. 25°C 0.5 g/l	2-p. 25°C 0.5 g/l	2-p. 25°C 0.5 g/l	2-p. 25°C 0.5 g/l
2-p. 25°C 1 g/l	2-p. 25°C 1 g/l	-	-
2-p. 45°C 0.05 g/l	2-p. 45°C 0.05 g/l	2-p. 45°C 0.05 g/l	2-p. 45°C 0.05 g/l
2-p. 45°C 0.5 g/l	2-p. 45°C 0.5 g/l	2-p. 45°C 0.5 g/l	2-p. 45°C 0.5 g/l
2-p. 45°C 1 g/l	2-p. 45°C 1 g/l	2-p. 45°C 1 g/l	2-p. 45°C 1 g/l
3-p. 25°C 0.05 g/l	3-p. 25°C 0.05 g/l	3-p. 25°C 0.05 g/l	3-p. 25°C 0.05 g/l
3-p. 25°C 0.5 g/l	3-p. 25°C 0.5 g/l	3-p. 25°C 0.5 g/l	3-p. 25°C 0.5 g/l
3-p. 25°C 1 g/l	3-p. 25°C 1 g/l	-	-
3-p. 45°C 0.05 g/l	3-p. 45°C 0.05 g/l	3-p. 45°C 0.05 g/l	3-p. 45°C 0.05 g/l
3-p. 45°C 0.5 g/l	3-p. 45°C 0.5 g/l	3-p. 45°C 0.5 g/l	3-p. 45°C 0.5 g/l
3-p. 45°C 1 g/l	3-p. 45°C 1 g/l	3-p. 45°C 1 g/l	3-p. 45°C 1 g/l
-	2-p. 45°C 1 g/l SSW	-	2-p. 45°C 1 g/l SSW
-	2-p. 45°C 1 g/l SSW	-	2-p. 45°C 1 g/l SSW
-	3-p. 45°C 1 g/l SSW	-	3-p. 45°C 1 g/l SSW

4.1.8 Method and Procedure for Property Analysis

Figure 4.11 shows a flowchart describing the interconnections between supportive experiments, main experiment, processing, and the mathematical mass-transfer model. It can be seen that the diffusion coefficients and swelling factors are obtained from the mathematical mass-transfer model, which takes data from the processed primary experimental result. The interfacial tension is calculated with the aid of the processed primary experimental results directly, but do also need a combination of auxiliary experiments and models, in addition to derived quantities from the primary experi-

ments. The mathematical mass-transfer model is described in chapter 4.2, while the data processing is described in chapter 4.1.5. Auxiliary experiments and models have been thoroughly described in chapter 3 - *Fundamental Properties of the Nanofluid and Hydrocarbon*. The properties is discussed in the chapter 5 - *Results and Discussion*

Dynamic and *equilibrium* are two terms which are used a lot in the analysis of the results. *Dynamic* refers to a property that changes with time until a potential equilibrium is reached, and is used in contexts were the analysis focuses on the time dependency. After a certain time-period, when a dynamic property has reached equilibrium, it is refered to as e.g. *Equilbrium IFT* or *Equilibrium Volume*, where the former means the interfacial tension at a time where it is no more change in interfacial tension, and the latter the volume in which there is no more increase as result of no more mass-transfer of CO_2. In order to compare volume change among different temperatures and pressure, the necessity of relative values are evident, i.e. the volume change normalised to its initial volume before CO_2 were introduced. For convenience, the phrase "*equilibrium volume*" is used for relative equilibrium volume increase, and the phrase "*absolute equilibrium volume* is used for the absolute equilibrium volume increase. The phrase *relative volume increase* is used for the relative dynamic increase with time.

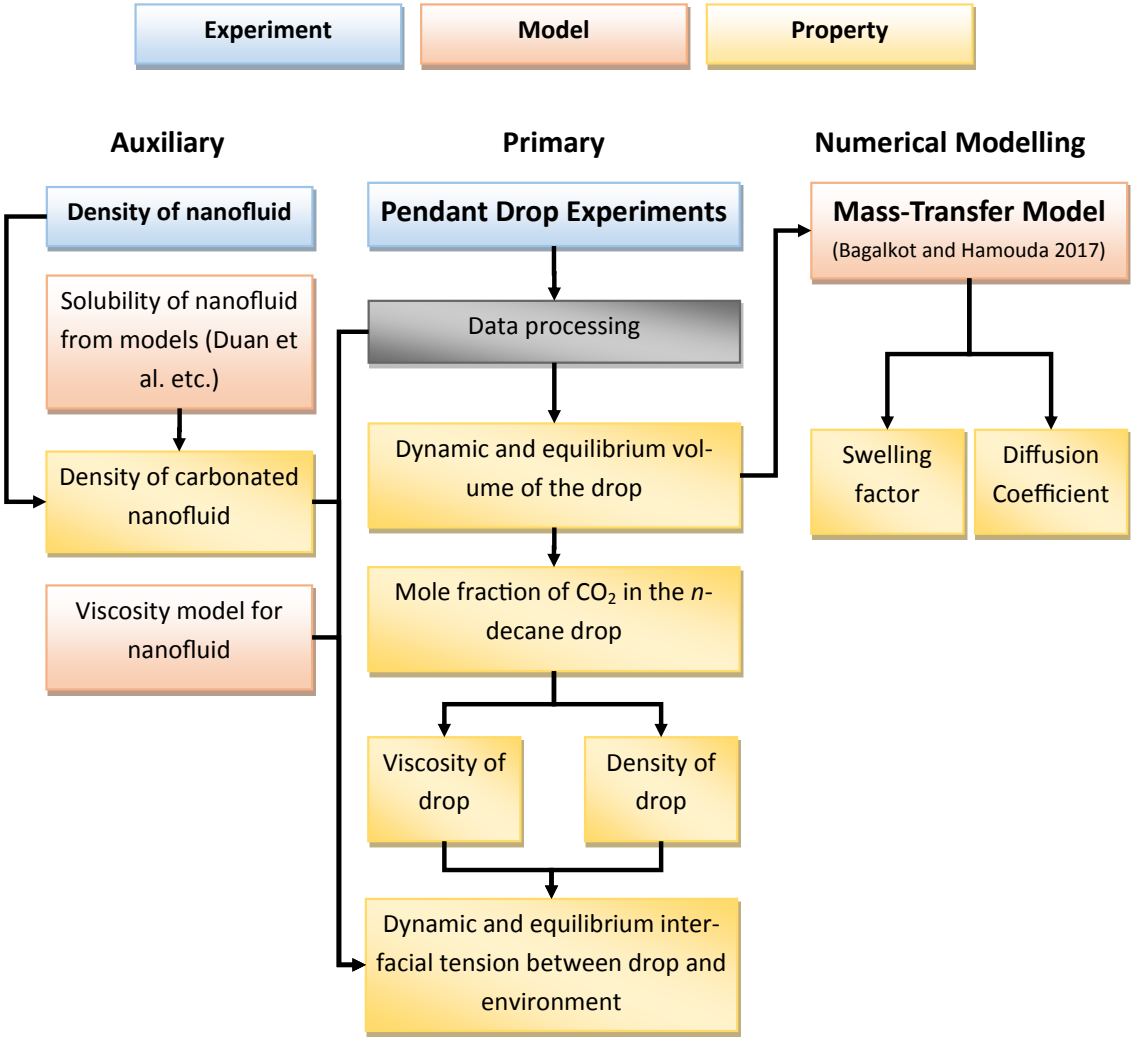

Figure 4.11: Flowchart showing the pathway of the auxiliary analysis, primary experiment and analysis together with numerical modelling and their interconnections

4.2 Mathematical Mass-Transfer Model

Bagalkot and Hamouda [43] have developed a method for experimentally finding and calculating the diffusion coefficient of CO_2 into a pendant drop. The method is an adaption of Yang and Gu's [77] method, with a simpler numerical solution. Both approaches is based on Fick's second law of diffusion, which is discussed in the theory section.

A set of equations are solved numerically with respect to the physical experiment. The equations are presented below. The diffusion process of CO_2 from the interface to the centre of the pendant drop is described by equation 2.3, which is Fick's second law of diffusion. Diffusion, and this equation have been discussed in the theory section.

The experiments and this model bases its calculations on an axisymmetric pendant drop, justifying the conversion of equation 2.3 from a tree-dimensional mass transfer problem in Cartesian coordinates, to a two-dimensional diffusion problem in cylindrical coordinates [43, 77]. Fick's second law of diffusion takes the form of equation 4.2 in cylindrical coordinates.

$$\frac{\partial C}{\partial t} = D\left[\frac{1}{r}\frac{\partial C}{\partial r} + \frac{\partial^2 C}{\partial r^2} + \frac{\partial^2 C}{\partial z^2}\right] \tag{4.2}$$

Where C is the concentration of CO_2 and D is the diffusion coefficient.

The average concentration indicates the amount of CO_2 diffused into the drop, and are calculated as a volumetric average by equation 4.3

$$C_{avg}(t) = \iint\limits_{(r,z)\in p_d} \frac{C(r,z)}{C_o} r dr dz \tag{4.3}$$

This concentration average is used in combination with experimentally found droplet volume increase to determine the swelling factor, as stated in equation 4.4, and then in combination with the swelling factor to find analytical volume stated in equation 4.5.

$$SF = 1 + \frac{\int_0^T \frac{[V_{exp}(t)-V_0]\cdot C_{avg}(t)}{V_{exp}^2} dt}{\int_0^T \frac{[C_{avg}^2(t)]}{V_{exp}^2} dt} \tag{4.4}$$

$$V(t) = V_0 + (SF-1)\cdot C_{avg}(t) \tag{4.5}$$

The best solution to this set of equations are obtained when the objective function, equation 4.6, is at its minimum. Equation 1 is the main equation that needs to

be solved and ultimately consists of two unknown variables. The concentration are therefore solved for, while varying the diffusion coefficient to look for the best fit.

$$E = \sqrt{\frac{1}{T}\int_0^T \frac{[V_{exp}(t) - V(t)]^2 dt}{V_{exp}^2(t)}} \cdot 100\% \tag{4.6}$$

Descretisation of the Diffusion Equation Fick's second law of diffusion is discretised by a combination of methods. The two second-order terms are discretised by the Crank-Nicholson Finite Difference method, while the temporal and the first order term is discretised by a two-point backward differencing method. This gives the four following expressions.

$$C_t = \frac{C_{i,j}^{n+1} - c_{i,j}^{n}}{\Delta t} \tag{4.7}$$

$$C_r = \frac{C_{i-1,j}^{n+1} - C_{i,j}^{n+1}}{\Delta r} \tag{4.8}$$

$$C_{rr} = \frac{1}{2}\frac{D}{\Delta r^2}\Big[\big(C_{i+1,j}^{n+1} - 2C_{i,j}^{n+1} + C_{i-1,j}^{n+1}\big) + \big(C_{i+1,j}^{n} - 2C_{i,j}^{n} + C_{i-1,j}^{n}\big)\Big] \tag{4.9}$$

$$C_{zz} = \frac{1}{2}\frac{D}{\Delta z^2}\Big[\big(C_{i,j+1}^{n+1} - 2C_{i,j}^{n+1} + C_{i,j-1}^{n+1}\big) + \big(C_{i,j+1}^{n} - 2C_{i,j}^{n} + C_{i,j-1}^{n}\big)\Big] \tag{4.10}$$

Letting $\frac{D}{2}\frac{\Delta t}{\Delta r^2} = \alpha$ and $\frac{D}{2}\frac{\Delta t}{\Delta z^2} = \beta$, transforms equation 4.2 into equation 4.11

$$C_{i,j}^{n+1} - C_{i,j}^{n} = \alpha \cdot A + \beta \cdot B \tag{4.11}$$

where

$$A = \big[\tfrac{2\Delta r}{r_i}(C_{i-1,j} + C_{i,j})^{n+1} + (C_{i+1,j} - 2C_{i,j} + c_{i-1,j})^{n+1} + (C_{i+1,j} - 2C_{i,j} + c_{i-1,j})^{n}\big]$$

and
$B = \big[(C_{i,j+1} - 2C_{i,j} + C_{i,j-1})^{n+1} + (C_{i,j+1} - 2C_{i,j} + C_{i,j-1})^{n}\big]$.

Note that n marks a point in time and are not an exponent.

Alternate Direction Implicit (ADI) is a method of solving what would have, in this case, been a multi-diagonal matrix. The ADI scheme was proposed in 1955 by Peaceman and Rachford, and instead of solving for the n+1 time step, one step are subdivided into two half steps and solved implicit in one dimension and explicit in the other. Which dimension that are solved implicit and explicit alternates for every half time step. The result are two tridiagonal matrices instead of one pentadiagonal. The method is unconditional stable and offers a relatively low computing cost [78].

The calculation-script is written and provided by Bagalkot and Hamouda, where five minute intervals are needed. The processing of raw data to achieve this is discussed in chapter 4.1.5.

4.3 Complete List of Chemicals

This list serves as an overview of all substances used during theis work, with key information and area of use.

4.3.1 Acetone

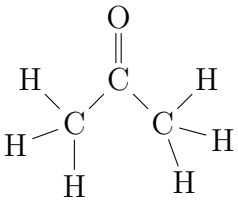

Molecular formula: C_3H_6O

Supplier: VWR International AS
Used for: Cleaning

H- and P-sentences:
H225: Highly flammable liquid and vapour H319: Causes serious eye irritation H336: May cause drowsiness or dizziness EUH066: Repeated exposure may cause skin dryness or cracking

P210: Keep away from heat, hot surfaces, sparks, open flames and other ignition sources. No smoking. P280: Wear protective gloves/protective clothing/eye protection/face protection. P305+P351+P338: IF IN EYES: Rinse cautiously with water for several minutes. Remove contact lenses if present and easy to do. Continue rinsing.

4.3.2 Carbon Dioxide

O=C=O

Molecular formula: CO_2

Used for: Diffusion experiments

H- and P-sentences:
H280: Contains gas under pressure; may explode if heated.
P403: Store in a well ventilated place.

4.3.3 Nanofluid

Nanoparticle: O=Si=O
Basefluid: Water

Molecular formula: SiO_2
Concentration: 30 wt%
Specific Gravity: 1.2
Nominal Particle Diameter: 20 nm
pH @ 25°C: 3
Viscosity @ 25°C: 5 cP Supplier: Nyacol^{TM} Nano Technologies

Used for: Diffusion experiments

Precautions
Minimum feasible handling, and temperatures should be maintained. Avoid contact with skin and eyes. Avoid generating mist during use. Use only in well ventilated area. Do not smoke. As a precautionary measure, the wearing of standard work gear is suggested.

4.3.4 *n*-Decane

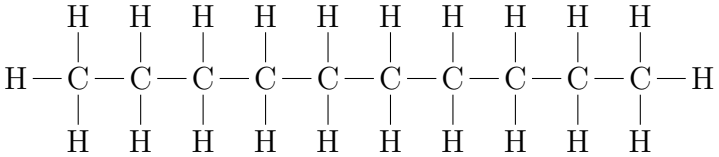

Molecular formula: $C_{10}H_{22}$
Purity: > 99% [79]
Supplier: Merck KGaA
Used for: Diffusion experiments

H- and P-sentences:
H226: Flammable liquid and vapou.
H304: May be fatal if swallowed and enters airways.

P301+310, P331 IF SWALLOWED: Immediately call a POISON CENTER or doctor/physician. Do NOT induce vomiting.

4.3.5 Water (DIW)

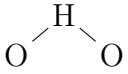

Molecular formula: H_2O
Purity:
Used for: General

Information:
The water used for experiments and cleaning. It is distilled and de-ionised. It is referred to as *DIW* throughout this thesis.

4.3.6 Synthetic Sea Water (SSW)

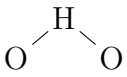

Molecular formula: H_2O
Purity:
Used for: Experiments

Information:
The water used for experiments. It is referred to as *SSW* throughout this thesis.

TABLE 4.6: Salt composition in synthetic sea water

Salt	**Concentration [g/l]**
$CaCl_2 \cdot 2H_2O$	1.91
$MgCl_2 \cdot 6H_2O$	9.05
$NaHCO_3$	0.17
NaCl	23.38
Na_2SO_4	3.41
KCl	0.75

4.4 Complete List of Equipment

4.4.1 Drop Shape Analyser

Manufacturer: EUROTECHNICA GmbH and Krüss GmbH
Model: PD-E1700 LL-H and DSA100 - Webpages: EUROTECHNICA, Krüss
Maximum pressure = 690 bar
Content:

- High resolution camera
- Light source
- HPHT PVT cell
- Thermostat
- Heating-coil
- Two piston-cylinders for introduction of fluids
- Pressure-gauges

4.4.2 Pump

Manufacturer: Gilson, Inc. [80]
Model: 305 Piston Pump
Rate: $10\mu l/min - 200ml/min$
Includes: Manometric module for minimising pressure fluctuations
Maximume pressure: 600 bar
Webpage: Gilson, Inc.

4.4.3 Turbidity Scanner

Manufacturer: Formulaction
Model: Turbiscan^{TM} Lab Expert
Maximum concentration: 95% [81]
Particle size range: 10 nm - 1 mm [81]

4.4.4 Densiometer

Manufacturer: Anton Paar
Model: DMA 4500
Temperature range: 0°Cto +90°C [82]
Pressure range: 0 to 10 bar [82]
Minimum sample size: 1 ml [82]
Accuracy: $5 \cdot 10^{-5} g/ml$ [82] / 0.03°C

4.4.5 Spectrophotometer

Manufacturer: Shimadzu Corporation
Model: UV-1700 PharmaSpec Double Beam Scanning UV-Vis Spectrophotometer
Range: 190.0 nm - 1100 nm ± 0.3 nm [83]
Absorbance: -0.5 to + 3.0 Abs ±0.004 Abs at 1.0 Abs [83]
Webpage: Shimadzu

4.4.6 De-ionisation

Manufacturer: Merck Millipore
Model: Milli-Q Integral 5 Water Purification System
Purity: < 1 unit/mL (particulates >0.22 μm - with the use of Millipak filter) [84]
Feed-water: Distilled

4.4.7 Wheighing Scale

Manufacturer: Mettler Toledo
Model: NewClassic MF MS104s/01
Accurancy: ± 0.0001 g

4.4.8 Magnetic Stirrer

Manufacturer: VWR
Model:VMS-C7

Chapter 5

Results and Discussion

A total of 182 individual pendant drop diffusion experiments have been carried out. DIW-CNF experiments have been conducted for 2 temperatures (25°C and 45°C), 9 pressures (10-90 bar $\Delta P = 10$), 3 concentrations (0.05, 0.5 and 1 g/l), and 2 different sets of environment (*saturated* - and *gradully saturated*, explained in ch. 4.1.2). All the *saturated* experiments have been carried out twice. SSW-CNF experiments have been carried out for 45°C, 10-90 bar,1 g/l , and for *saturated* and *gradually saturated environments*. It has also been conducted a 24 hours long *Pendant drop diffusion - high pressure and high temperature (PDD-HPHT)* experiment without CO_2 present, in order to observe possible effects on volume without CO_2. In addition to the PDD-HPHT experiments it has also been conducted spectrophotometry-experiments at atmospheric conditions. These two sets of experiments coupled with each other confirmed a low possibility of nanoparticle migration across the NF/*n*-decane interface, and are discussed in chapter 3.7. This *Results- and Discussion-chapter* is concerned with the analysis of the diffusion experiments, as it is the major part of the thesis and the fact that all other experiments have been conducted to achieve values or information concerning the diffusion, all the other results are presented in chapter 3 - *Fundamental Properties of the Nanofluid and Hydrocarbon*. More over, a number of different experiments of varying magnitude have been carried out and discussed in chapter 3, these experiments were conducted to justify assumptions qualitatively (e.g. solubility) and to obtain specific values quantitatively (e.g. density of CNF). A lot of different properties are needed in the analysis of the results, and analytical and empirical models have been extensively used, they are also described in chapter 3.

The *Results and Discussion* is organised in a way that the fundamental properties and observations are discussed in a natural way building on each other, where conclusions in a succeeding sub-section may confirm an observation, suggestion or statement in a preceding one. This is clearly mentioned where it is relevant. Since the fundamental concept of all these experiments is to record the volume change, the first sub-chapter is presenting the volume variation (increase) of the drop, extensive tables with all the data is presented in Appendix D. Mole fraciton of CO_2 in decane, density, viscosity, interfacial tension, and diffusion coefficient is presented after the volume change sub-chapter. Tables may be found in appendix E and F.

5.1 Volume Change

5.1.1 Volume Change vs. Time

When CO_2 mass-transfer occurs across the interface between CNF and the *n*-decane drop, the oil will swell. Figure 5.1 shows the relative volume change versus time, for the 1 g/l DIW-CNF for both *saturated* and *gradually saturated* environments. All the curves represent different experiments conducted at a constant pressure and temperature. Each plot represents volume variation at different pressure (10- 90 bar) at fixed temperature of either 25°C or 45°C. The effect of pressure can be compared individually within either of the plots at the current conditions. The effect of temperature can be observed between the plots in the abscissa-direction. The effect of phase can be observed in the ordinate-direction. Similar analyses has been carried out for 0.5 g/l and 0.05 g/l, presented in figure 5.2 and 5.3. It is observed (fig. 5.1 to 5.3) that at 25°C, the swelling increases with pressure until phase-change of CO_2 occurs. (64 bar at 25°C), after this point, the equilibrium volume is lower than just before this pressure, but then increases again as pressure increase. However, a different phenomenon is observed for 45°C, where, contrary to 25°C, the phase is changing from gaseous to super critical and not from gaseous to liquid. Why this matters is suggested to be the sudden change in density of the former. The density change of pure CO_2 have been discussed in chapter 2.2, and density of the CO_2 saturated *n*-decane drop will be discussed later in this chapter. Further, the rate at which volume change occurs, e.g. the mass-transfer rate of CO_2, is higher for *saturated* environment than for *gradually saturated*, this is observed for both temperatures. It is also qualitatively observed that the magnitude of volume change is higher for the temperature, which might be due to higher solubility of CO_2 in nanofluid and *n*-decane at 25°C compared to 45°C, as discussed in chapter 5.2. Moreover, the magnitude of the equilibrium volume seems to some extent to be independent of the two different saturation environments, this is logical as the *gradually saturated* experiments essentially are converted into *saturated* environment the moment the nanofluid is fully saturated with CO_2. It is also observed that the rate of volume increase slows with time. As mass-transfer rate is driven by concentration gradient, it is logical that the rate of swelling decreases with time, as the drop gets more and more saturated with CO_2 and the gradient decreases. However, for*gradually saturated* environments at high pressure ($P > 60$ bar) it is observed an increase in swelling rate with time, until just before saturation point. This might be attributed to the gradual saturation of the nanofluid, and more and more CO_2 becomes available for the *n*-decane with time. Two factors are believed to play a vital role in this behaviour; 1) the solubility of CO_2 in *n*-decane is higher than in nanofluid, 2) the amount of nanofluid is much greater than the volume of *n*-decane. The proposed mechanism is that as more and more nanofluid becomes saturated, it exists and increasing availability of CO_2 to the *n*-decane, not corresponding directly to the nanofluids concentration because of the excess volume. According to this statement, equal amounts of nanofluid and *n*-decane should result in a linear increase of the drop volume. Near to equilibrium, the *gradually saturated* experiments experience a more sudden saturation than the saturated experiments, creating a flat curve rapidly.

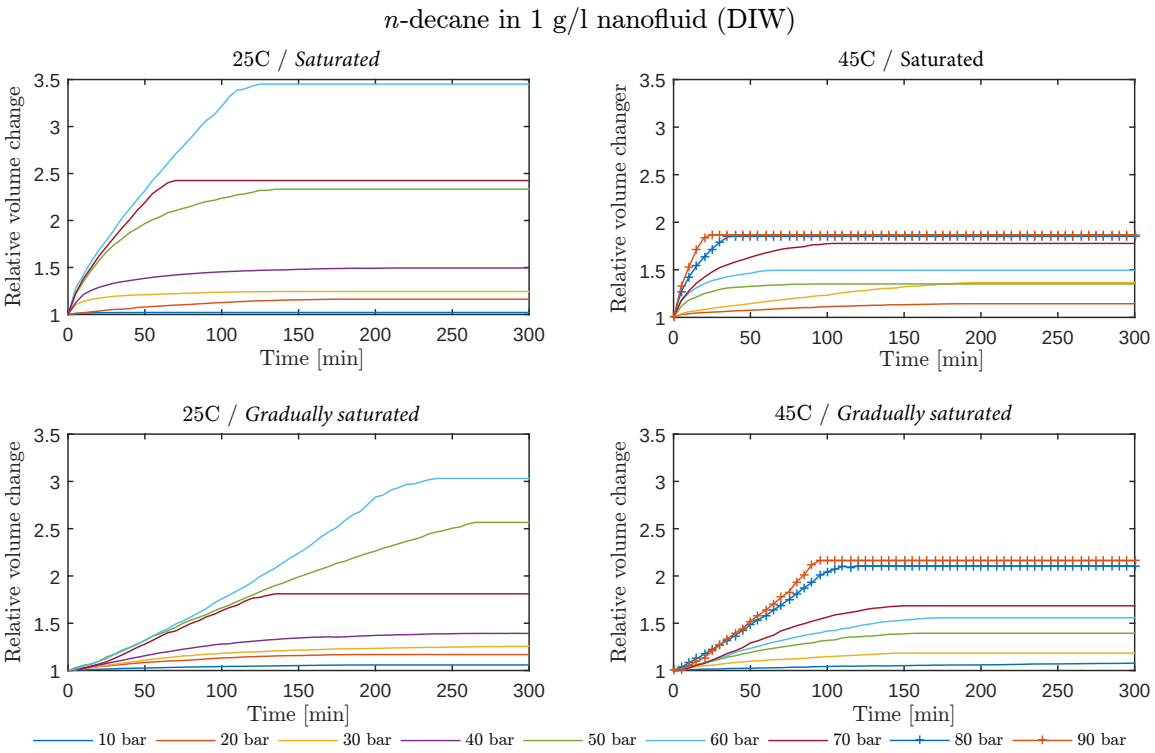

Figure 5.1: Volume change of an n-decane drop surrounded by DIW-CNF 1 g/l at 25°C and 45°C. Every pressure line marks a separate experiment

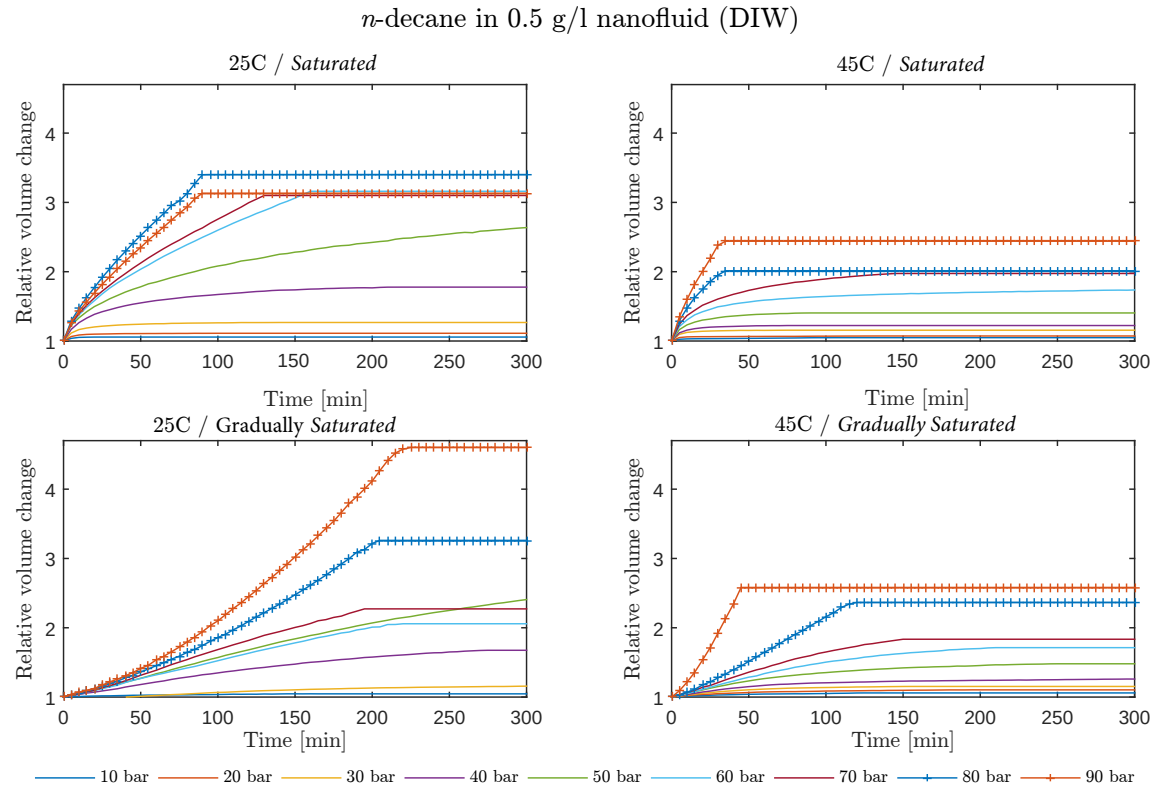

Figure 5.2: Volume change of an n-decane drop surrounded by DIW-CNF 0.5 g/l at 25°C and 45°C. Every pressure line marks a separate experiment

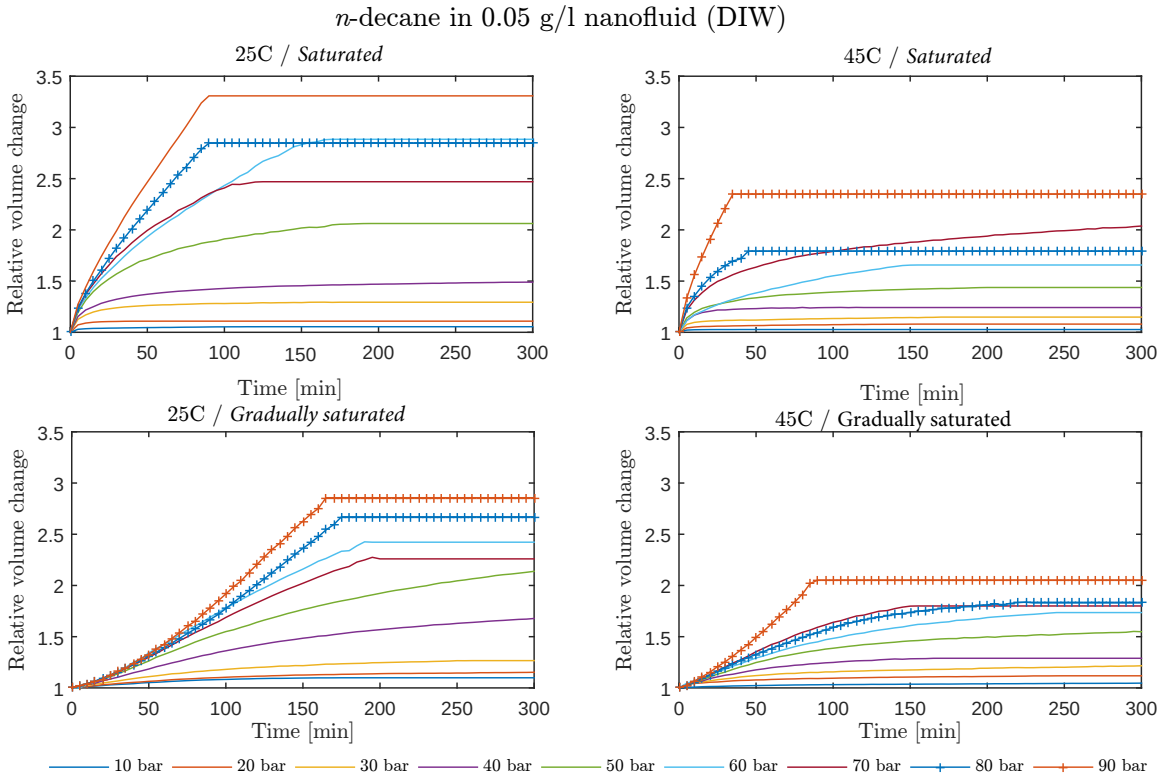

Figure 5.3: Volume change of an n-decane drop surrounded by DIW-CNF 0.05 g/l at 25°C and 45°C . Every pressure line marks a separate experiment.

5.1.2 Comparison of Concentrations vs. Pressure

The behaviour of relative increase in volume among different concentrations of DIW-CNF is compared at different pressures. Four plots have been created, which presents the comparison for *saturated* and *gradually saturated* environments for both temperatures. Figure 5.4 and 5.5 shows the comparison among all the concentrations with a *saturated* environment at 25°C and 45°C, respectively. Figure 5.6 and 5.7 shows the comparison among all the concentrations with a *gradually saturated* environment at 25°C and 45°C, respectively.

Comparison of all concentrations at 25°C - Saturated and Gradually Saturated

It is observed in the two figures (5.6, 5.7) that the magnitude of swelling increase with pressure until phase change occurs. Even though the magnitude differs among concentrations of DIW-CNF, this phenomenon occurs for all of them. It can also be observed that the difference in magnitude is less significant at lower pressures. The increase in swelling with pressure seems to be exponential initially, and then gradually fade as pressure becomes higher. An interesting phenomenon, which is already mentioned in chapter 5.1.1, is the sudden decrease in swelling when crossing the CO_2 phase-change pressure. This decrease is believed to not result from a lower mass transfer of CO_2, but rather from a density change of the CO_2 as it changes into liquid. The sudden increase in CO_2 density when crossing this pressure has already been discussed in the theory chapter (ch. 2.2). This suggestion is also further substantiated in figure 5.22, where the mole fraction of CO_2 vs. pressure is plotted along with the relative volume change. Beyond the phase-change point, the volume continues to increase with pressure. This is consistent with the proposed CO_2 density-relation, where the increase in CO_2 density is sudden at phase-change point, but then increases very slowly. This suggests that enough CO_2 is entering the drop to counteract the compressing due to higher density with pressure. It is also suggested that the solubility of CO_2 in the environment (CNF) plays a significant role in the volume change, the reason for this is the concentration difference which drives the mass-transfer process. A higher amount of CO_2 in the surrounding phase would yield a possibility of larger mass-transfer across the interface befor eequalization of the CO_2 gradient, and hence a higher concentration of CO_2 in the drop-phase. The solubility of the environment have been discussed in the methodology chapter (3.2), where the solubility follows a general trend of rapid increase with pressure initially (P <60 bar for 25°C, P <90 for 45°C) and then gradually fade off. It marks a distinct point around the phase change where the increase in solubility with pressure significantly reduces. All this suggest that the volume change or swelling of the drop is largely dependent in the two factors, solubility in the surrounding phase, and the density of the CO_2.

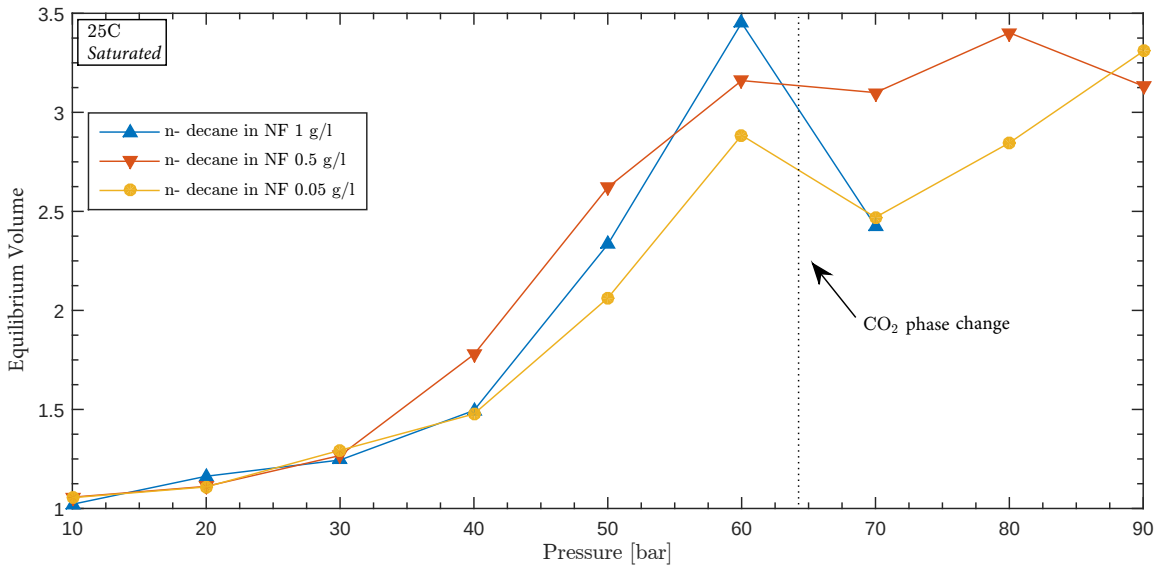

Figure 5.4: Equilibrium volume of an n-decane drop surrounded by DIW-CNF at 25°C , *saturated*. Every point marks a separate experiment

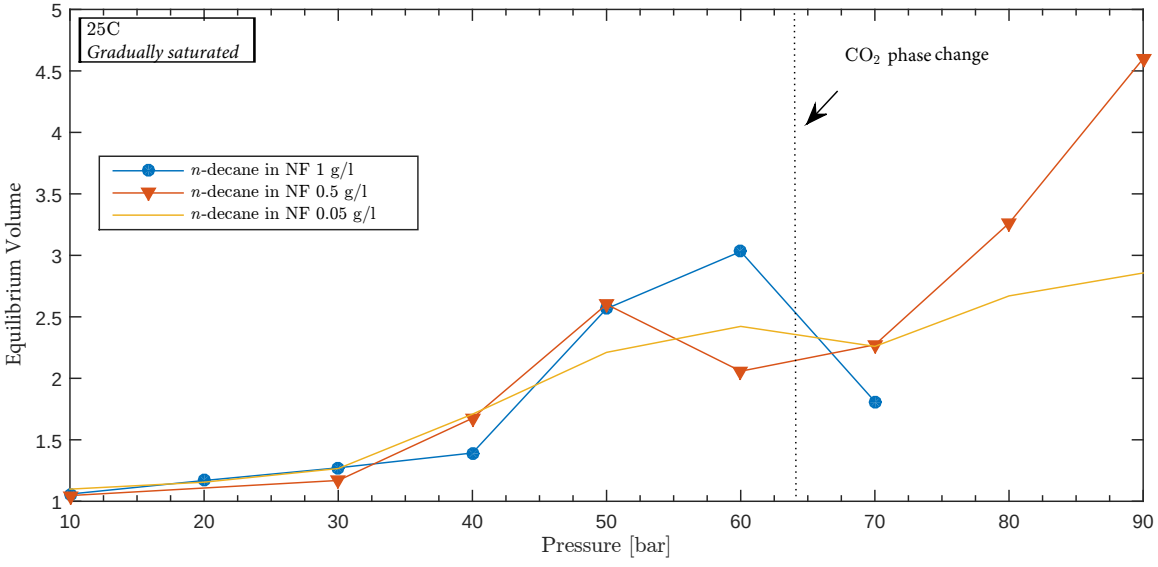

Figure 5.5: Equilibrium volume of an n-decane drop surrounded by DIW-CNF at 25°C , *gradually saturated*. Every point marks a separate experiment

Comparison of all concentrations at 45°C - Saturated and Gradually Saturated

In figure 5.6 and 5.7, the comparison among concentrations of nanofluid at 45°C for saturated and gradually saturated environments are presented, respectively. An important distinction between 25°C and 45°C is the phase change of CO_2, contrary to 25°C the phase change at 45°C with pressure crosses over the gaseous-super critical line, and not the gaseous-liquid. Across this line (45°C 74 bar), the density change of CO_2 is continuous. The phase change does also occur at a higher pressure. With the exception of *saturated environment* for 0.05 g/l DIW-CNF, the phenomenon of a lowered volume change across the phase-change boarder is not observed as it is for 25°C, contrary, the rate of increase with pressure seems to be higher after the CO_2 reaches phase change pressure. The decrease for *saturated* 0.05 g/l DIW-CNF environment might be attributed to experimental error, but the trend from the *gradually saturated* experiments shows a similar trend relative to the two other concentrations, which may indicate that the phenomenon is somehow related to the concentration of nanofluid, either for the two other concentrations, or for the 0.05 g/ itself. This particular observation remains unexplained. Other than the phenomena at, and across, the phase change boarder, similar observations are made for both 25°C and 45°C.

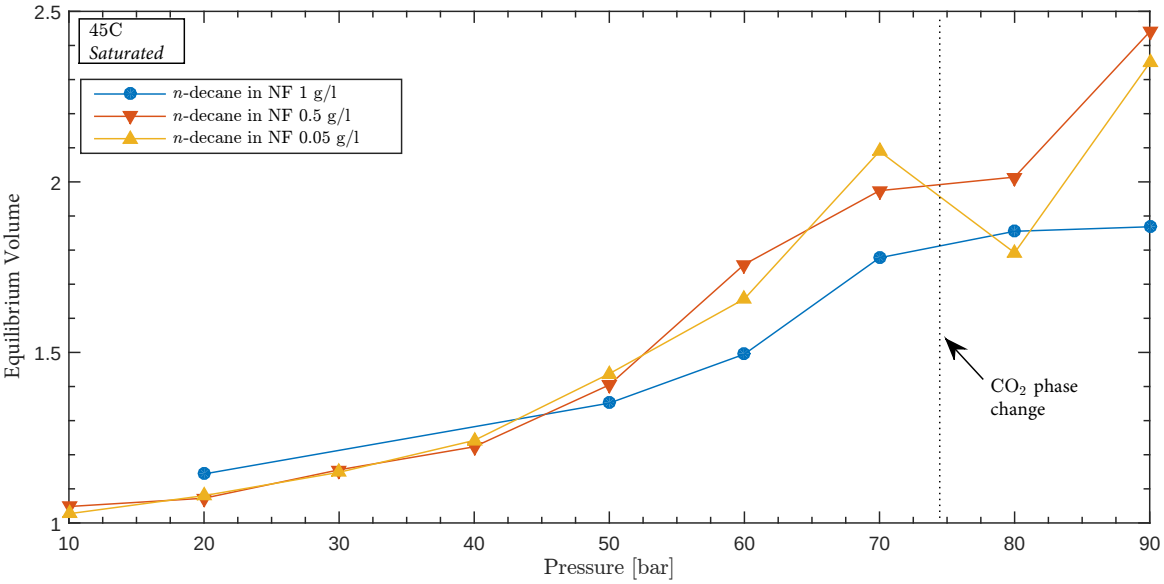

Figure 5.6: Equilibrium volume of an *n*-decane drop surrounded by DIW-CNF at 45°C , *saturated*. Every point marks a seperate experiment

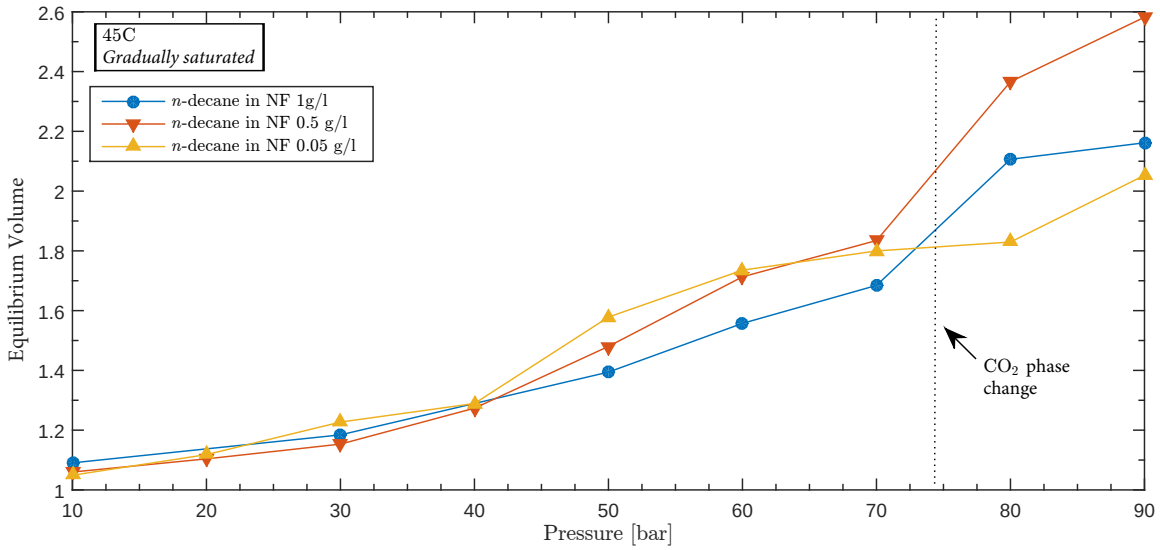

Figure 5.7: Equilibrium volume of an n-decane drop surrounded by DIW-CNF at 45°C *gradually saturated*. Every point marks a seperate experiment

5.1.3 Dependency on Nanofluid Concentration

To observe the effect of nanofluid concentration on the equilibrium volume increase, four plots (Fig. 5.8, 5.9, 5.10 and 5.11) are generated which compares all the pressure in a single plot for the 2 different phase-sets (*saturated* and *gradually saturated*) and the two different temperatures (25°C and 45°C). The plots have equilibrium volume in the ordinate-direction and the three concentrations in the abscissa-direction. With the exception of some few cases, it can clearly be observed a trend that 0.5 g/l have a slightly lower swelling than the two other concentrations at low pressures (P $<$ 40 bar), but at higher pressures clearly shows greater swelling (equilibrium volume) than the two others (0.05 g/l and 1 g/l). 0.05 and 1 g/l seems to perform quite similarly. It seems to be some inconsistancies right around phase-change. These statements are true for all four cases (both temperatures for *saturated* and *gradually saturated* environments). These observations offer great insight for EOR-applications, first of all it shows that it exists an optimum concentration of nanoparticles, dependent on what is preferred. In the case of mobility alteration and reconnection of waterblocked oil ganglia, the system of silica-nanofluid/n-decane suggest that the optimum is between 0.05 g/l and 1 g/l, and probably close to 0.5 g/l. If these observations extrapolate to crude oil (which would need verification), injecting carbonated 0.5 g/l nanofluid would probably yield the highest recovery since the relative permeability of displaced phase is increased the most, due to viscosity reduction (discussed in ch. 5.4) as a result of more CO_2 being transferred into the oil. This is neglecting any effect silica nanoparticles have when it adsorbs on the rock. Maghzi *et al.* 2012 [85] , suggests that silica nanoparticles are altering the rock properties towards more water-wet due to adsorption on the surface, which would be preferable in an EOR-perspective. However, it is suggested that an increasing concentration of nanoparticles might the best for rock alteration. [85]. An optimum concentration considering all the aspects should exist, where effects on both fluid alteration and rock alteration are accounted for. Moreover, from experiments presented in chapter 3.7 - *Possible Mass-Transfer of*

Nanofluid, it is likely that nanoparticles/nanofluid is not transferred into the oil-phase. The optimum concentration for equilibrium volume is suggested to relate to alteration of the environmental phase, namely that the nanofluid acts as a solubility promoter of CO_2 in the water-basefluid, and that the higher content of CO_2 creates a greater concentration gradient, allowing for more CO_2 to enter the drop before the gradient becomes zero. It has been confirmed qualitatively by experiments (ch. 3.2) that nanofluid has a greater solubility than its respective basefluid (SSW and DIW). This section is relating nanofluid concentration to equilibrium volume change, and other effects that might be caused by the nanofluid is discussed in their respective chapters.

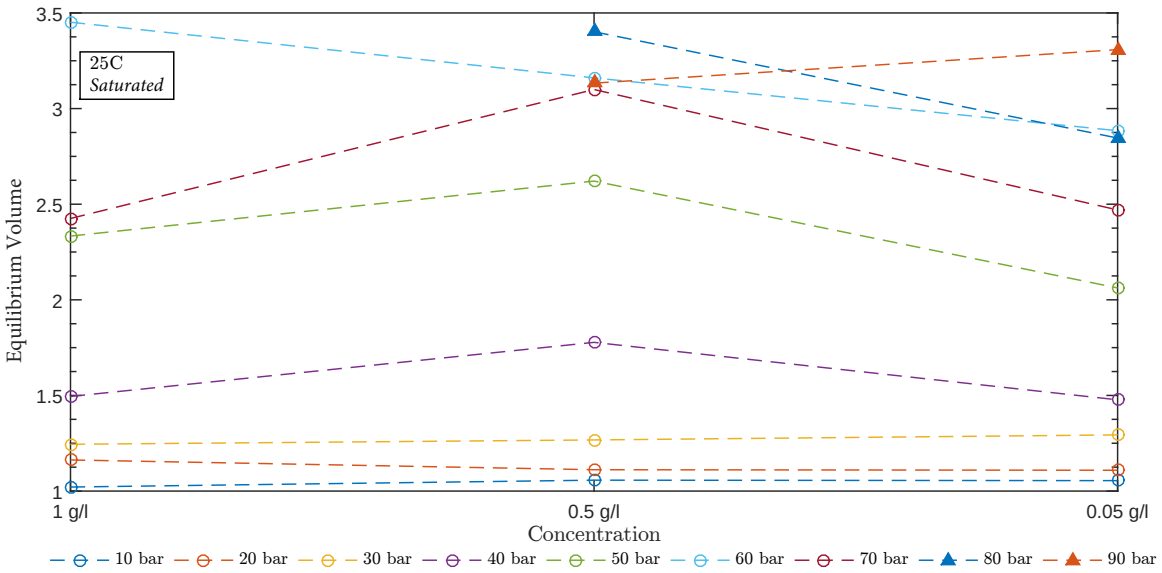

Figure 5.8: Comparison between pressure of equilibrium volume of an n-decane drop versus concentration of nanofluid (DIW-based) *saturated*, 25°C. Every point marks a seperate experiment

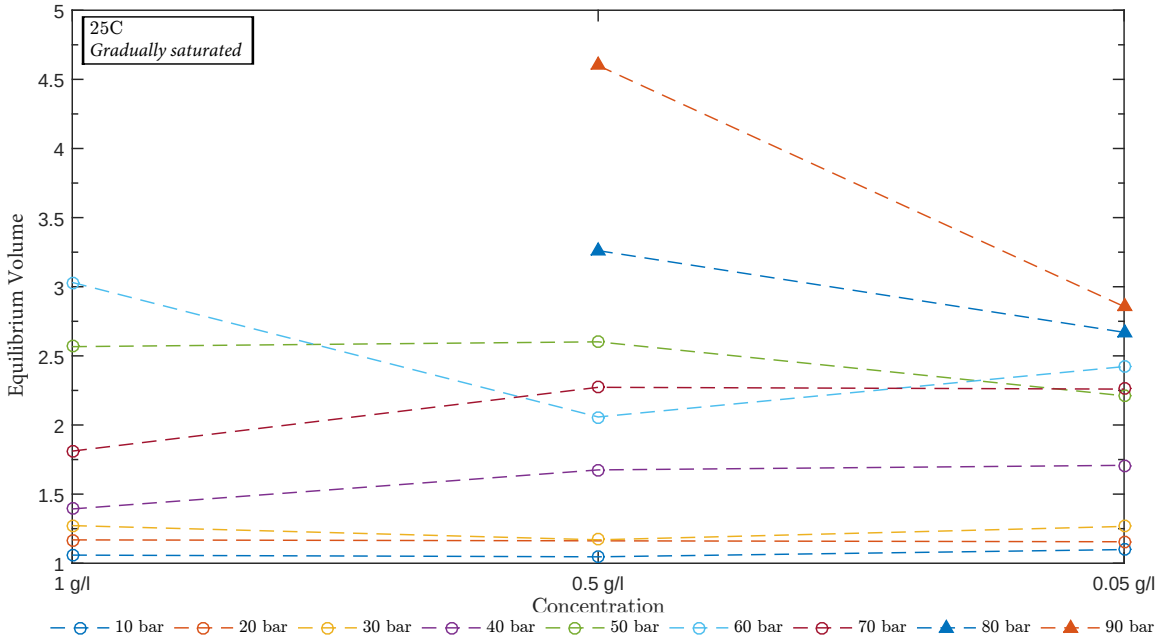

Figure 5.9: Comparison between pressure of equilibrium volume of an n-decane drop versus concentration of nanofluid (DIW-based) *gradually saturated* 25°C. Every point marks a seperate experiment

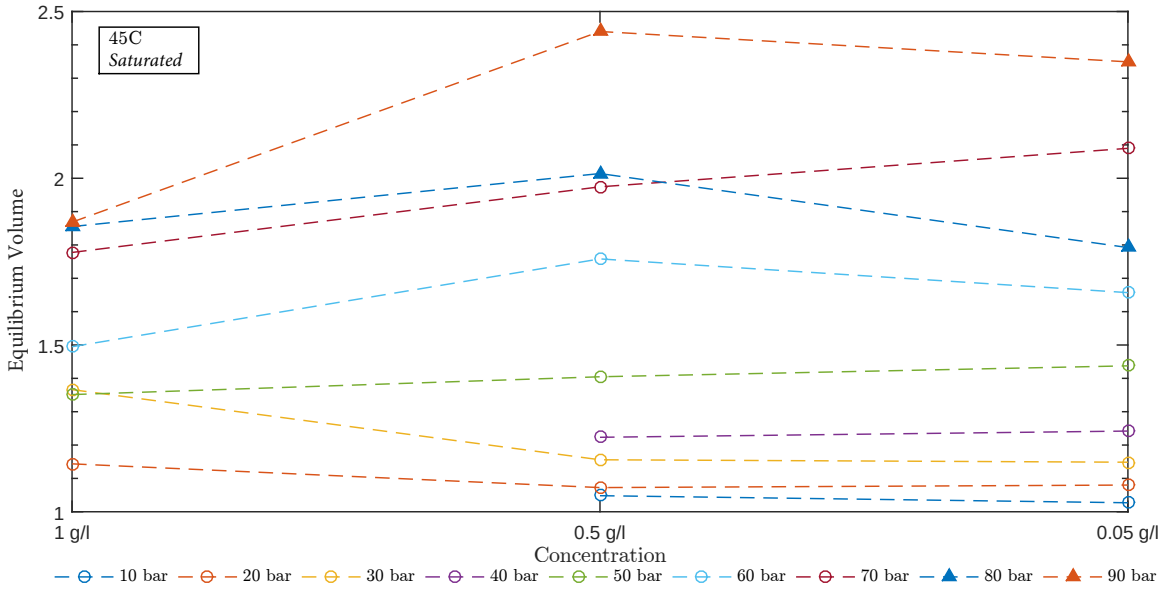

Figure 5.10: Comparison between pressure of equilibrium volume of an n-decane drop versus concentration of nanofluid (DIW-based) *saturated*, 45°C. Every point marks a seperate experiment

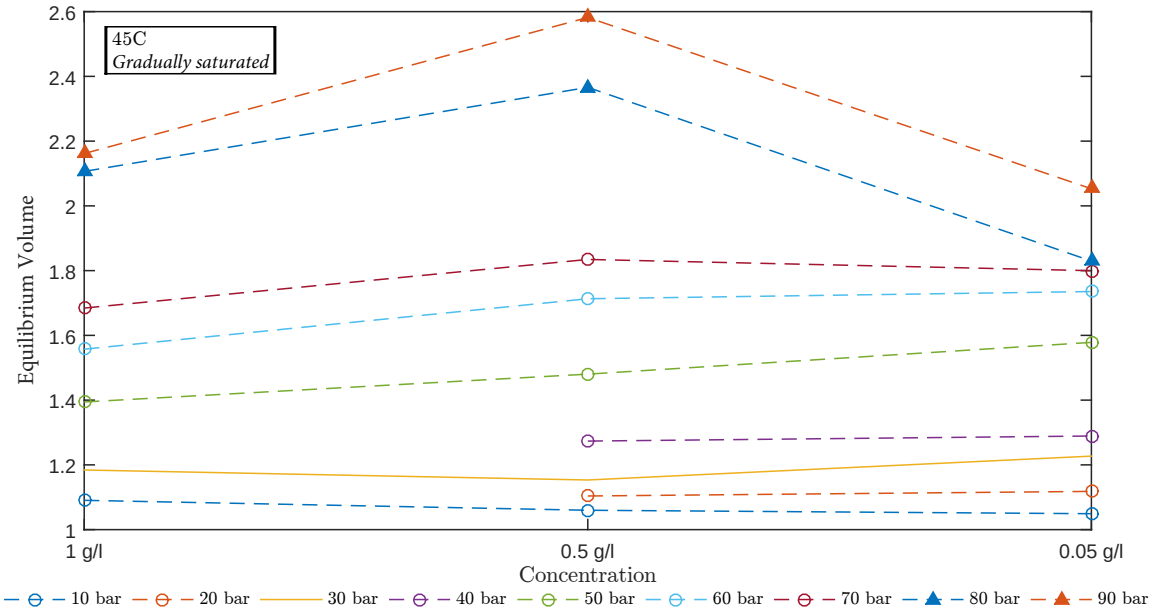

Figure 5.11: Comparison between pressure of equilibrium volume of an n-decane drop versus concentration of nanofluid (DIW-based) at *gradually saturated* 45°C. Every point marks a seperate experiment

The effect of Nanofluid Concentration Compared to Water

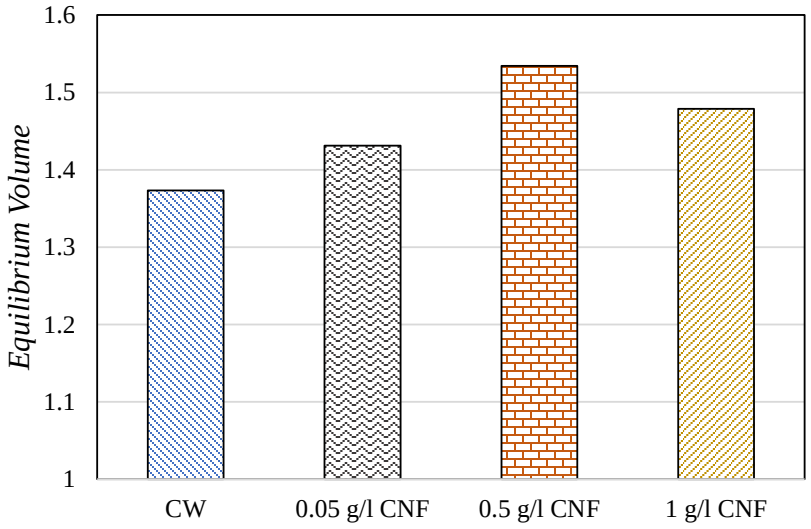

Figure 5.12: Equilibrium volume of an n-decane drop surrounded by CW, 0.05 g/l CNF, 0.5 g/l CNF and 1 g/l CNF at 25°C and 40 bar.

Volume data for n-decane surrounded by carbonated water (CW) has been provided by Hamouda and Bagalkot for comparison purposes. Figure 5.12 shows the equilibrium volume of n-decane surrounded by pure carbonated water at 40 bar and 25°C, as well as for carbonated nanofluid with three concentration. This barplot illustrates the increased swelling of oil caused by the presence of nanofluid. The reason for this ability have been discussed in great detail in past and future chapters. However, at these particular conditions the optimum nanofluid concentration (0.5 g/l) results in a swelling 12% higher than that of pure carbonated water. The exact values are CW = 1.373437217, 0.05 g/l CNF = 1.431144962, 0.5 g/l CNF = 1.534486828, 1 g/l CNF = 1.47868567. The swelling of the oil offer great EOR-opportunities as the viscosity is reduced, the relative permeability is increased, the mobility ratio in a CWI/CNFI scenario would be superior to a conventional waterflood in the sense that the injection fluid is increasing the mobilisation of the displaced fluid while displacing it. Swelling is also reported to reconnect trapped oil-ganglia and reduce the residual oil saturation.

5.1.4 Comparison of *Saturated* and *Gradually Saturated* Environments

Two different sets of phases-sets are investigated in this work. *saturated*, which is saturated carbonated nanofluid together with the drop of n-decane, the nanofluid is saturated at the moment the experiment commences. The second phase-set is *gradually saturated*, which is free CO_2 and nanofluid together with the n-decane drop at the commencement of the experiment. As the *gradually saturated* experiment is carried out, the CO_2 gradually diffuses first into the nanofluid and then in the n-decane drop, eventually making the nanofluid saturated. This process is best observed in the previously discussed relative volume change vs. time (5.1.1). In this current section, the equilibrium volume is presented, and theoretically, the *gradually saturated*

experiments have been transformed into *saturated* at this point. However, differences among the sets are observed. This section is organised in a way where six plots are presented (Fig 5.13 to 5.18), a particular plot presents the data for both phase-sets at a particular temperature and concentration of nanofluid. One phenomenon that seems valid for all cases with regards to phase is that a *saturated* environment seems to be more heavily affected by the phase-change of CO_2. It does exist individual observations for the different concentrations that are discussed further. However, the impact of phase seems to be small compared to e.g. pressure or temperature, as far as volume is concerned. This statement can be verified by observing that the change with pressure is generally larger than the change caused by phase. Temperature comparison for both phases is discussed in chapter 5.1.5. It is important to stress that this statement is intended for the volume increase only, and does not say anything about the effect of phase on other properties. Additionally this EOR-method may be utilised in an EOR/CCS combination, where significant amounts of the injected CO_2 is trapped in the reservoir at the end of the reservoirs lifetime. Experiments on this matter is reported in the literature and is discussed in the introduction of this thesis.

Environment: NF 1 g/l DIW-based

Figure 5.13 shows the equilibrium volume for the two scenarios (*saturated* and *gradually saturated*) at 25°C for 1 g/l DIW-CNF environment, while figure 5.14 shows the corresponding experiments for 45°C. In the former, it can be observed that the the environmental scenario seems insignificant at the lower pressures, but around and after the phase-change of CO_2 (64 bar) there is a distinct difference. At 60 and 70 bar, the equilibrium volume of the *gradually saturated* experiments are lower. At 45°C similar observations are made for the independency of phase at lower pressures, but after the phase-change, which for 45°C is from gaseous to super critical, equilibrium volume is significantly higher for the *gradually saturated* experiments. This is opposite of what is observed at 25°C. Unfortunately, only 1 pressure is recorded above phase-change for this particula system (25°C 1 g/l DIW-CNF), hence, it is difficult to establish if this is an experimental error or a possible trend. The lowered equilibrium volume from 60 to 70 bar at 25°C is due to phase-change of CO_2 from gaseous to liquid state, and has been discussed in chapter 5.1.2.

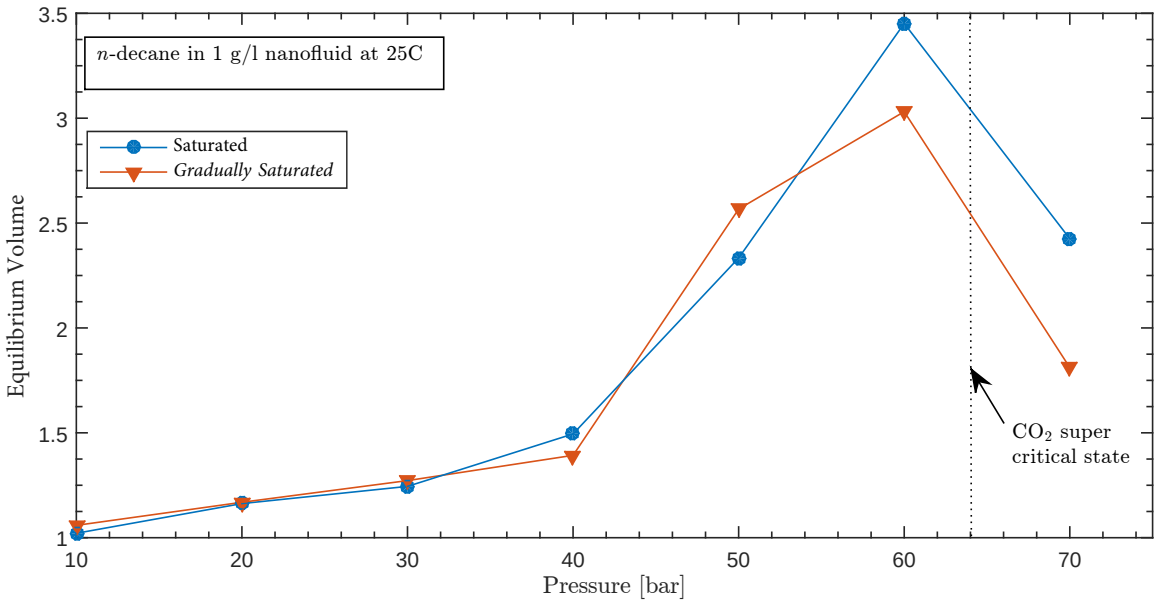

Figure 5.13: Comparison between phases on equilibrium volume of an n-decane drop surrounded by 1 g/l DIW-CNF at 25°C. Every point marks a separate experiment

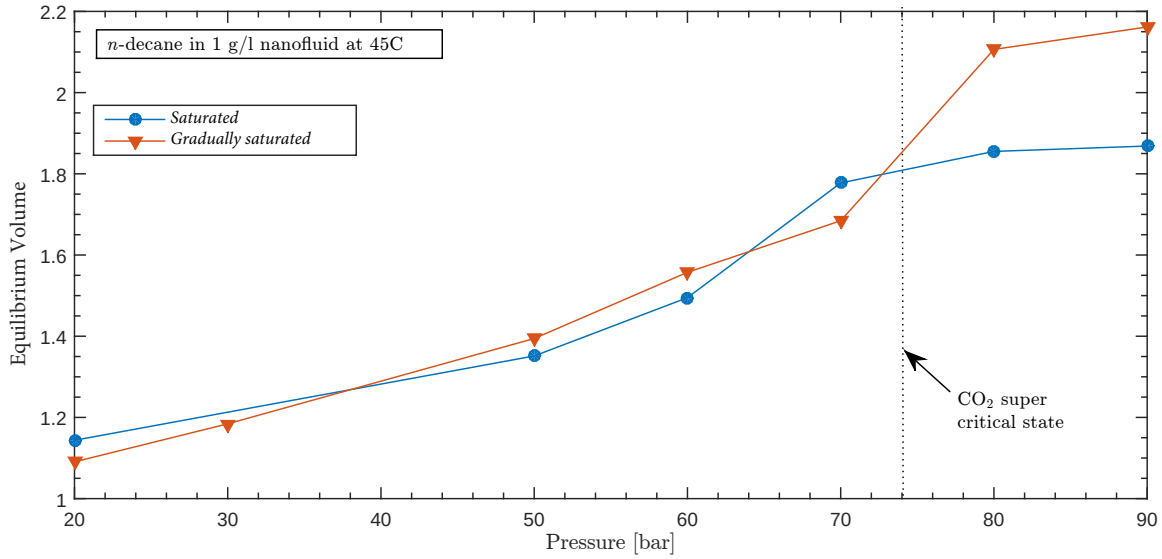

Figure 5.14: Comparison between phases on equilibrium volume of an n-decane drop surrounded by 1 g/l DIW-CNF at 45°C. Every point marks a separate experiment

Environment: NF 0.5 g/l DIW-based

Figure 5.15 shows the relative volume increase for the two phase-sets at 25°C for 0.5 g/l DIW-CNF environment, while figure 5.16 shows the corresponding experiments for 45°C. For both of them, similar observations are made as in figure 5.13 and 5.14 (1 g/l DIW-CNF), concerning the small dependency on whether the environment is *saturated* or *gradually saturated* with CO_2 at low pressures (P < 60 bar). For figure 5.15 it can be observed that the *gradually saturated* experiments behave quite counter intuitively around the phase-change pressure, it is believed that the 60 bar experiment has too equilibrium volume, this is based on the former observation of reduction of equilibrium volume after the phase-change. However, the *gradually saturated* experiments are seen to supersede *saturated* experiments at 90 bar. At 45 °C (Fig. 5.14), the *gradually saturated* experiments supersede after the super critical pressure.

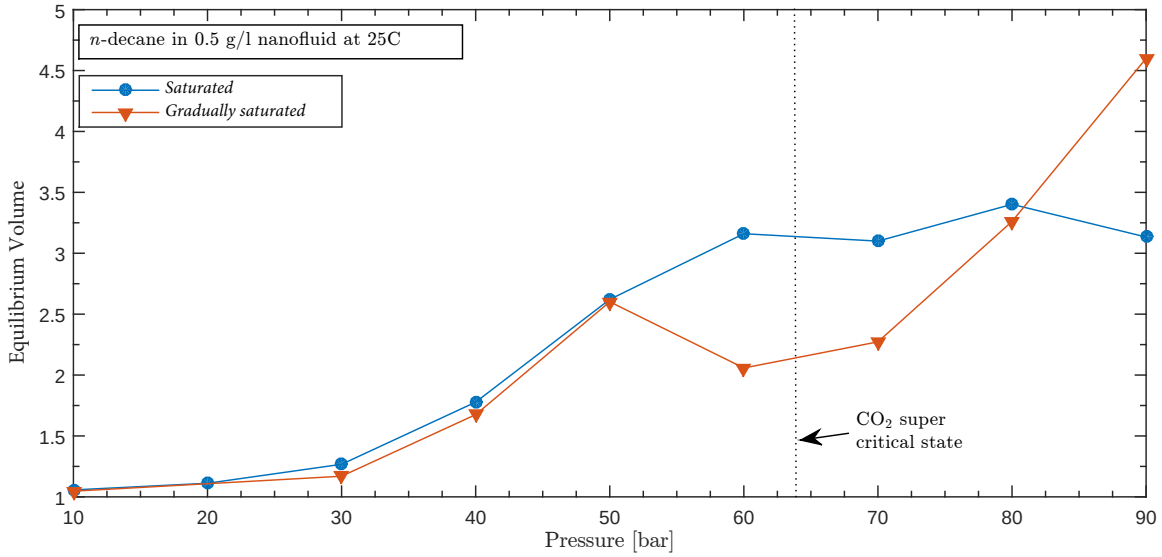

Figure 5.15: Comparison between phaseson equilibrium volume of an *n*-decane drop surrounded by 0.5 g/l DIW-CNF at 25°C. Every point marks a separate experiment

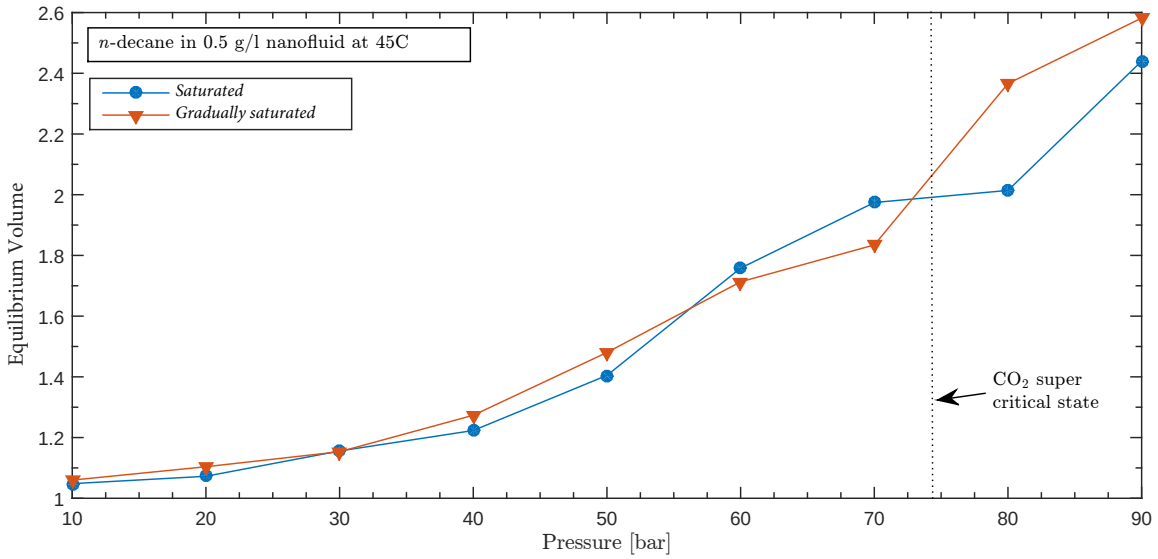

Figure 5.16: Comparison between phases on equilibrium volume of an n-decane drop surrounded by 0.5 g/l DIW-CNF at 45°C. Every point marks a separate experiment

Environment: NF 0.05 g/l DIW-based

Figure 5.17 shows the relative volume increase for the two phase-sets at 25°C for 0.05 g/l DIW-CNF environment, while figure 5.18 shows the corresponding experiments for 45°C. In both of the scenarios, the *gradually saturated* experiments have a tendency to be a little higher than the *saturated* for lower pressure. The *saturated* experiments crosses over around the phase-change border.

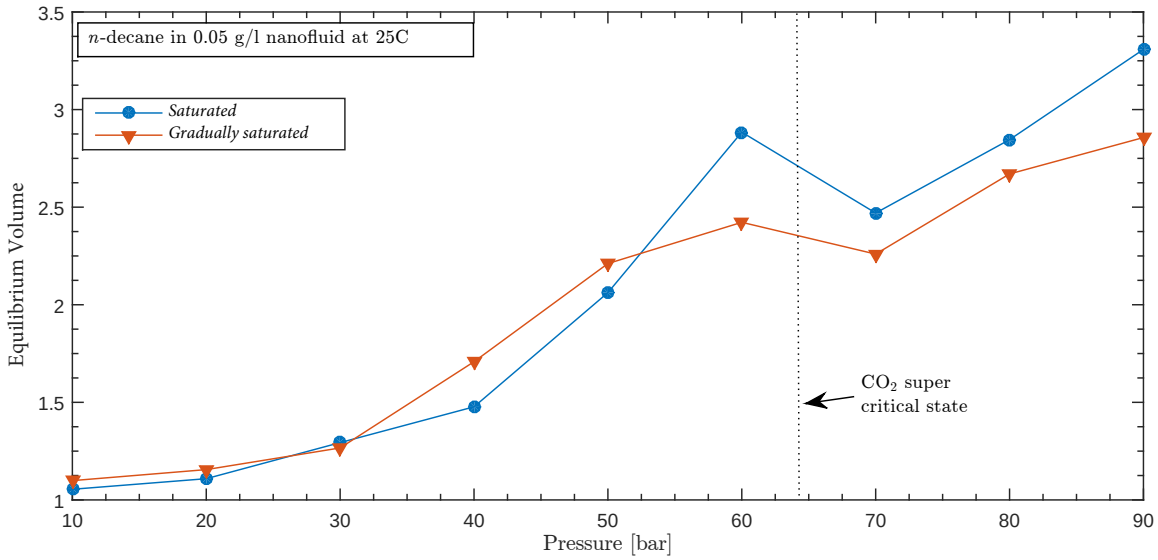

Figure 5.17: Comparison between phases on equilibrium volume of an n-decane drop surrounded by 0.05 g/l DIW-CNF at 25°C. Every point marks a separate experiment

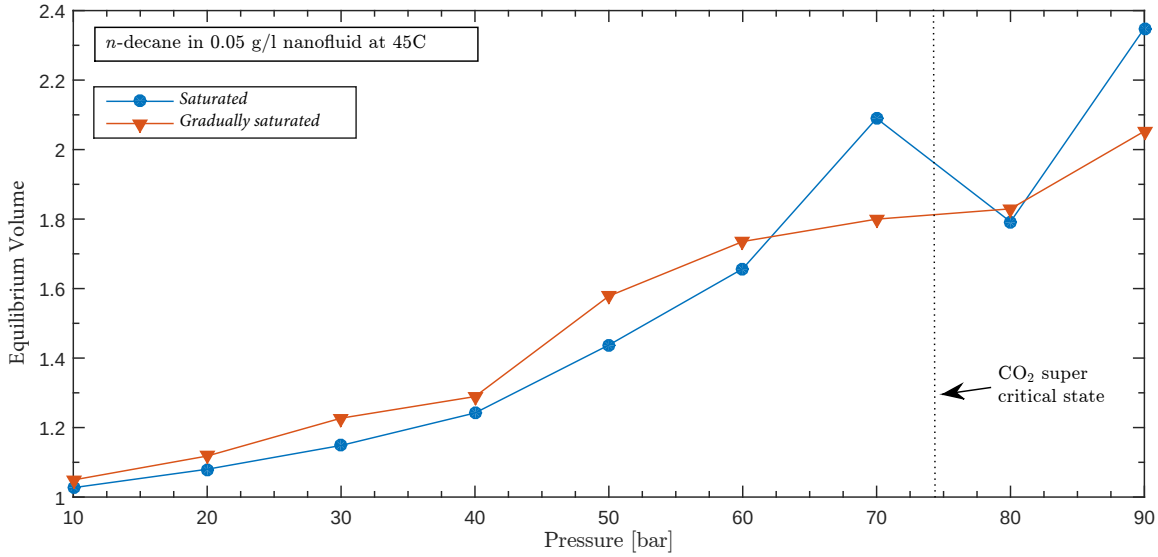

Figure 5.18: Comparison between phases on equilibrium volume of an n-decane drop surrounded by 0.05 g/l DIW-CNF at 45°C. Every point marks a separate experiment

Concentration Gradient in *n*-decane

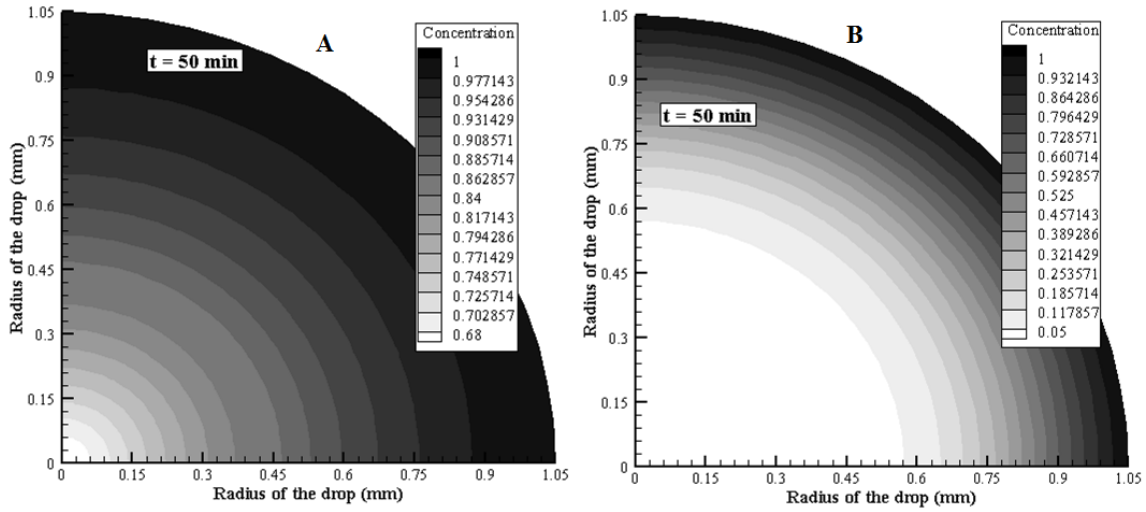

Figure 5.19: Representation of diffusion of CO_2 into n-decane from DIW-CNF *saturated* (A) and *gradually saturated* (B). The contour-plots are calculated with the Mathematical Mass-Transfer model, with the experimental data at t = 50 min, for 0.5 g/l CNF 25°C at P = 30 bar

Figure 5.19 is depicting the distribution of CO_2 in an n-decane drop, under the same pressure and temperature at a particular point in time (t = 50 min). The environment of nanofluid is the same, but the mode of the experiment differs in that figure 5.78-A shows an experiment which is commenced with the environment at CO_2 *saturated* conditions, and 5.19-B shows an experiment where the environment is *gradually saturated* with CO_2. These figures illustrates the effect of the CO_2 concentration gradient in the environment-phase very well, in the sense that these to scenarios have similar equilibrium volume (can be seen in fig. 5.15), but the *gradually saturated*

experiment reach it after a longer time-period (can be seen in fig. 5.1). The rate of diffusion into, and through out, the *n*-decane drop is slower in the *gradually saturated* experiments. The concentration gradient in that environment is also known to be lower than the *saturated* environment by definition, which also means a lower driving force for CO_2 diffusion. Considering that this particular example also represents a scenario where one experiment just have less CO_2 present, this proves the relationship between rate of volume increase in the drop, and solubility of the environment, where it is suggested that the rate of volume increase of the drop increases with higher environment solubility. This statement has to be made by pretending that the different concentration gradients is due to lower solubility of CO_2 in one of them, which is not true in this particular case, but the argument is still valid.

5.1.5 Dependency on Temperature

The temperature effect is presented by plotting all concentrations in one plot for both temperatures. This is done separately for *saturated* and *gradually saturated* environments. At lower pressures (P $<$ 40 bar), the temperature seems to play a minuscule role. However, at higher pressures, 25 °C experience a much larger equilibrium volumes than 45°C. It can also be seen that the effect of phase change is more significant at lower temperature. The higher equilibrium volume at lower temperatures may be attributed to a higher solubility of CO_2 in the environment (nanofluid) at lower temperatures. The effect of higher solubility have already been discussed in the results (ch. 5.1.2), and the solubility is accounted for in chapter 3.2 - *CO_2 Solubility in Nanofluid, DIW and SSW*. The experiments seems to be a bit more consistent for *saturated* than *gradually saturated* experiments. In figure 5.21 *gradually saturated* 25°C 0.5 g/l NF, a remarkable equilibrium volume of 4.599 is recorded. It is uncertain whether this result is valid or not, but according to every other observation discussed, this is one of the conditions that should perform the greatest, with respect to equilibrium volume increase, among the conditions studied in this work.

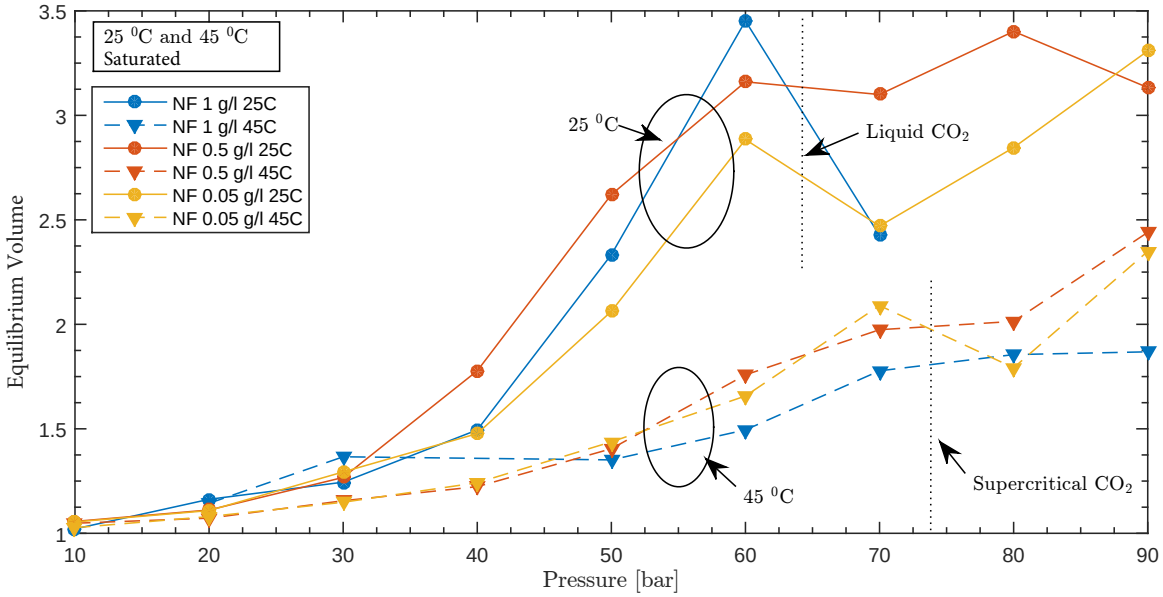

Figure 5.20: Equilibrium volume of an n-decane drop, comparison of all concentrations of DIW-based nanofluid at 2 different temperatures. Environment: *saturated*. Every point marks a seperate experiment

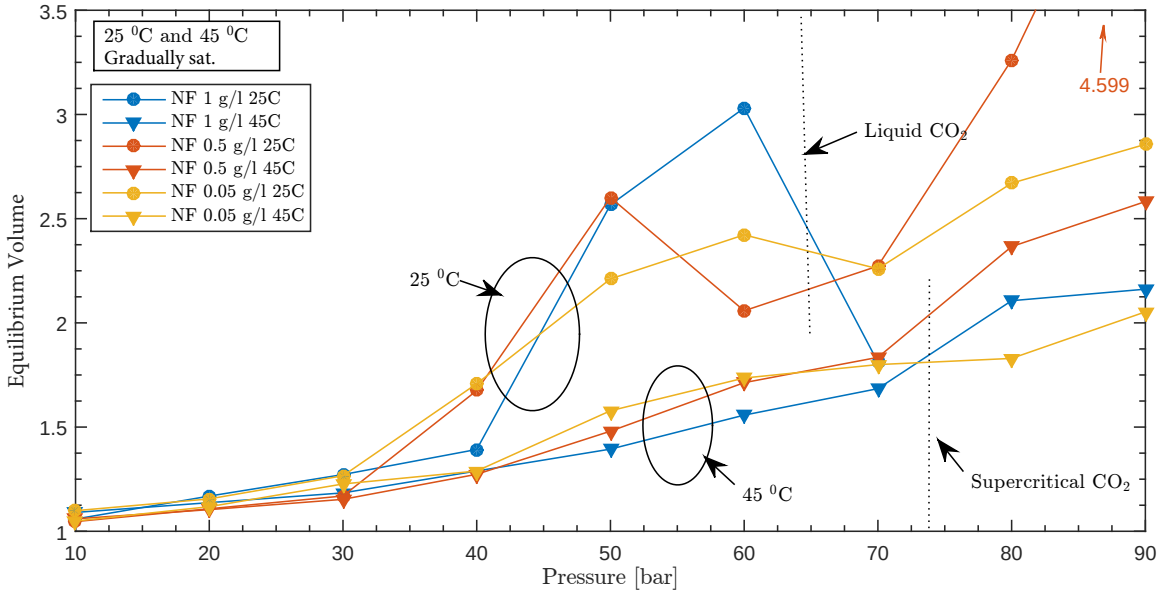

Figure 5.21: Equilibrium volume of an n-decane drop, comparison of all concentrations of DIW-based nanofluid at 2 different temperatures. Environment: *gradually saturated*. Every point marks a seperate experiment

5.1.6 Relative Volume, Mole Fraction and Solubility Comparison

To investigate the reason for the sudden drop in volume increase at phase change, the mole fraction of CO_2 in the *n*-decane drop is plotted simultaneously as relative volume increase. However, mole fraction sensitivity will be discussed further in chapter 5.2. Figure 5.22 shows the aforementioned plot, which depicts the properties of 1 g/l DIW-CNF, *gradually saturated* at 25 °C. It can be seen that the amount of CO_2 present in the *n*-decane drop unconditionally increases with pressure, while the volume increase experiences a drop across the pressure at which the CO_2 changes phase from gaseous to liquid. This means that density change has to be a contributing factor to the lower equilibrium volume increase at 70 bar. Further, it may be observed that mole fraction and volume increase follows a similar trend before the phase-change. For pressures both lower and above the phase-change do the density follow a quite moderate change compared to the dramatic change at phase-change pressure. It has also been suggested that solubility of CO_2 in the environmental phase plays a significant role in the swelling process, this has been discussed, and it is argued that the greater amount of CO_2 in the environment offers a greater concentration gradient, that in turn transfer more CO_2 to the drop before the gradient equalizes. Figure 5.23 shows the comparison between solubility and volume increase. It is confirmed that nanofluid probably do not enter the drop-phase (ch. 3.7), However, a potential change in solubility of CO_2 in the drop-phase in the case of nanoparticles/nanofluid present, is believed to be of lower significance as the solubility of CO_2 in the nanofluid is the limiting factor.

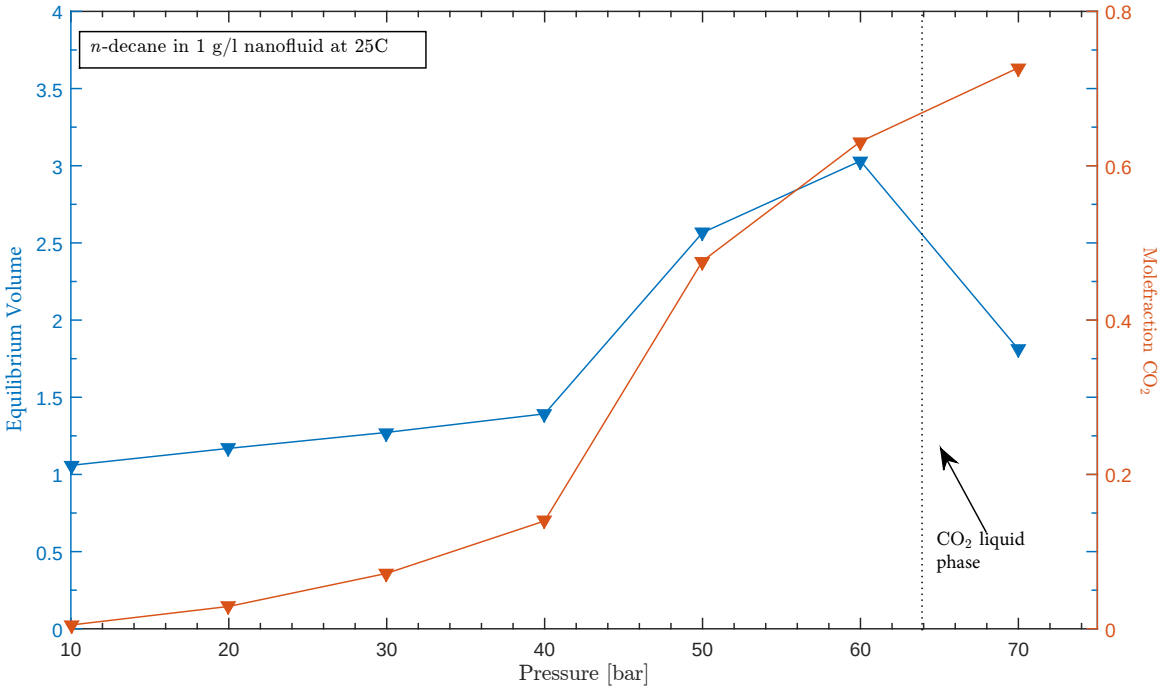

Figure 5.22: Equilibrium volume and mole fraction of CO_2 in an *n*-decane drop. Environment: *saturated* 1 g/l DIW-CNF. Every point marks a seperate experiment

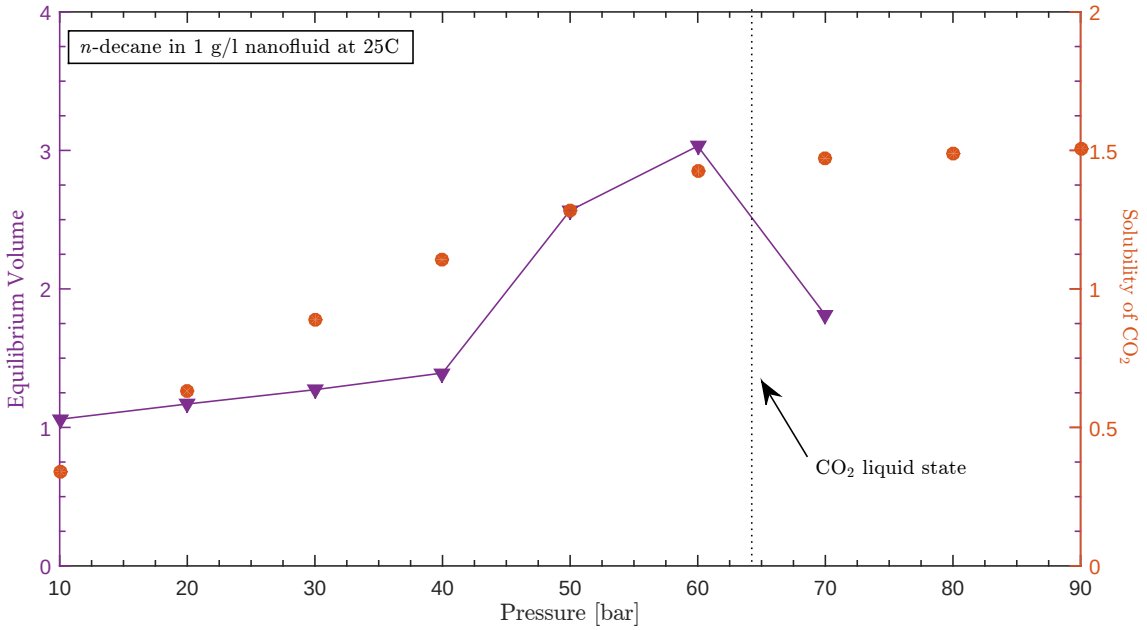

Figure 5.23: Equilibrium volume and mole fraction of CO_2 in an *n*-decane drop. Environment:*gradually saturated* 1 g/l DIW-CNF. Every point marks a seperate experiment

5.1.7 Summarising Points on Volume Increase and Equilibrium Volume

- The state of matter of CO_2 is important, volumetric behaviour across phase-change border differs between 25°C and 45°C. It is suggested that the reason is phase-change from gaseous state to liquid state of the former, and phase-change from gaseous state to super critical state of the latter. This do also result in different density behaviour of the CO_2, where there is a sudden, dramatic increase for the former, and a smooth, continuous exponential increase for the latter.

- The rate of mass-transfer is higher at 25°C than 45°C, which might be attributed to higher solubility, which leads to a greater concentration gradient and greater driving force for diffusion at lower temperatures.

- The rate of mass transfer increases with pressure, the same argument as made in the previous bullet-point, about solubility increase can be made for this statement.

- The magnitude of the equilibrium volume is higher at 25°C than for 45°C. It is suggested that this is caused by the greater solubility of CO_2 in the surrounding nanofluid at lower temperatures, which results in greater mass-transfer before equalization of the concentration gradient.

- The rate of volume increase slows down as time increases with an initially *saturated* system at the commencement of the experiments. This is logical as the mass-transfer is driven by a concentration gradient which is decreasing with time. The opposite effect is however **initially** observed when the experiments

are commencing in the *gradually saturated* system, the rate of volume increase slows down with time.

- The equilibrium volume increases with pressure for all concentrations of nanofluid, this seems to be unconditionally true at 45°C, and partially true at 25°C, where the equilibrium volume experience a decrease at 70 bar, and then continues to increase. This decrease is concluded to result from the density increase when CO_2 changes state of matter (phase) to liquid. The isothermal limit in which the phase-change would be from gaseous to super-critical and not gaseous to liquid is 31.03°C.

- For pressures above 30 bar, maximum equilibrium volume is generally observed for the intermittent concentration of nanofluid (0.5 g/l), it is argued and reasoned that this is due to 0.5 g/l nanofluid promotes a higher solubility of CO_2 in the environment. This also means that it exists a possible optimum concentration of nanofluid with regards to EOR, in which the mobility of displaced oil can be reduced to offer greater recovery.

- The concentration of nanofluid seems to be less significant at lower pressures, this might be because the solubility of CO_2 in the basefluid (DIW) is originally low at those conditions.

- The increase in equilibrium volume with pressure experiense an increasing growth with pressure, which fades off at higher pressures.

- Equilibrium volume is continuously increasing with pressure until the phase-change pressure of CO_2 is superseded. The equilibrium volume experiences a reduction at this point and then continues to increase. This is evident at 25°C. For 45°C, a similar phenomenon is observed, but the equilibrium volume do not drop below the volume at the preceding pressure.

- Even though the equilibrium volume is reduced at the phase-change boarder, the mole fraction of CO_2 in the *n*-decane drop is continuously increasing, and the phenomenon is therefore suggested to be caused by the density change of CO_2. This statement is confirmed by comparing densities, mole fraction and equilibrium volume. Moreover, this study have carried out experiments on both sides of the gaseous/liquid phase-line for CO_2 as well as on both sides of the gaseous/supercritical phase-line. This has revealed the great influence of the state of matter of CO_2, and especially the density effects on swelling. The effects extends heavily to the interfacial tension which is discussed later in the *Results and Discussion*

- The solubility of CO_2 in the surrounding phase is believed to play an important role in the magnitude of the volume increase. This is rooted in the existence of a greater concentration gradient that needs to be equalised.

- Contrary to at 25°C, the rate of volume increase at 45°C is observed to have a tendency of being higher after phase-change. This can again be caused by the fact that after phase-change, systems at 25°Cand 4°Cexperience different state of matter of the CO_2

- *Saturated* systems seems to be affected to a greater extend by CO_2 phase-change.
- 0.5 g/l DIW-CNF as surrounding phase results in a slightly lower equilibrium volume at low pressures, but clearly outperforms the two other concentration at higher pressures, with respect to swelling. The performance seems a bit inconsistent right around CO_2 phase change pressure. But an effect of the nanofluid concentration is evident.
- The effect of temperature on volume increase is low for low pressures, but large as pressure increases.
- Lower temperature results in greater volume increase. This is one of the reasons solubility of CO_2 in the surrounding phase is believed to play a vital role.

5.2 Mole Fraction

Diffusion of CO_2 into the drop occurs, and the equilibrium mole fraction of CO_2 in n-decane is obtained on the premise that the change in drop volume from $t = 0$ to $t = t_{equilibrium}$ has to be the volume of CO_2 present.The equilibrium mole fraction is obtained by equation 5.1 to 5.2.

$$MF_{CO_2} = \frac{n_{CO_2}}{n_{CO_2} + n_{C_{10}}}, \tag{5.1}$$

where MF is mole fraction and n is the total number of moles. The mole fraction can then be calculated by applying the change in volume and well known properties of the two components from the literature. The results in equation 5.2, which is directly applied to calculate the mole fraction of CO_2 in the drop based on experimentally obtained volume data.

$$MF_{CO_2} = \frac{\frac{\Delta V \cdot \rho_{CO_2}(p,t)}{MW_{CO_2}}}{\frac{\Delta V \cdot \rho_{CO_2}(p,t)}{MW_{CO_2}} + \frac{V_0 \cdot \rho_{C10}(p,t)}{MW_{C_{10}}}}, \tag{5.2}$$

where ΔV is the change in volume, V_0 is the initial volume of pure n-decane, ρ is the density of the pure substance at the given pressure and temperature, MW is molecular weight, and the sub-scripts, CO_2 and C_{10}, is carbon dioxide and n-decane, respectively.

5.2.1 Effect of the Nanofluid concentration on CO_2 content in the *n*-decane drop.

Figure 5.24 shows the equilibrium mole fractions of CO_2 in the drop, for the three different concentrations of nanofluid as environmental-phase, at 25°Cand pressure range from 10 to 90 bar. The experiments were carried out with CO_2 saturated nanofluid, i.e. at the commencement of the experiment, the nanofluid are saturated with CO_2, with a continuous supply.

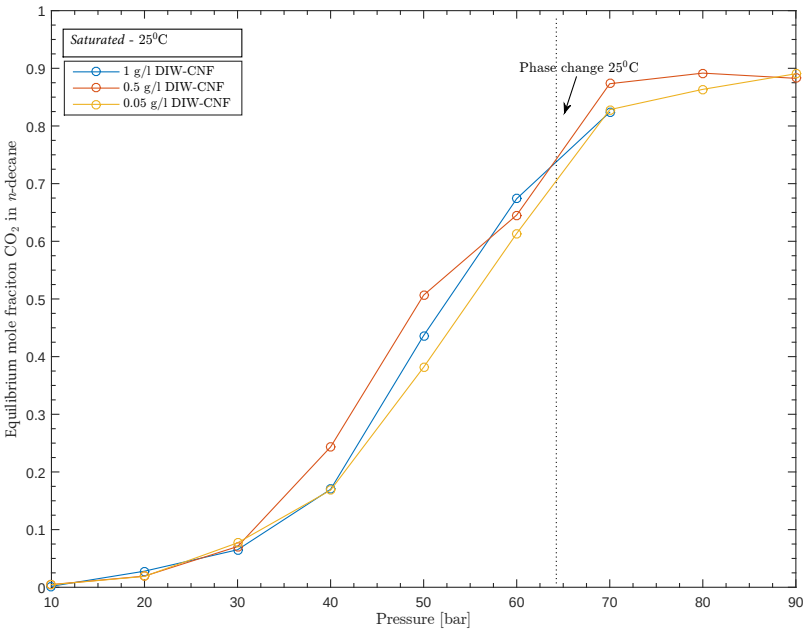

Figure 5.24: Equilibrium mole fraction of CO_2 in *n*-decane. Comparison of mole fraction of CO_2 in *n*-decane, for saturated nanofluids at 25°Cand pressures from 10 to 90 bar.

It is observed that the general trend is an exponential growth, which fades and flattens out into an S-curve. This is true for all three concentrations of nanofluid (0.05, 0.5 and 1 g/l). As it can be seen, the equilibrium CO_2 content in *n*-decane increases with pressure, as expected. Three main observations. At low pressures (P <30/40 bar), there is almost no difference in the CO_2 content for the different nanofluid concentrations. A steep increase of CO_2 mole fraction in the *n*-decane is evident as the pressure increases above about 30/40 bar. The third observation is that the CO_2 mole fractions of the different nanofluid concentrations become more similar above the point of phase change ($\approx$ 65 bar). Additionaly, it can be seen that the mole fraction do not behave the same as the volume when the pressure is beyond phase-change pressure for CO_2. Interestingly, this shows that the trend in amount of CO_2 that is transported into *n*-decane is not affected in the same fashion as volume by the state of matter of CO_2. Moreover, it is observed that the mole fractions is similar among concentrations at low pressure ($P < 40$) bar and at high pressure ($P > 80$) bar. In the interval 40 bar $\leq$ P $\leq$ 80 bar, an environment consisting of 0.5 g/l nanofluid generally achieves a higher mole fraction of CO_2 than the two others (with the expetion at 60 bar, which might be experimental error). It has also been observed in the volume increase section that this concentration is a possible optimum.

Figure 5.25 depicts a similar plot as figure 5.24, but for a *gradually saturated* environment. A similar trend as for *saturated* experiments is observed. It is believed that 60 bar 0.05 g/l DIW-CNF is an erroneous reading.
Figure 5.25 through 5.27 shows the mole fraction of all concentrations versus pressure for *saturated* 25°C, *gradually saturated* 25°C, *saturated* 45°C and *gradually saturated* 45°C, repsectively. The 0.5 g/l DIW-CNF seems to generally transfer more CO_2 to the drop. 0.05 g/l is behaving very similar to 0.5 g/l, while 1 g/l DIW-CNF result in

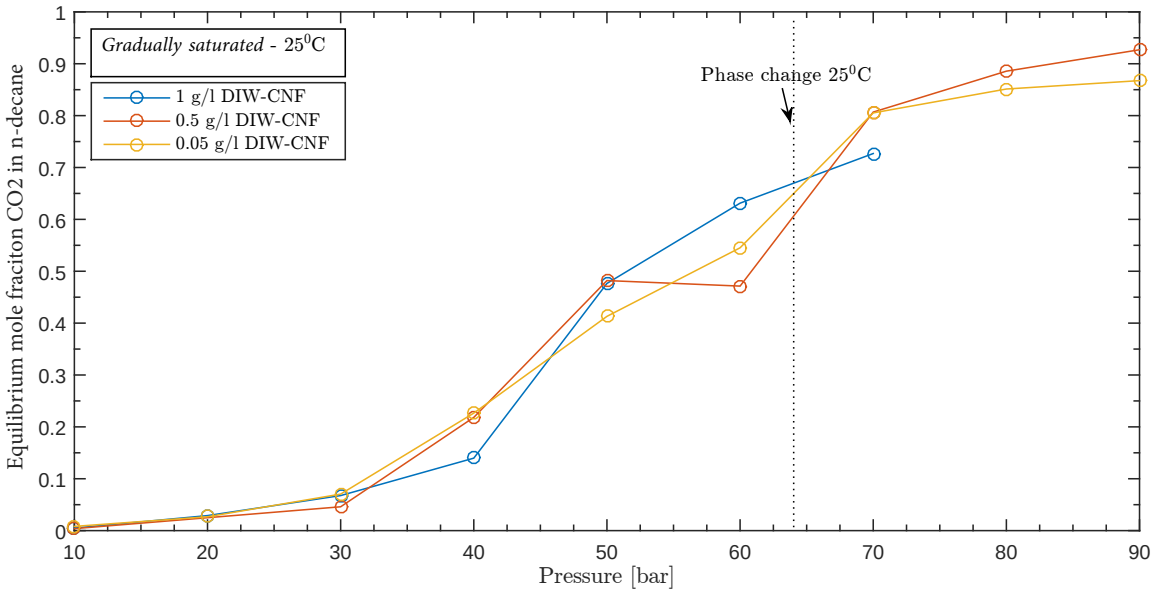

Figure 5.25: Equilibrium mole fraction of CO_2 in *n*-decane. Comparison of mole fraction of CO_2 in *n*-decane, for *gradually saturated* nanofluids at 25°Cand pressures from 10 to 90 bar.

the *n*-decane drop containg the least CO_2. The mole fraction of CO_2 in the drop is, among others, directly related to the behaviour of viscosity of the drop. As discussed in the respective *viscosity*-discussion, a reduced viscosity lessens the resistance of oil to flow, in this case *n*-decane. It can therefor be said on a general basis that the more CO_2 transported into the oil, the better for the recovery. The highest mole fraction, generally as a result of 0.5 g/l nanofluid environment, can therefore be said to be the optimum concentration (among the three investigated) for EOR in this particular isolated scenario. Moreover, a higher mole fraction of CO_2, results in a greater oil swelling (discussed in section 5.1), increased relative permeability and increased mobility ratio. Effectively this means that the displacing phase during CNFI actually mobilises the displaced phase and alters the mobility ratio between them as injection is carried out.

In figure 5.26, the 0.05 g/l DIW-CNF point at 80 bar is believed to be a bit low, and that the trend should follow a similar patern as the two other concentrations. However, if it is correct, it would mean that the particular concentration of nanofluid makes the mass-transfer behave differently across the pressure at which the CO_2 changes from gaseous phase to super critical. This is not seen in other cases and deemed unlikely. Further, it may then be noted that that this trend (low point at 80 bar) is seen in both approaches (*saturated* and *gradually saturated*, however, it is lower in the case of *gradually saturated* approach.

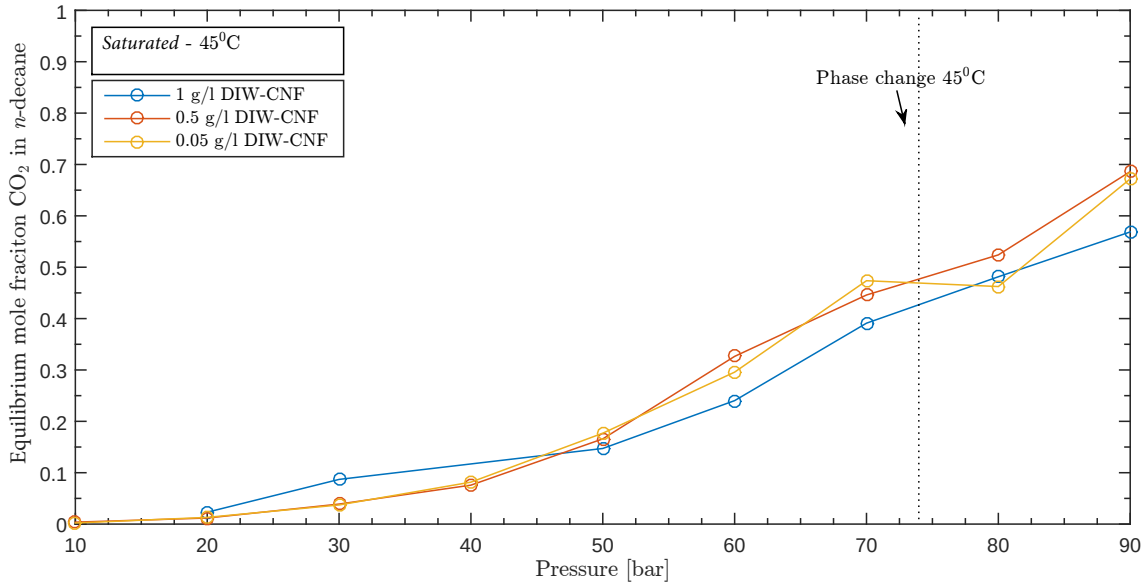

Figure 5.26: Equilibrium mole fraction of CO_2 in n-decane. Comparison of mole fraction of CO_2 in n-decane, for *saturated* nanofluids at 45°Cand pressures from 10 to 90 bar.

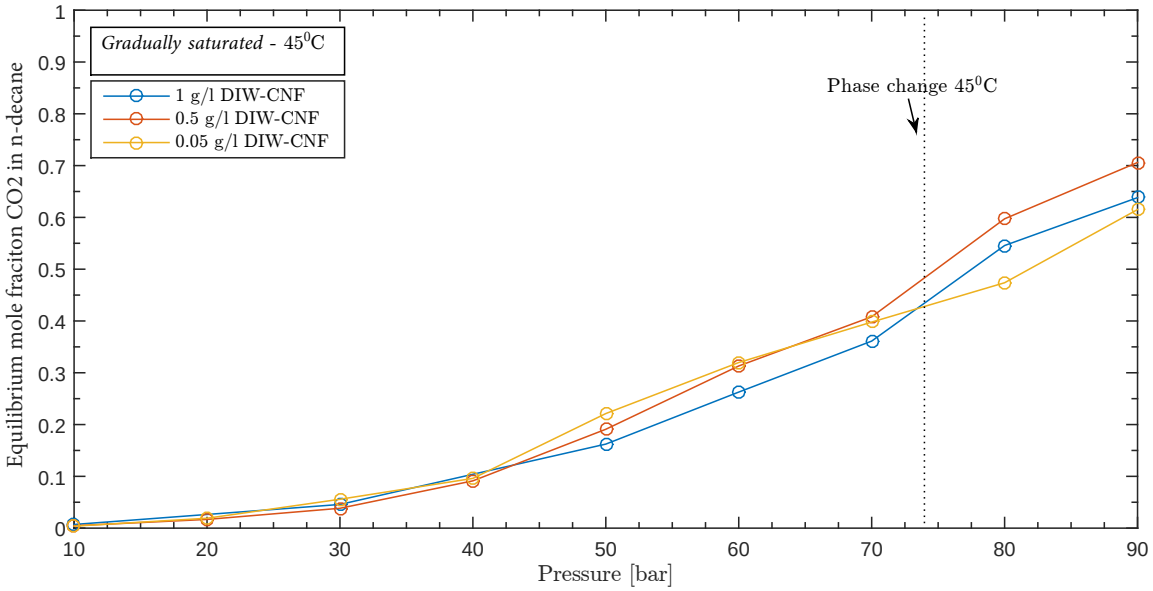

Figure 5.27: Equilibrium mole fraction of CO_2 in n-decane. Comparison of mole fraction of CO_2 in n-decane, for *gradually saturated* nanofluids at 45°Cand pressures from 10 to 90 bar.

5.2.2 Effect of Temperature on CO_2 content in the *n*-decane drop.

Figure 5.28 shows the comparison of 25°C and 45°C for *saturated* 1 g/l DIW-CNF, where it can be observed that the temperature plays a less significant role on the mole fraction for pressures lower than 40 bar. At 40 bar the lower temperature starts to deviate largely, and much more CO_2 is present at a particular pressure than for 45°C. Two major differences between 25°C and 45°C are present; 1) the phase-change of CO_2 occurs over the dew-point line for 25°C, while CO_2 at 45°C transform directly from gaseous state to super critical. This has previously been argumented for not playing a signifacnt role on the equilibrium mole fraction. 2) Solubility of CO_2 in DIW-NF at 25°C is higher than at 45°C. The mole fraction reached a plateau at 70 bar when the temperature was 25°C, where further increase with pressure is minimal, this plateau is probably reached for 45°C outside of the range of these experiment. It is done sensitivity on all scenarios with respect to temperature (*gradually saturated and saturated for 0.05, 0.5 and 1 g/l*),which is plotted in figures 5.28 to 5.33. There are 2/104 data-points that are believed to be erroneous, in the sense that they deviate in an un-natural fashion. In addition, these deviations occur in regions where previous plots have showed to be stable. The two points are 80 bar 45°C in fig. 5.30 and 60 bar 25°Cin fig. 5.33. The comparison among temperatures results in the conclusion that much higher mass transfer of CO_2 occurs at lower temperatures in the DIW-CNF/*n*-decane system. This can again be attributed to the higher solubility of the environment-phase at lower temperatures, discussed in chapter 5.1. Comparing the mole fraction further strengthens this argument, as the solubility of the basefluid (DIW) do also reach a plateau at 70 bar for 25°Cand 100 bar (outside the range of the experiments) at 45°C. This can be seen in figure 3.13, presented in chapter 3.

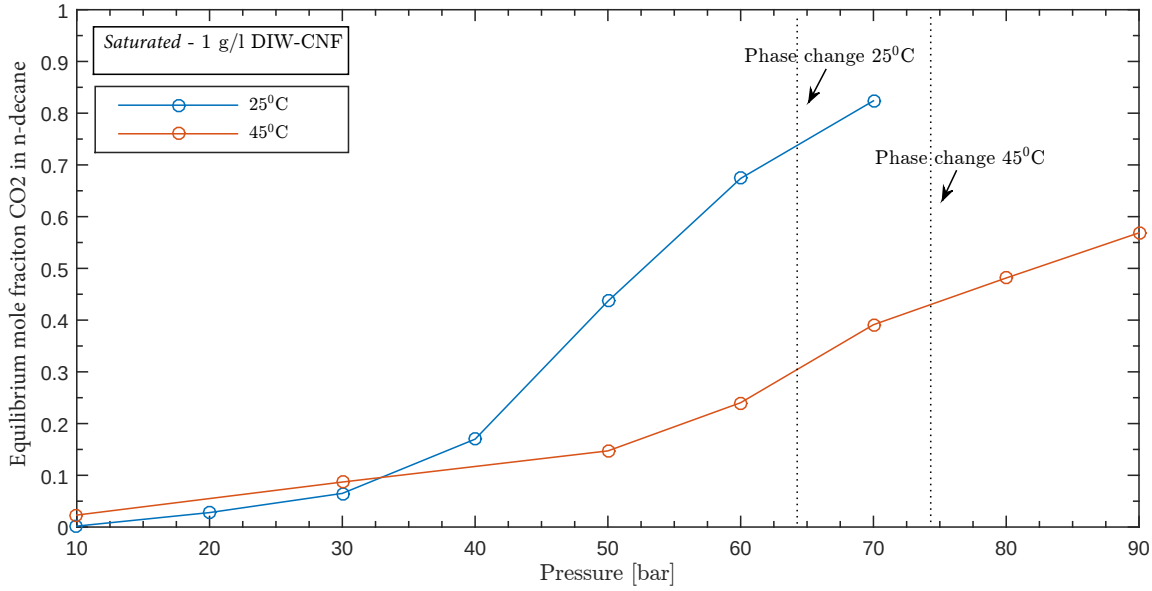

Figure 5.28: Equilibrium mole fraction of CO_2 in *n*-decane. Comparison among temperatures. Environment: DIW-CNF 1 g/l, *saturated*

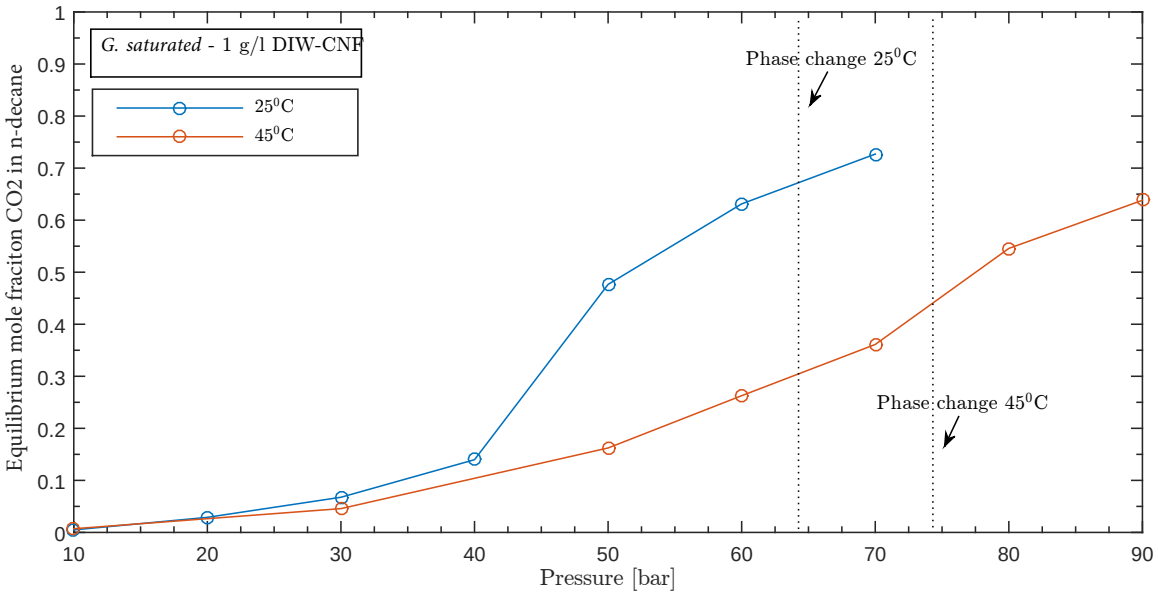

Figure 5.29: Equilibrium mole fraction of CO_2 in *n*-decane. Comparison among temperatures. Environment: DIW-CNF 1 g/l, *gradually saturated*

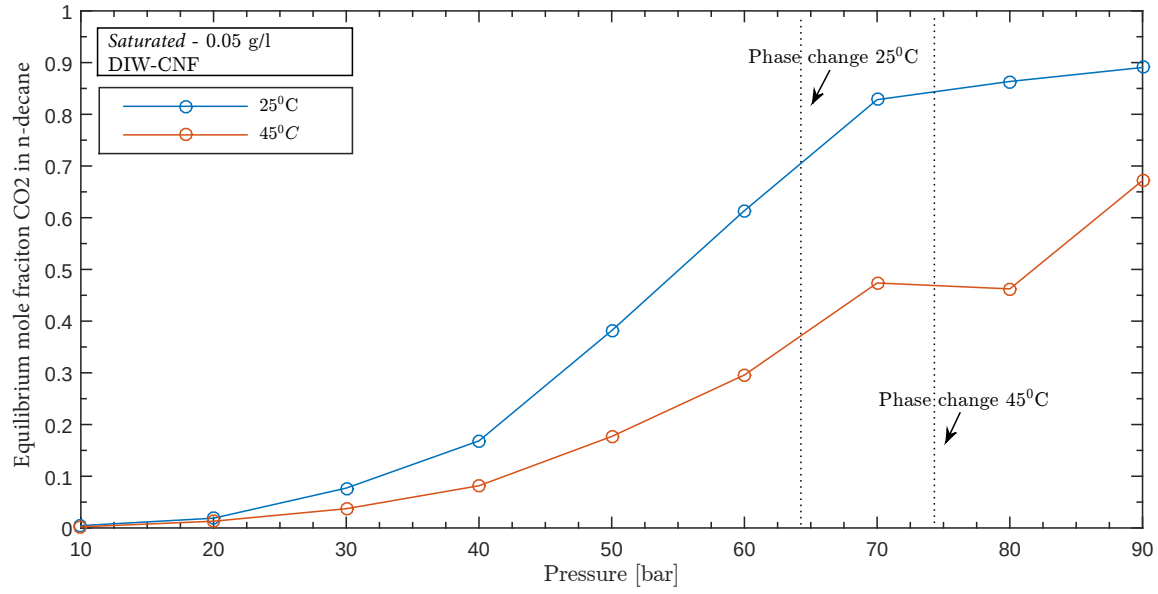

Figure 5.30: Equilibrium mole fraction of CO_2 in *n*-decane. Comparison among temperatures. Environment: DIW-CNF 0.05 g/l, *saturated*

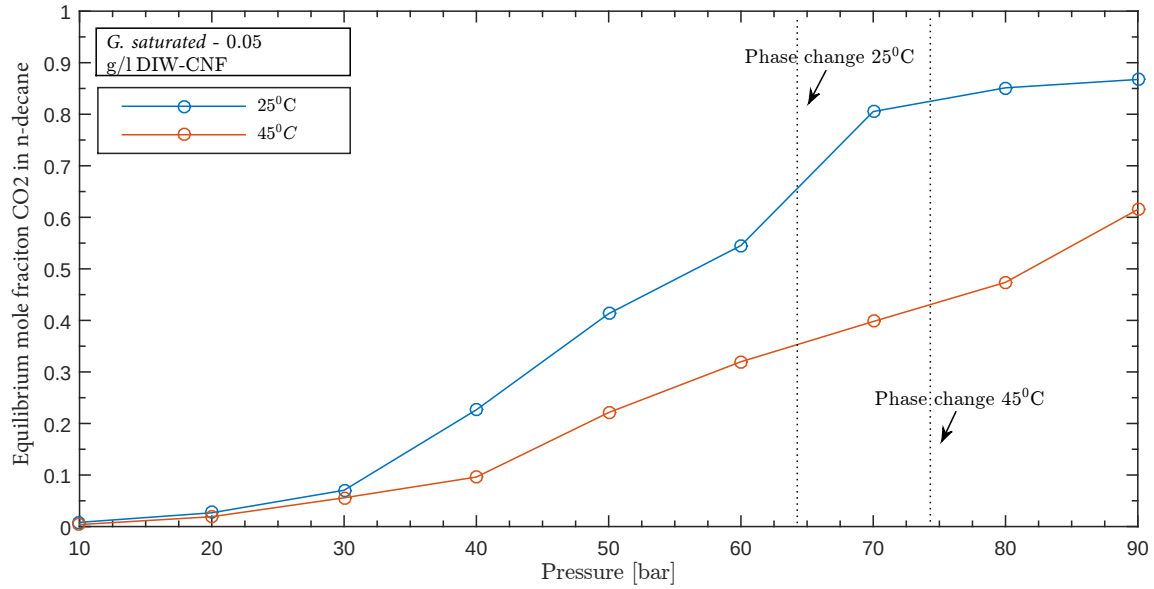

Figure 5.31: Equilibrium mole fraction of CO_2 in *n*-decane. Comparison among temperatures. Environment: DIW-CNF 0.05 g/l, *gradually saturated*

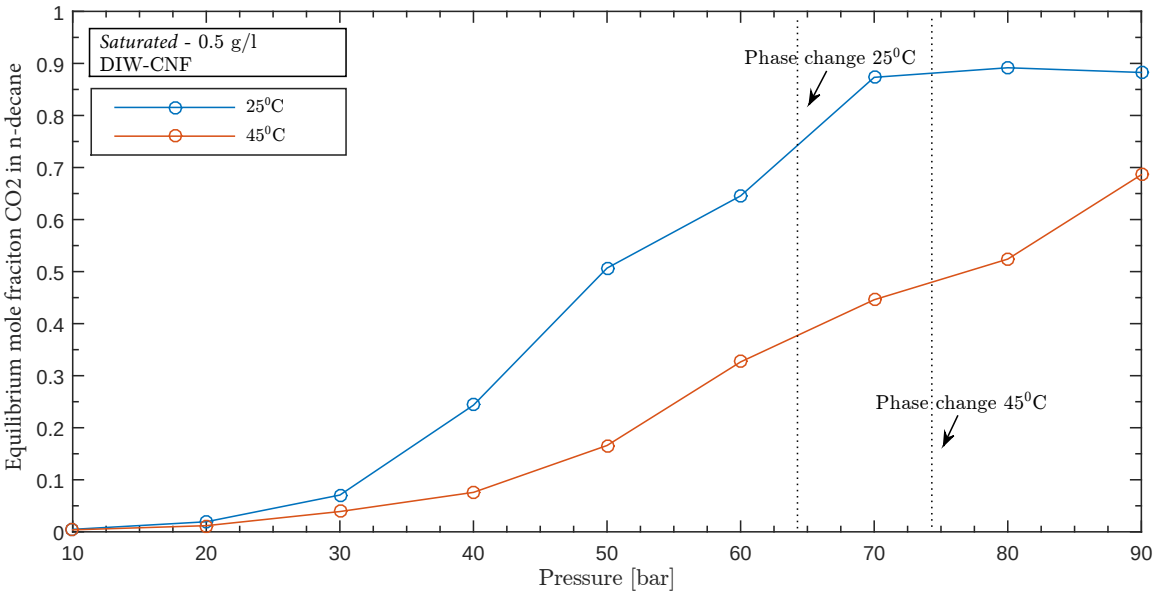

Figure 5.32: Equilibrium mole fraction of CO_2 in *n*-decane. Comparison among temperatures. Environment: DIW-CNF 0.5 g/l, *saturated*

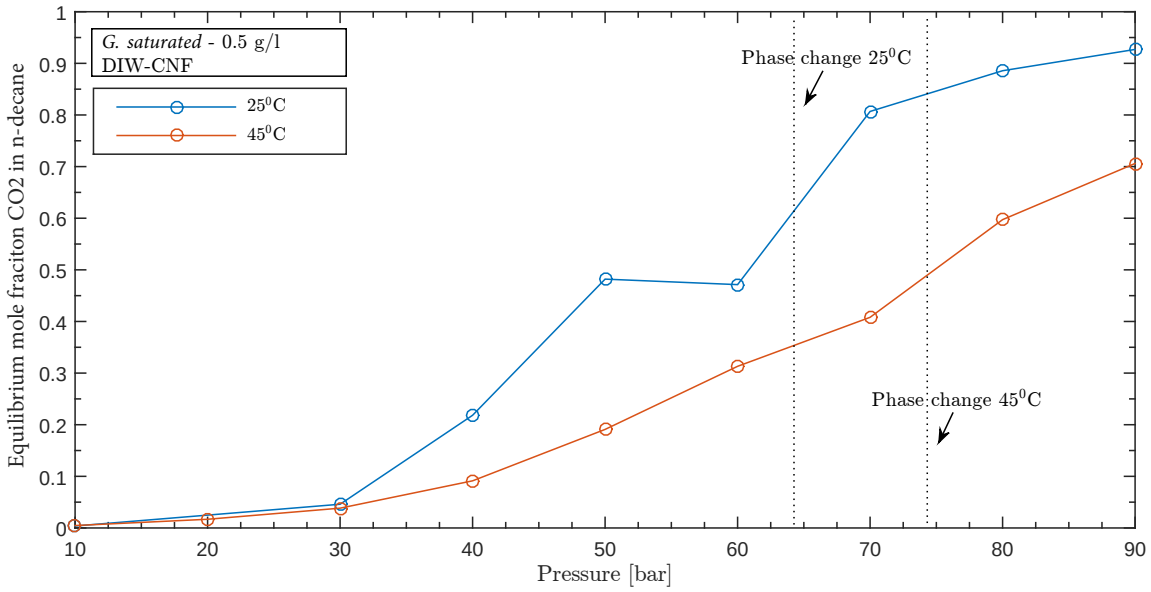

Figure 5.33: Equilibrium mole fraction of CO_2 in *n*-decane. Comparison among temperatures. Environment: DIW-CNF 0.5 g/l, *gradually saturated*

5.2.3 Comparison Among *Saturated* and *Gradually Saturated* Environment

The scenarios at different temperatures are plotted simultaneously as the same scenarios with different surrounding environments in figur 5.34 to 5.36 in order to investigate the significancy of environment on transfer of CO_2 and mole fraction. The environment seems to have a low significancy comparing it to the effect of temperature, the variance seen amongenvironments are probably within the error margin. However, it can be noted that *saturated* environments might result in a bit more CO_2 present in the drop, even though it is very slightly. Comparing the impact of saturation-mode to effect of temperature on the equilibrium mole fraction, it may be concluded that temperature plays a more significant role on the equilibrium mole fraction than saturation-mode. This may be linked to the solubility, as discussed. However, it is important to stress that the claim about insignificany of environment (*saturated* or *gradually saturated*) is only for equilibrium mole fraction. As soon as the time-perspective and dynamic mole fraction is taken into consideration large differences are evident, this is because the equilibrium mole fraction do not say anything about how long time it took to reach equilibrium. This time-period differs from the *saturated* and *gradually saturated* experiments. This has already been discussed in section 5.1. Accounting for the duration is essential when it comes to CCS and EOR, to be able to know whether the equilibrium is reached, or how much CO_2 have been transferred. Diffusion is discussed in section 5.6.

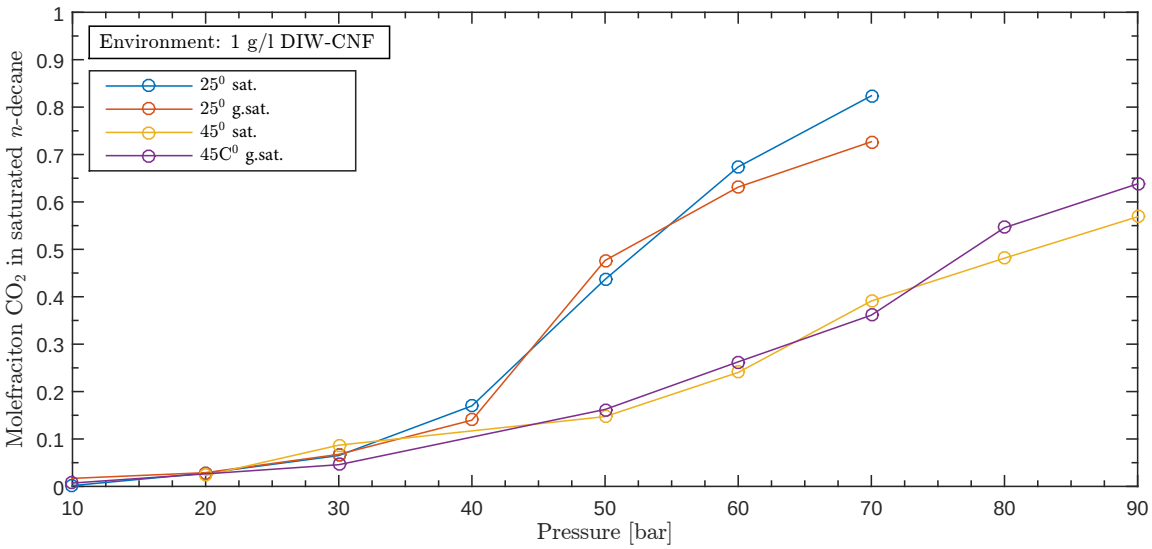

Figure 5.34: Equilibrium mole fraction of CO_2 in *n*-decane. Comparison among environments. Environment: DIW-CNF 1 g/l

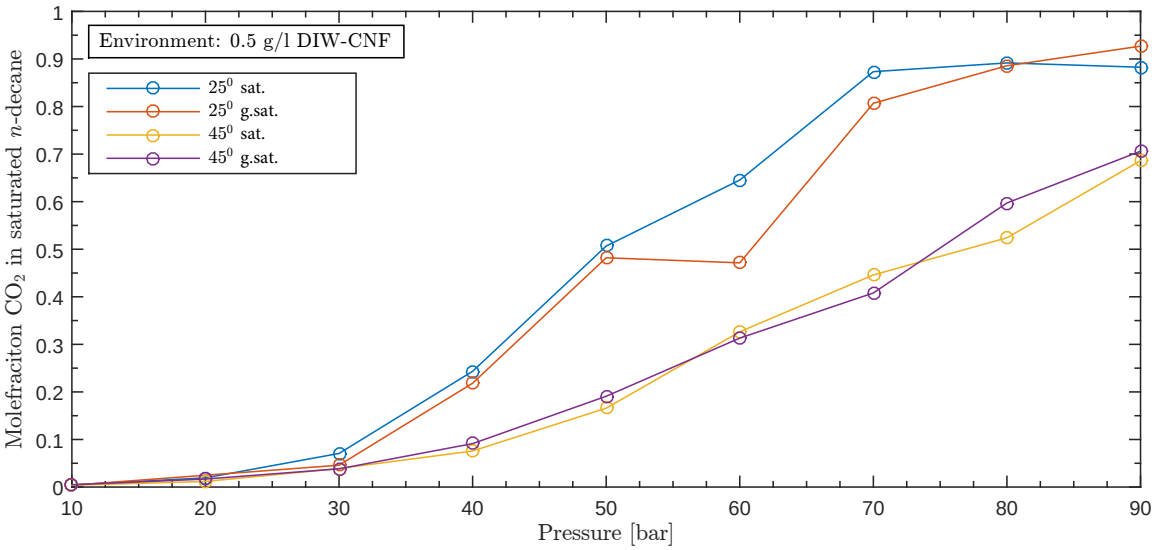

Figure 5.35: Equilibrium mole fraction of CO_2 in n-decane. Comparison among environments. Environment: DIW-CNF 05 g/l

[h]

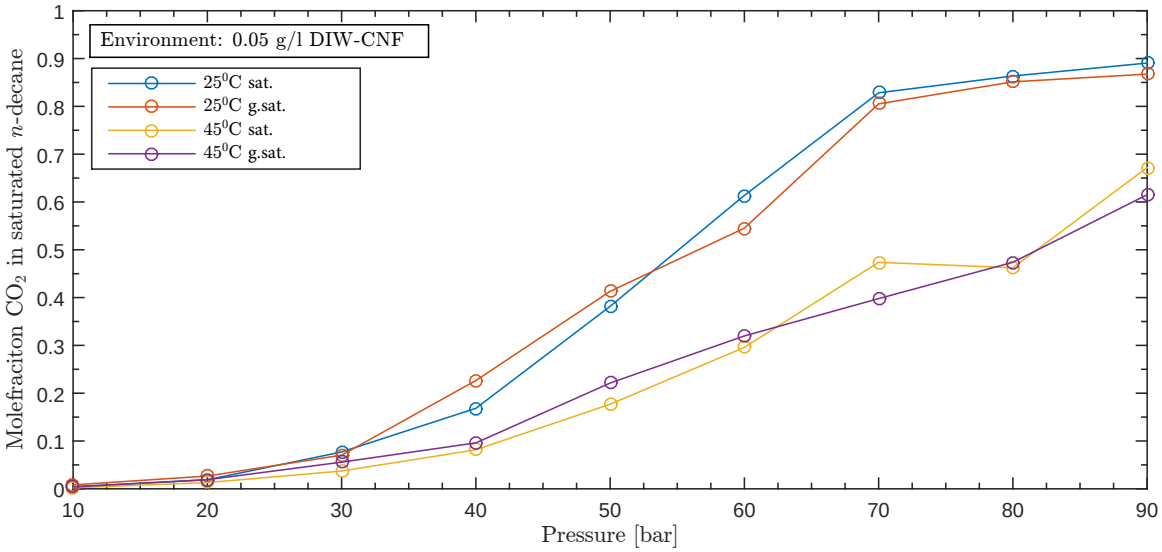

Figure 5.36: Equilibrium mole fraction of CO_2 in n-decane. Comparison among environments. Environment: DIW-CNF 005 g/l

5.2.4 Summarising Points on Equilibrium Mole Fraction

- The behaviour of equilibrium mole fraction with pressure is unaffected by whether free CO_2 is in a gaseous , liquid or super critical state. i.e no sudden changes in the mole fraction trend is observed as pressure is increased past $P = P_{liq}$ and $P = P_{cri}$.
- The concentration of the nanofluid has little influence on the equilibrium mole fraction at pressures below 40 bar.
- The highest equilibrium mole fraction is generally caused by an environment of 0.5 g/l DIW-CNF for 40 bar $\leq$ P $\leq$ 80 bar.
- Overall, the 0.5 g/l DIW-CNF results in the highest equilibrium mole fraction.
- The effect of temperature on equilibrium mole fraction is small at P $<$ 40 bar.
- Lower temperatures shows signifant higher equilibrium mole fraction at P $\geq$ 40 bar
- CO_2 solubility in the environment is most likely the major contributor to the behaviour of equilibrium mole fraction in the drop
- The environment (*saturated* or *gradually saturated*) do not substantially affect the equilibrium mole fraction, as the magnitude at equilibrium is not affected by the time it took the achieve it.
- The effect of temperature and pressure is the dominant contributors to the behaviour of the equilibrium mole fraction.

5.3 Density of an *n*-decane Drop Surrounded by Carbonated Nanofluid

When CO_2 is transported into the *n*-decane drop, the density of the drop is altered. As mass-transfer is governed by the concentration gradient of CO_2 between the environment and the drop, the transport will be larger initially, when the gradient is the greatest. As more and more CO_2 is transported, the gradient reduces, and the mass-transfer will therefore be slower and slower with time. Figure 5.37 shows the dynamic density change of the drop with time, at 30 bar. At this pressure, CO_2 is lighter than *n*-decane and a decrease in drop density can be observed as CO_2 is transported into the drop. It is important to understand the dynamic density behaviour of the drop when for instance considering the dynamic interfacial tension, which is discussed in chapter 5.5. When the CO_2 gradient is redused to zero, the amount of CO_2 in the drop is constant, it follows that the density also reaches equilibrium at this point. The equilibrium for this particular case is reached just after 200 minutes. For equilibrium interfacial tension calculations, this equilibrium density is used as input.

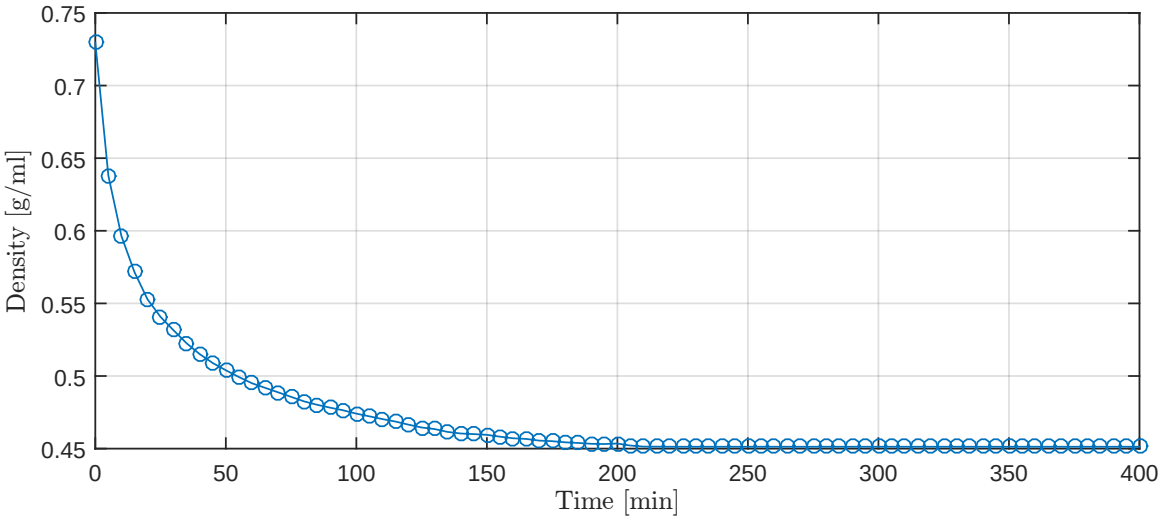

Figure 5.37: Dynamic density of an *n*-decane drop surrounded by CO_2 saturated 0.5 g/l nanofluid at 25°C

5.3.1 The Effect of Nanofluid Concentration on the Density of a CO_2-containing *n*-decane drop

Figure 5.38 compares the density of the *n*-decane drop exposed to environments of the 3 different concentrations of DIW-CNF. It may be observed a slight difference in density of the drops occurs at pressure lower than the phase-change region of CO_2 (P<64 bar). It does however seem evident that the density of a drop exposed to the 0.5 g/l DIW-NF have a tendency to be lower of the three concentrations (0.05, 0.5 and 1 g/l. Once the CO_2-liquid-region is attained, the density experiences a large shift for greater density. These observations together with the observations made in the *volume change chapter* (ch.5.1), where the volume experiences a dip across the phase-change pressure, complement each other. This also suggests that the density

of CO_2 have a significant effect on the density of the *n*-decane drop in this system. It also confirms the contribution of CO_2 density on the volume increase of the drop. Figure 5.4 refers back to the volume plot.

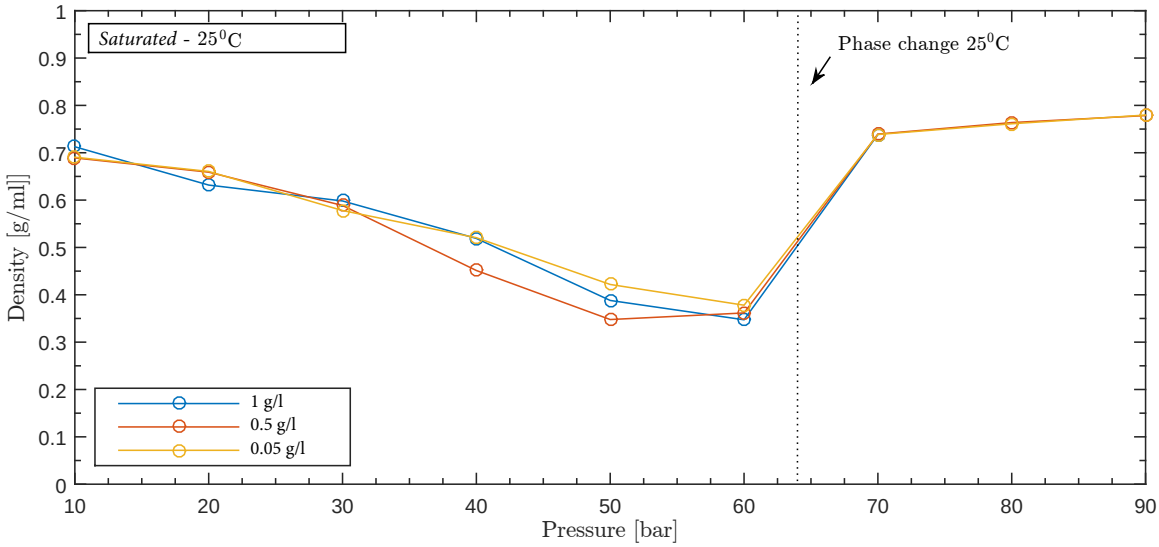

Figure 5.38: Density comparison of *n*-decane in a CO_2/*n*-decane/NF (0.05 g/, 0.5 g/l, 1 g/l) system at *saturated*, 25°C.

Density of the *n*-decane drop surrounded by the three concentrations (0.05, 0.5, and 1 g/l) at 45°Care compared in figure 5.39, the behaviour of the drop-density when CO_2 crosses to super critical state from gaseous may be observed. A similar trend of decrease in density of the drop can be observed for pressures below 70 bar, it is however observed to a lesser extent. It is observed a decrease in the density of the drop with pressure, but the rate at which this happens is lower for the higher temperature. When the pressure for super critical CO_2 is reached, the density of the drop increases slightly. Contrary to CO_2 at 25°C, the density change with pressure at 45°Cis continuous (ch. 2.2) and do not experience a sudden jump. The slope of the density increase do however increase. Despite this, there is a slight increase in the density across the phase-change pressure at 45°C. It is suggested that the increased solubility and swelling, as well as the density of CO_2 is contributing factors to the *n*-decane drop density. The increased solubility in the environment results in higher driving force for diffusion, a higher swelling, and in combination with CO_2 density, these factors are suggested to be the governing properties with respect to density of the drop until super critical state for CO_2 is reached. After the critical point is reached, the solubility of the environment increases, but not quit eas much, the swelling do also therefore increase a bit, which favours density decrease. However, the CO_2 density increases with a higher rate a this point and becomes dominant, which results in an elevated drop density. However, this is not observed in figure 5.41, where the density of the drop at 45°Cin a *gradually saturated* environment is plotted. This will be discussed in the next section, where phase-sets are compared. It is generally observed a larger difference among concentrations for *gradually saturated*, and especially at 45°C, where and environment of 0.5 g/l DIW-CNF certainly has the lowest density.

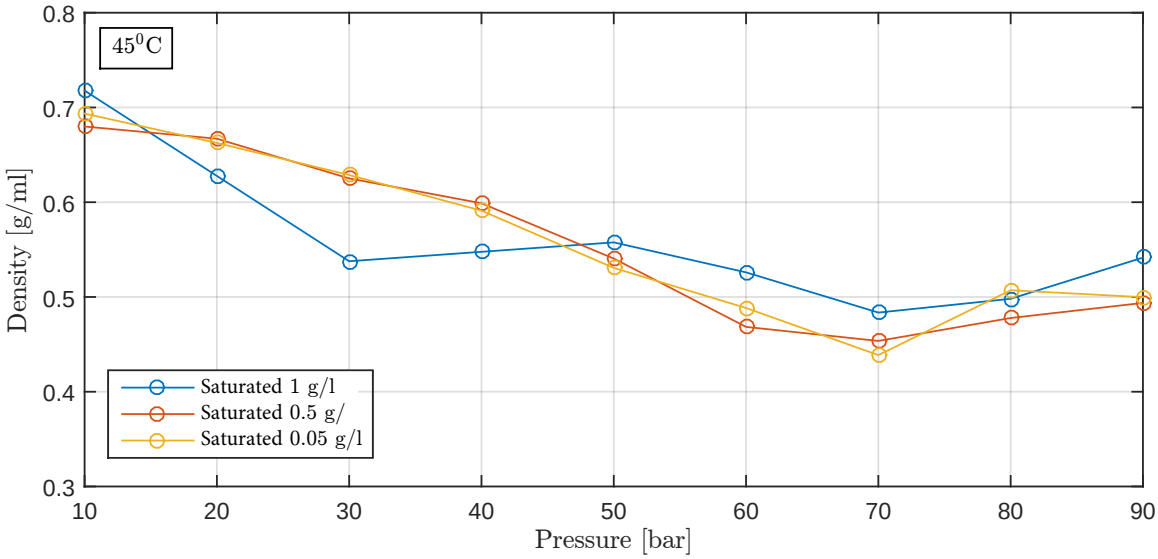

Figure 5.39: Density comparison of *n*-decane in a CO_2/*n*-decane/NF (0.05 g/, 0.5 g/l, 1 g/l) system at *saturated*, 45°C.

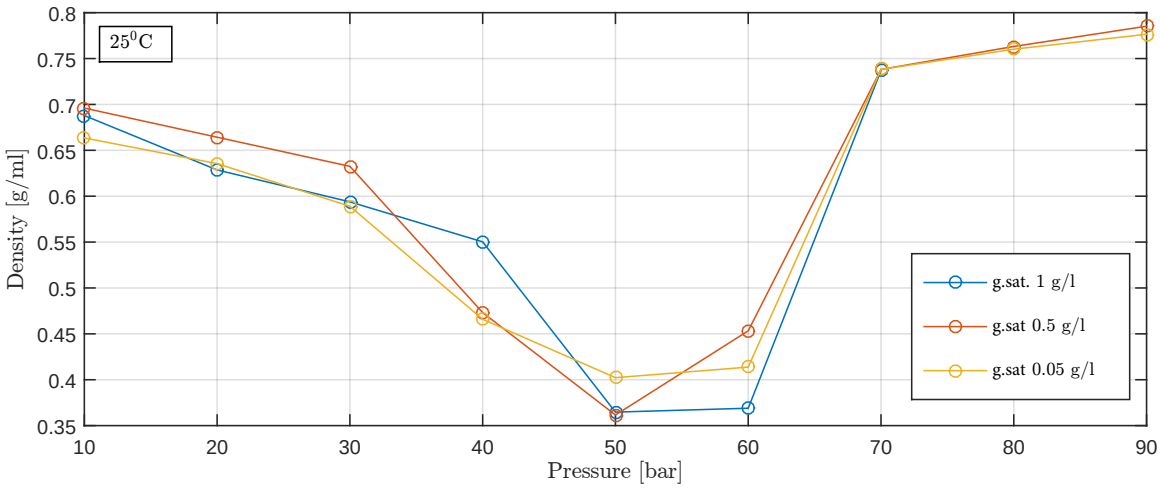

Figure 5.40: Density comparison of *n*-decane in a CO_2/*n*-decane/NF (0.05 g/, 0.5 g/l, 1 g/l) system at *gradually saturated*, 25°C.

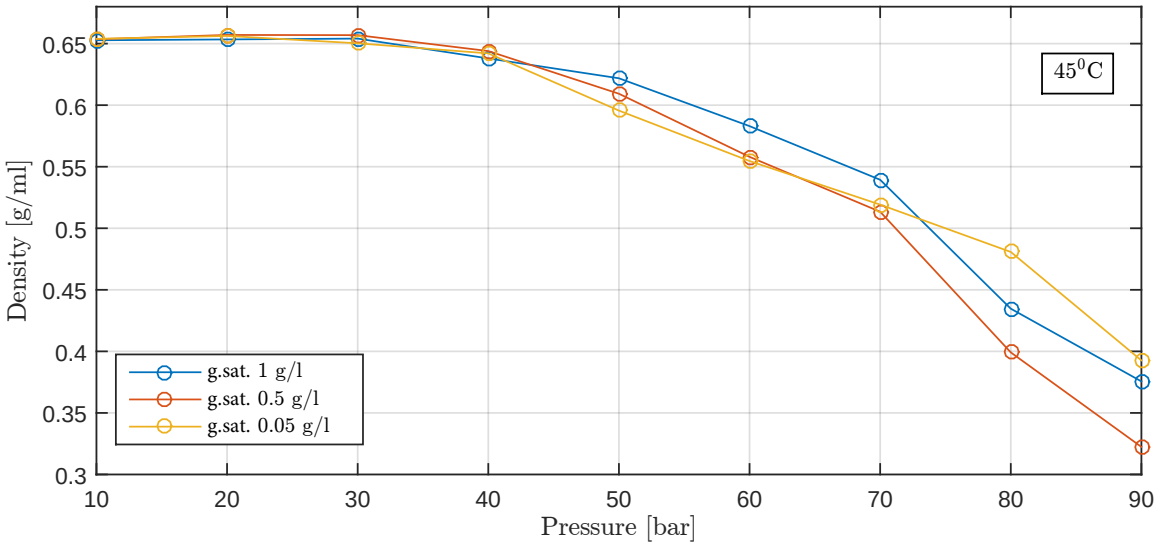

Figure 5.41: Density comparison of *n*-decane in a CO_2/*n*-decane/NF (0.05 g/, 0.5 g/l, 1 g/l) system at *gradually saturated*, 45°C.

5.3.2 The effect of *saturated* and *gradually saturated* CO_2 Environments on a CO_2-conaining *n*-decane drop

Figure 5.42 compares the two environments (*saturated* and *gradually saturated*) for 25°Cfor all concentrations (0.05, 0.5 and 1 g/l). The environment do not seem to have much effect for the lower temperature. Similar observations as for the *saturated* 25°Cenvironment can be observed for the *gradually saturated* 25°C also. It is somewhat larger differences at pressures lower than 70 bar. Quite interestingly, in the liquid region of CO_2 (P > 64 bar) there is almost no difference in the density of the drop. This is suggested to be due to the large density increase of CO_2, which shifts it to be very close to the density of pure *n*-decane. The influence of varying amount of CO_2 in the drop then becomes insignficant in determining the behaviour of the total drop density.

Figure 5.43 shows the same plot as Figure 5.42, but for 45°C, the same observations can not be made. For the *saturated*, there is a distinct increase in the density of the drop after supercritical CO_2 pressure is reached, which is not observed for the *gradually saturated*. Instead, a coninously distinct decrease is observed for the whole pressure range. The explenation has to be a lower transport of CO_2 across the interface between nanofluid and *n*-decane, as CO_2 would at these pressures elevate the density upwards as the density of CO_2 is greater than the pure *n-decane*. Generally, it is also observed more variation in the *gradually saturated*.

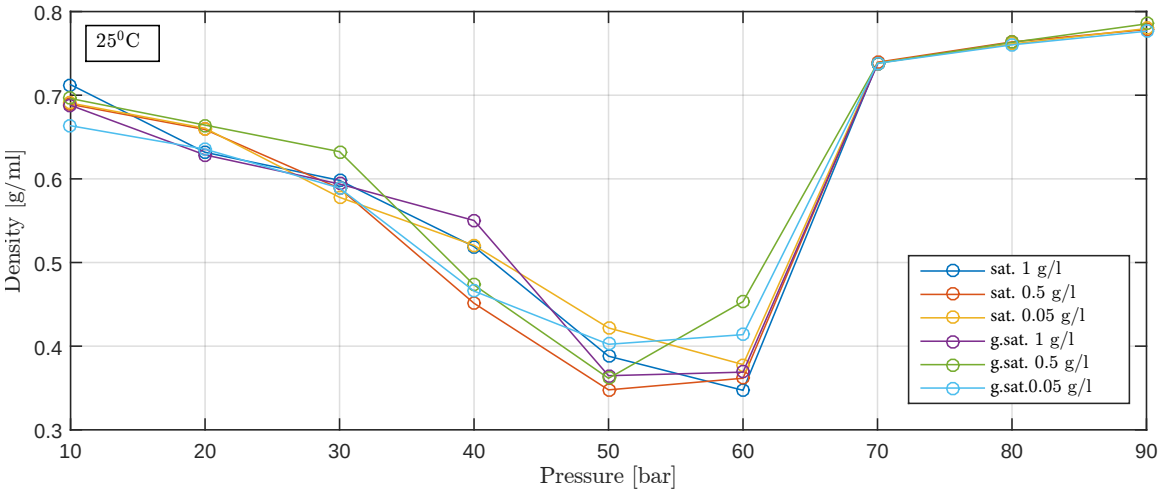

Figure 5.42: Density comparison of *n*-decane in a CO_2/*n*-decane/NF (0.05 g/, 0.5 g/l, 1 g/l) system at *saturated*- and *gradually saturated*, 25°C.

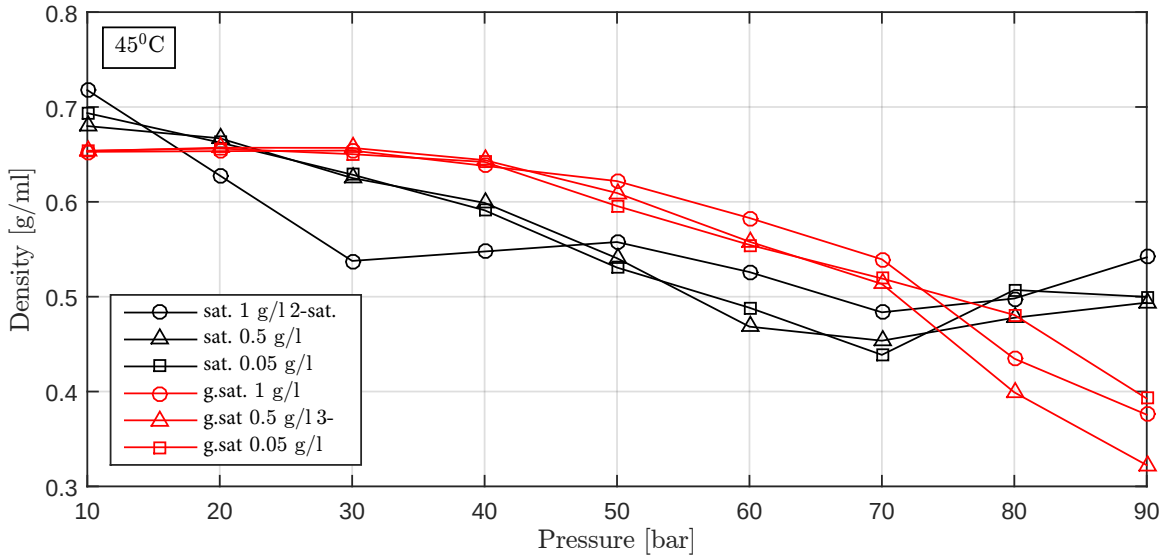

Figure 5.43: Density comparison of *n*-decane in a CO_2/*n*-decane/NF (0.05 g/, 0.5 g/l, 1 g/l) system at *saturated*- and *gradually saturated*, 45°C.

5.3.3 The effect of Temperature on a CO_2-conaining *n*-decane drop

Figure 5.44 and 5.45 shows the comparison of all the concentrations for the two temperatures, for *saturated* and *gradually saturated*, respectively. The lower pressures seems to be less important on density when it comes to temperature. It can be observed in both figures (Fig. 5.44 and 5.45), that the densities are quite similar for pressures lower than 40 bar, especially for *gradually saturated* (Fig. 5.45). It can be clearly seen that 25°C experience a greater negative change in drop density than 45°C and the extreme effect across the phase-change boarders are much more evident when changing from gaseous to liquid, than from gaseous to super critical. The phenomenon of more similar densities among environments at these pressures are evident. It is believed that the 30 bar 45°C 1 g/l point which is lower than the 25°C for the same pressure is an error.

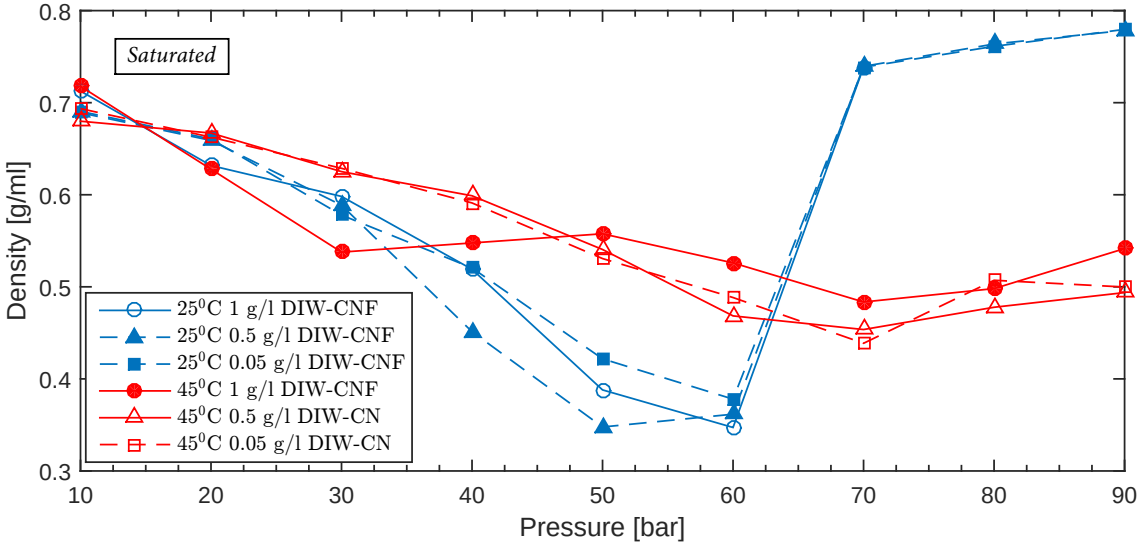

Figure 5.44: Density comparison of *n*-decane in a CO_2/*n*-decane/NF (0.05 g/, 0.5 g/l, 1 g/l) system at *saturated*, 25 and 45°C.

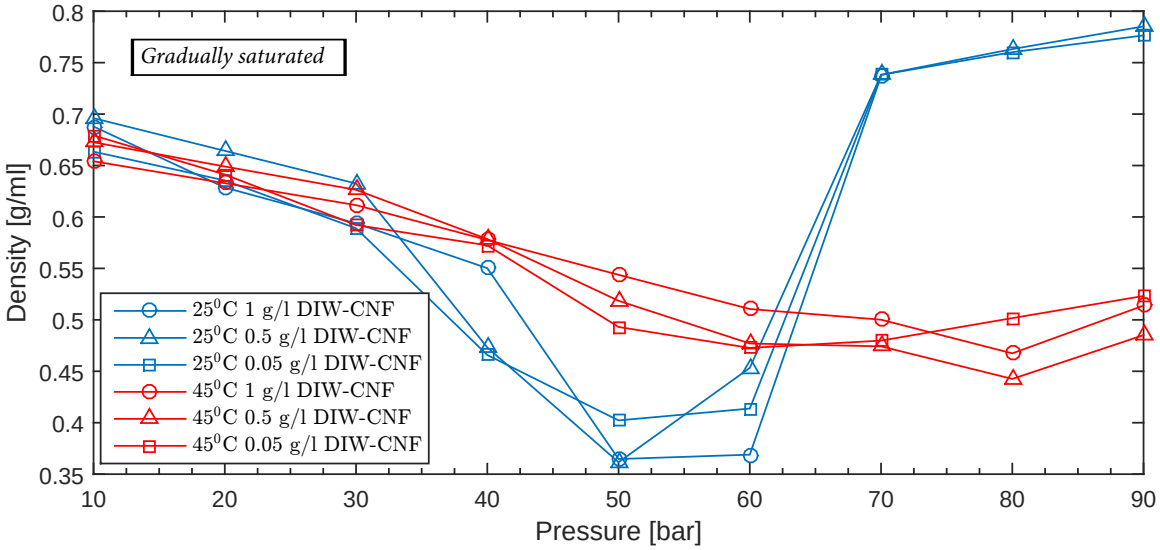

Figure 5.45: Density comparison of *n*-decane in a CO_2/*n*-decane/NF (0.05 g/, 0.5 g/l, 1 g/l) system at *gradually saturated*, 25 and 45°C.

5.4 Viscosity

5.4.1 Comparison Among Concentrations

The viscosity with pressure is presented in figure 5.46 to 5.49. It can be observed that it behaves inverse of the mole fraction,

$$\mu \propto MF^{-1},$$

which is logical as the viscosity is calculated based on mole fraction of CO_2 pressent. It is, however, still a derived value from experiments as the volume, and hence mole fraction, is obtained experimentally. The viscosity decreases with pressure, and it seems like the 0.5 DIW-CNF environment performs best. Similar behaviour as observed in other properties is observed around phase change for *saturated*. In terms of mobility alteration for EOR, the 0.5 DIW-CNF would yield a better result in both *saturated* 25°C and 45°C scenarios according to *n*-decane/CNF experiments. For *saturated* environment, the decrease in viscosity becomes larger with pressure until liquid phase change of CO_2, where it still decreases, but flattens out. For 45°Cthe decrease seems to become unconditionally greater with pressure, within this pressure range. The difference in viscosity among concentrations are smaller at lower pressures.

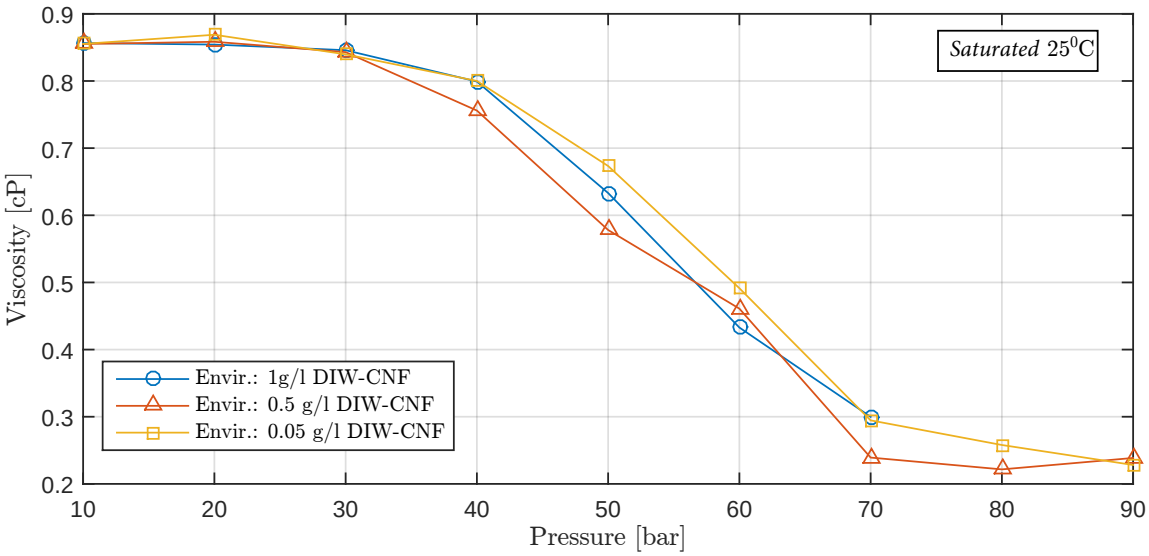

Figure 5.46: Viscosity comparison of n-decane in a CO_2/n-decane/NF (0.05 g/, 0.5 g/l, 1 g/l) system at *saturated*, 25°C.

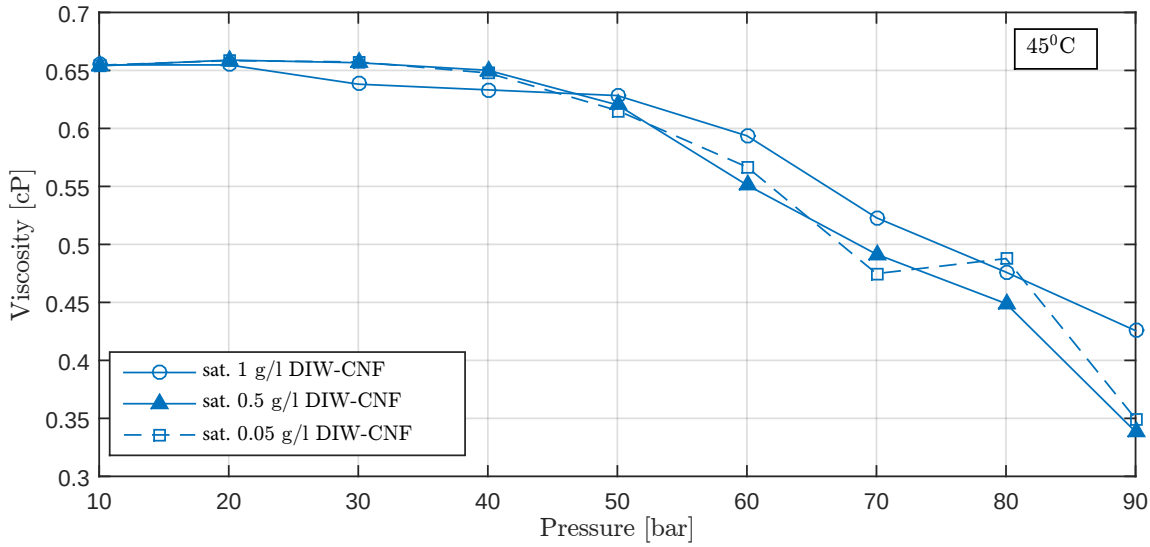

Figure 5.47: Viscosity comparison of n-decane in a CO_2/n-decane/NF (0.05 g/, 0.5 g/l, 1 g/l) system at *saturated*, 45°C.

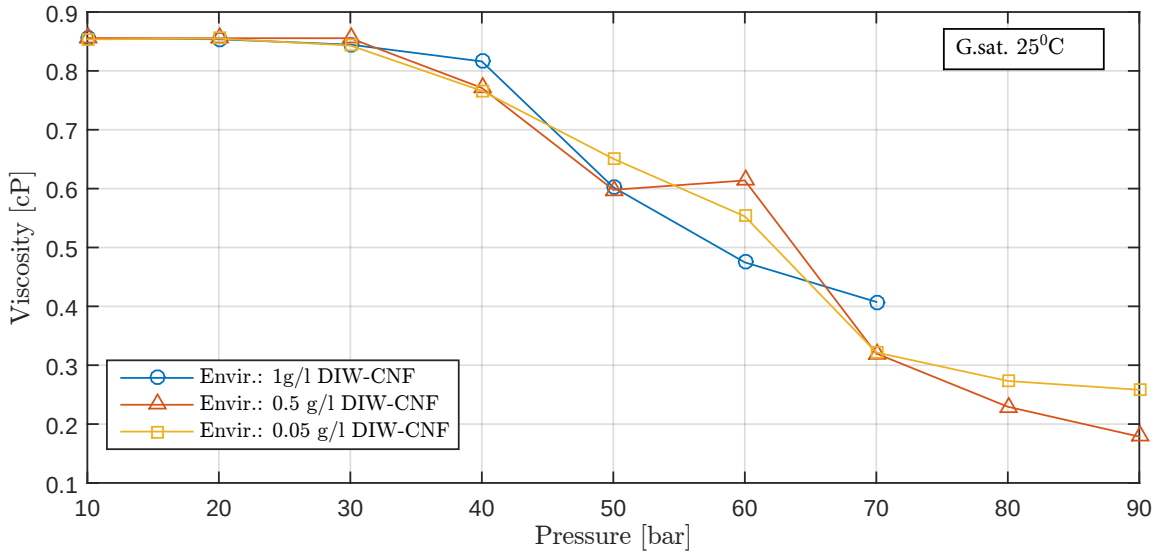

Figure 5.48: Viscosity comparison of *n*-decane in a CO_2/*n*-decane/NF (0.05 g/, 0.5 g/l, 1 g/l) system at *gradually saturated*, 25°C.

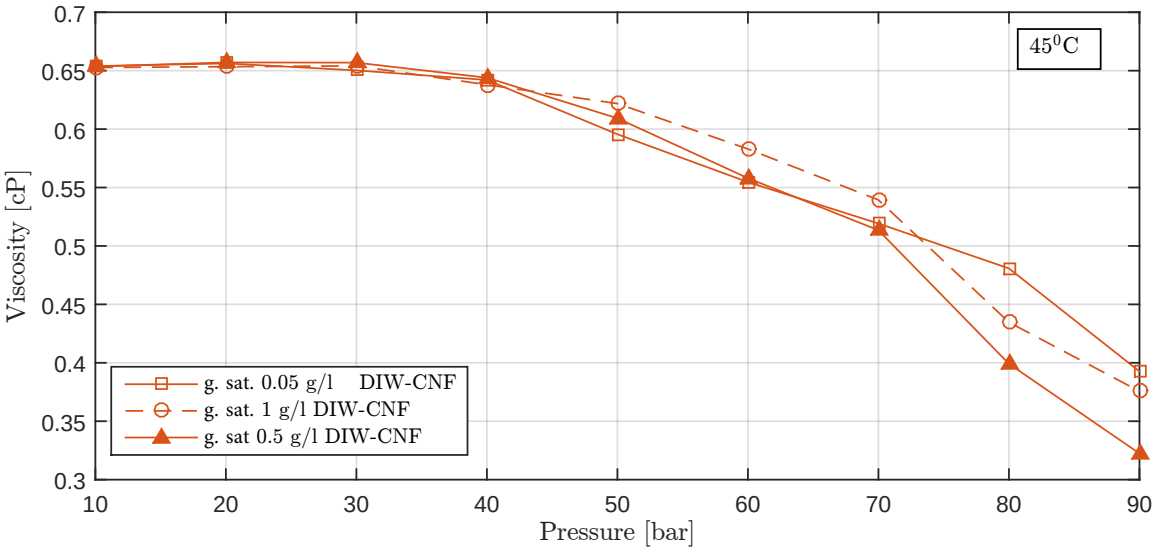

Figure 5.49: Viscosity comparison of *n*-decane in a CO_2/*n*-decane/NF (0.05 g/, 0.5 g/l, 1 g/l) system at *gradually saturated*, 45°C.

5.4.2 Comparison Among Phase-Sets

Figure 5.50 and 5.51 shows the phase-set-comparison of both 25°Cand 45°C, which seems to play an insignificant role on the equilibrium viscosity. At lower pressures there is almost no difference, at higher pressure the difference between the cases are a little bit larger, but the differences are not decided into *saturated*-or *gradually saturated*, and it can be concluded that the phase do not matter on the equilibrium viscosity.

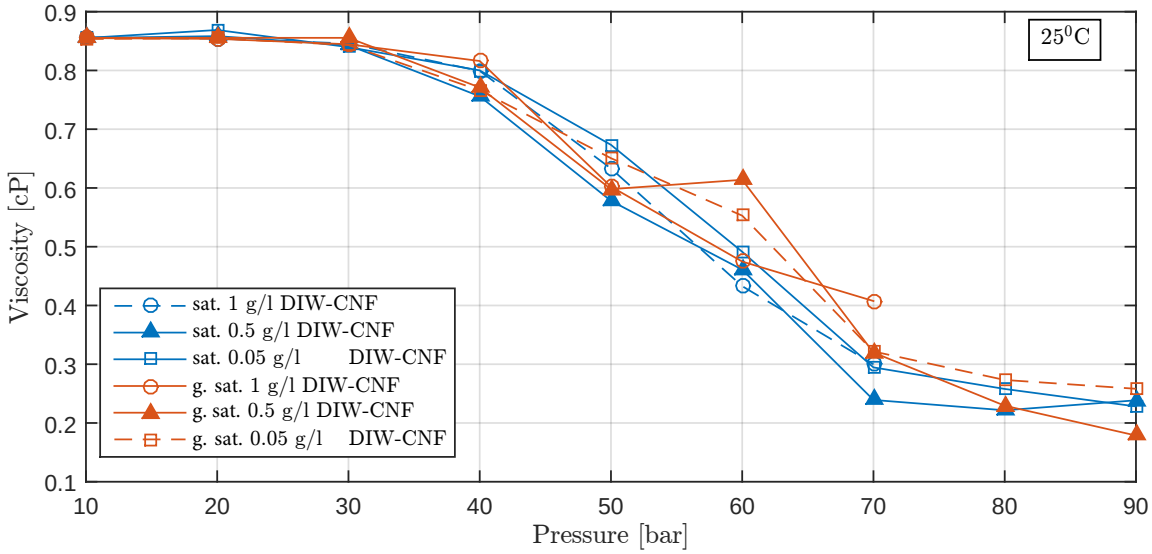

Figure 5.50: Viscosity comparison of *n*-decane in a CO_2/*n*-decane/NF (0.05 g/, 0.5 g/l, 1 g/l) system at *saturated*- and *gradually saturated*, 25°C.

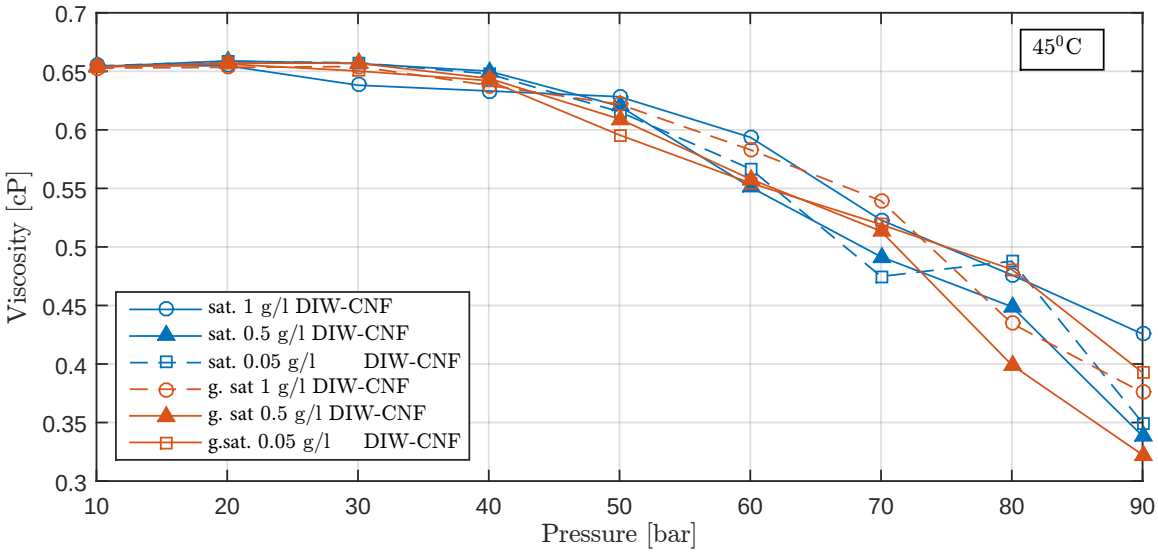

Figure 5.51: Viscosity comparison of *n*-decane in a CO_2/*n*-decane/NF (0.05 g/, 0.5 g/l, 1 g/l) system at *saturated*- and *gradually saturated*, 45°C.

5.4.3 Comparison Among Temperature

Figure 5.52 shows the comparison among temperatures at *saturated* conditions, where at lower pressures, the viscosity at 25°C is higher than for 45°C, this is as expected because only small amounts of CO_2 is present in the drop, and the *n*-decane becomes less prone to resist flowing at higher temperatures because of greater movement of the molecules. However, as the pressure increases, more CO_2 enter the drop at 25°C-conditions than for 45°C-conditions, and a crossing point becomes evident, where the effect of more CO_2 entering the drop overcomes the effect of reduced viscosity from temperature. This point occurs around 50 bar for both *saturated* and *saturated* environments. This means that temperature in itself is more dominant on viscosity at pressures < 50 bar, but the solubility, driving force, swelling and effect of CO_2 becomes the dominant factor in drop viscosity at greater pressures.

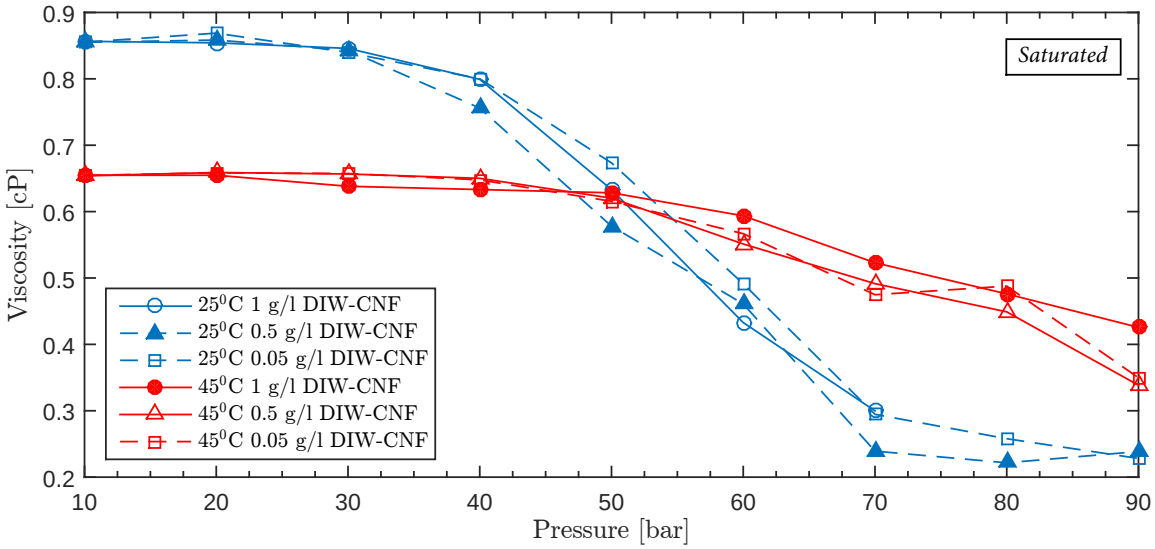

Figure 5.52: Viscosityy comparison of *n*-decane in a CO_2/*n*-decane/NF (0.05 g/, 0.5 g/l, 1 g/l) system at *saturated*, 25 and 45°C.

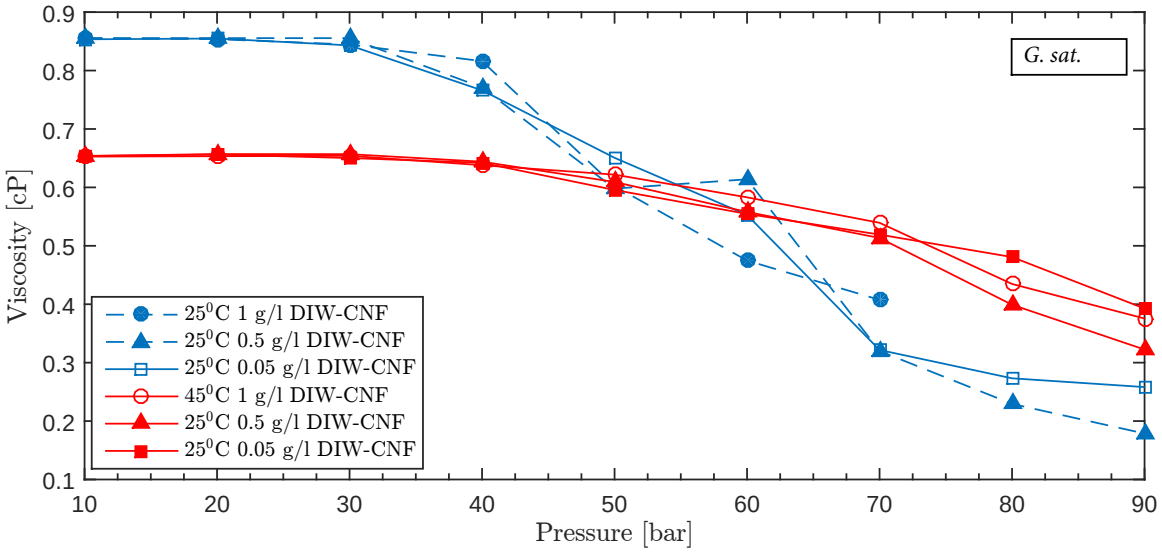

Figure 5.53: Viscosity comparison of *n*-decane in a CO_2/*n*-decane/NF (0.05 g/, 0.5 g/l, 1 g/l) system at *gradually saturated*, 25 and 45°C.

5.5 Interfacial Tension Between the Pendant *n*-decane drop and Carbonated Nanofluid

Interfacial tension (IFT) is calculated with th DSA4 software provided by Krüss, this software has viscosity and density of both the drop and the environment as input, and calculates the IFT based on that input together with the profile-shape of the drop and its contact angle relative to a baseline. The baseline is the intersection between the drop and the capillary tube. However, the software is only capable of static input parameters for viscosity and density, which means that in a dynamic process like CO_2 diffusion into *n*-decane, it is crucial to understand which values to feed as input. The equilibrium IFT is the most valuable parameter for analysis done in this work, as it can be evaluated in the light of diffusion coefficients. Thus the density of the drop at equilibrium volume is used as input. This ensures that the IFT calculated by DSA4 will be correct when the dynamic calculation of IFT reaches equilibrium. This also means data-points presented of a dynamic IFT is not neccesarrily the true value until equilibrium is reached. A procedure for calculating correct dynamic IFT is suggested, but not applied due time limitations. The proposed method would; 1) Be to generate large tables with the dynamic density of the drop for all 188 scenarios. A spreadsheet capable of generating these tables has been made, and used for obtaining equilibrium density. 2) Create a program, possibly in Python, with utilisation of the pygui-package to automate a stop/start routine of the IFT calculation, and input the respective density at any given point in time. Creating this program in itself is not too difficult, but as the dynamic density needs to be given at one exact point in time, it is difficult to automatically stop the DSA4 calculation at precisely that time-step, especially as the speed of calculation is not uniform. A solution might be to use pixel-recognition of the time-numbers, or simply doing it manually. However, the time consumed by either making the program, or do it manually is far from a justifiable time utilisation, at least in the time-frame of this thesis-work. However, it

is done for one case for comparison and general discussion, and to emphasise that it must be accounted for in dynamic IFT calculations, this is discussed in section 5.5.1. It is important to stress that even though these limitations exist, a lot of information can be extracted, and one can be confident of the values presented as equilibrium IFT, as well as the length of the time-period before equilibrium is reached.

5.5.1 The Effect of Pressure on Dynamic Interfacial Tension

Figure 5.54 depicts the flaw of utilising a static density input in the Krüss software. One graph shows the dynamic IFT calculated with static density input, while the other shows the same case, but the density input has been manually changed in time intervals of five minutes to generate a dynamic density input. As discussed (sec. 5.5), this is extremely tedious work and done only for this particular case. The points beetween 80 and 120 bar for the dynamic-density case was intentionally not generated due to time prioritising.

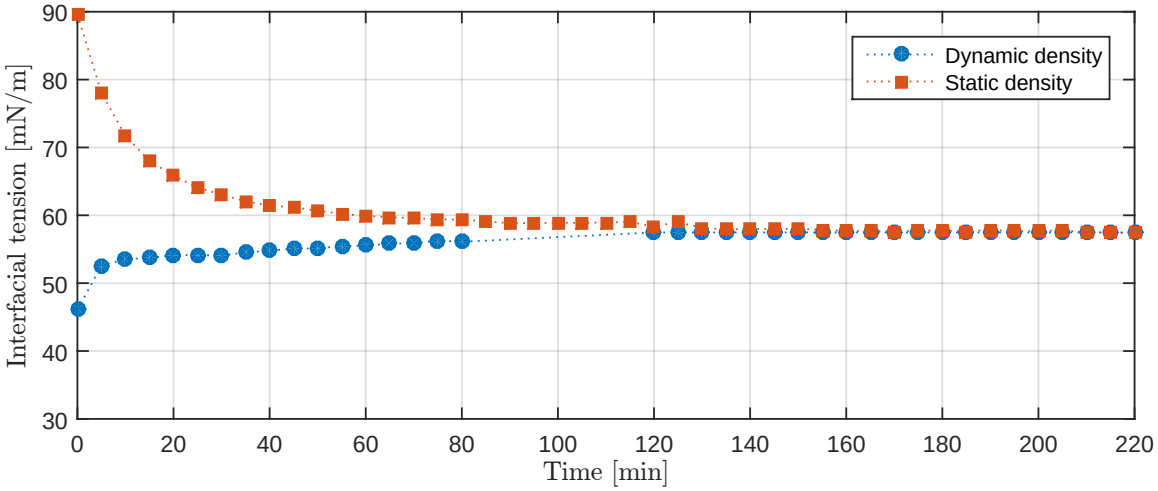

Figure 5.54: Comparison of dynamic interfacial tension [mN/m] for the same record with static and dynamic density as input. (40 bar).

It can be observed (fig. 5.54) that regardless of dynamic or static density input, the equilibrium IFT is identical, this is because of the input of equilibrium density in the static case. The fact that they are identical was known before this comparison by knowing the method of the Krüss DSA4 software calculations, and this serves as proof for validity of presented equilibrium IFT. The dynamic density do actually follow a similar trend as the dynamic IFT calculated with static density (may be seen in fig. 5.37), which is the reason for the reverse trends between dynamic- and static-density calculated IFT. Reducing the density of the drop, effectively increases the density difference over the interface, which increases the IFT, this is seen explicitly in in terms of CW/CNF surroundings, and *n*-decane drop. In terms of CO_2 free gas diffusing into oil, the opposite is evident as the density difference is reduced, and not increased, by diffusion of CO_2. This is duscussed more in section 5.5.2, where the effect of pressure on the IFT is discussed.

Studying figure 5.55, which is plotted with the use of static IFT, it does not accomadate discussion around the magnitude of the dynamic IFT values, however, it is

observed that the equilibrium IFT between the drop and the environment is increased with pressure. At 25°C, the IFT decreases drastically when the pressure at which free CO_2 changes state of matter is surpassed (64 bar). This phase-change is from gaseous to liquid state. This is unexpected results, and is extensively discussed, justified and confirmed in the comparison versus pressure (ch. 5.5.2). The current section will focus on the behaviour with time. The change to equilibrium occurs smoothly, but at higher pressures ($P \geq 50$ bar) tend to oscillate before equilibrium is reached. The IFT is dependent on the density difference (see discussion on fig. 5.61), which is changing at difference rates for the different cases, but also on the shape of the drop, which tries to minimise its surface area and energy. The oscillations are believed to be an effect of a rapid increase and a more unstable achievement of minimum energy at the surface. Figure 5.56, 5.57 and 5.57 shows the oscillations individually for representation purposes. The oscillations seems to be generally larger for *gradually saturated* environments than for *saturated ones*.

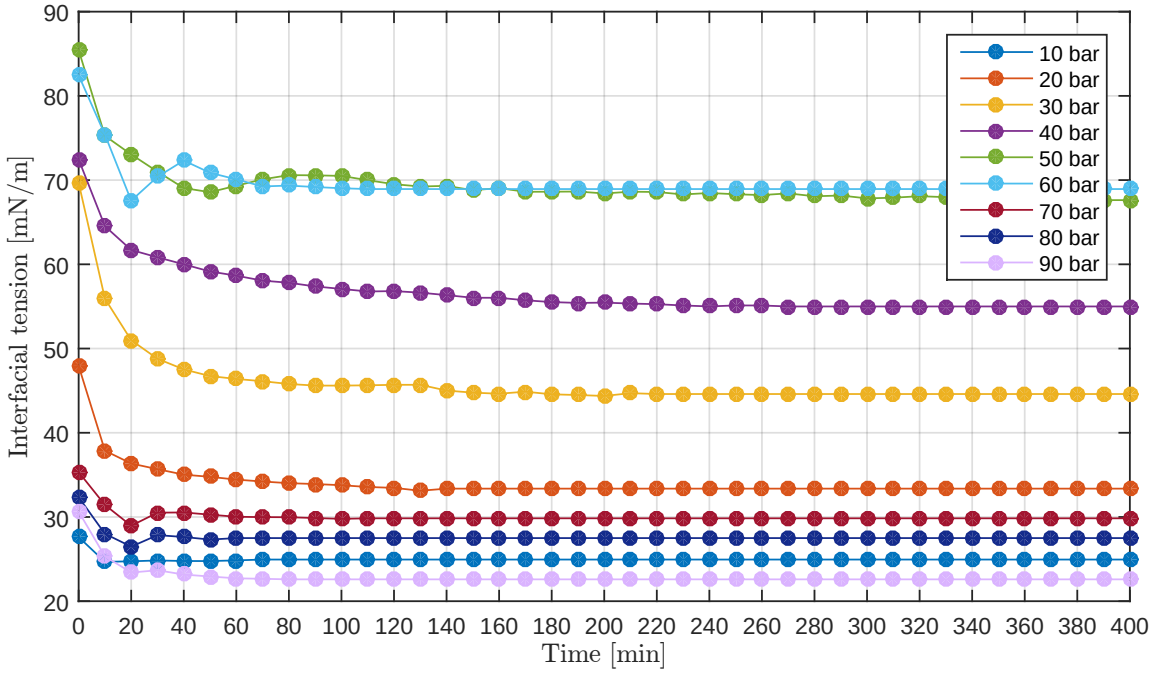

Figure 5.55: Comparison amongst pressure for interfacial tension [mN/m] vs. time. Environment 0.5 g/l DIW-CNF 25°C, *saturated*.

Figure 5.56 is a plot a CO_2 *saturated* environment at 25C 0.5 g/l nanofliud , $P = 40$ and 50 bar, which is the cases among the ones with highest relative volume increase. The oscillations to reach equilibrium IFT can clearly be seen. Figure 5.57 show the same phenomenon for a *gradually saturated* 90 bar. The difference between the two cases is that one is CO_2 in gaseous state, and in the other CO_2 is in liquid state. Figure 5.58 shows a similar phenomenon for 80 bar 45 C, where the CO_2 is in super critical state. Hence it can be concluded that the oscillations to reach equilibrium occurs no matter the initial phase of the environment, it also occurs regardless of the state of matter of CO_2. It is important to note that the plots illustrating oscillation is genreated with static density. However, the density change do not oscillate, so the oscilation would still have been present if the IFT were calculated with dynamic

density. It might however have changed the magnitude.

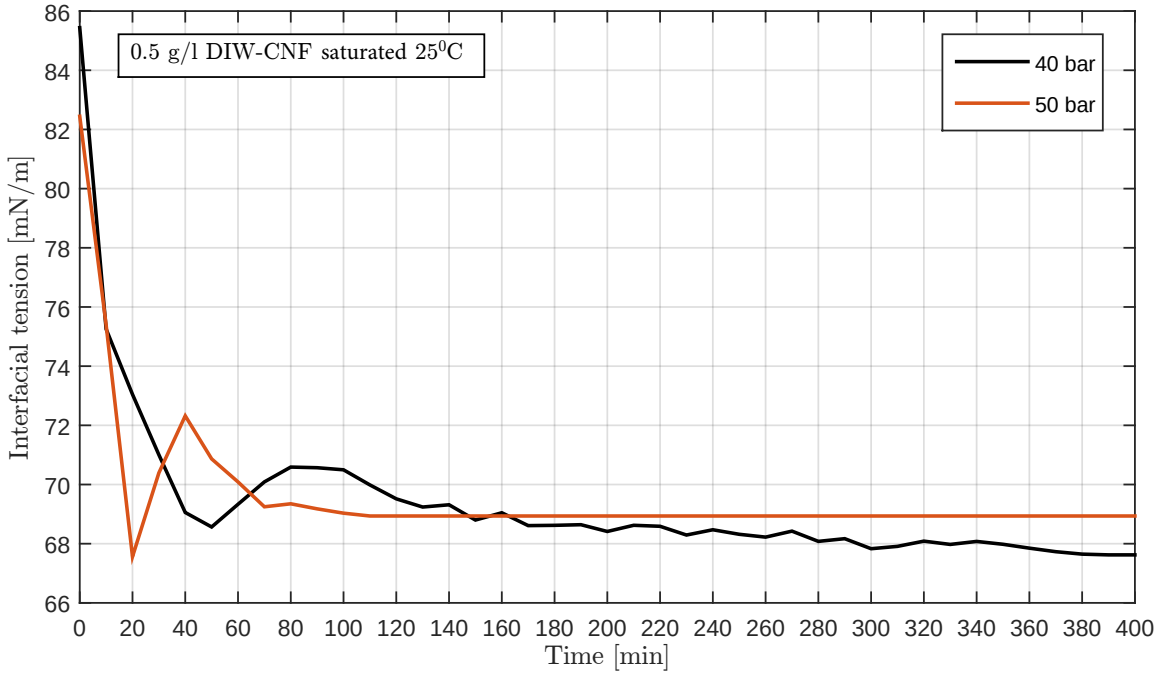

Figure 5.56: Interfacial tension [mN/m] vs. time.Environment 0.05 g/l DIW-CNF 25°C, *saturated*, 40 and 50 bar

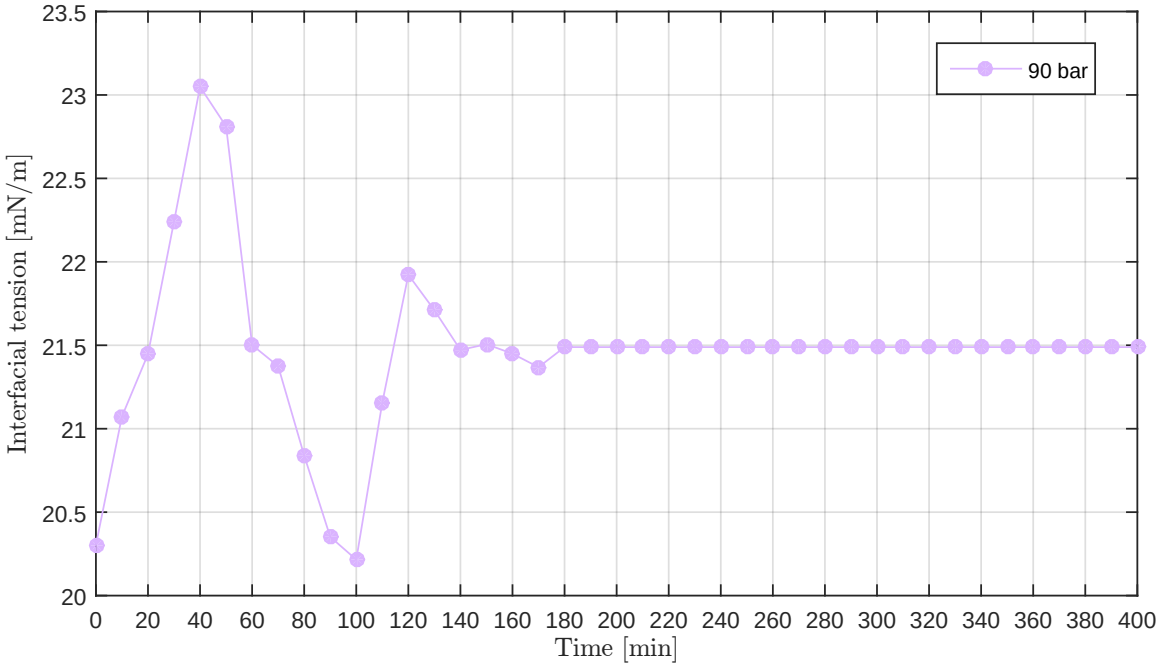

Figure 5.57: Interfacial tension [mN/m] vs. time.Environment 0.5 g/l DIW-CNF 25°C, *gradually saturated*, 90 bar

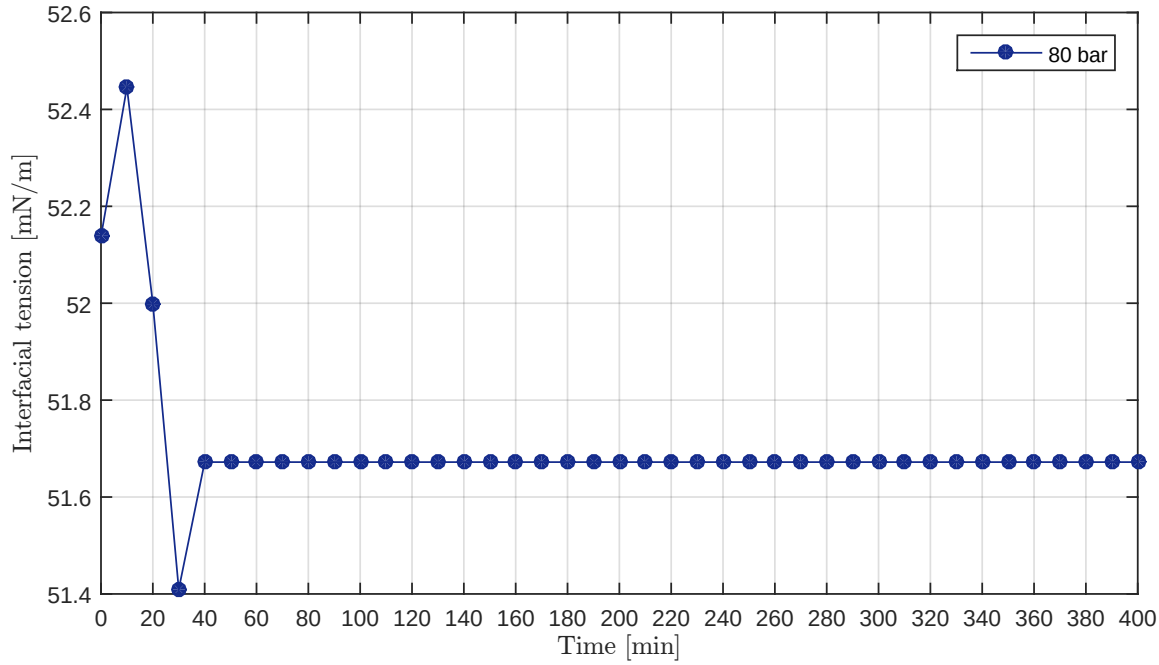

Figure 5.58: Interfacial tension [mN/m] vs. time.Environment 1 g/l DIW-CNF 45°C, *saturated*, 80 bar

5.5.2 The Effect of Nanofluid Concentration and Pressure on Equilibrium Interfacial Tension

Comparison at 25°C

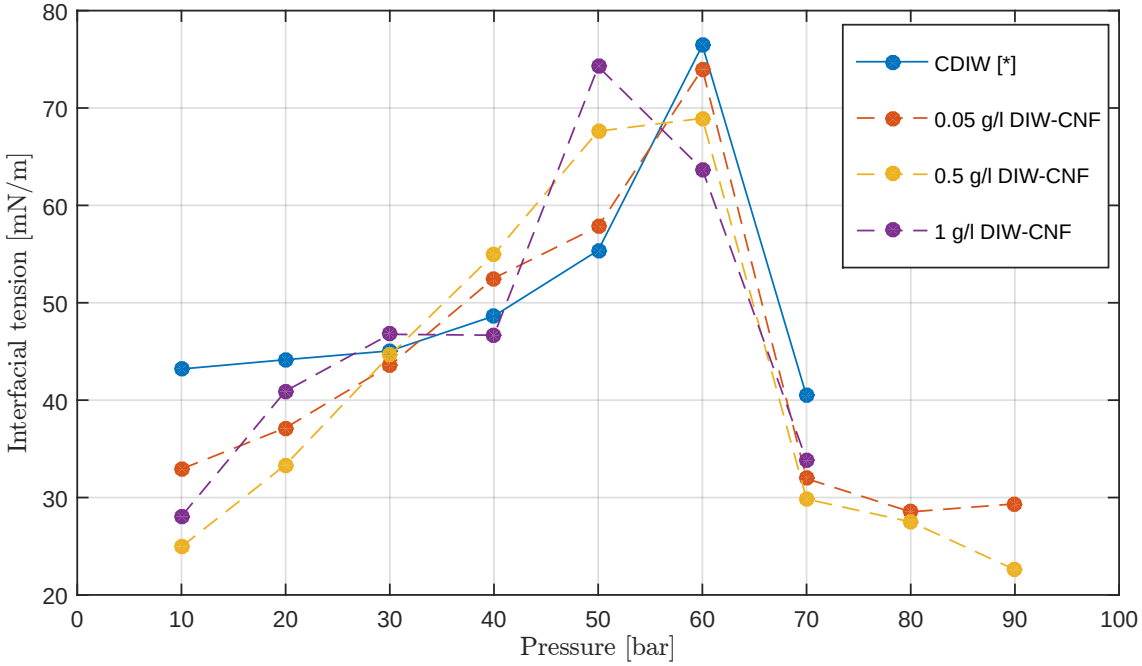

Figure 5.59: Comparison amongst concentration for interfacial tension [mN/m] vs. pressure. Environment 25°C, *saturated*. * Data-points provided by Hamouda/Bagalkot for comparison.

Observations for Figure 5.59 and 5.60

- IFT increases with pressure, until CO_2 reaches phase-change pressure to liquid.
- Rate of volume change increases with pressure (See chapter 5.1).
- Volume changer increases with pressure (See figure 5.1).
- Solubility of CO_2 in nanofluid and and *n*-decane increase with pressure (See chapter 3.2).

Discussion Miscibility of an injected gas with oil is achieved by reducing IFT to zero, which is done by increasing the pressure. Figure 5.59 and 5.60 does however show that for carbonated nanofluid, the IFT between the environment and n-decane increases with pressure below the CO_2 phase change point. This is believed to be an effect of CO_2 diluting the nanofluid. When IFT increases, the barrier for mass transfer of CO_2 from the nanofluid to the oil enlargens, since volume change and rate of which it occurs also increases, it is evident that magnitude if IFT cannot be the sole contributing factor for rate or amount of mass transfer across this interface. As figure 5.61 shows, the IFT is largely dependent on the density difference between the

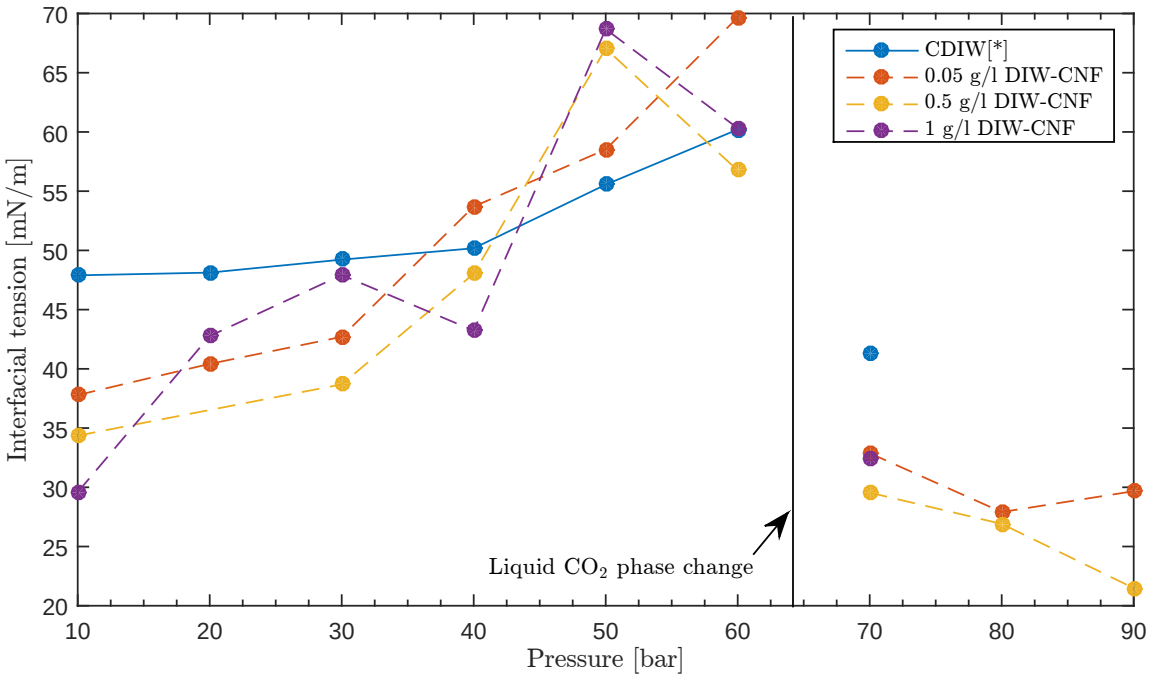

Figure 5.60: Comparison amongst concentration for interfacial tension [mN/m] vs. pressure. Environment 25°C, *gradually saturated*. * Data-points provided by Hamouda/Bagalkot for comparison.

two phases. CO_2 dissolved in nanofluid does not affect the density dramatically, but while pressurising from 10 to 60 bar, the solubility of CO_2 in nanofluid is almost quadroupled, from ≈ 0.3 to $1.3 mol/kg$. Thus, establishing a greater driving force. Higher solubility in nanofluid with pressure do also offer a greater supply of CO_2 available for the decane drop. It is observed in figure 5.2 that the relative volume change of the decane drop can be as high as 3, which constitutes a CO_2 content of about two thirds. The CO_2 content in the decane drop is therefore dramatically reducing the density of the drop (P¡ 64 bar 25°C), and density difference of the phases are increased.

Proposed Mechanism

- Increased solubility of CO_2 in nanofluid caused by increased pressure is increasing the CO_2 concentration gradient, and potential for CO_2 transport.
- Mass-transfer driving force is increased with increased solubility of CO_2 in the nanofluid.
- Increased solubility of CO_2 in the nanofluid offer a greater supply of CO_2 to the decane drop before the concentration gradient equalises between the environment and the drop.
- More CO_2 transfered to the decane drop lowers its density as $\rho_{CO_2} < \rho_{C10}$, for
- Drop density do therefor decrease with pressure, while nanofluid density increase with pressure

- The increased $\Delta\rho$ increases the IFT.
- When the pressure at which CO_2 changes to liquid phase is reached, the density of the drop drastically increase, the $\Delta\rho$ drastically decreaase, and IFT decrease. This is true fir 25°C, where the CO_2 density becomes larger than the decane density. At 45°C, the CO_2 phase change occurs from gaseous to super critical conditions, and not to liquid, therefor the density of CO_2 do not surpass the density of decane, and the increase in IFT is only lowered, and not reduced.

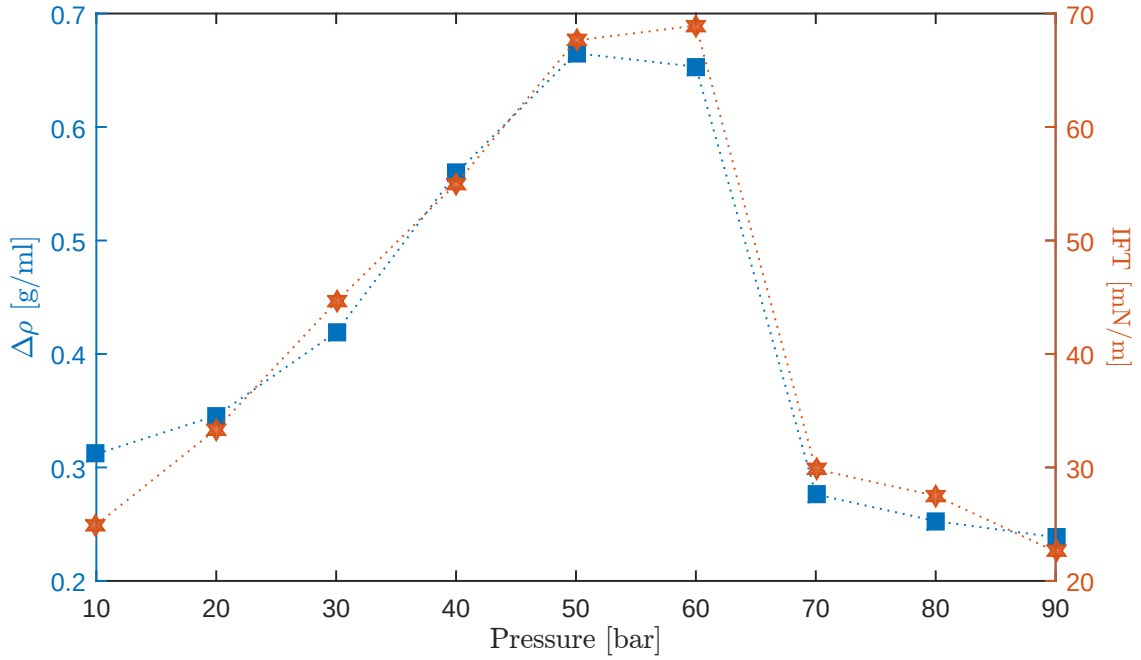

Figure 5.61: Comparison interfacial tension [mN/m] and density difference between environment- and drop-phase (0.5 g/l DIW-NF and *n*-decane. 25°C, *saturated*.

Figure 5.61 shows the great correlation between density difference of the drop and environment, and IFT. $\Delta\rho$ and IFT is plotted on two separate axes.

Comparison Interfacial tension vs. Pressure at 45°C

Compared to other properties, the IFT seems to behave more different from each other in terms of temperature sensitivity, both for *saturated* and *gradually saturated* environments. For 45°C, a similar phenomenon of rapid decrease in IFT is not observed, at least to the same extend. As it is stated that IFT is related to the density difference, and the density development for CO_2 with pressure at 45°C is smooth, no dramatic change crossing this pressure is expected. However, decrease in IFT across this pressure is observed for 2 out of 3-cases with a *saturated* environment. In figure 5.62, it is maybe a possibility that 0.5 g/l 70 bar, could have been higher, so a decrease in IFT would have been seen across the boarder. However, for both *saturated* and *gradually saturated* environment, no distinct decrease in IFT is observed, and the solubility of CO_2 in the environment might be more dominant, as the density increase of CO_2 is quite smooth and slow, while the solubility increases flattens out similarly to what is observed for IFT at 45°C. It is therefore suggested that at 45°C, solubility of the environment is the dominant property dictating the behaviour of IFT.

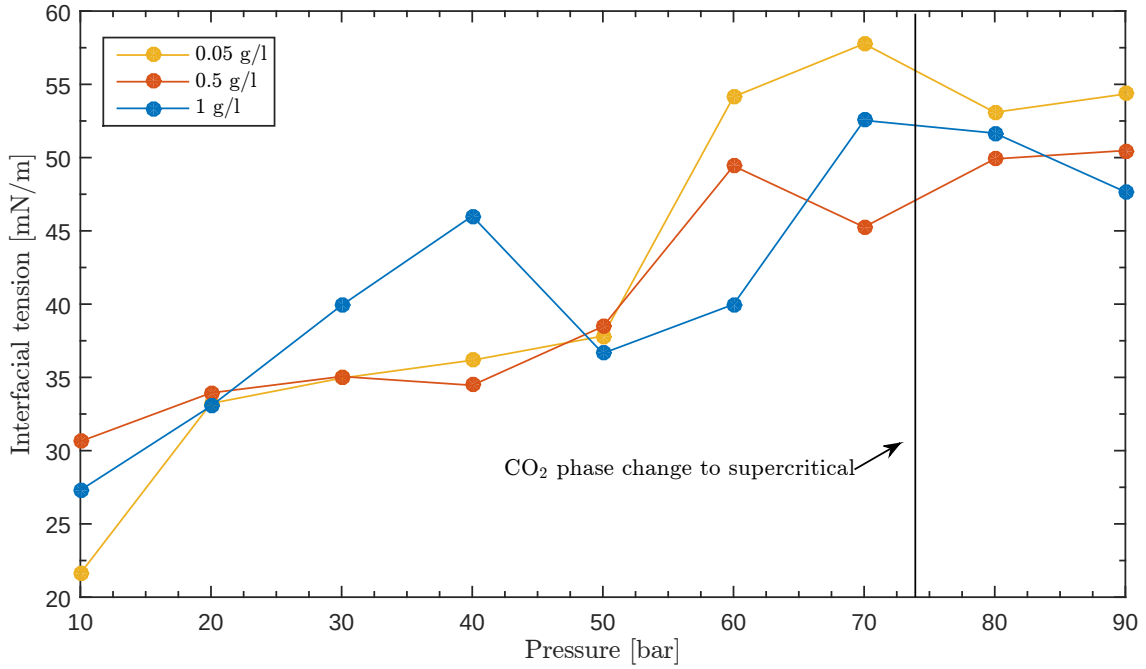

Figure 5.62: Comparison amongst concentration for interfacial tension [mN/m] vs. pressure. Environment 45°C, *saturated*.

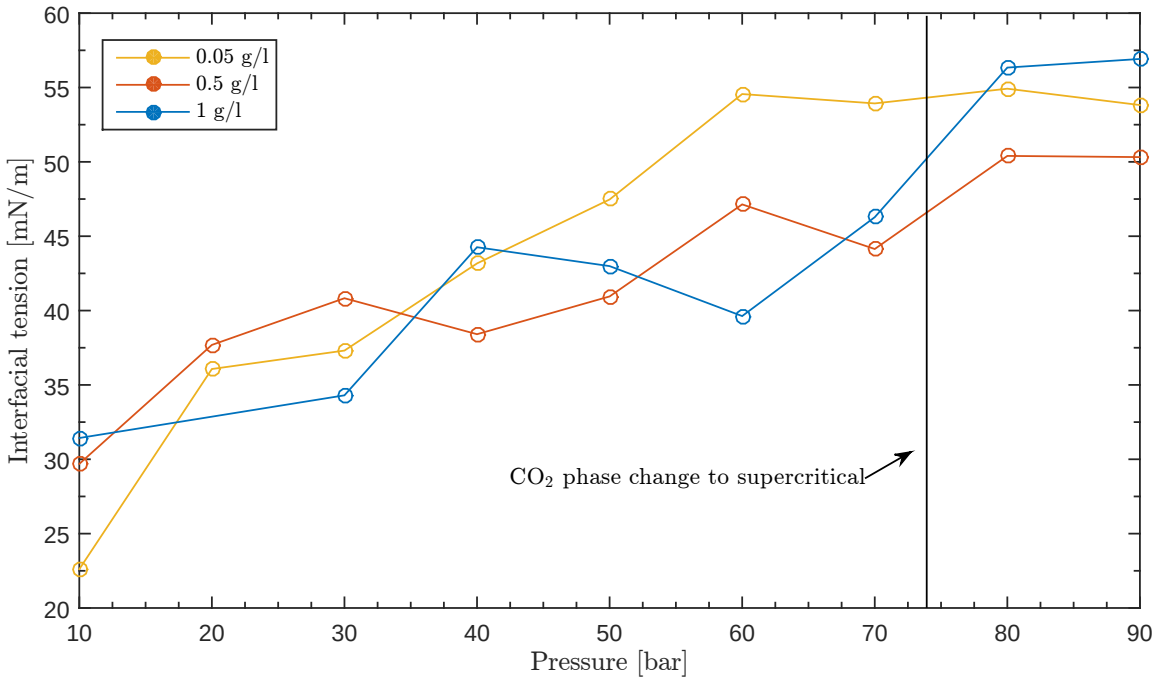

Figure 5.63: Comparison amongst concentration for interfacial tension [mN/m] vs. pressure. Environment 45°C, *gradually saturated*.

Coments on the Dependancy of Concentration
Contrary to properties like volume increase and mole fraction, the local variation among concentrations are fluctuating quite a lot. However, considering figure 5.59 and 5.60, 0.5 g/l nanofluid environment results in the lowest IFT, compared to 0.05 and 1 g/l, after phase-change pressure. This is natural as the IFT is dependent on density, this concentration has the highest content of CO_2, which is actually reducing the density difference at these pressure. Interestingly 0.5 g/l nanofluid concentration has a low IFT at lower pressures (P $<$ 40 bar) also, which cannot be a density effect caused by more CO_2 present, as at that pressure, more CO_2 would increase the IFT. However, it might that less CO_2 is present at those pressures. Additionally, at these pressures, DIW, which has the lowest content of CO_2 (Fig. 5.12), shows by far the highest IFT, these observations might indicate that nanoparticles are modifying the interface between the *n*-decane and the basefluid/nanofluid.

5.5.3 The Effect of Temperature on Equilbrium Interfacial Tension

Figure 5.64 shows that the IFT at 25°C is higher below 60 bar for that of 45°C. This can be attributed to both the lower solubility of CO_2 at 45°C, less CO_2 in drop, and lower $\Delta\rho$. However, increasing the temperature do also lower the IFT. 25°C IFT lies above 45°C until the phase change of CO_2 for 25°C at 64 bar, where it drops below. This is interesting as one would expect the IFT to ultimately be lower for higher temperatures. With all the mechanisms discussed for this system, the combinations of mechanisms have a fascinating outcome, resulting in IFT being lower at low temperatures for the higher pressures. Increasing the pressure further is of course expected to lower them both down to 0, when miscibility is achieved.

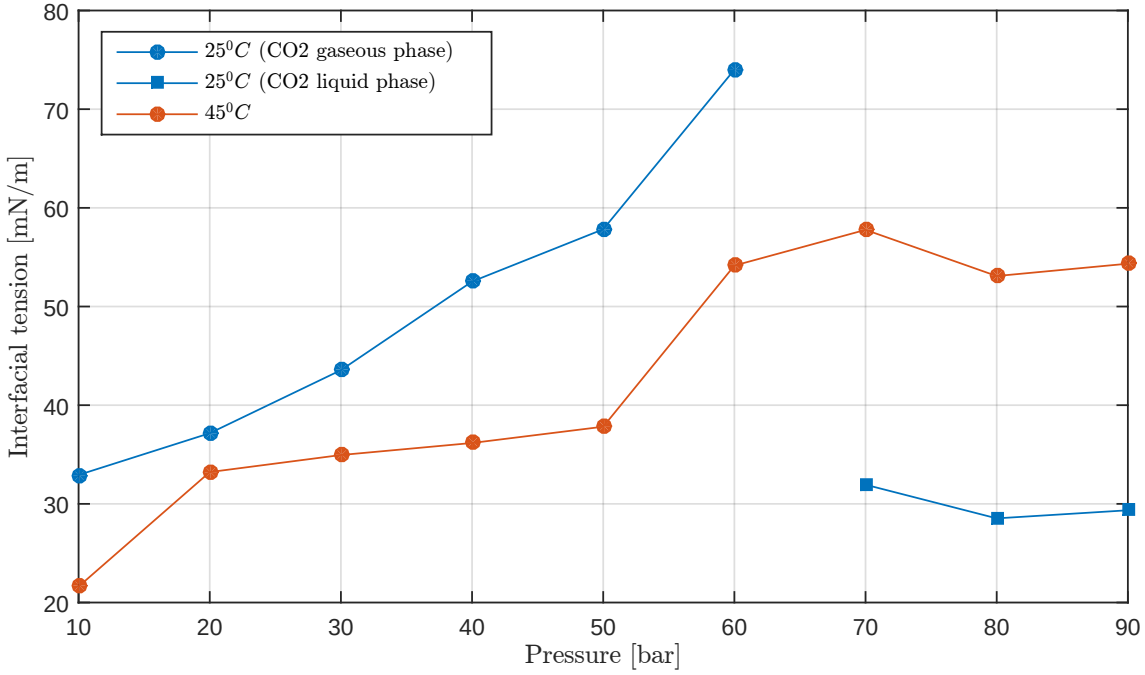

Figure 5.64: Comparison amongst temperature for interfacial tension [mN/m] vs. pressure. Environment: 0.05 g/l DIW-CNF, *saturated*.

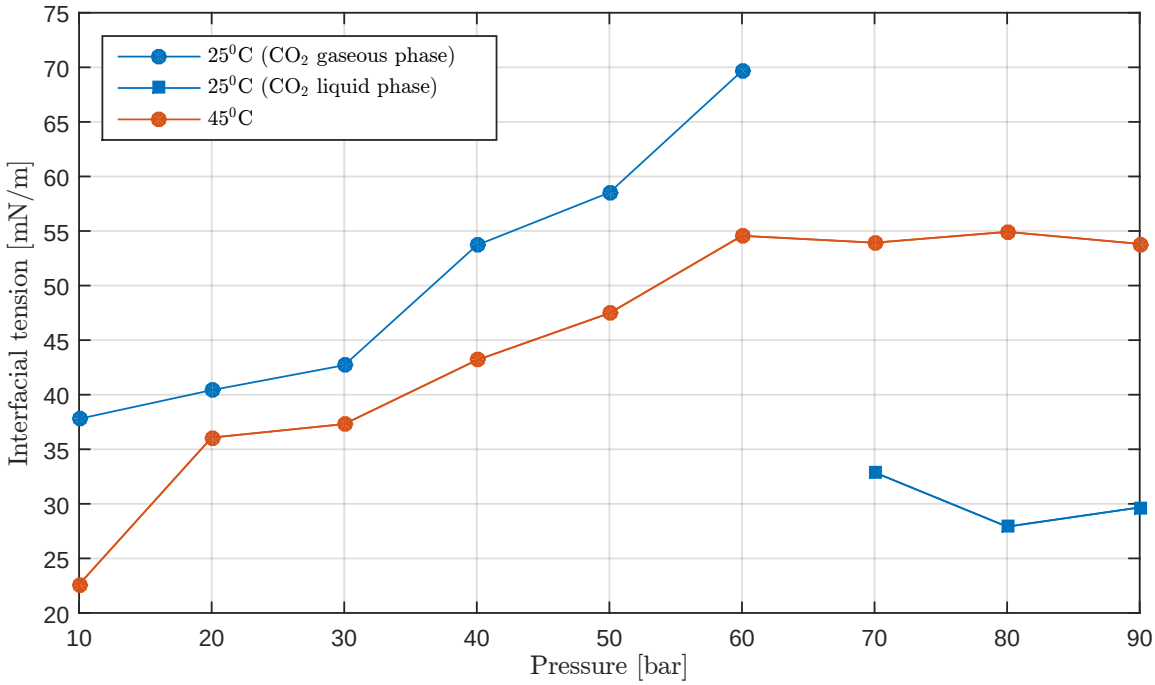

Figure 5.65: Comparison amongst temperature for interfacial tension [mN/m] vs. pressure. Environment: 0.05 g/l DIW-CNF, *gradually saturated*.

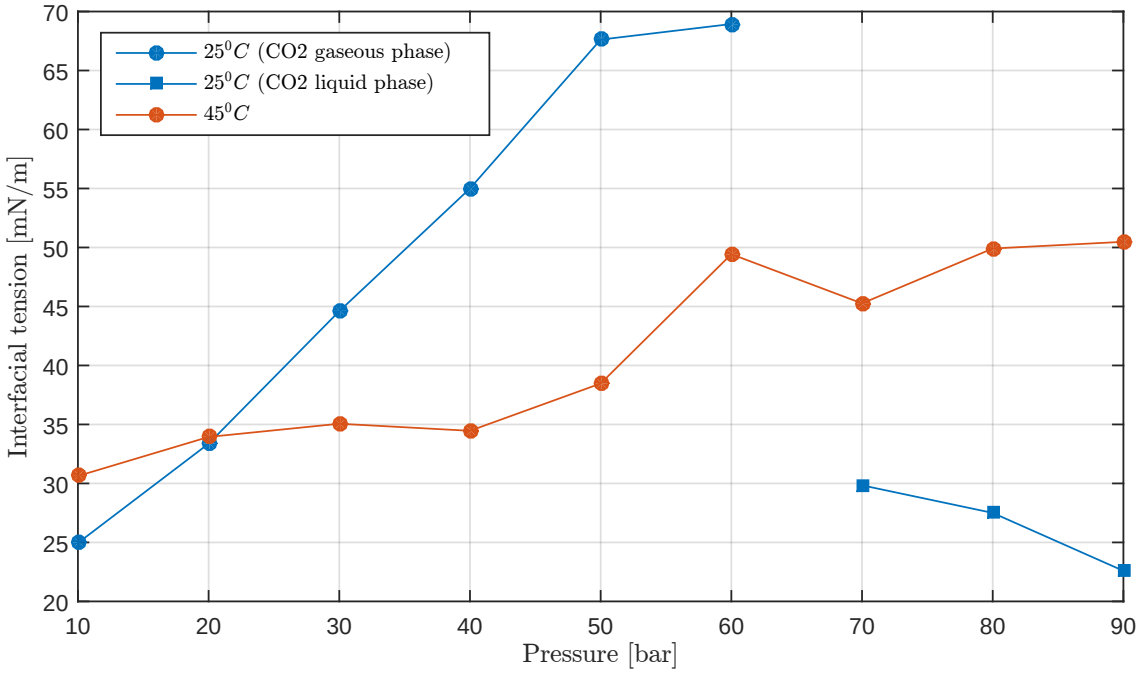

Figure 5.66: Comparison amongst temperature for interfacial tension [mN/m] vs. pressure. Environment: 0.5 g/l DIW-CNF,*saturated*.

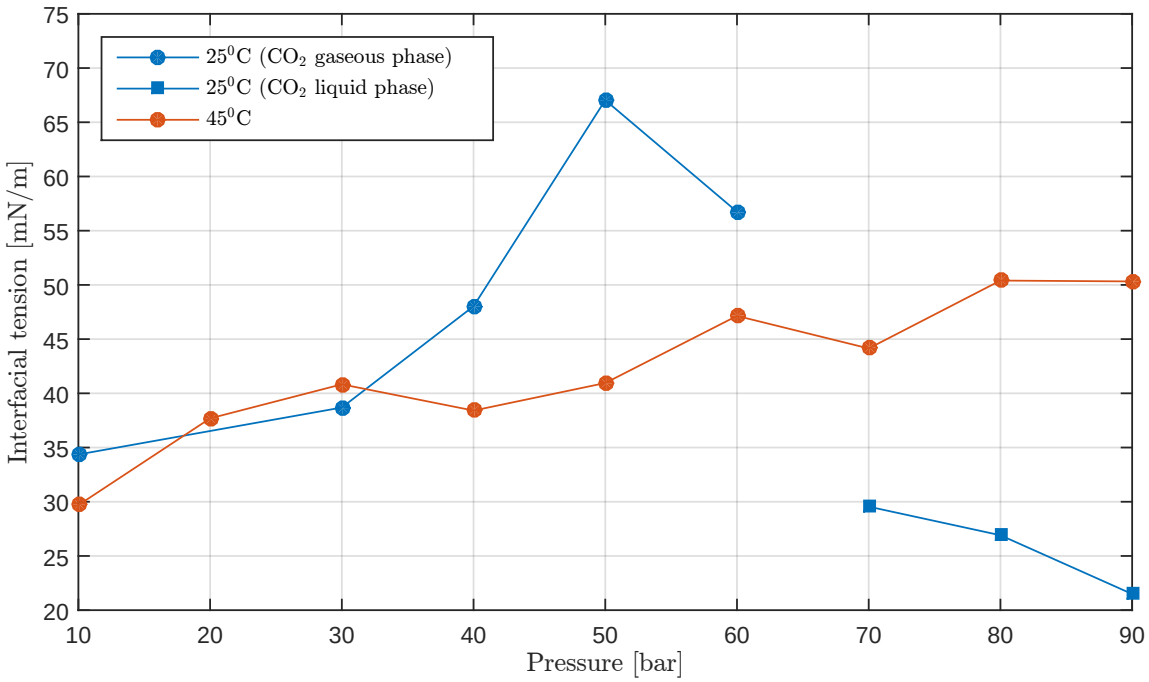

Figure 5.67: Comparison amongst temperature for interfacial tension [mN/m] vs. pressure. Environment: 0.5 g/l DIW-CNF, *gradually saturated*.

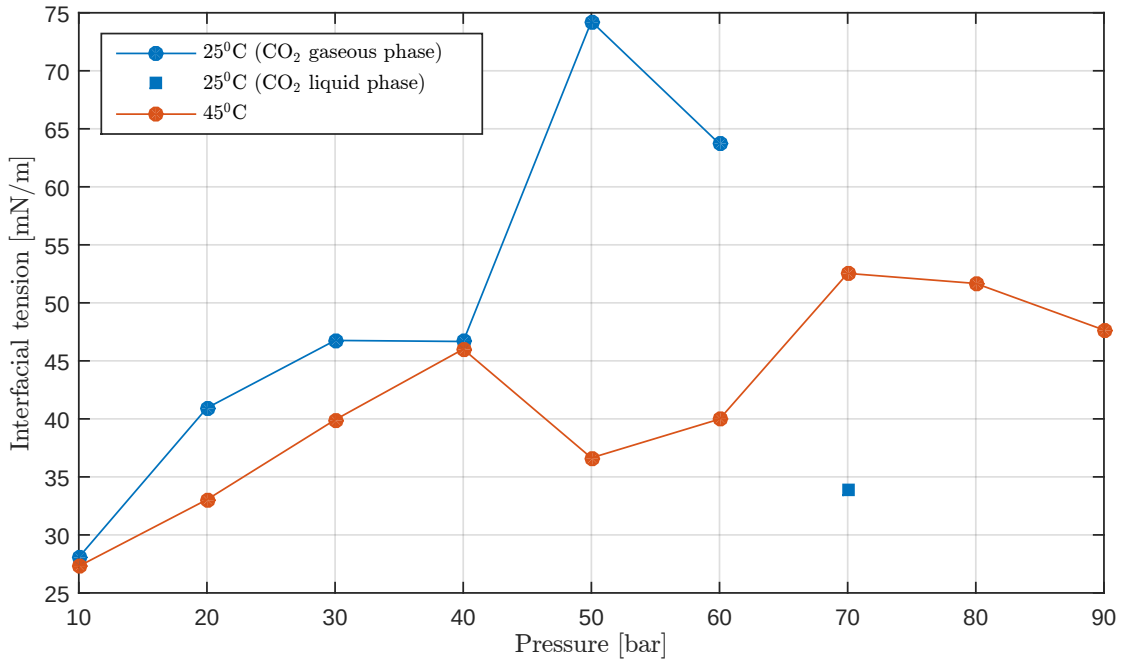

Figure 5.68: Comparison amongst temperature for interfacial tension [mN/m] vs. pressure. Environment: 1 g/l DIW-CNF, *saturated*.

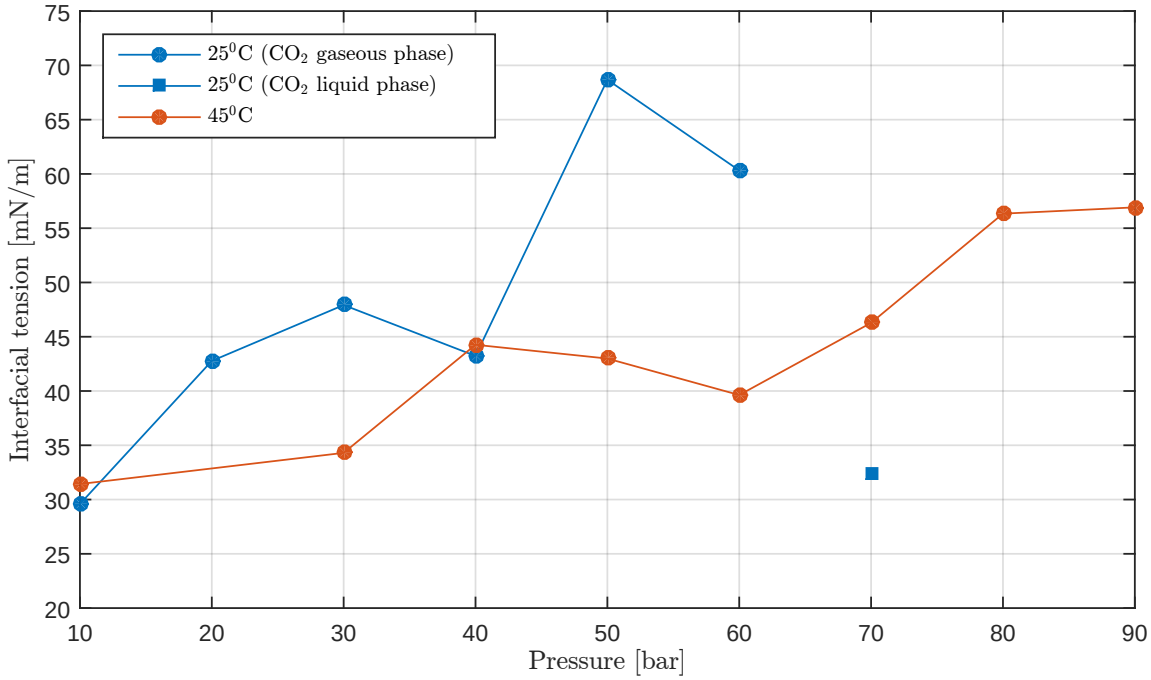

Figure 5.69: Comparison amongst temperature for interfacial tension [mN/m] vs. pressure. Environment: 1 g/l DIW-CNF, *gradually saturated*.

5.5.4 The Effect of *saturated* and *gradually saturated* CO_2 Environments on Equilibrium Interfacial Tension

Figure 5.70 shows a comparison at 25°C for*saturated* and *gradually saturated* environments. It can be observed that the *gradually saturated* is a bit lower than the *saturated* at the lowest pressures ($P < 30bar$), but that the slope at which the IFT increases with pressure is steeper, it do also peek at 50 bar, and not 60 bar, which *saturated* does. After the peek at 50 bar, the *gradually saturated* cases is generally slightly lower than the *saturated* scenarios. Figure 5.71 shows the same plot for 45°C, where no clear distinction can be made, however, the *saturated* experiments seem to have a slightly higher variance among themselves.

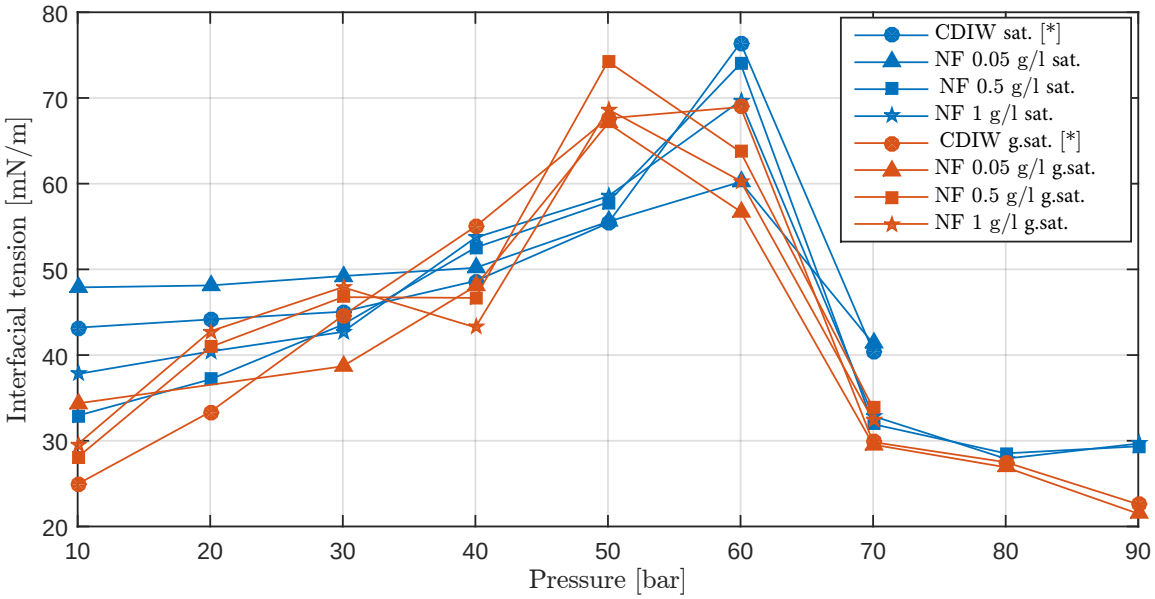

Figure 5.70: Comparison amongst phase (all concentrations) for interfacial tension [mN/m] vs. pressure. Environment: 25°C. * Data-points provided by Hamouda/Bagalkot for comparison.

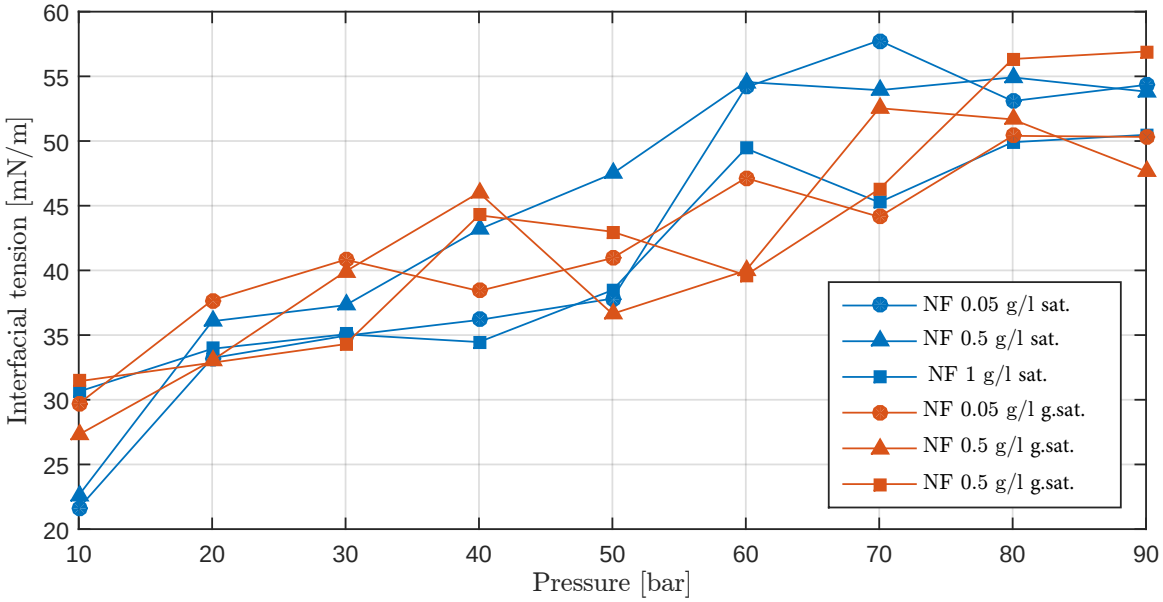

Figure 5.71: Comparison amongst phase (all concentrations) for interfacial tension [mN/m] vs. pressure. Environment: 45°C. * Data-points provided by Hamouda/Bagalkot for comparison.

5.5.5 Summarising Points on Interfacial Tension

- It is verified that using the equilibrium density results in correct equilibrium IFT, even though the calculation is made dynamically. The *dynamic* points before equilibrium is reached is however not correct when static equilibrium density is used as input.
- It is confirmed that dynamic density input is crucial for calcualting the dynamic interfacial tension.
- Transition from unsteady IFT, to equilibrium occurs smoothly, but do experience oscillations at pressures higher than 50 bar.
- The CO_2 solubility of the environment has a large effect on the behaviour of IFT, this is because the solubility is closely related to the concentration gradient and mass transport, and therefore dictates the amount of CO_2 in the drop. The amount of CO_2 in the drop affects the density difference largely, which is directly proprtional to IFT.
- IFT increase with pressure until P $>$ 60 (64) bar at 25°C, and P $>$ 70 (74) bar at 45°C. This is related to density of CO_2.
- $IFT \propto \Delta\rho$
- It is indicated that nanoparticles are capable of modifying the interface between basefluid/nanofluid and *n*-decane
- Increase in temperature lowers the IFT, but at pressures higher than 64 bar, density differences become dominant. At those conditions, a temperature of 25°C results in a lower IFT than 45°C

5.6 Diffusion Coefficient

Figure 5.72 shows the diffusion coefficients of CO_2 into *n*-decane, it is observed that the diffusion coefficient decreases with pressure up until 60 bar. As discuseed in chapter 3.2, solubility of CO_2 in both nanofluid and *n*-decane increases with pressure, which generates a higher concentration gradient (ΔC) of CO_2, and a greater driving force for mass-transfer. In the case of gas diffusing into heavy oil (CO_2, CH_4, C_2H_6,C_3H_8), a higher pressure result in higher diffusion coefficient, accoridng to Yang *et al.* [12] [77]. However, in this study, the opposite is observed in the case of CO_2 diffusing from carbonated water or nanofluid into *n*-decane. The opposite phenomenon may be credited to the increase in interfacial tension with pressure (Discussed in chapter 5.5), which acts as an opposing force to the mass-transfer across the interface. Moreover, an increased solubility of both species constitutes a greater availability of CO_2, and a greater source of CO_2 for being transported into the *n*-decane drop. It is clear from the experiments conducted, and discussed in chapter 5.1 - Volume Change, and chapter 5.2 - Mole Fraction, that more CO_2 confidently enters the drop as pressure increases. It can therefore be stated that IFT is the dominant factor affecting diffusion coefficient, which also is seen in the results from Yang *et al* [42], where it can be said that $D \propto IFT^{-1}$. The reason for the opposite phenomenon on diffusion coefficient from carbonated water compared to diffusion from free gas phase, is the opposite effect on IFT, which is a result on the increase in $\Delta\rho$ with pressure, and not decrease, as it is for free gas diffusion. All this has previously been explained and confirmed.

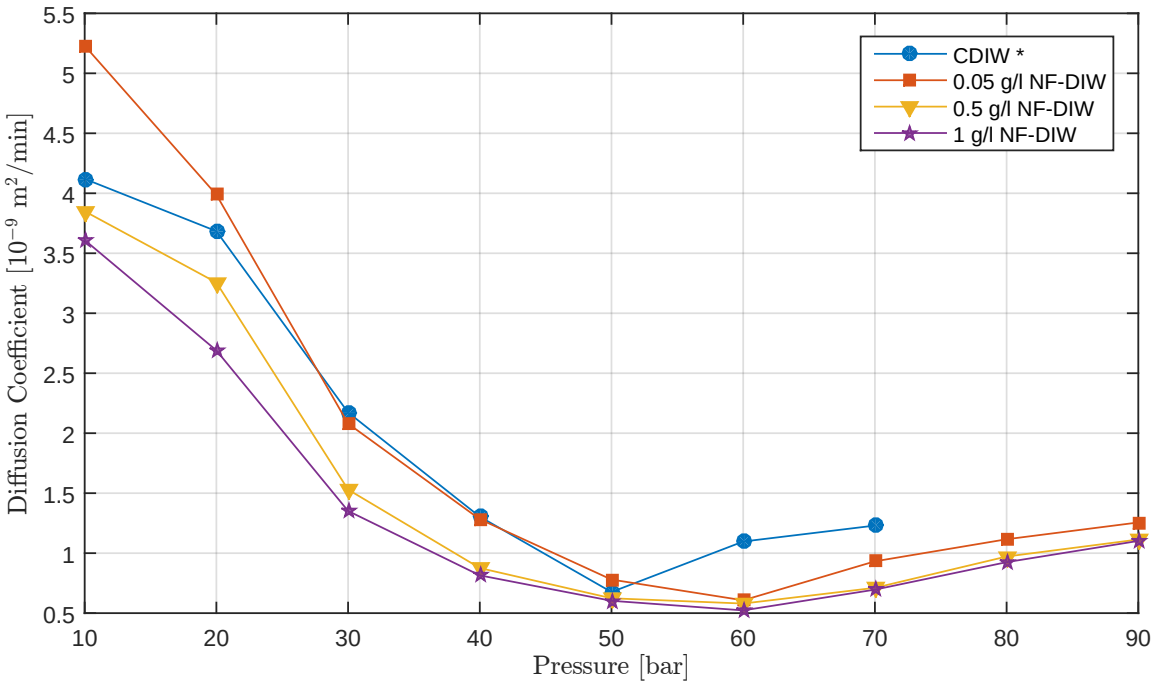

Figure 5.72: Diffusion Coefficient of CO_2 into *n*-decane at 25°C. *saturated*

The swelling factor at 25°C and *saturated* conditions is plotted against pressure in figure 5.73. The swelling factor, discussed in chapter 4.2 is calculated, based on raw

experimental data, according to equation 5.3

$$SF = 1 + \frac{\int_0^T \frac{[V_{exp}(t) - V_0] \cdot C_{avg}(t)}{V_{exp}^2} dt}{\int_0^T \frac{[C_{avg}^2(t)]}{V_{exp}^2} dt} \tag{5.3}$$

It is observed an increased swelling factor with pressure for pressures until 60 bar, then a slight dip at 70, and a slow increase again. A higher interfacial tension suggests a lower diffusion coefficient, a lower diffusion coefficient is observed when IFT is higher, thus it is suggested that IFT is the governing factor. Beyond 60 bar, the diffusion coefficient increase with pressure, which is consistent with the claim for IFT beeing governing, as the reverse phenomenon is observed for IFT, namely increased IFT with pressures up until 60 bar, and then decrease. The reason for the IFT behaviour is discussed in chapter 5.5, figure 5.61, and relates to mole fraction of CO_2 present, and its density.

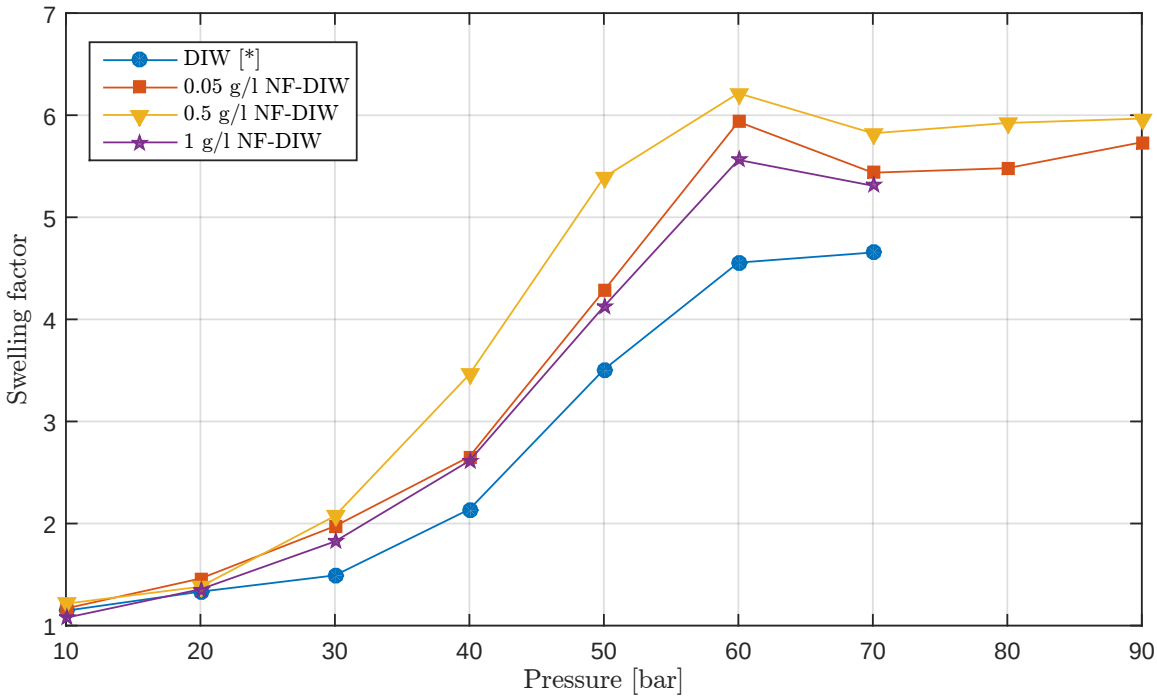

Figure 5.73: Swelling factor of *n*-decane in the presence of DIW-CNF at 25°C. *saturated*

CO_2 Concentration Gradient at Varying Pressure

Figure 5.74 shows four individual experiments, all at the similar conditions, except a varying pressure (10, 30, 50 and 80 bar). The figure depicts the concentration gradient of CO_2 in the *n*-decane drop at a particular point in time (t = 50 min), during a CO_2 *saturated* experiments at 25°C with the environment nanofluid having a concentration of 0.5 g/l. The increased rate of swelling with pressure can be visualised with the increased drop radius. Comparing the concentration gradients in the drops reflects the diffusion coefficients in that the lowest pressure have the

greates concentration, the gradual decrease for the two intermittent pressures, before the gradient becomes greater again for the highest pressure. This is exactly what is predicted by the diffusion coefficients. The diffusion coefficients experience a degrease with pressure until P = $P_{CO_2,sat}$ or P = $P_{CO_2,cri}$, as a result of the behaviour of IFT. Moreover, an important feature of this plot, together with the diffusion coefficients is that they are complementary to the ineterfacial tension calculation. Meaning that since the diffusion coefficient and the IFT is calculated with two unrelated methods (Only related with the physical observed volume change of the drop), they validate each other by portraying similar phenomena. This results have a major significance as it interrelates the experimental and numerical calculations.

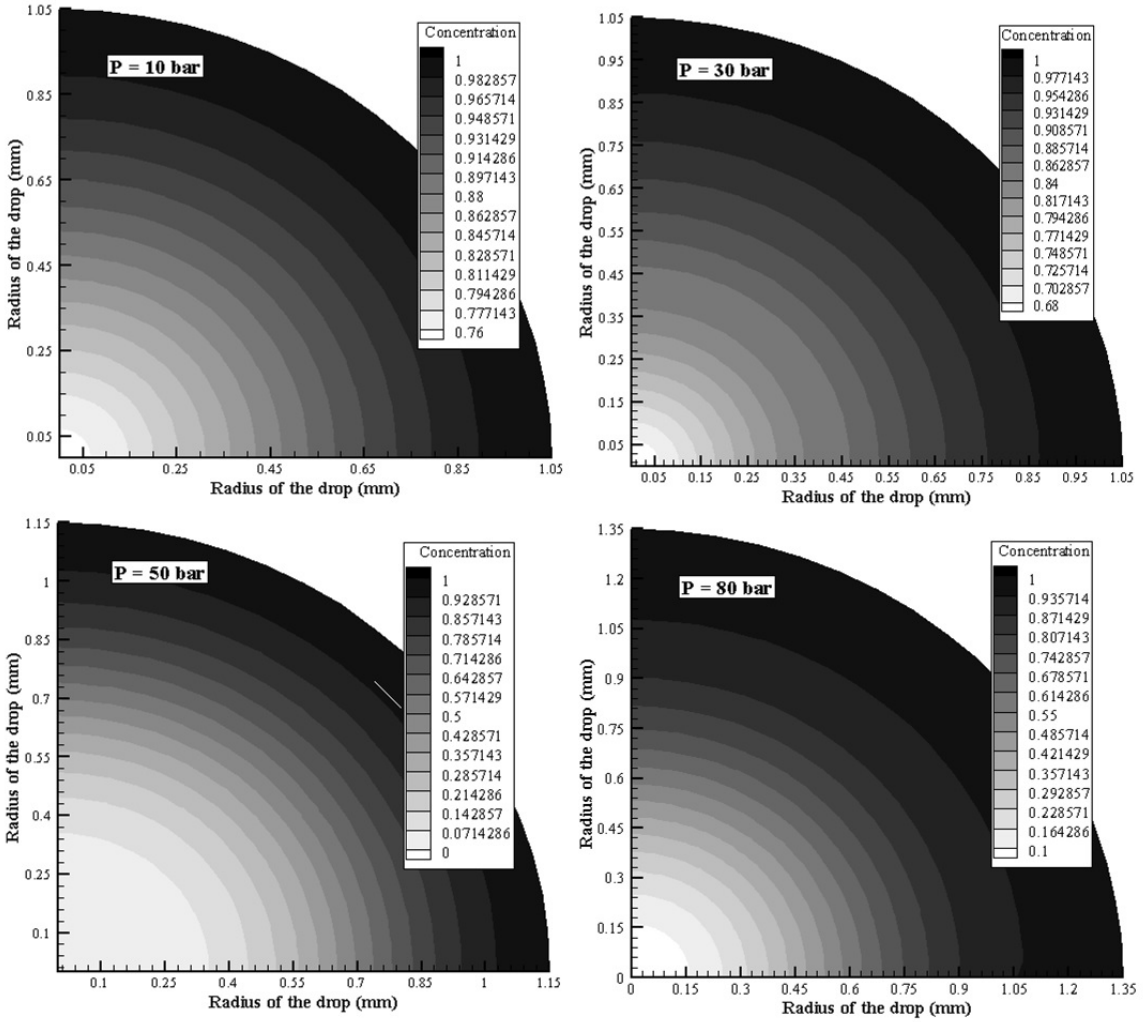

Figure 5.74: Representation of diffusion of CO_2 into *n*-decane from *saturated* DIW-CNF for 4 pressures (10 bar, 30 bar, 50 bar and 80 bar). The contour-plots are calculated with the Mathematical Mass-Transfer model, with the experimental data at t = 50 min, for 0.5 g/l CNF 25°C

5.6.1 Effect of Temperature on the Diffusion Coefficient

Comparing diffusion coefficient among temperatures (Fig. 5.75) reveals a higher diffusion coefficient at higher temperature, at all pressures (10 - 90 bar). When the temperature increases the solubility decrease, and the amount of CO_2 available decreases, resulting in a lower concentration gradient for CO_2, which pulls in the direction of a lower diffusion coefficient. However, the IFT do also decreases with temperature (Chapter 5.5), which acts in favour of a higher diffusion coefficient. Additionally, a higher temperature constitutes a higher entropy of the system, more Brownian motion, and faster diffusion. In summation, the diffusion coefficient is ultimately dependent on interfacial tension (decrease with increase), solubility (increase with increase) and temperature (increase with increase). Interfacial tension is largely dependent on the density of the drop, which decreases up until 60 bar, and then decrease (CO_2 density related). Therefore, the IFT is also largely dependent on solubility.

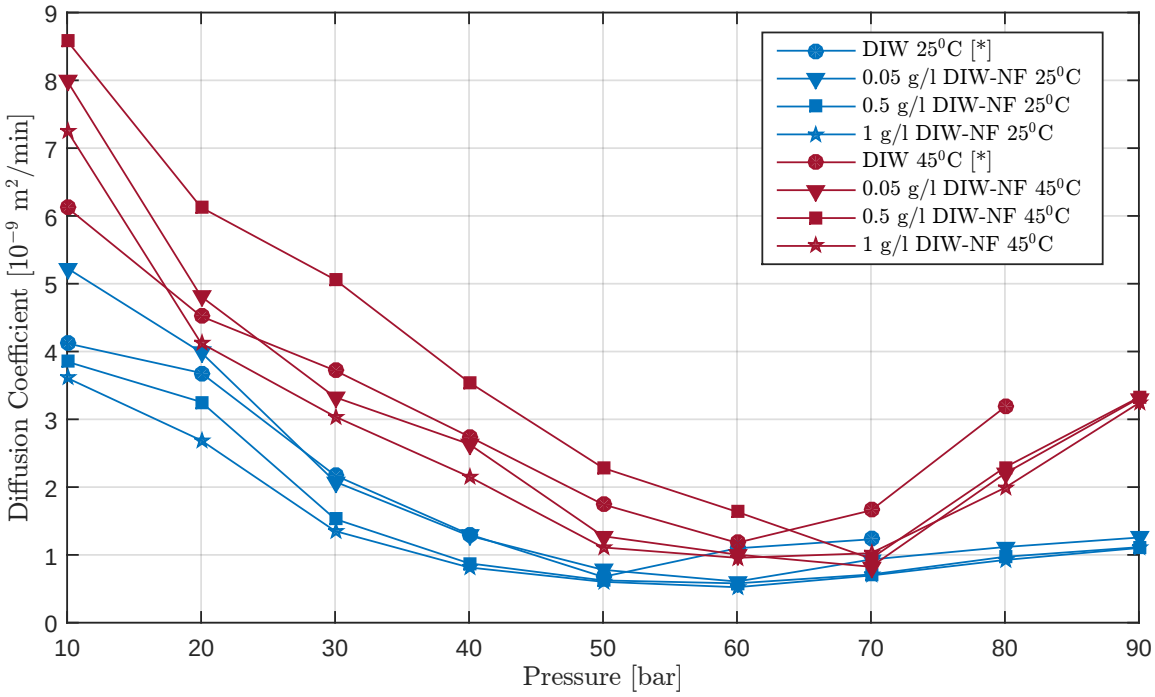

Figure 5.75: Diffusion coefficient of CO_2 into *n*-decane from saturated DIW-CNF. 25 and 45°C.

5.6.2 The Effect of *Saturated* and *Gradually Saturated* CO_2 Environments on Diffusion Coefficient

When comparing *saturated* and *gradually saturated* conditions (Fig. 5.76 to 5.80), the exact same trends are observed, regarding initial decrease and then an increase after phase-change pressure is surpassed. IFT is credited with being the most dominant or governing factor. However, it is interesting to observe how much lower the diffusion coefficient for *gradually saturated* environments are, it is approximately one order of magnitude less. This is explainable with the fact that CO_2 has to diffuse through

water, and the concentration gradient between the environment and drop is much lower than for the *saturated* scenarios. The diffusion in a *gradually saturated* system with CO2/nanofluid/*n*-decane will be slowed down by the dissolution and diffusion of CO_2 into nanofluid. An illustration of the concentration gradients may be found in chapter 4.1.2, Fig 4.3.

Figure 5.76 shows the comparison of the two environments (*saturated* and *gradually saturated*), at 25°C. For the *saturated* scenario, it seems a bit arbitrary which concentration of nanofluid has the higher diffusion coefficient. However, the diffusion coefficient is affected by a number of things, including the degree of swelling and the rate of mass-transfer. The degree of swelling is higher in cases with greater concentration gradient. Diffusion coefficient is dependent on how fast and how much it swells (Swelling factor). Ultimately, the lowest swelling might give the largest diffusion coefficient. This means that many factors are pulling in different directions, which is believed to be the seemingly large variance in the diffusion coefficient. For instance, 0.5 g/l NF-DIW is observed to consistently have the largest swelling factor in figure 5.73 for *saturated* environment at 25°C, however, in figure 5.76 it is observed to be in the lower half with regards to diffusion coefficient. Further, it may be observed that the diffusion coefficient at *gradually saturated* scenarios is always lower than the respective *saturated* scenario for any given pressure.

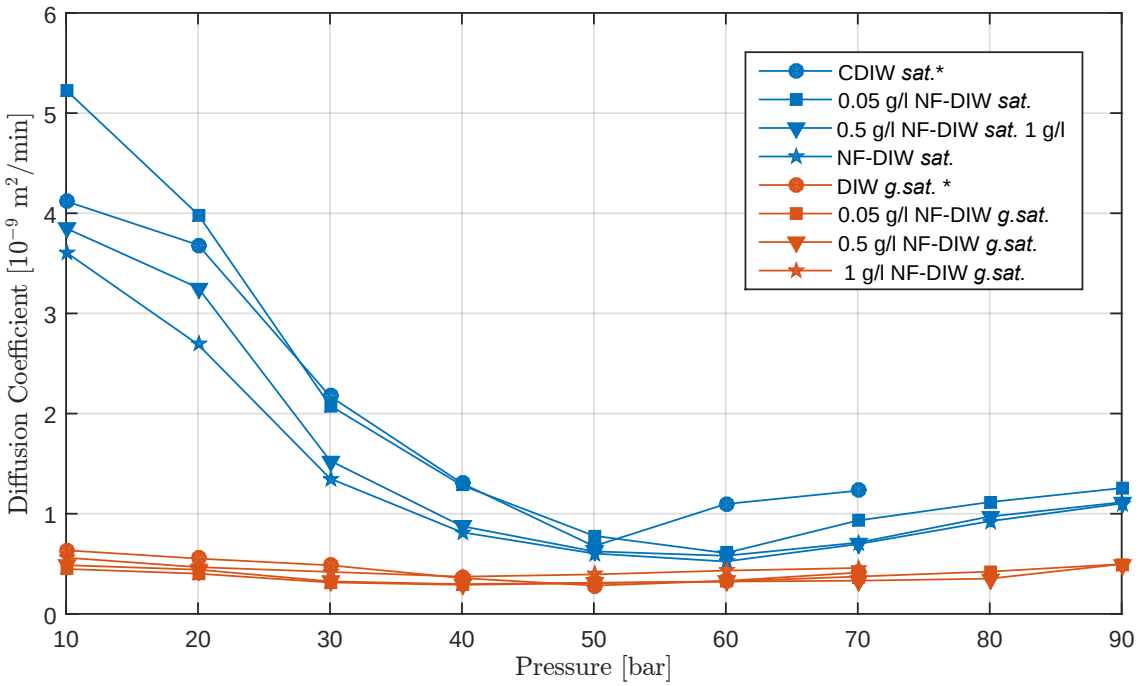

Figure 5.76: Diffusion coefficient of CO_2 into *n*-decane from DIW-CNF. 25°C *saturated* and *gradually saturated*

The same figure as presented earlier (fig. 5.19) is also presented below as figure 5.77. This figure illustrates the concentration of CO_2 in the drop at one particular point in time (t = 50 min), for the two secenarios, *saturated* and *gradually saturated* environments. It may be observed that much more CO_2 is accumulated in the drop for the former scenario. This illustrates very well the differences among diffusion co-

efficients, where the rate at which CO_2 entered the drop according to the magnitude of the concentration gradient and larger driving-force can be visualised.

Figure 5.78 shows the *gradually saturated* scenario at 25°C. This is the same values as in figure 5.76, but plotted without the *saturated* scenario in order to get a better scale. It may be observed that the trend is similar, but compared to the *saturated* scenario it is much lower in magnitude. However, this means that the saturation-mode is affecting the diffusion coefficient to a greater extent than what concentration of nanofluid does. This is logical, as the saturation-mode governs the concentration gradient, which again governs the mass-transfer (Together with IFT).

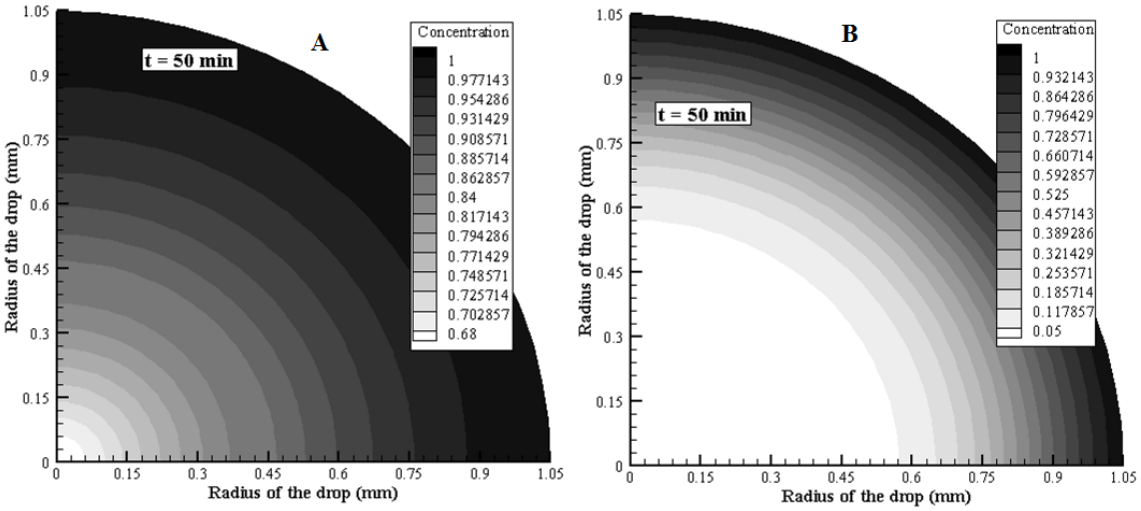

Figure 5.77: Representation of diffusion of CO_2 into *n*-decane from DIW-CNF *saturated* (A) and *gradually saturated* (B). The contour-plots are calculated with the Mathematical Mass-Transfer model, with the experimental data at t = 50 min, for 0.5 g/l CNF 25°C at P = 30 bar

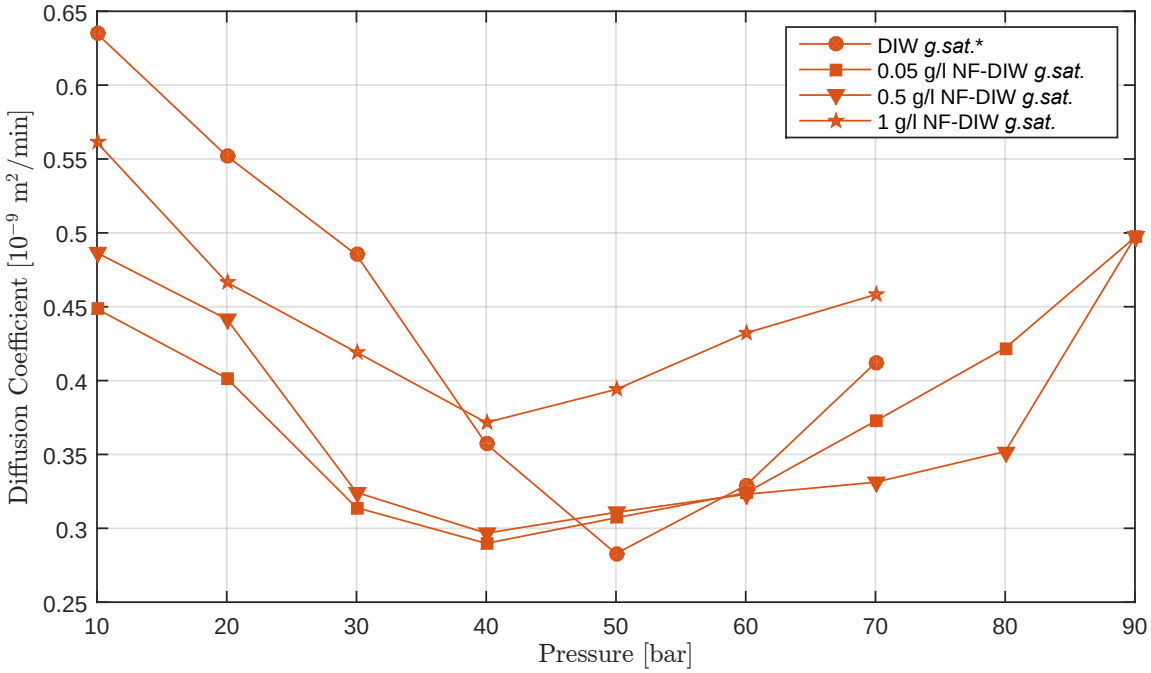

Figure 5.78: Diffusion coefficient of CO_2 into *n*-decane from unsaturated DIW-CNF. 25°C *gradually saturated*

Figure 5.79 and 5.80 shows similar graphs as figure 5.76 and 5.78, but for 45°C. I.e. the first plot shows the comparison among *saturated* and *gradually saturated* environments, while the latter shows the *gradually saturated* alone. In figure 5.79 it can be observed that for the *gradually saturated* scenario, the different cases of concentrations are extremely close to each other. Consulting figure 5.80 reveals that it is indeed some variation, but this is assumed to be within the error margin. This means that at 45°C, in a *gradually saturated* environment, the concentration of nanofluid becomes insignificant for the magnitude of the diffusion coefficient.

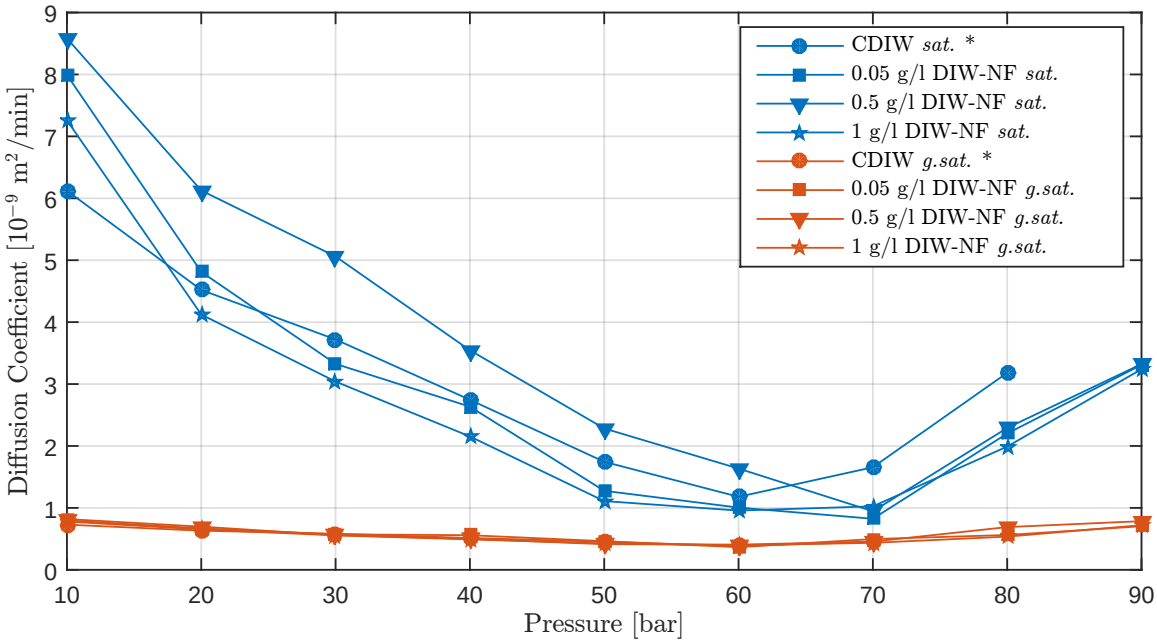

Figure 5.79: Diffusion coefficient of CO_2 into *n*-decane from DIW-CNF. 45°C *saturated* and *gradually saturated*

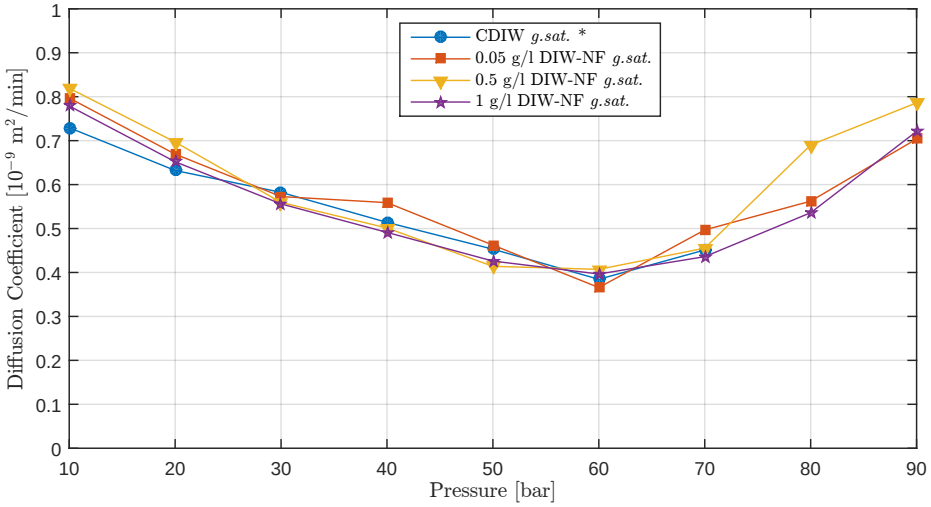

Figure 5.80: Diffusion coefficient of CO_2 into *n*-decane from unsaturated DIW-CNF. 45°C *gradually saturated*

5.6.3 Swelling Factors

Figure 5.81 and 5.82 depicts the swelling factors with sensitivity on the saturation-mode in the former, and sensitivity on the temperature in the latter. It may be observed that for both cases it can be stated that at low pressures (P < 40) shows no significant differences, this might be to the relatively low swelling at low pressures. The swelling factor for *saturated* conditions becomes ≈ 50% higher than that of *gradually saturated* at pressures above 50 bar (Fig. 5.81). This can also be said about the relationship between temperatures, but in that case, the 25°C scenarios behave differently from 45°C at, and around, phase-change pressure for CO_2. This results in a slightly less difference at higher pressures (P > 60 bar). In both sensitivity studies

(Fig. 5.81 and 5.82), it is very clear that cases containing nanofluid forms a group separate from pure carbonated water. In its respective scenario CNF do result in a greater swelling factor than CW. Moreover, the 0.5 g/l CNF, do unconditionally result in the highest swelling factor. This observation really strengthens the claim that 0.5 g/l is the optimum concentration among the three investigated (0.05, 0.5 and 1 g/l). It is also convenient, that the optimum most likely is the concentration in the middle of the two others, as it would not be possible to propose this unless lower readings were observed on both sides.

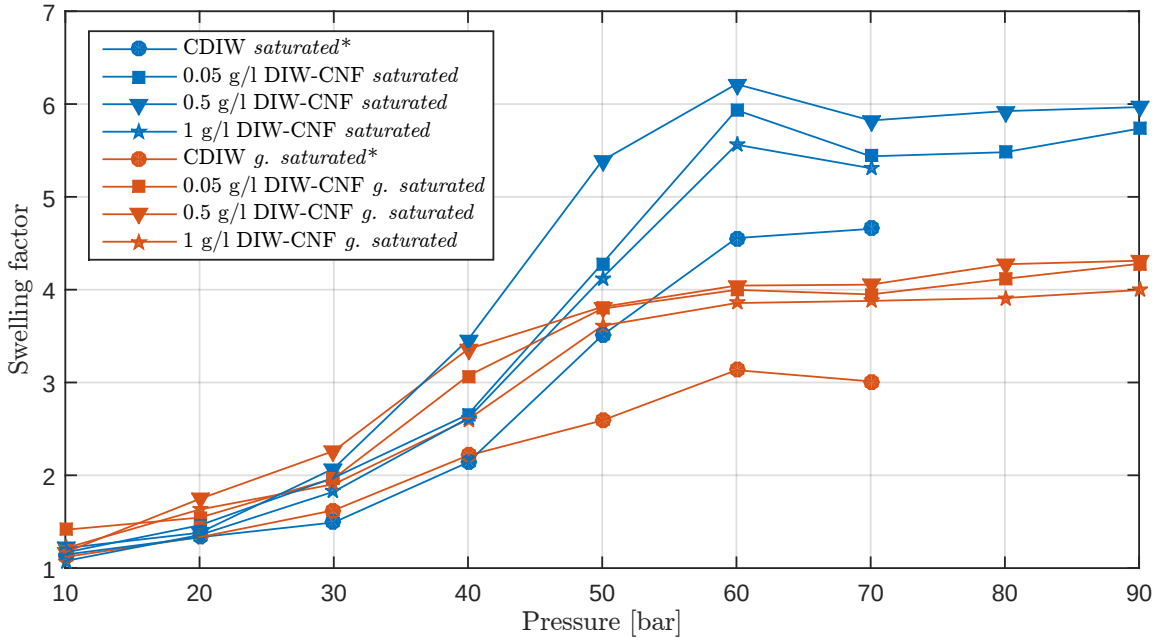

Figure 5.81: Swelling factor of an *n*-decane drop surrounded by *saturated DIW-CNF*. 25°C textitsaturated and *gradually saturated*

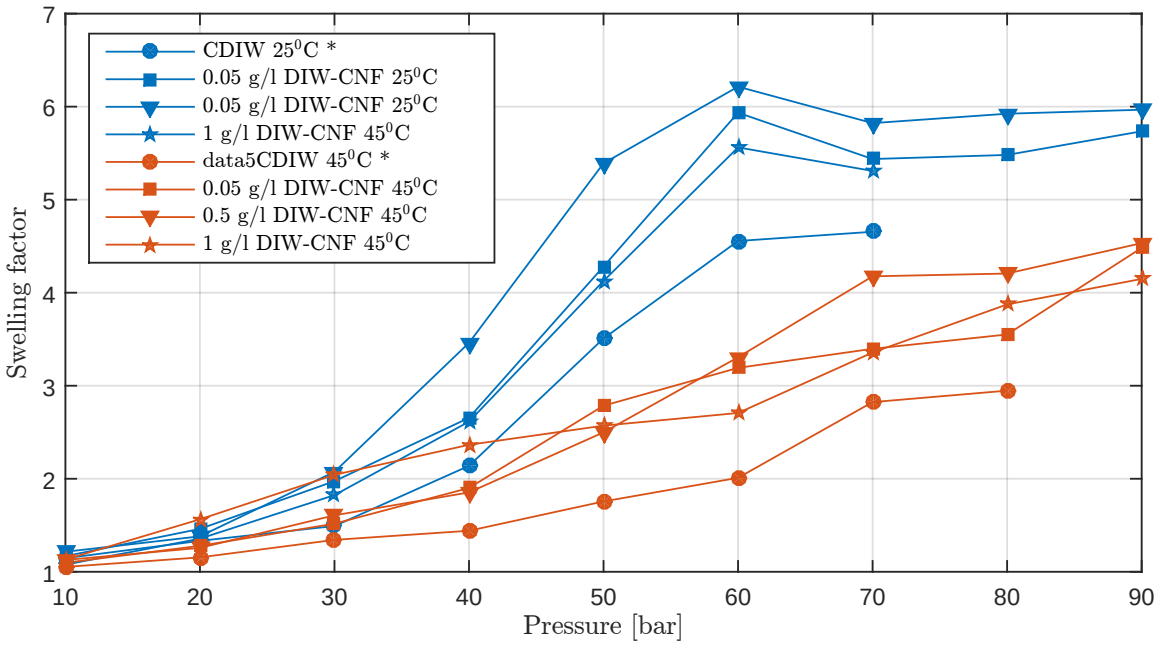

Figure 5.82: Swelling factor of an n-decane drop surrounded by *saturated DIW-CNF* at 25°C and 45°C

5.6.4 Sumarising Points for Diffusion Coefficient and Swelling Factor

- The diffusion coefficient decreases with pressure until phase-change pressure for CO_2 ($\approx$ 64 bar for 25°C, and 74 bar for 45°C), then the diffusion coefficient increases with pressure
- $D \propto IFT^{-1}$.
- For diffusion from carbonated water/nanofluid, the opposite trend in diffusion coefficient with pressure occurs, compared to diffusion of free gas into oil. This is explainable, and related to $IFT \propto \Delta\rho$.
- Swelling factor increases with pressure.
- Diffusion coefficient calculation and IFT calculation is complementary to each other, in the sense that the only thing that relates their calculation method is the same physical raw data recordings. Since both calculated properties shows similar phenomena (i.e. IFT increase with pressure - D decrease with pressure), it validates the calculation and confidence in the results and analysis is strengthen.
- Higher temperature results in higher diffusion coefficient.
- Diffusion coefficient are higher for CO_2 *saturated* scenarios, than for *gradually saturated scenarios*.
- At 45°C*gradually saturated* scenarios, there is no variation in diffusion coefficient with change in nanofluid concentration.

- There is no significant difference in swelling factor with temperature or saturation-mode at P $<$ 40 bar.
- Carbonated nanofluid (0.05, 0.05, 1 g/l) do unconditionally result in higher swelling factor than carbonated water.
- 0.5 g/l CNF do unconditionally result in highest swelling factor.

$$D = f(IFT, sol)$$
$$SF = f(sol), SF \neq f(IFT)$$

5.7 Synthetic Sea Water (SSW)

Experiments with SSW-NF have been carried out for one concentration of nanofuid (1 g/l), one temperature (45°C), five pressures (10, 30, 50, 70 and 90 bar) and for *saturated* and *gradually saturated* conditions, a total of 10 experiments, which also have a DIW-NF counterpart (1 g/l DIW-NF 45°C). Since most conventional mechanism have already been discussed for DIW-NF, the discussion surrounding synthetic sea water (SSW) will be arranged as a comparison to DIW-NF. The number of SSW-NF experiments are not enough to suggest mechanisms and behaviour with certainty, as it for instance is only conducted at one temperature. Carrying out these experiments, and include them in this thesis, is intended for qualitative comparison, and more experiments on this matter are planned for future research.

5.7.1 Volume Change

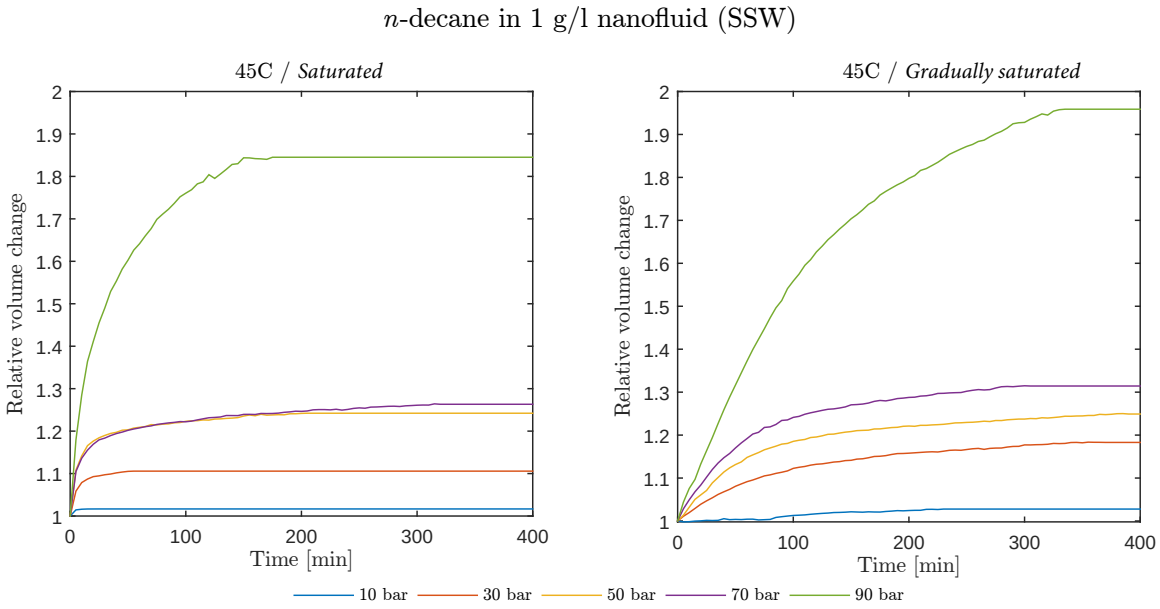

Figure 5.83: Dynamic of an *n*-decane drop surrounded by SSW-CNF 1 g/l at 45°C.

The dynamic volume of *n*-decane surrounded by SSW-CNF can be seen in figure 5.83, for both *saturated* and *gradually saturated* environments. It may be observed

that as previously discussed for DIW-CNF, the *saturated* environment results in a faster achievment of equilibrium volume, due to the greater concentration gradient. The equilibrium volume is increasing with pressure for both scenarios, and a massive jump at 90 bar is observed for both. These experiments are conducted at 45°C, which means that the pressure at which free CO_2 reaches super critical state is 74 bar. This pressure is crossed between the experiment conducted at 70 bar, and the ones conducted at 90 bar. It is not certain wheter the observation of a higher equilibrium volume for the *gradually saturated* experiment is correct.

A possibly important observation for further analysis is made in chapter 3.3, it is seen that carbonated SSW-NF have lower density than carbonated DIW-NF, while pure SSW have greater density than pure DIW. The saltwater saltwater is heavier than freshwater, but the phenomenon regarding carbonated water is explained by the lower solubility of CO_2 in water when salts are added. Dissolution of CO_2 in water are increasing its weight, and by that mechanism, CO_2 saturated SSW becomes lighter than CO_2 saturated DIW.

Figure 5.84 compares the equilibrium volume of the *n*-decane drop exposed to SSW-CNF for *saturated* and *gradually saturated* experiments. It can be observed that the equilibrium volumes are similar for P = 10 to P = 70 bar, and may be regarded as being similar. However, the equilibrium volume at 90 bar is deviating from this fashion, and it is uncertain whether it is an experimental error or not. If it is true, it means that somehow the *gradually saturated* experiments are able to form a greater CO_2 gradient between the environment and the drop. However, this is deemed unlikely, and the difference is most probably experimental error.

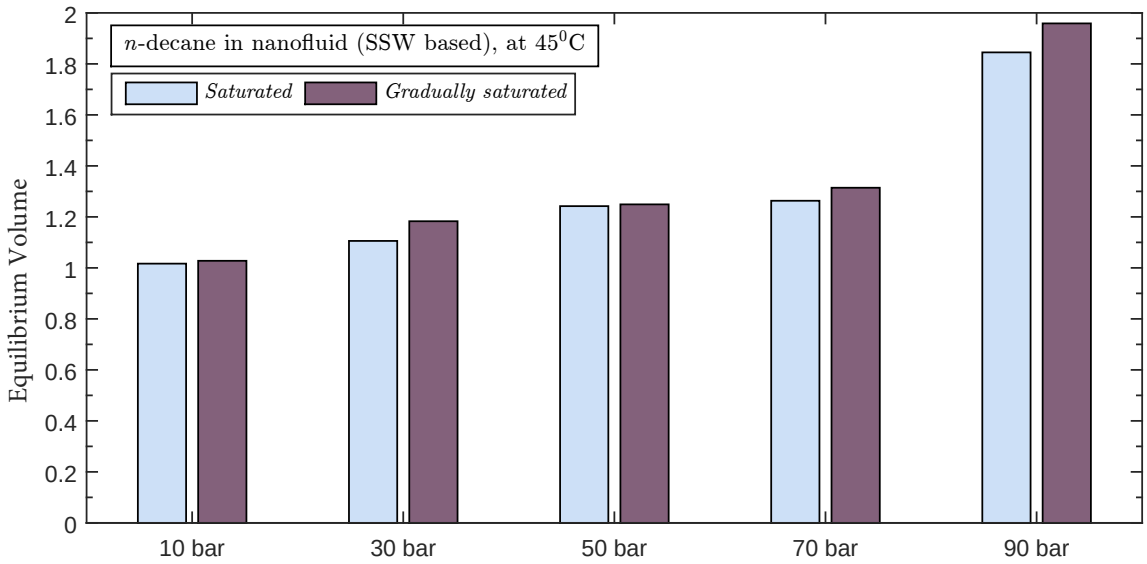

Figure 5.84: Equilibrium volume of an *n*-decane drop surrounded by SSW-CNF 1 g/l at 45°C.

Figure 5.85 compares equilibrium volume of the *n*-decane drop between SSW-CNF and DIW-CNF *saturated* environments, which effectively is to compare the degree of swelling. As expected, the swelling is lower for for SSW-CNF, whih is suggested

to mainly be caused by lower solubility of CO_2 in SSW than DIW. A lower CO_2 content results in a lower CO_2 gradient between the environment and the drop. The concentration gradient determines the amount of CO_2 transported into the drop before the gradient equalises. This is extensively discussed in chapter 5.1.2, together with the behaviour of mass-transport with pressure. However, the effect of SSW-CNF environment seems to be less significant at pressures higher than the critical pressure for free CO_2. If correct, this might be an interesting observation in terms of EOR offshore, where saltwater is readily available for waterflooding, and freshwater is not. Additionally, critical pressure and temperature for CO_2 is not hard to reach, and are often a given in offshore oil reservoirs.

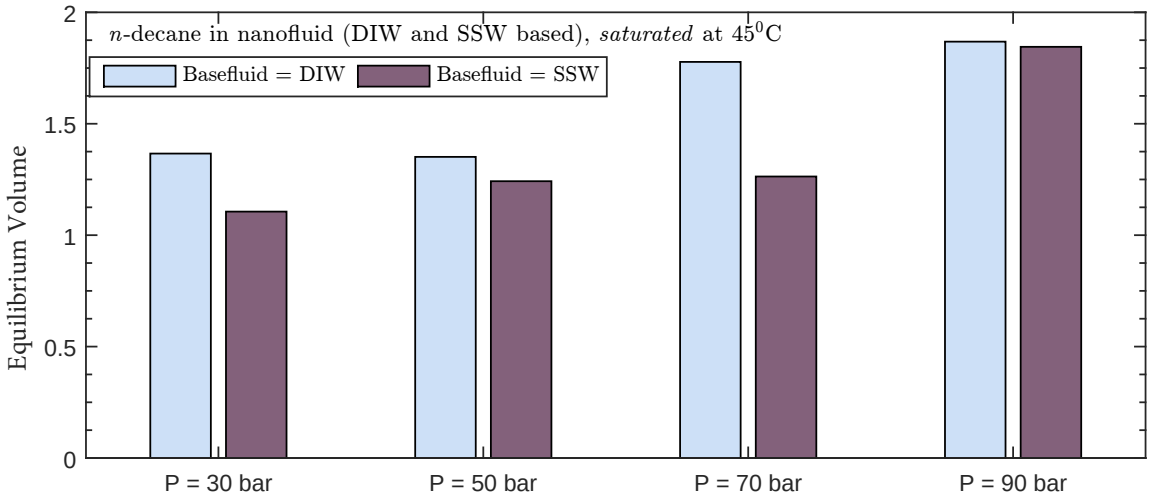

Figure 5.85: Comparison of equilibrium volume of an n-decane drop surrounded by SSW-CNF 1 g/l and a drop surrounded by DIW-CNF at 1 g/l at 45°C, *saturated* environment

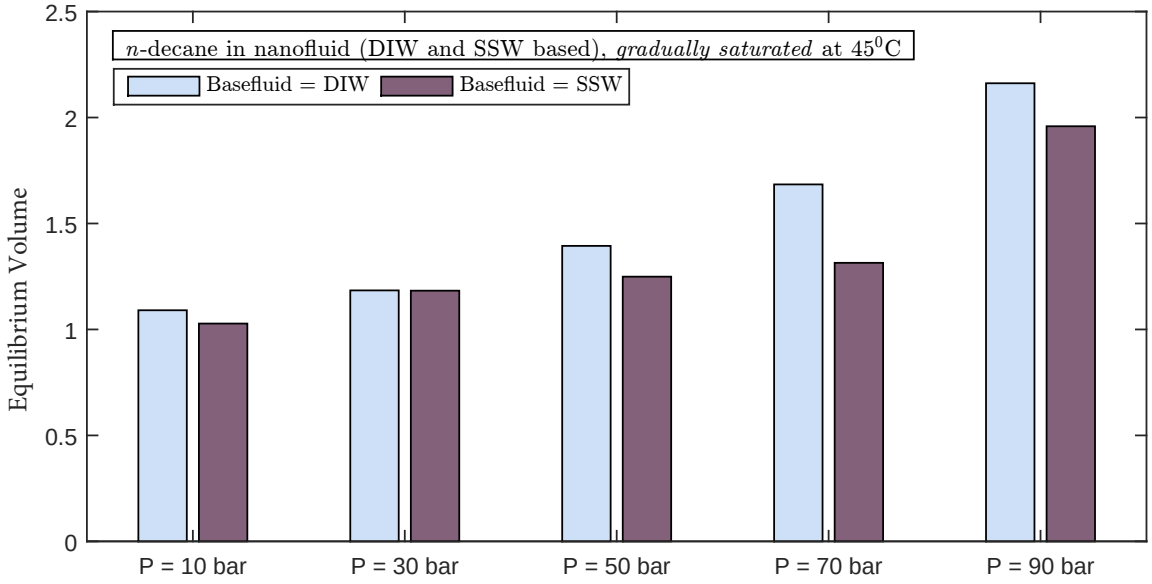

Figure 5.86: Comparison of equilibrium volume of an n-decane drop surrounded by SSW-CNF 1 g/l and a drop surrounded by DIW-CNF at 1 g/l at 45°C, *gradually saturated* environment

The *gradually saturated* comparison between DIW-CNF and SSW-CNF may be observein figure 5.86. As expected, SSW tends to result in a lower swelling. Similar observations for 90 bar as in the *saturated* comparison (Fig. 5.85) is not observed, i.e. the swelling of n-decane exposed to SSW-CNF is lower than the exposed to DIW-CNF. This might suggest that the SSW reading for 90 bar in figure 5.85 is erroneous. Moreoverm it might be observed that the behaviour with pressure is slightly different for SSW-CNF than DIW-CNF (fig. 5.86), in the sense that DIW-CNF experience a steeper increase in equilibrium volume with pressure.

5.7.2 Mole Fraction

Mole fraction of CO_2 present in the n-decane drop at equilibrium volume is presented in figure 5.87, 5.88 and 5.89, where DIW-CNF and SSW-CNF at *saturated* and *gradually saturated* conditions. SSW-CNF is compared among the two environments, respectively. The equilibrium mole fractions reflects what is observed in the equilibrium volume section, but takes density into account. The effect of density is not so evident at 45°C because of the smooth transition of free CO_2 density when critical pressure is surpassed. Mole fractions are important in the calculation of density and viscosity and extensively described in chaper 5.2. The relative comparison between SSW-CNF environment and DIW-CNF environment have been done in the previous section (Volume).

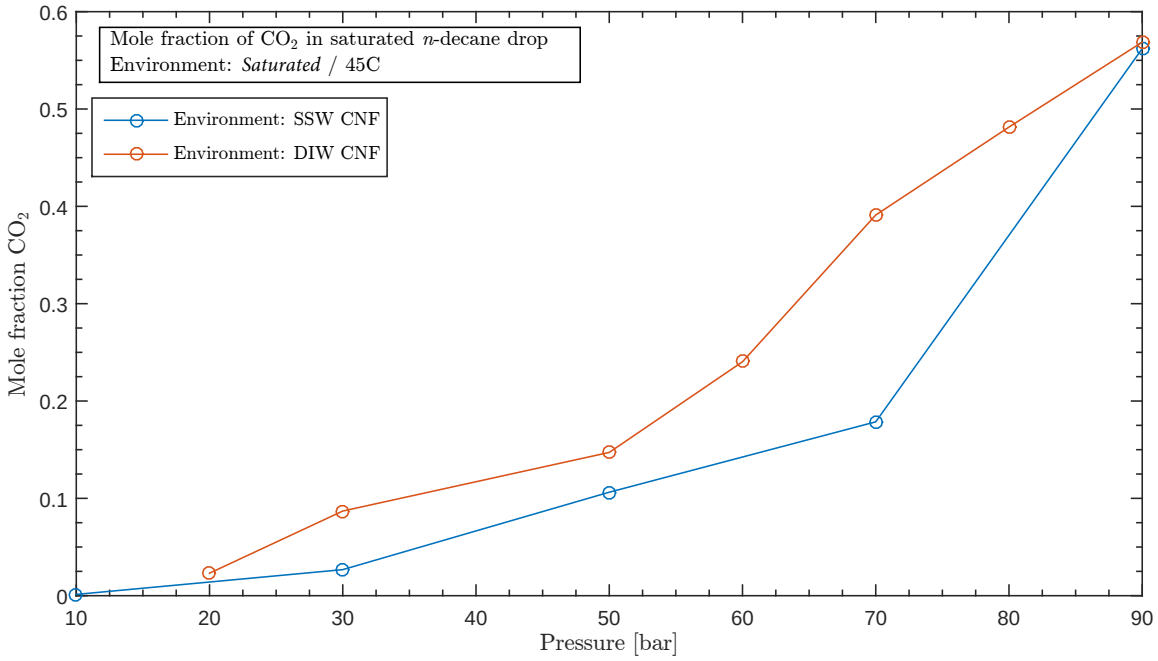

Figure 5.87: Comparison of equilibrium mole fraction of an n-decane drop surrounded by SSW-CNF 1 g/l and a drop surrounded by DIW-CNF at 1 g/l at 45°C, *saturated* environment

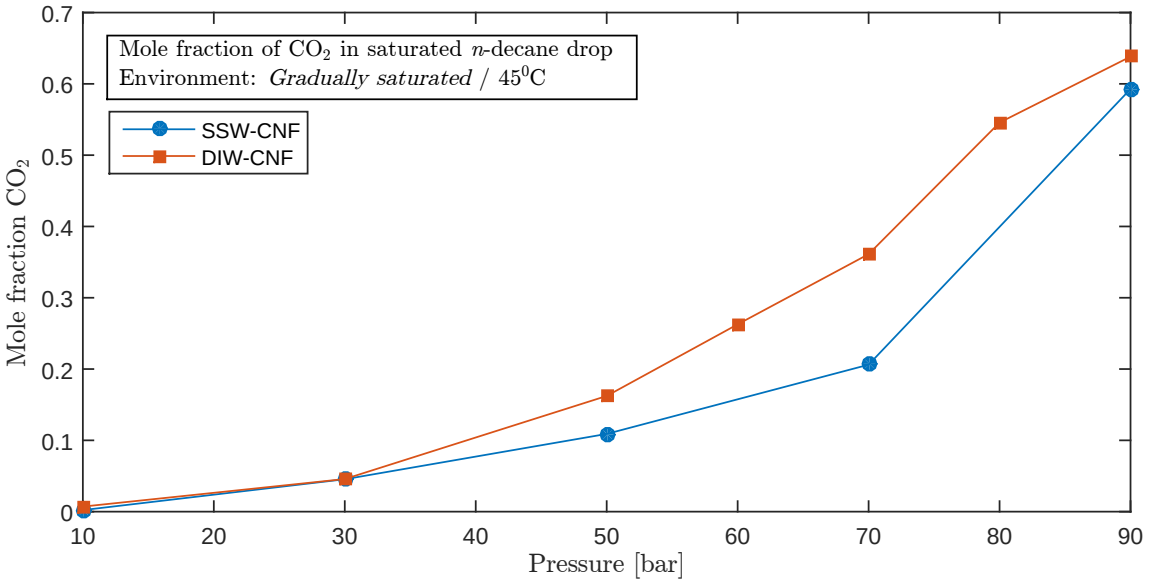

Figure 5.88: Comparison of equilibrium volume of an n-decane drop surrounded by SSW-CNF 1 g/l and a drop surrounded by DIW-CNF at 1 g/l at 45°C, *gradually saturated* environment

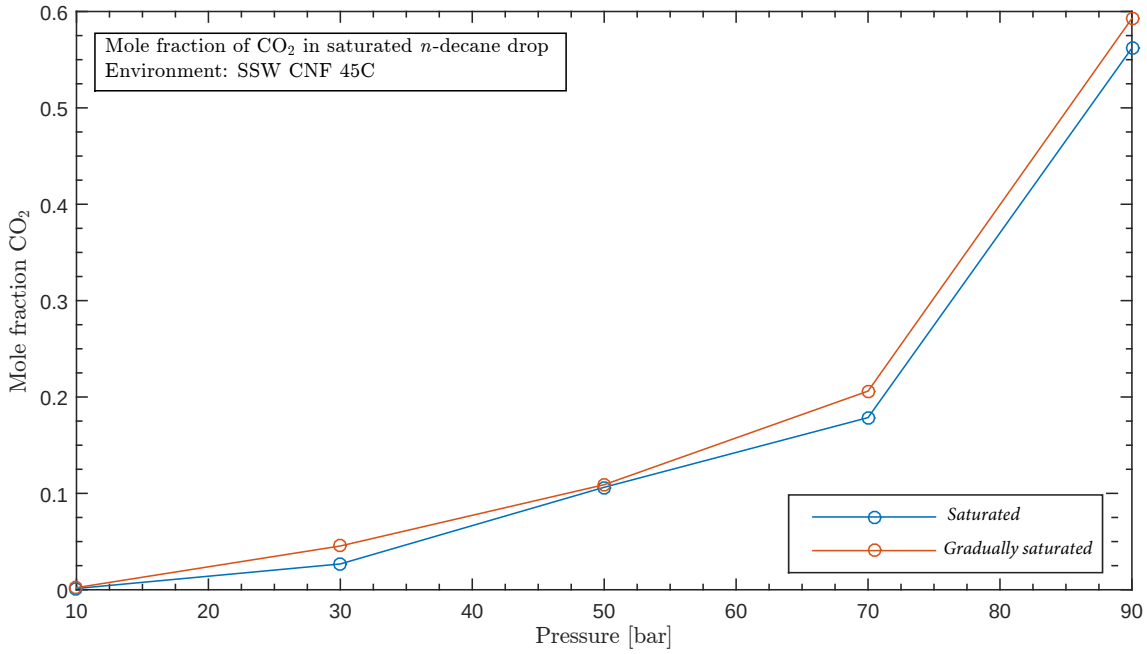

Figure 5.89: Comparison of equilibrium volume of an n-decane drop surrounded by SSW-CNF 1 g/l at 45°C, *saturated* and *gradually saturated* environment

5.7.3 Density

The method for calculating density of the drop at equilibrium is discussed in chapter 3.5. Figure 5.90 compares the density of the *n*-decane drop at *saturated* and *gradually saturated* conditions. It may be observed that the density is always higher for the *sarated* environment, but the difference is quite small, considering the scale. The difference is the largest at P = 30 bar, and smallest at P = 50 bar. What is known from the DIW-CNF experiments is also that the density of the drop is largely dependent on the density of CO_2, the fact that density of CO_2 experience a higher increase from 80 to 90 bar, than from for instance 60 to 70 (Ch. 2.2, Fig. 2.4), may be masking an effect of crossing the critical pressure. In the DIW-CNF experiments it is consistently observed a density increase of the drop across the critical pressure during *saturated* environment experiments, while it is not seen for the *gradually saturated* experiments. For SSW-CNF experiments it is observed in neither, which may be a result of data-points every twenty bar, and not every tenth.

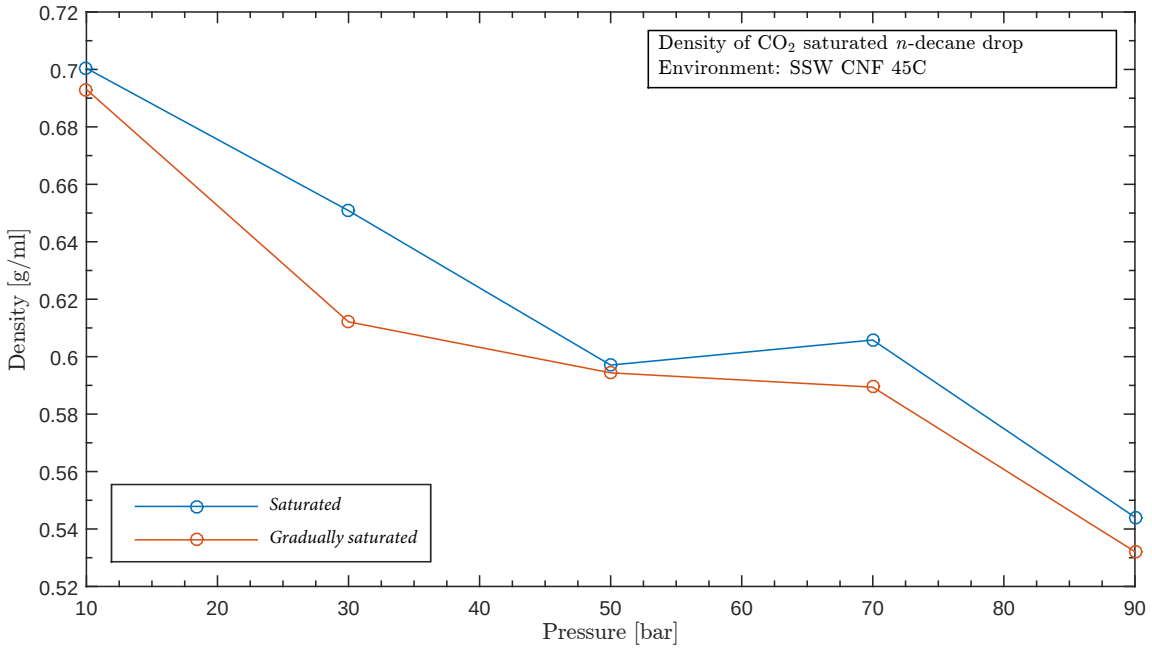

Figure 5.90: Comparison of equilibrium density of an *n*-decane drop surrounded by SSW-CNF 1 g/l at 45°C, *saturated* and *gradually saturated* environment

Figure 5.91 compares SSW-CNF and DIW-CND *saturated* environments, it can be seen that the *n*-decane drop exposed to SSW-CNF generally experience a greater density, which is due to the lower content of CO_2 present(Observed in mole frac. fig.5.87). This is also the reason for the more similar densities at 90 bar, where the volume and mole fraction is similar, this have been discussed. The aforementioned increase in density of the drop at 90 bar can be observed for the DIW-CNF environment, where it becomes obvious that a data-point at 80 bar for SSW-CNF is indeed needed to be able to compare the trends.

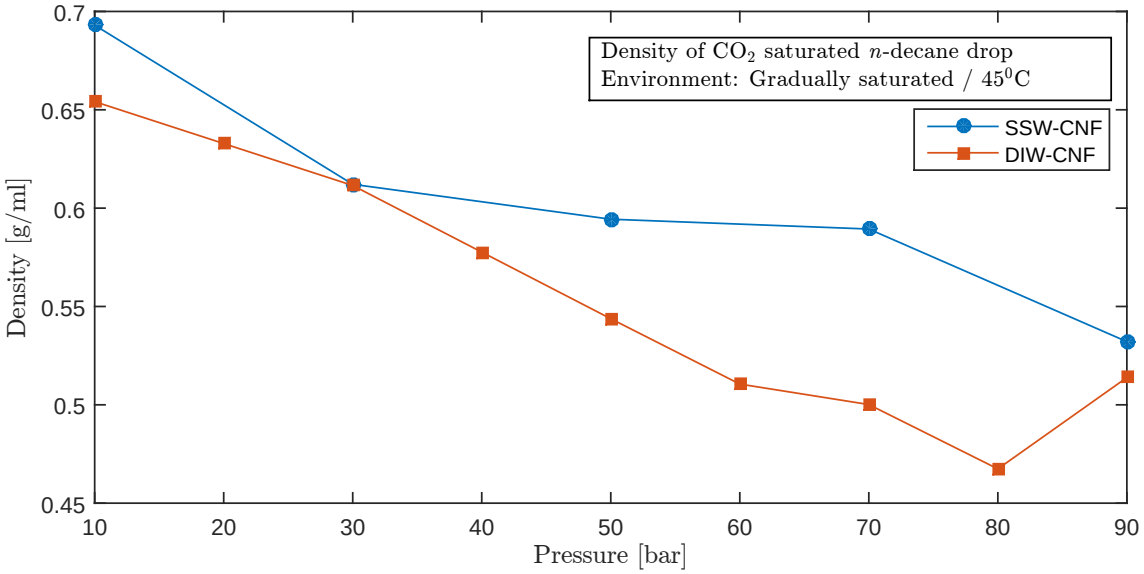

Figure 5.91: Comparison of equilibrium density of an n-decane drop surrounded by SSW-CNF 1 g/l and a drop surrounded by DIW-CNF at 1 g/l at 45°C, *gradually saturated*

5.7.4 Viscosity

The method for calculating viscosity of the drop at equilibrium is discussed in chapter 3.5. Figure 5.92 shows the comparison among the two saturation-modes of the environment (*saturated* and *gradually saturated*), for an n-decane drop surrounded SSW-CNF. The viscosity is of the two cases is so similar, they can maybe be regarded as the same, from the discussion on mole fraction it is shown that the moles of CO_2 present are also quite similar in the two cases. Previous discussion on density (fig. 5.90) shows that there exists a percent-wise larger difference in equilibrium density, which means that the viscosity is less dependent on the amount of CO_2 present, than what density is

Figure 5.93 shows that the viscosity of the n-decane drop is greater in an SSW-CNF *saturated* environment than DIW-CNF, this is a result of lower content of CO_2 which otherwise would have reduced the viscosity. It is also observed that the viscosity becomes more or less similar at P = 90 bar, due to similar CO_2 content.

Figure 5.94 is a similar plot as 5.93, but for *gradually saturated* environments. Similar trends can be observed for them. Comparing all three figures (5.92, 5.93, and 5.94) it is evident that the viscosity change for all cases where $P \leq 50$ bar is experiencing minimal change with pressure. A rapid decrease occurs for the DIW-CNF at pressure where $P > 50$ bar, this phenomenon seems to be delayed for the SSW-CNF cases, but that the equilibrium viscosity at P = 90 bar is still in the same range. That means that SSW-CNF experiences a delayed, but steeper decline in viscosity with pressure.

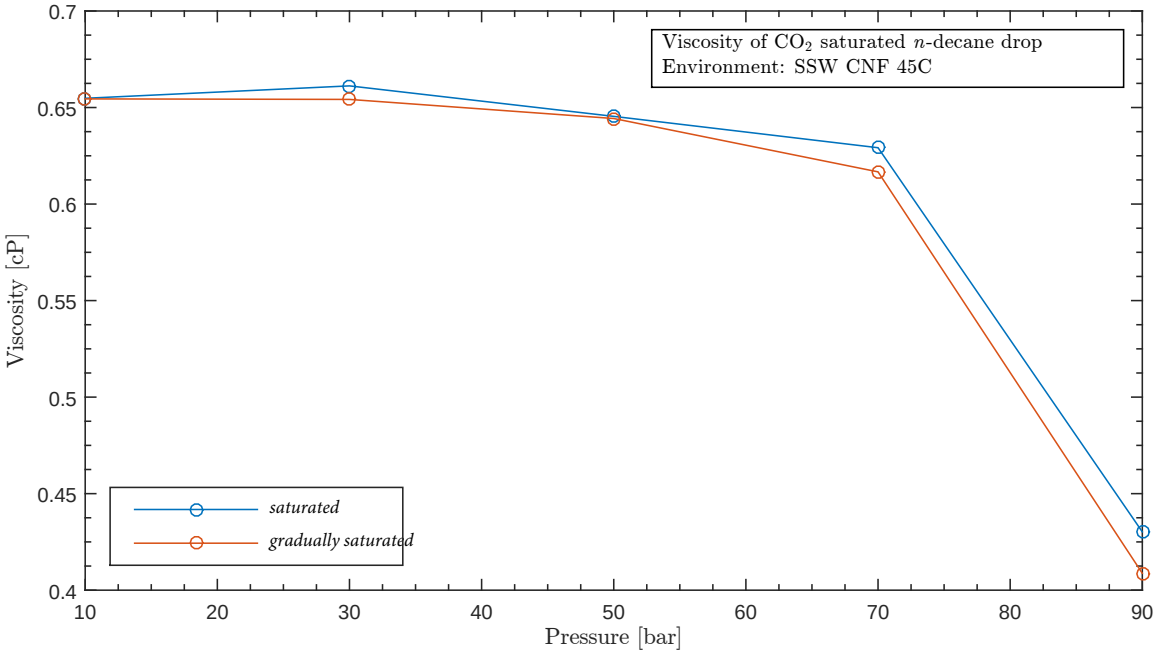

Figure 5.92: Comparison of equilibrium viscosity of an n-decane drop surrounded by SSW-CNF 1 g/l at 45°C, *saturated* and *gradually saturated* environment

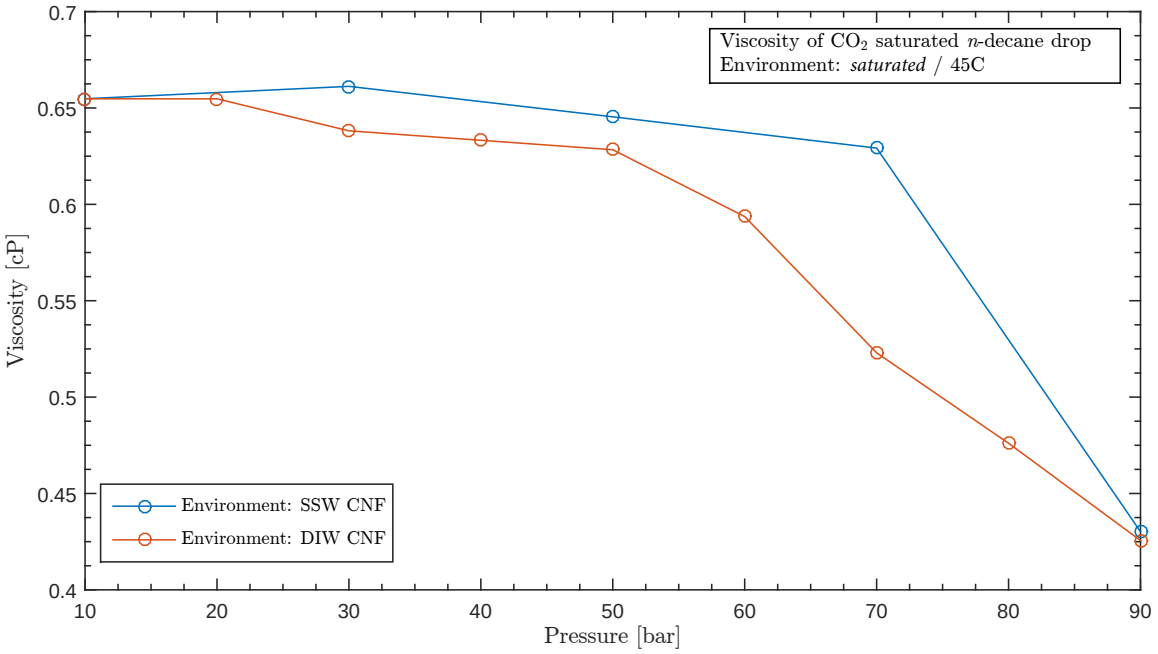

Figure 5.93: Comparison of equilibrium viscosity of an n-decane drop surrounded by SSW-CNF 1 g/l and a drop surrounded by DIW-CNF at 1 g/l at 45°C, *saturated*

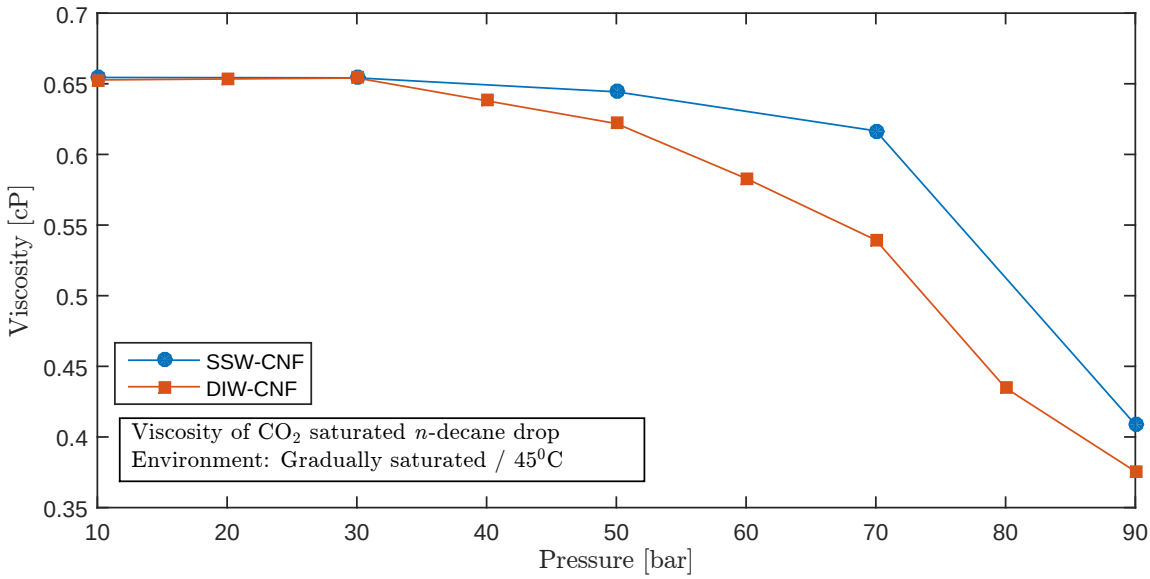

Figure 5.94: Comparison of equilibrium density of an n-decane drop surrounded by SSW-CNF 1 g/l and a drop surrounded by DIW-CNF at 1 g/l at 45°C, *gradually saturated*

5.7.5 Interfacial Tension, Swelling Factor, and Diffusion Coefficients

The interfacial tension for the *n*-decane drop with SSW and DIW based CNF at 45°C for *saturated* and *gradually saturated* environments are compared in figure 5.95. It is observed that the SSW-CNF environment result in a lot less variance in the trend, but that both environments results in an increase in IFT with pressure, due to CO_2 being transported into the drop. This have been extensively discussed in section (5.5). At 25 °C, the IFT experience a large decrease at the 70 bar data-point, due to the shift in CO_2 density, this shift is not evident at 45°C, since the phase-change of CO_2 goes from gaseous to super critical and not from gaseous to liquid. Morover, it is observed that the interfacial tension in an SSW-CNF environment is generally lower than for a DIW-NF environment. To factors are believed to play a role; 1) The lower solubility of SSW, which lead to lower concentration gradient, which leadss to less CO_2 being transported across the SSW-CNF / *n*-decane interface, which lead to a lower density difference ($\Delta\rho$) between the phases and a lower IFT. 2) The lower density of SSW-CNF compared to DIW-CNF is probably also reducing the density difference between the environment and the drop, and contributing to reducing IFT.

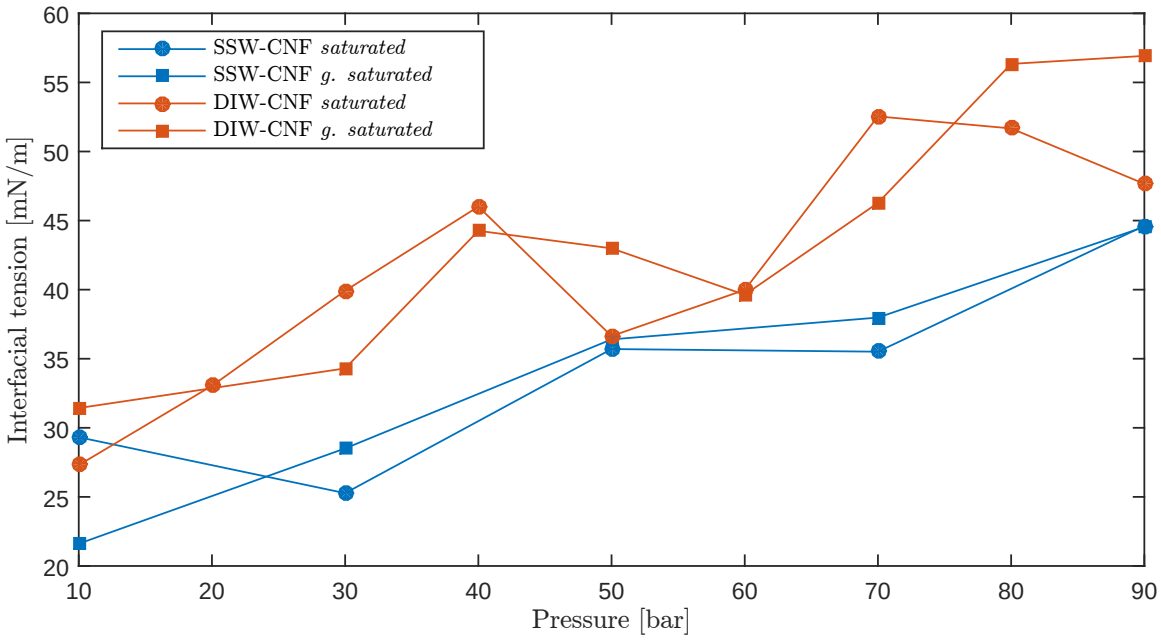

Figure 5.95: Comparison interfacial tension of an *n*-decane drop for SSW and DIW based CNF at 45°C for *saturated* and *gradually saturated* environments.

The swelling factor of *n*-decane is compared between being exposed to SSW-CNF or DIW-CNF in figure 5.96. A difference is observed between them, where DIW-CNF results in a greater swelling factor. Both of them follow a similar trend with pressure, where the rate of increase also changes from P = 50/60 bar to P = 70 bar. The swelling factor takes both time to reach equilibrium, and the degree of swelling into account. The dynamic volume change of both DIW-CNF and SSW-CNF at 50 bar (where the swelling factor difference is large) is plotted in figure 5.97 for illustration. The plot is generate with raw data obtained from the recorded drops.

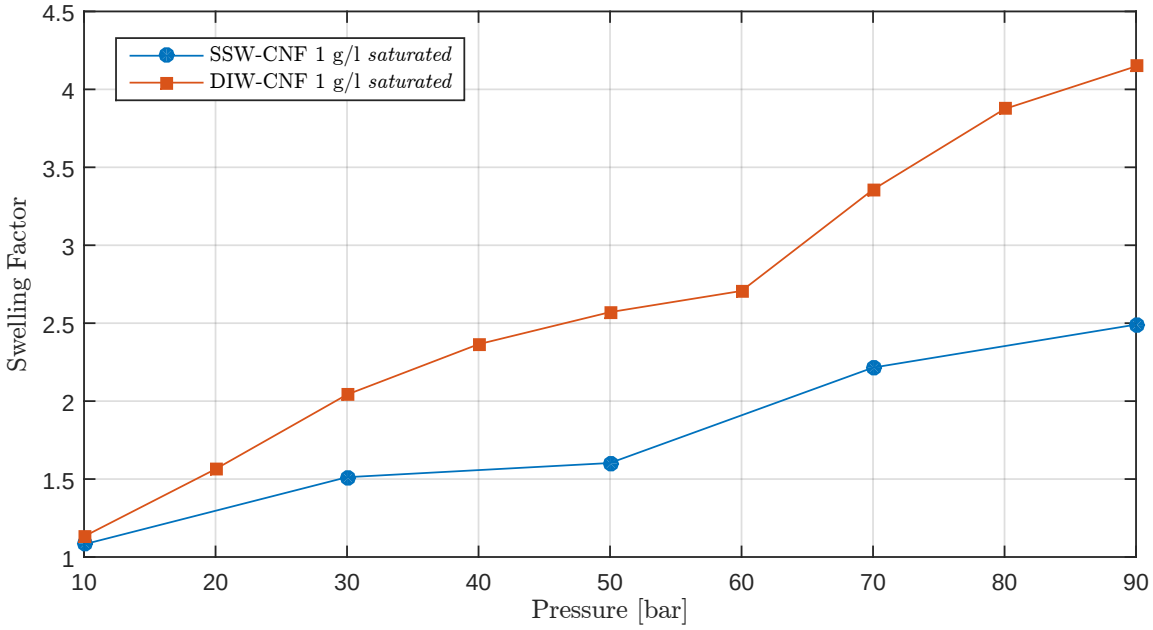

Figure 5.96: Comparison of swelling factor of SSW and DIW based CNF at 45°C for *saturated* environment.

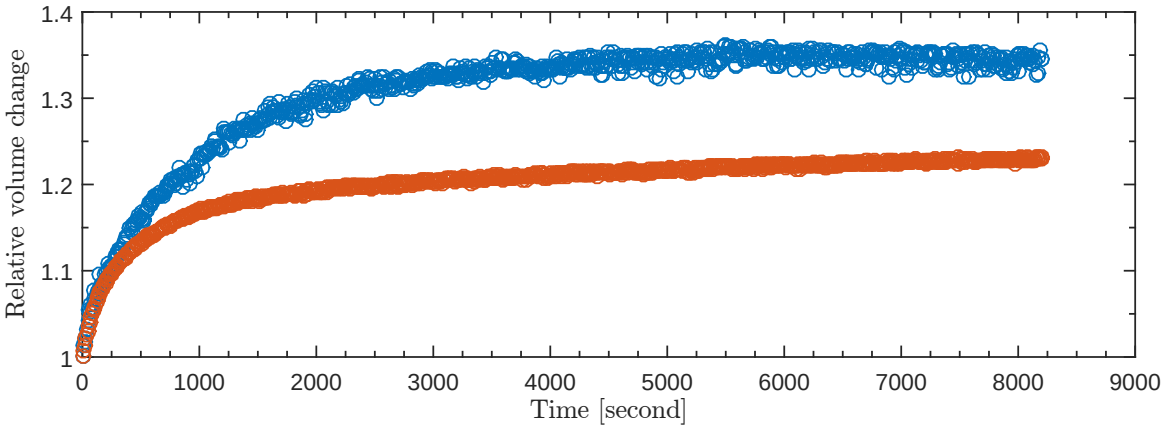

Figure 5.97: Dynamic volume change of an n-decane drop exposed to carbonated nanofluid. Both scatter plots show the swelling at 50 bar and 25°C. where the orange points are SSW, and the blue are DIW-based nanofluid

The diffusion coefficients for both DIW-CNF and SSW-CNF environment are plotted in figure 5.98. It may be observed that the scenario with SSW-CNF do not follow a similar trend as DIW-CNF environment does, further investigations into SSW are needed to say something concrete about this behaviour. As stated, the driving force for diffusion is given by the concentration gradient of CO_2, which generally is lower for SSW-CNF. However, between $40 < P < 80$ the diffusion coefficient how SSW-CNF is the greatest. It must be noted that swelling factor plays a role on the diffusion coefficient, but it is a phenomenon worth further investigation. Notably, at P = 50 bar, the IFT of SSW-CNF and DIW-CNF is in the similar range (Fig. 5.95).

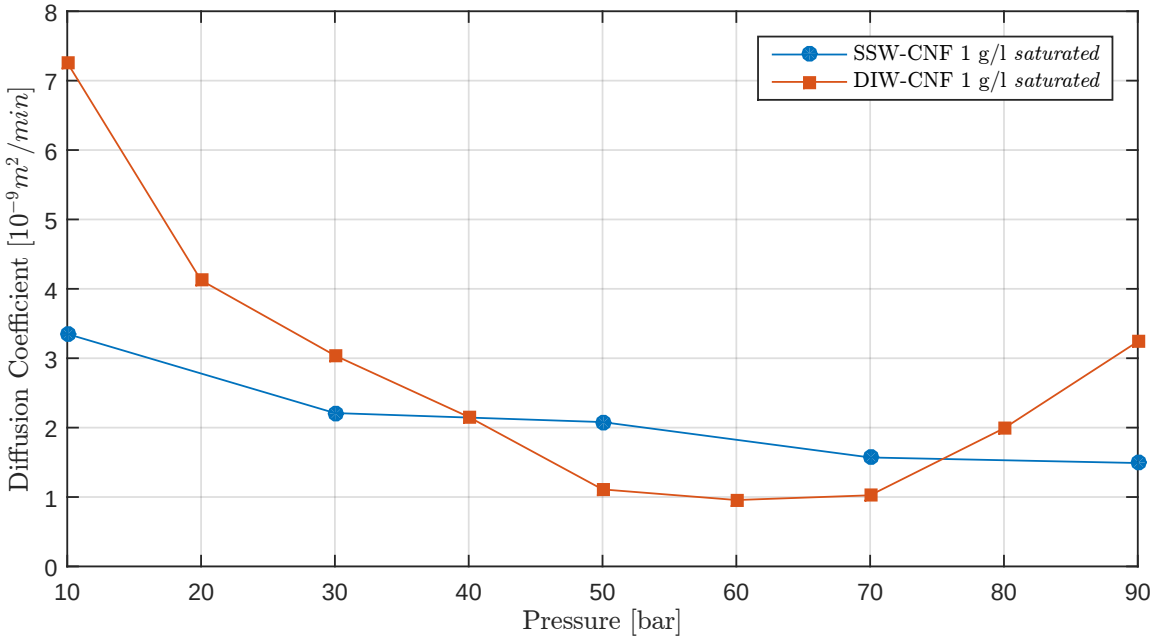

Figure 5.98: Comparison of diffusion coefficient of SSW and DIW based CNF at 45°C for *saturated* environment.

5.7.6 Summarising Points on SSW

- Carbonated SSW is lighter than carbonated DIW.
- An environment of SSW-CNF generally results in a lower equilibrium volume for an *n*-decane drop exposed to it, compared to DIW-CNF.
- The equilibrium density of an *n*-decane drop exposed to SSW-CNF is generally higher than a drop exposed to DIW-CNF.
- The equilibrium viscosity is less affected by CO_2 content variations than equilibrium density.
- An *n*-decane drop exposed to SSW-CNF experience a similar viscosity as an *n*-decane drop exposed to DIW-CNF at P = 90 bar.
- The viscosity of an *n*-decane drop exposed to either DIW-CNF or SSW-CNF is minimally affected by pressure variations for pressures lower than 50 bar.

- The equilibrium viscosity of an n-decane drop exposed to SSW-CNF experience a delayed, but steeper, decrease with pressure, compared to an n-decane drop exposed to DIW-CNF.
- An SSW-CNF environment results in lower IFT between the n-decane drop and the environment, compared to DIW-CNF environment.
- An SSW-CNF environment results in a lower swelling factor of an n-decane drop, compared to DIW-CNF environment.
- An SSW-CNF environment generally results in a lower CO_2 diffusion coefficient into n-decane, but do supersede DIW-CNF environment at 50 bar $\leq$ P $\leq$ 70 bar.

Chapter 6

Summary and Conclusion

This study has been done in order to enhance the understanding of mechanisms related to carbonated water injection, and the possibilities of improving the process with utilisation of nanotechnology. Pendant drop diffusion experiments have been carried out at 25°C and 45°C, 10-90 bar, for three concentrations (0.05, 0.5 and 1.0 g/l) of water-based silica nanofluid, and one concentration (1 g/l) of synthetic sea water-based nanofluid. Two saturation schemes of CO_2 in the nanofluid have been explored, one initially CO_2 saturated, and one gradually saturated. These saturation schemes may represent the difference between a CO_2 gas injection process, and a carbonated water injection process, respectively. *n*-decane was introduced as a drop to a PVT cell through a capillary tube, and exposed to carbonated nanofluid. The change in volume, resulting from the CO_2 mass-transport across the interface between the drop and the surroundings, were recorded and analysed. Complementing the physically obtained dynamic volume data with a numerical modelling offered for quantification and analysis of several properties.

Drop-volume increase has shown to generally be greater when the pressure is higher, and to be inversely related to temperature. This is also true for the rate at which volume change occurs. The solubility of CO_2 in the environment, and the resulting concentration gradient, is likely to cause this relationship. The concentration gradient is the driving-force for mass-transfer, and is reduced alongside transport; this means that rate of volume increase declines over time. The effect of temperature on mass transport was shown to be most evident at pressures higher than 50 bar. The degree of transport together with the density of CO_2, was observed to be deterministic for the total drop density.

The viscosity of the drop is counterintuitively shown to increase with temperature because of the CO_2 mass-transport into the *n*-decane, where the effect of increased solubility of CO_2 in the water with lower temperature is dominant to the direct effect of temperature on viscosity.

Pressure-temperature regions of gaseous, liquid and supercritical CO_2 have shown to be important to understand, where unexpected results of increased interfacial tension and decreased diffusion coefficient with an increase in pressure have been vali-

dated by two methods. Transition from gaseous to both supercritical and liquid state reverse this trend for diffusion coefficient. Transition from gaseous to liquid reverse it dramatically for interfacial tension, and it is found that density difference of the phases is predominantly affecting this property.

Interfacial tension is reduced by more than 50% by the transition from gaseous to liquid CO_2 region. The CO_2 solubility of the environment showed a large effect on the behaviour of interfacial tension, this is because the solubility is closely related to the concentration gradient, and therefore dictates the amount of CO_2 that is transported into the drop. It has been shown that a higher temperature reduces the interfacial tension. However, after transition to liquid CO_2 region, the reduced density difference, as a result of more CO_2 present, becomes so dominant that the interfacial tension is lower at 25°C than 45°C.

Diffusion coefficients, as observed in the literature, increased by a higher temperature, and was observed to be inversely related to interfacial tension. Contrary to free gas diffusion, the latter results in a decrease in the diffusion coefficient with increasing pressure in the gaseous CO_2 region. When the CO_2 was introduced to the system simultaneously as the drop, the CO_2 diffusion coefficient for transport into the drop were greatly reduced. This is natural as CO_2 has to dissolve and diffuse through the nanofluid before it reaches the drop.

Nanofluid showed to improve swelling factor relative to pure carbonated water. A possible optimum concentration for improving EOR properties in the CWI-process was found with 0.5 g/l water-based nanofluid, suggested to be caused by solubility improvement of CO_2 in water, and generating a greater concentration gradient.

Synthetic Sea Water-based nanofluid, compared to DIW-CNF at 45°C, generally resulted in a lower equilibrium volume for an *n*-decane drop exposed to it. Probably caused by the reduction in CO_2 solubility in the water by adding salts, and thereby lower the concentration gradient between the environment and the drop. Viscosity was seen to be less affected by the variation of CO_2 content than density, and at 90 bar had a similar value viscosity as a drop exposed to DIW-CNF. However, the viscosity experienced a delayed decrease, but a steeper slope as the pressure increased, which resulted in the similarities between DIW- and SSW-CNF at 90 bar. The CO_2 diffusion coefficient from the SSW-CNF into the drop was generally lower than DIW-CNF, but did surpass at pressures between 50 and 70 bar

Opportunities for utilising carbonated water injection, coupled with nano-EOR, to improve the possibilities for carbon storage, and enhance oil recovery has been indicated by this study. By investigating the CO_2 mass-transfer in gaseous, liquid and supercritical regions, it showed that those pressure-temperature ranges possibly are under-studied.

Bibliography

[1] S. Angus, B. Armstrong, and K. De Reuck, "Carbon dioxide: International thermodynamic tables of the fluid state-3," *Carbon Dioxide: International Thermodynamic Table of the Fluid State*, 1976.

[2] R. Span and W. Wagner, "A new equation of state for carbon dioxide covering the fluid region from the triple-point temperature to 1100 k at pressures up to 800 mpa," *Journal of physical and chemical reference data*, vol. 25, no. 6, pp. 1509–1596, 1996.

[3] "NIST thermophysical properties of fluid systems." `http://webbook.nist.gov/chemistry/fluid/`. Accessed: 2017-05-16.

[4] N. N. T. Inc., "Data sheet nyacol dp9711."

[5] U. Nations, "Adoption of the paris agreement, 21st conference of the parties," 2015.

[6] R. K. Pachauri, M. R. Allen, V. R. Barros, J. Broome, W. Cramer, R. Christ, J. A. Church, L. Clarke, Q. Dahe, P. Dasgupta, *et al.*, *Climate change 2014: synthesis report. Contribution of Working Groups I, II and III to the fifth assessment report of the Intergovernmental Panel on Climate Change*. IPCC, 2014.

[7] B. Petroleum, "Bp energy outlook 2016 edition," *Outlook to*, vol. 2035, 2016.

[8] N. Mungan, "Carbon dioxide flooding-fundamentals," *Journal of Canadian Petroleum Technology*, vol. 20, no. 01, 1981.

[9] R. M. Brush, H. J. Davitt, O. B. Aimar, J. Arguello, J. M. Whiteside, *et al.*, "Immiscible co2 flooding for increased oil recovery and reduced emissions," in *SPE/DOE Improved Oil Recovery Symposium*, Society of Petroleum Engineers, 2000.

[10] and others, "Method for producing oil by means of carbon dioxide," Dec. 30 1952. US Patent 2,623,596.

[11] L. Holm, V. Josendal, *et al.*, "Mechanisms of oil displacement by carbon dioxide," *Journal of petroleum Technology*, vol. 26, no. 12, pp. 1–427, 1974.

[12] C. Yang and Y. Gu, "Diffusion coefficients and oil swelling factors of carbon dioxide, methane, ethane, propane, and their mixtures in heavy oil," *Fluid Phase Equilibria*, vol. 243, no. 1, pp. 64–73, 2006.

[13] E. F. Righi, J. Royo, P. Gentil, R. Castelo, A. Del Monte, S. Bosco, *et al.*, "Experimental study of tertiary immiscible wag injection," in *SPE/DOE Symposium on Improved Oil Recovery*, Society of Petroleum Engineers, 2004.

[14] B. Caudle, A. Dyes, *et al.*, "Improving miscible displacement by gas-water injection," 1958.

[15] D. Green and G. Willhite, "Enhanced oil recovery, vol. 6," *SPE Textbook Series, TX, USA*, 1998.

[16] M. Sohrabi, A. Emadi, S. A. Farzaneh, S. Ireland, *et al.*, "A thorough investigation of mechanisms of enhanced oil recovery by carbonated water injection," in *SPE Annual Technical Conference and Exhibition*, Society of Petroleum Engineers, 2015.

[17] L. Kern, "High pressure gas-carbonated water miscible displacement process," Apr. 2 1974. US Patent 3,800,874.

[18] W. R. Shu, "Carbonated waterflooding for viscous oil recovery using a co2 solubility promoter and demoter," Nov. 15 1983. US Patent 4,415,032.

[19] M. Seyyedi, M. Sohrabi, and A. Farzaneh, "Investigation of rock wettability alteration by carbonated water through contact angle measurements," *Energy & Fuels*, vol. 29, no. 9, pp. 5544–5553, 2015.

[20] N. Mosavat and F. Torabi, "Experimental evaluation of the performance of carbonated water injection (cwi) under various operating conditions in light oil systems," *Fuel*, vol. 123, pp. 274–284, 2014.

[21] Z. Duan, R. Sun, C. Zhu, and I.-M. Chou, "An improved model for the calculation of co 2 solubility in aqueous solutions containing na+, k+, ca 2+, mg 2+, cl-, and so 4 2-," *Marine Chemistry*, vol. 98, no. 2, pp. 131–139, 2006.

[22] Y. Dong, B. Dindoruk, C. Ishizawa, E. J. Lewis, *et al.*, "An experimental investigation of carbonated water flooding," in *SPE Annual Technical Conference and Exhibition*, Society of Petroleum Engineers, 2011.

[23] G. Shu, M. Dong, S. Chen, and P. Luo, "Improvement of co 2 eor performance in water-wet reservoirs by adding active carbonated water," *Journal of Petroleum Science and Engineering*, vol. 121, pp. 142–148, 2014.

[24] A. Alizadeh, M. Khishvand, M. Ioannidis, and M. Piri, "Multi-scale experimental study of carbonated water injection: an effective process for mobilization and recovery of trapped oil," *Fuel*, vol. 132, pp. 219–235, 2014.

[25] H. Yang, L. James, and T. Johansen, "Carbonated water injection for eor in one dimensional flow with constant pressure boundaries,"

[26] M. Sohrabi, N. I. Kechut, M. Riazi, M. Jamiolahmady, S. Ireland, and G. Robertson, "Coreflooding studies to investigate the potential of carbonated water injection as an injection strategy for improved oil recovery and co2 storage," *Transport in porous media*, vol. 91, no. 1, pp. 101–121, 2012.

[27] M. Sohrabi, M. Tavakolian, A. Emadi, M. Jami, and S. Ireland, "Improved oil recovery and injectivity by carbonated water injection," in *International Symposium of the Society of Core Analysts held in Aberdeen, Scotland, UK, August*, pp. 27–30, 2012.

[28] M. Sohrabi, M. Riazi, M. Jamiolahmady, S. Ireland, and C. Brown, "Carbonated water injection (cwi) studies," in *29th Annual Workshop & Symposium, IEA Collaborative Project on Enhanced Oil Recovery*, pp. 3–5, 2008.

[29] M. Sohrabi, M. Riazi, M. Jamiolahmady, S. Ireland, and C. Brown, "Carbonated water injection for oil recovery and co 2 storage," in *Sustainable energy UK conference: meeting the science and engineering challenge, Oxford, UK*, 2008.

[30] M. Riazi, M. Sohrabi, M. Jamiolahmady, S. Ireland, *et al.*, "Oil recovery improvement using co2-enriched water injection," in *EUROPEC/EAGE Conference and Exhibition*, Society of Petroleum Engineers, 2009.

[31] M. Sohrabi, M. Riazi, M. Jamiolahmady, S. Ireland, and C. Brown, "Mechanisms of oil recovery by carbonated water injection," in *SCA annual meeting*, 2009.

[32] N. I. Kechut, M. Riazi, M. Sohrabi, M. Jamiolahmady, *et al.*, "Tertiary oil recovery and co2 sequestration by carbonated water injection (cwi)," in *SPE International Conference on CO2 Capture, Storage, and Utilization*, Society of Petroleum Engineers, 2010.

[33] M. Riazi, M. Sohrabi, and M. Jamiolahmady, "Experimental study of pore-scale mechanisms of carbonated water injection," *Transport in porous media*, vol. 86, no. 1, pp. 73–86, 2011.

[34] N. I. Kechut, M. Sohrabi, M. Jamiolahmady, *et al.*, "Experimental and numerical evaluation of carbonated water injection (cwi) for improved oil recovery and co2 storage," in *SPE EUROPEC/EAGE Annual Conference and Exhibition*, Society of Petroleum Engineers, 2011.

[35] N. I. Kechut, M. Jamiolahmady, and M. Sohrabi, "Numerical simulation of experimental carbonated water injection (cwi) for improved oil recovery and co 2 storage," *Journal of Petroleum Science and Engineering*, vol. 77, no. 1, pp. 111–120, 2011.

[36] M. Sohrabi, N. I. Kechut, M. Riazi, M. Jamiolahmady, S. Ireland, and G. Robertson, "Safe storage of co 2 together with improved oil recovery by co 2-enriched water injection," *Chemical Engineering Research and Design*, vol. 89, no. 9, pp. 1865–1872, 2011.

[37] M. Riazi, M. Jamiolahmady, and M. Sohrabi, "Theoretical investigation of pore-scale mechanisms of carbonated water injection," *Journal of Petroleum Science and Engineering*, vol. 75, no. 3, pp. 312–326, 2011.

[38] M. R. Riazi, "A new method for experimental measurement of diffusion coefficients in reservoir fluids," *Journal of Petroleum Science and Engineering*, vol. 14, no. 3-4, pp. 235–250, 1996.

[39] Y. Zhang, C. Hyndman, and B. Maini, "Measurement of gas diffusivity in heavy oils," *Journal of Petroleum Science and Engineering*, vol. 25, no. 1, pp. 37–47, 2000.

[40] S. R. Upreti and A. K. Mehrotra, "Diffusivity of co2, ch4, c2h6 and n2 in athabasca bitumen," *The Canadian Journal of Chemical Engineering*, vol. 80, no. 1, pp. 116–125, 2002.

[41] C.-d. Yang and Y.-a. GU, "A new method for measuring solvent diffusivity in heavy oil by dynamic pendant drop shape analysis," in *SPE Annual Technical Conference and Exhibition. Denver: Society of Petroleum Engineers*, 2003.

[42] D. Yang, P. Tontiwachwuthikul, and Y. Gu, "Dynamic interfacial tension method for measuring gas diffusion coefficient and interface mass transfer coefficient in a liquid," *Industrial & engineering chemistry research*, vol. 45, no. 14, pp. 4999–5008, 2006.

[43] N. Bagalkot and A. A. Hamouda, "Experimental and numerical method for estimating diffusion coefficient of the carbon dioxide into light components," *Industrial & Engineering Chemistry Research*, vol. 56, no. 9, pp. 2359–2374, 2017.

[44] M. F. Fakoya and S. N. Shah, "Emergence of nanotechnology in the oil and gas industry: Emphasis on the application of silica nanoparticles," *Petroleum*, 2017.

[45] R. Saidur, K. Leong, and H. Mohammad, "A review on applications and challenges of nanofluids," *Renewable and sustainable energy reviews*, vol. 15, no. 3, pp. 1646–1668, 2011.

[46] M. V. Bennetzen, K. Mogensen, *et al.*, "Novel applications of nanoparticles for future enhanced oil recovery," in *International Petroleum Technology Conference*, International Petroleum Technology Conference, 2014.

[47] B. Ju, T. Fan, and M. Ma, "Enhanced oil recovery by flooding with hydrophilic nanoparticles," *China Particuology*, vol. 4, no. 1, pp. 41–46, 2006.

[48] B. Ju and T. Fan, "Experimental study and mathematical model of nanoparticle transport in porous media," *Powder Technology*, vol. 192, no. 2, pp. 195–202, 2009.

[49] L. Hendraningrat and O. Torsæter, "Effects of the initial rock wettability on silica-based nanofluid-enhanced oil recovery processes at reservoir temperatures," *Energy & Fuels*, vol. 28, no. 10, pp. 6228–6241, 2014.

[50] L. Hendraningrat, S. Li, and O. Torsæter, "A coreflood investigation of nanofluid enhanced oil recovery," *Journal of Petroleum Science and Engineering*, vol. 111, pp. 128–138, 2013.

[51] R. Li, P.-X. Jiang, C. Gao, F. Huang, R. Xu, and X. Chen, "Experimental investigation of silica-based nanofluid enhanced oil recovery: The effect of wettability alteration," *Energy & Fuels*, 2016.

[52] S. Al-Anssari, A. Barifcani, S. Wang, and S. Iglauer, "Wettability alteration of oil-wet carbonate by silica nanofluid," *Journal of colloid and interface science*, vol. 461, pp. 435–442, 2016.

[53] C. O. Metin, J. R. Baran, and Q. P. Nguyen, "Adsorption of surface functionalized silica nanoparticles onto mineral surfaces and decane/water interface," *Journal of Nanoparticle Research*, vol. 14, no. 11, p. 1246, 2012.

[54] B. Suleimanov, F. Ismailov, and E. Veliyev, "Nanofluid for enhanced oil recovery," *Journal of Petroleum Science and Engineering*, vol. 78, no. 2, pp. 431–437, 2011.

[55] E. A. Taborda, V. Alvarado, C. A. Franco, and F. B. Cortés, "Rheological demonstration of alteration in the heavy crude oil fluid structure upon addition of nanoparticles," *Fuel*, vol. 189, pp. 322–333, 2017.

[56] M. Corcione, "Empirical correlating equations for predicting the effective thermal conductivity and dynamic viscosity of nanofluids," *Energy Conversion and Management*, vol. 52, no. 1, pp. 789–793, 2011.

[57] A. Haghtalab, M. Mohammadi, and Z. Fakhroueian, "Absorption and solubility measurement of co 2 in water-based zno and sio 2 nanofluids," *Fluid Phase Equilibria*, vol. 392, pp. 33–42, 2015.

[58] A. Fathollahi and B. Rostami, "Carbonated water injection: Effects of silica nanoparticles and operating pressure," *The Canadian Journal of Chemical Engineering*, vol. 93, no. 11, pp. 1949–1956, 2015.

[59] J. Crank, *The mathematics of diffusion*. Oxford university press, 2 ed., 1979.

[60] W. F. Smith, *Principles of Materials Science and Engineering*. McGraw-Hill, Inc, 2 ed., 1990.

[61] Y. Suehiro, M. Nakajima, K. Yamada, and M. Uematsu, "Critical parameters of {xCO 2+(1- x) CHF 3} forx=(1.0000, 0.7496, 0.5013, and 0.2522)," *The Journal of Chemical Thermodynamics*, vol. 28, no. 10, pp. 1153–1164, 1996.

[62] A. A. Hamouda and E. Maevskiy, "Oil recovery mechanism (s) by low salinity brines and their interaction with chalk," *Energy & Fuels*, vol. 28, no. 11, pp. 6860–6868, 2014.

[63] Z. Duan and R. Sun, "An improved model calculating co 2 solubility in pure water and aqueous nacl solutions from 273 to 533 k and from 0 to 2000 bar," *Chemical geology*, vol. 193, no. 3, pp. 257–271, 2003.

[64] Z. Duan, R. Sun, C. Zhu, and I.-M. Chou, "An improved model for the calculation of co 2 solubility in aqueous solutions containing na+, k+, ca 2+, mg 2+, cl-, and so 4 2-," *Marine Chemistry*, vol. 98, no. 2, pp. 131–139, 2006.

[65] Z. Duan, J. Hu, D. Li, and S. Mao, "Densities of the co2–h2o and co2–h2o–nacl systems up to 647 k and 100 mpa," *Energy & Fuels*, vol. 22, no. 3, pp. 1666–1674, 2008.

[66] Z. Duan, N. Møller, and J. H. Weare, "An equation of state for the ch4-co2-h2o system: I. pure systems from 0 to 1000 c and 0 to 8000 bar," *Geochimica et Cosmochimica Acta*, vol. 56, no. 7, pp. 2605–2617, 1992.

[67] W. Duangthongsuk and S. Wongwises, "Measurement of temperature-dependent thermal conductivity and viscosity of tio 2-water nanofluids," *Experimental thermal and fluid science*, vol. 33, no. 4, pp. 706–714, 2009.

[68] G. Batchelor, "The effect of brownian motion on the bulk stress in a suspension of spherical particles," *Journal of fluid mechanics*, vol. 83, no. 01, pp. 97–117, 1977.

[69] D. A. Drew and S. L. Passman, "Theory of multicomponent fluids," 1999.

[70] H. Brinkman, "The viscosity of concentrated suspensions and solutions," *The Journal of Chemical Physics*, vol. 20, no. 4, pp. 571–571, 1952.

[71] X. Wang, X. Xu, and S. U. S. Choi, "Thermal conductivity of nanoparticle-fluid mixture," *Journal of thermophysics and heat transfer*, vol. 13, no. 4, pp. 474–480, 1999.

[72] F. Herning and L. Zipperer, "Calculation of the viscosity of technical gas mixtures from the viscosity of individual gases," *Gas u. Wasserfach*, vol. 79, p. 69, 1936.

[73] A. L. Graham, "On the viscosity of suspensions of solid spheres," *Applied Scientific Research*, vol. 37, no. 3-4, pp. 275–286, 1981.

[74] "US Research Nanomaterials, INC silicon dioxide." `http://www.us-nano.com/inc/sdetail/408`. Accessed: 2017-03-10.

[75] N. Masoumi, N. Sohrabi, and A. Behzadmehr, "A new model for calculating the effective viscosity of nanofluids," *Journal of Physics D: Applied Physics*, vol. 42, no. 5, p. 055501, 2009.

[76] "Shimadzu the measurement principle used by a spectrophotometer." `http://www.shimadzu.com/an/uv/support/fundamentals/structure.html`. Accessed: 2017-05-25.

[77] C. Yang and Y. Gu, "New experimental method for measuring gas diffusivity in heavy oil by the dynamic pendant drop volume analysis (dpdva)," *Industrial & engineering chemistry research*, vol. 44, no. 12, pp. 4474–4483, 2005.

[78] P. Niyogi, C. S.K., and L. M.K., *Introduction to Computational Fluid Dynamics*. Pearson Education India, 2006.

[79] A. Hamouda, O. Valderhaug, R. Munaev, H. Stangeland, *et al.*, "Possible mechanisms for oil recovery from chalk and sandstone rocks by low salinity water (lsw)," in *SPE Improved Oil Recovery Symposium*, Society of Petroleum Engineers, 2014.

[80] "Gilson, Inc. 305 pump user's guide." `http://www.gilson.com/Resources/305_Pump_Users_Guide.pdf`. Accessed: 2017-06-3.

[81] "Labcompare turbiscan lab stability analyzer from formulaction sa." http://www.labcompare.com/25100-Stability-Analyzers/4864758-Turbiscan-LAB-Stability-Analyzer/. Accessed: 2017-06-3.

[82] "Rofa anton paar density meter specifications." http://www.rofa.at/Leaflet/Apaar/DMA4500.pdf. Accessed: 2017-06-3.

[83] "Scinteck shimadzu uv-1700 double beam scanning uv-vis spectrophotometer." http://www.scinteck.com/shimadzu-1700-double-beam-scanning-uv-vis-spectrophotometer.html. Accessed: 2017-06-3.

[84] "Merck Millipore zrxq005ww milli-q integral 5 water purification system." https://www.merckmillipore.com/NO/en/product/Milli-Q-Integral-5-Water-Purification-System,MM_NF-ZRXQ005WW?ReferrerURL=https. Accessed: 2017-06-5.

[85] A. Maghzi, S. Mohammadi, M. H. Ghazanfari, R. Kharrat, and M. Masihi, "Monitoring wettability alteration by silica nanoparticles during water flooding to heavy oils in five-spot systems: A pore-level investigation," *Experimental Thermal and Fluid Science*, vol. 40, pp. 168–176, 2012.

Appendix A

Full Experimental setup

A: CO2 supply and Pressure Maintenance System

Used for supply of CO2 to the PVT cell. When V.A - 2, 2A, 2B and 3 are open, the liquid pump (P.A) acts as pressure support for the PVT cell. Refilling of C.A - 2 can be done from C.A - 1 throug valve V.A - 1B and 2B

C.A - 1: High pressure piston cylinder, for CO2 supply to C.A - 2.

C-A - 2: Piston cylinder with pressure corresponding to the PVT cell pressure.

P.A: Automatic liquid pump for pressure support.

B: Drop Generation System

Used for drop generation through the capillary tube. Drops are generated by bringing the cylinder pressure slightlly above the PVT cell pressure, and valve V.B - 2 are gently opened. The size of a drop are determined by addition of force to the piston. At satisfactory a satisfactory magnitude, valve V.B - 2 are closed.

LC.B - 1: Supply of liquid to the piston cylinder

C.B - 1: Manually operated piston cylinder

C: Liquid Environment Delivery System

Used for supply of liquid environmental phase. Applying force to the piston while valve V.C - 2 is open will fill the PVT cell with ther respective liquid.

LC.C - 1: Supply of liquid to the piston cylinder

C.C - 1: Manually operated piston cylinder

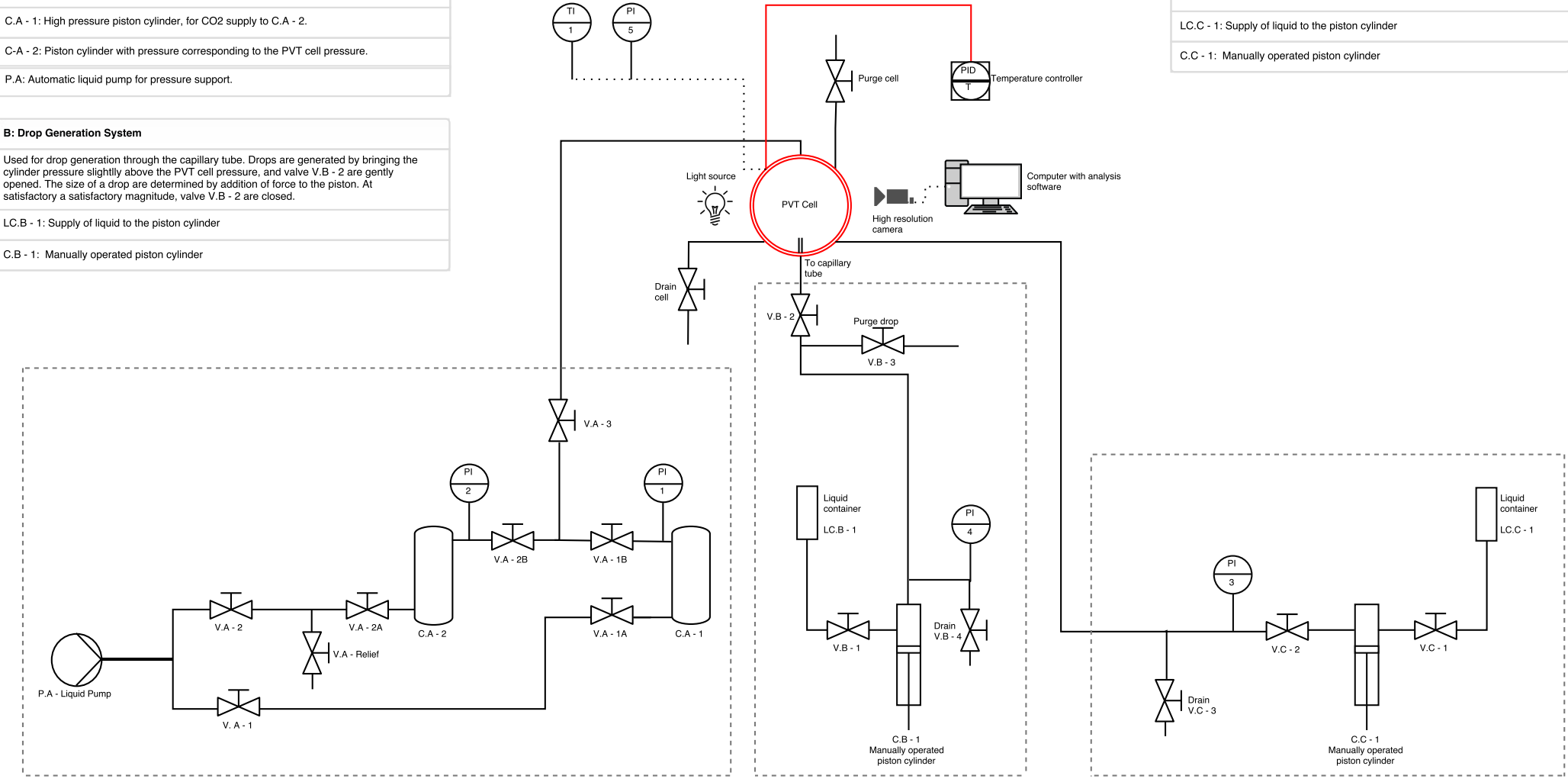

A: CO2 and Pressure Maintenance System

B: Drop Generation System

C: Liquid Environment Delivery System

Appendix B

Risk Assessment

Report for risk assessment

1. **Department (institute/section):** Department of Petroleum Engineering

2. **Date of risk assessment:** 3/2/2017

3. **Definition of area that is risk assessed (with limitations, premise and simplifications):**

    a) **Room:** [redacted]

    b) **Activity /lab work:** Investigate physical properties when surrounding a decane droplet with CO_2, water and nanofluid. This is done in a PVT cell.

4. **Risk assessment performed by:**

Name and position:

Ole Morten Isdahl

M.Sc. student

5. **Document information**

Version:

Valid from date:

Approved by/ Signature laboratory manager /Lab engineer:

Purpose: Determine mass transfer of carbon dioxide into decane, and other physical properties at various conditions.

General description of work:

- Fill a PVT cell (25 ml volume) with roughly 80 % water, containing nanofluid. (Max 2g/l)
- The experimental pressure range from 10 to 80 bar. (Maximum allowed pressure = 690 bar).
    - The system provided by EUROTECHNICA (PD-E170 LL-H) has a maximum working pressure of 690 bar.
- Introduce a decane drop through a capillary tube.
- Carbon dioxide is supplied from two cylinders in series (separated by valves). One at high pressure (200 bar) and one at working pressure (10-80 bar). The cylinder at working pressure have pressure support from a liquid pump during operation. Similar cylinders have previously been tested at 600 bar.
- Acetone is used for some cleaning
- Temperature will range from 25 to 45 °C (Maximum allowed temperature = 70 °C)

Identified hazards:

Chemicals used			
Name	**R - phrases**	**S - phrases**	**Should be substituted**
Acetone	H225: Highly flammable liquid and vapour H319: Causes serious eye irritation H336: May cause drowsiness or dizziness EUH066: Repeated exposure may cause skin dryness or cracking	P210: Keep away from heat, hot surfaces, sparks, open flames and other ignition sources. No smoking. P280: Wear protective gloves/protective clothing/eye protection/face protection. P305+P351+P338: IF IN EYES: Rinse cautiously with water for several minutes. Remove contact lenses if present and easy to do. Continue rinsing.	
Carbon dioxide	H280: Contains gas under pressure; may explode if heated	P403: Store in a well ventilated place.	
n-decane	H226: Flammable liquid and vapour. H304: May be fatal if swallowed and enters airways	P301+310, P331 IF SWALLOWED: Immediately call a POISON CENTER or doctor/physician. Do NOT induce vomiting.	
Nanofluid Nyacol DP9711 Identification of Substance: SiO_2+water	List of hazard phrases: None, as silicon dioxide is not classified according to regulation (EC) 1272/2008 (CLP). Avoid contact with skin, may cause skin irritation or dryness. Avoid contact with eyes, may cause irritation.	Minimum feasible handling, and temperatures should be maintained. Avoid contact with skin and eyes. Avoid generating mist during use. Use only in well ventilated area. Do not smoke. As a precautionary measure, the wearing of standard work gear is suggested.	

Descriptions of tasks				
Critical operations / activities of task	**Risk**: (What can go wrong)?	**Measure**	**Responsible / deadline**	**Completed**
Refilling of high pressure CO_2 cylinder	Leakage or bursting	Proper inspections of connections and gauges. As this operation is rare, consultation from experienced persons are available (?)		
Handling chemicals	Exposure, spillage	Handle with care and use gloves, coat and protective glasses (Use of gas mask in case of acetone)		
Operating valves	Opening incorrect valves / valve failure. Worst case: • CO_2 to atmosphere (~0.3m^3) • Spillage of 30 ml 2 g/l SiO_2+water nanofluid (pH >> 3) + ~5 µl n-decane	A detailed flowchart of the whole system has been made and are consulted during operations. Use of protective gloves, coat and glasses.		

Discussion/Proposed changes

No proposed changes.

Some facts
The PVT cell may contain acidic water (max 25 ml) due to dissolved CO_2 (pH ~ 3). However, in case of pressure release, the CO_2 will come out of solution and pH increase.
The whole system is corrosion free (Except the tubing which contains pure CO_2).
The high pressure cylinder (or identical) has previously been tested at 600 bar and are in this experiment only pressurised to a maximum of 200 bar.
The experimental setup is, if no changes occurs, operated at maximum 1/8 of the maximum working pressure. (Max. 80 bar pressure for the experiments. Maximum operating pressure is 690 bar).
The room for the setup is well ventilated.
The 200 bar cylinder of CO_2 has a volume of approximately 550 ml, which means a leak would yield a maximum of 0.3 m^3 of CO_2 at atmospheric conditions (25 °C).

Appendix C

Written MATLAB-scripts

C.1 CO_2 solubility: Parent-script

```
clear
clc

% CO2 SOLUBILITY IN PURE WATER AND AQUEOUS SOLUTIONS



% Model written based on "An improved model calculating CO2
    solubility in pure water and aqueous NaCl solutions from 273 to
    533 K and from 0 to 2000 bar" by Zhenhao Duan and Rui Sun (2003),
     and "An improved model for the calculation of CO2 solubility in
    aqueous solutions containing Na+, K+, Ca2+, Cl-, and SO42-" by
    Zhenhao Duan and Rui Sun (2005). Valid range T[K]: 273 < T < 533
    , P[bar]: 0 < P < 2000, [m/kg]: 0 < m < 4.3

%% INPUT
check = 1;
% (1/0) 1 = Only calculate value. 0 = Produce surface plot of whole
    valid interval.


Pmin = 0;      % Minimum pressure [Bar]
Pmax = 2000;   % Maximum pressure [Bar]
Tmin = 273;    % Minimum Temperature [Kelvin]
Tmax = 533;    % Maximum Temperature [Kelvin]

% SSW composition
mNa     = 0.45;       % Molality [mol/kg]
mK      = 0.01;       % Molality [mol/kg]
mCa     = 0.013;      % Molality [mol/kg]
mMg     = 0.045;      % Molality [mol/kg]
mCl     = 0.525;      % Molality [mol/kg]
mSO4    = 0.024;      % Molality [mol/kg]

if check == 1;
    P = 50;      %[bar]
    T = 298.15; %[K]
    solubility = CO2sol(P,T,mNa,mCa,mK,mMg,mCl,mSO4)
```

```
    return
end

% Creating solubility matrix of the whole valid interval

Prange = linspace(Pmin,Pmax,(Pmax-Pmin)+1);
Trange = linspace(Tmin,Tmax,(Tmax-Tmin)+1);
for j = 1:(Tmax-Tmin)+1
    T = Trange(j);
    for i = 1:(Pmax-Pmin)+1
        P = Prange(i);
        solubility(i,j) = CO2sol(P,T,mNa,mCa,mK,mMg,mCl,mSO4);
    end
end

solubility(imag(solubility)~=0) = 0;
mesh(Trange,Prange,solubility)
```

C.1.1 Function called by the main solubility script

```
function[CO2insolution] = CO2sol(P,T,mNa,mCa,mK,mMg,mCl,mSO4)

% CHECK IF WITHIN VALID RANGE

if T < 273 || T > 533
        disp('Temperature out of range!')
        return;
end
if P < 0 || P > 2000
        disp('Pressure out of range!')
        return;
end
if mNa < 0 || mNa > 4.3
        disp('Consentration of Na out of range!')
        return;
end
if mCa < 0 || mCa > 4.3
        disp('Consentration of Ca out of range!')
        return;
end
if mK < 0 || mK > 4.3
        disp('Consentration of K out of range!')
        return;
end
if mMg < 0 || mMg > 4.3
        disp('Consentration of Mg out of range!')
        return;
end
if mCl < 0 || mCl > 4.3
        disp('Consentration of Cl out of range!')
        return;
end


% Calulation of fugacity coefficient (Non-iterative). Fitted to the
   iterative EoS from 2003 paper, but with updated parameters for
   increased accuracy.
```

```
36
37 % Calculating test parameter
38 if T < 305
39     P1 = (1.1617*T^2-545.9*T+65929)*10^(-2);
40     % CO2 saturation pressure fitted to data from http://www.linde-
           gas.ro. R^2 = 1
41
42     elseif T >= 305 && T < 405;
43         P1 = 75+(T-305)*1.25;
44     elseif T >= 405
45         P1 = 200;
46 end
47
48 % Fitting region 1
49 if T >= 273 && T < 573 && P<P1
50     c1 = 1; c2 = 4.7586835*10^(-3); c3 = -3.3569963*10^(-6);
51     c4 = 0; c5 = -1.3179396; c6 = -3.8389101*10^(-6); c7 = 0;
52     c8 = 2.2815104*10^(-3); c9 = 0; c10 = 0; c11 = 0; c12 = 0;
53     c13 = 0; c14 = 0; c15 = 0;
54 end
55
56 % Fitting region 2
57 if T >= 273 && T < 340 && P >= P1 && P < 1000
58     c1 = -7.1734882*10^(-1); c2 = 1.5985379*10^(-4);
59     c3 = -4.9286471*10^(-7); c4 = 0;  c5 = 0;
60     c6 = -2.7855285*10^(-7);  c7 = 1.1877015*10^(-9);
61     c8 = 0;  c9 = 0; c10 = 0; c11 = 0; c12 = -96.539512;
62     c13 = 4.4774938*10^(-1); c14 = 101.81078;
63     c15 = 5.3783879*10^(-6);
64 end
65
66 % Fitting region 3
67 if T >= 273 && T < 340 && P >= 1000
68     c1 = -6.5129019*10^(-2); c2 = -2.1429977*10^(-4);
69     c3 = -1.1444930*10^(-6); c4 = 0; c5 = 0; c6 = -1.1558081*10^(-7);
70     c7 = 1.1952370*10^(-9); c8 = 0; c9 = 0; c10 = 0; c11 = 0;
71     c12 = -221.34306; c13 = 0; c14 = 71.820393; c15 =
           6.6089246*10^(-6);
72 end
73
74 % Fitting region 4
75 if T >= 340 && T < 435 && P >= P1 && P < 1000
76     c1 = 5.0383896; c2 = -4.4257744*10^(-3); c3 = 0; c4 = 1.95727333;
77     c5 = 0; c6 = 2.4223436*10^(-6); c7 = 0; c8 = -9.3796135*10^(-4);
78     c9 = -1.5026030; c10 = 3.0272240*10^(-3); c11 = -31.3777342;
79     c12 = -12.847063; c13 = 0; c14 = 0; c15 = -1.5056648*10^(-5);
80 end
81
82 % Fitting region 5
83 if T >= 340 && T < 435 && P >= 1000
84     c1 = -16.063152; c2 = -2.7057990*10^(-3); c3 = 0;
85     c4 = 1.4119239*10^(-1); c5 = 0; c6 = 8.1132965*10^(-7);
86     c7 = 0; c8 = -1.1453082*10^(-4); c9 = 2.3895671;
87     c10 = 5.0527457*10^(-4); c11 = -17.763460; c12 = 985.92232;
88     c13 = 0; c14 = 0; c15 = -5.4965256*10^(-7);
89 end
90
```

```
% Fitting region 6
if T >= 435 && P >= P1
    c1 = -1.5693490*10^(-1); c2 = 4.4621407*10^(-4);
    c3 = -9.1080591*10^(-7); c4 = 0; c5 = 0; c6 = 1.0647399*10^(-7);
    c7 = 2.4273357*10^(-10); c8 = 0; c9 = 3.5874255*10^(-1);
    c10 = 6.3319710*10^(-5); c11 = -249.89661; c12 = 0; c13 = 0;
    c14 = 888.76800; c15 = -6.6348003*10^(-7);
end

% Table for calculating parameters
a1 = (c2+c3*T+c4/T+c5/(T-150))*P;
a2 = (c6+(c7*T)+(c8/T))*P^2;
a3 = (c9+(c10*T)+(c11/T))*log(P);
a4 = (c12+(c13*T))/P;
a5 = c14/T;
a6 = c15*(T^2);

% Fugacity coefficient
phi = c1 + a1 + a2 + a3 + a4 + a5 + a6;


% Emprical calculation of water vapour pressure and mole frac CO2 in
    gas.

% Assumes water vapour pressure in mixtures are the same as for pure
    water.

Tcw = 647.29;       % Critical temperature of water [K]
Pcw = 220.85;       % Critical pressure of water [Bar]
t = (T-Tcw)/Tcw;

b1 = -38.640844;
b2 = 5.8948420;
b3 = 59.876516;
b4 = 26.654627;
b5 = 10.637097;

PH2O = ((Pcw*T)/Tcw)*(1+b1*(-t)^1.9 + b2*t + b3*t^2 + b4*t^3 + b5*t
    ^4);
yco2 = (P-PH2O)/P; % mole frac CO2 in vapour.

% Calculating interaction parameters
% Par(T,P) = f1 + f2T + f3/T + f4T^2 + f5/(630-T) + f6P + f7PlnT+ f8P
    /T + f9P(630-T) + f10P^2/(630-T)^2 + c11TlnP

% Myu-CO2
m1 = 28.9447706; m2 = -0.0354581768; m3 = -4770.67077; m4 =
    1.02782768*10^(-5);
m5 = 33.8126098; m6 = 9.04037140*10^(-3); m7 = -1.14934031*10^(-3);
m8 = -0.307405726; m9 = -0.0907301486; m10 = 9.32713393*10^(-4);

% lambdaco2Na
l1 = -0.411370585; l2 = 6.07632013*10^(-4); l3 = 97.5347708; l4 = 0;
l5 = 0; l6 = 0; l7 = 0; l8 = -0.0237622469; l9 = 0.0170656236; l10 =
    0;
l11 = 1.41335834*10^(-5);

```

```
% zetaco2NaCl
z1 = 3.36389723*10^(-4); z2 = -1.98298980*10^(-5); z3 = 0; z4 = 0;
z5 = 0; z6 = 0; z7 = 0; z8 = 2.12220830*10^-3; z9 =
    -5.24873303*10^-(3);
z10 = 0; z11 = 0;

%

myuco2RT = m1 + m2*T + m3/T + m4*T^2 + m5/(630-T) + m6*P + m7*P*log(T
    ) + (m8*P)/T + m9*P/(630-T) + (m10*P^2)/((630-T)^2);
lambdaco2Na = l1 + l2*T + l3/T + l4*T^2 + l5/(630-T) + l6*P + l7*P*
    log(T) + (l8*P)/T + l9*P/(630-T) + (l10*P^2)/((630-T)^2) + l11*T*
    log(P);
zetaco2NaCl = z1 + z2*T + z3/T + z4*T^2 + z5/(630-T) + z6*P + z7*P*
    log(T) + (z8*P)/T + z9*P/(630-T) + (z10*P^2)/((630-T)^2) + z11*T*
    log(P);

%% Calulating CO2 solved in water [moles/kg]

d1 = -myuco2RT;
d2 = -2*lambdaco2Na*(mNa+mK+2*mCa+2*mMg);
d3 = -zetaco2NaCl*mCl*(mNa+mK+mMg+mCa);
d4 = 0.07*mSO4;
lnmco2 = log(yco2*phi*P)+d1+d2+d3+d4;
CO2insolution = exp(lnmco2);
end
```

C.2 Program for Calculating Density of CW

```
clear
clc
format long

P = [1 2 3 4 5 6 7 8 9];          % Pressure [MPa]
T = [(273.15+25) (273.15+45)];  % Temperature [K]

MH2O = 18.01528;       %Molecular weight H2O [g/mol]
MCO2 = 44.01;          %Molecular weight CO2 [g/mol]

%Density(T(1),P(1-9))of water [g/cm3]
rhoH2OT1 = [0.99745 0.9979 0.99835 0.9988 0.99925 0.99969 1.0001
    1.0006 1.001];

%Density(T(2),P(1-9))of water [g/cm3]
rhoH2OT2 = [0.99061     0.99104 0.99148 0.99191 0.99234 0.99278
    0.99321 0.99364 0.99407];

%Density(T(1,2),P(1-9))of water [g/cm3]
rhoH2O = [rhoH2OT1;rhoH2OT2];

% Table of parameters
A11 = 0.38384020*10^(-3);    A21 = -0.57709332*10^(-5);
A12 = -0.55953850;           A22 = 0.82764653*10^(-2);
A13 = 0.30429268*10^3;       A23 = -0.43813556*10^1;
A14 = -0.72044305*10^5;      A24 = 0.10144907*10^4;
A15 = 0.63003388*10^7;       A25 = -0.86777045*10^5;
```

```
26
27 for t = 1:2
28
29     % Parameterization
30     A1 = A11*T(t)^2+A12*T(t)+A13+A14*T(t)^(-1)+A15*T(t)^(-2);
31     A2 = A21*T(t)^2+A22*T(t)+A23+A24*T(t)^(-1)+A25*T(t)^(-2);
32
33     for p = 1:length(P)
34
35         % Molar volume of water [cm3/mol]
36         V1 = MH2O/rhoH2O(t,p);
37
38         % CO2 solubility [mol/g] (Calls function)
39         SCO2 = CO2sol((P(p)*10),T(t),0,0,0,0,0,0)*10^-3;
40
41         % CO2 solubility [g/g]
42         SmCO2 = SCO2*MCO2;
43
44         % Total mass of CO2 [g]
45         massCO2 = (SmCO2*V1*rhoH2O(t,p))/(1-SmCO2);
46
47
48         NCO2 = massCO2/MCO2;      % Moles of CO2
49         xCO2 = NCO2(NCO2+1);      % Molefrac CO2
50         xH2O = 1-xCO2;            % Molefrac H2O
51
52
53         % Solution volume
54         V = V1*(1+(A1+A2*P(p))*xCO2);
55
56         % Appearant volume of CO2
57         VappCO2 = (V-xH2O*V1)/xCO2;
58
59         % Toital volume
60         Vtot = V1*xH2O+VappCO2*xCO2;
61
62         %Density of solution
63         rho(t,p) = (xCO2*MCO2+xH2O*MH2O)/Vtot;
64
65     end
66 end
67
68 plot(P,rho)
```

C.2.1 Changes done for Density of NF

```
1
2 % Preliminary calculaiton of water and nanoparticle mole fractions
3 rho_np = 2.65; % [g/ml]
4 rho_h2o = 0.99705; % [g/ml];
5 C_np = 0.05; %[g/l]
6 V = 1*10^-3; % [ml]
7 m_NP = C_np*V;
8 MW_H2O = 18.01528;
9 MW_NP = 60.08;
10
11
```

```
m_H2O = (1-m_NP/rho_np)*rho_h2o;
N_H2O = m_H2O/MW_H2O;
N_NP = m_NP/MW_NP;
xxH2O = N_H2O/(N_H2O+N_NP);
xNP = 1-xxH2O;




        % Molar volume of water [cm3/mol]
        V1 = (xxH2O*MW_H2O+xNP*MW_NP)/rhoH2O(t,p);

        % CO2 solubility [mol/g] (Calls function)
        SCO2 = NANOFACTOR*CO2sol((P(p)*10),T(t),0,0,0,0,0,0)*10^-3;
```

C.3 Program for Calculating Viscosity of Carbonated Nanofluid

```
clear
clc
format long


% Preliminary calculaiton of water, CO2 and nanoparticle mole
    fractions
rho_np = 2.65; % [g/ml]
rho_h2o = 0.99705; % [g/ml];
C_np = 0.05 % 0.5 % 1.0; %[g/l]
V = 1*10^-3; % [l]
m_NP = C_np*V; %(g/ml)
MW_H2O = 18.01528;
MW_NP = 60.08;
MW_CO2 = 44.01;

m_H2O = (1-m_NP/rho_np)*rho_h2o;
N_H2O = m_H2O/MW_H2O;
N_NP = m_NP/MW_NP;
xxH2O = N_H2O/(N_H2O+N_NP);
xNP = 1-xxH2O;

MW_NF = (xxH2O*MW_H2O+xNP*MW_NP); % g/mol
N_NF = MW_NF^(-1); % mol/g


myu_CO225 = [0.01503 0.01520 0.01548 0.01593 0.01670 0.01832 0.06160
    0.06679 0.07065];
myu_CO245 = [0.01598 0.01613 0.01636 0.01669 0.01718 0.01791 0.01905
    0.02105 0.02548];
myu_CO2 = [myu_CO225;myu_CO245];

%Viscosity of Nanofluid
%25C
myu_NF125 = [0.9190     0.9188  0.9186  0.9183  0.9181  0.9179
    0.9177  0.9175  0.9173];
myu_NF0525 =  [0.9039   0.9037  0.9035  0.9032  0.9030  0.9028
```

```
    0.9026  0.9024  0.9022];
myu_NF00525 = [0.8912   0.8909  0.8907  0.8905  0.8903  0.8901
    0.8899  0.8897  0.8895];
%45C
myu_NF145 = [0.6157     0.6159  0.6160  0.6161  0.6163  0.6164
    0.6166  0.6167  0.6169];
myu_NF0545 =  [0.6056   0.6057  0.6059  0.6060  0.6062  0.6063
    0.6064  0.6066  0.6067];
myu_NF00545 = [0.5971   0.5972  0.5973  0.5975  0.5976  0.5977
    0.5979  0.5980  0.5982];


myu_NF1 = [myu_NF125;myu_NF145]; % 1 g/l
myu_NF05 = [myu_NF0525;myu_NF0545]; % 0.5 g/l
myu_NF005 = [myu_NF00525;myu_NF00545]; % 0.05 g/l

dens1gl1 = [0.99835 0.99883 0.99931 0.99979 1.00027 1.00075 1.00123
    1.00171 1.00218];
dens1gl2 =[0.99610 0.99631 0.99652 0.99673 0.99694 0.99715 0.99736
    0.99757 0.99778];
dens1gl =[dens1gl1;dens1gl2];
dens05gl1 = [0.99797 0.99836 0.99875 0.99914 0.99953 0.99992 1.00031
    1.00070 1.00109];
dens05gl2 = [0.99541 0.99564 0.99587 0.99610 0.99633 0.99657 0.99680
    0.99703 0.99726];
dens05gl =[dens05gl1;dens05gl2];
dens005gl1 = [0.99774 0.99815 0.99855 0.99896 0.99936 0.99976 1.00017
     1.00057 1.00097];
dens005gl2 = [0.99085 0.99114 0.99142 0.99171 0.99200 0.99229 0.99258
     0.99287 0.99316];
dens005gl = [dens005gl1;dens005gl2];

%NIST
rhoH2OT1 = [0.99745     0.9979  0.99835 0.9988  0.99925 0.99969
    1.0001  1.0006  1.001];
rhoH2OT2 = [0.99061     0.99104 0.99148 0.99191 0.99234 0.99278
    0.99321 0.99364 0.99407];
rhoH2O = [rhoH2OT1;rhoH2OT2];

P = [10 20 30 40 50 60 70 80 90];
T = [(273.15+25) (273.15+45)];


for t = 1:2
    for p = 1:9

    % CO2 solubility [mol/g] (Calls function)
    SCO2 = (1+0.07*(dens1gl(t,p)-rhoH2O(t,p))/(dens1gl(t,p)-rhoH2O(t,
        p)))*CO2sol(P(p),T(t),0,0,0,0,0,0)*10^-3 %Do with bot sol

    % Mole frac CO2
    x_CO2 = SCO2/(N_NF+SCO2);
    %Mole frac NF
    x_NF = 1-x_CO2;

    myu_CNF1(t,p) = ((x_CO2*myu_CO2(t,p)*sqrt(MW_CO2)+x_NF*myu_NF1(t,
        p)*sqrt(MW_NF))/((x_CO2*sqrt(MW_CO2)+x_NF*sqrt(MW_NF))));
```

```
76
77
78
79      SCO2 = (1+0.07*(dens05gl(t,p)-rhoH2O(t,p))/(dens1gl(t,p)-rhoH2O(t
            ,p)))*CO2sol(P(p),T(t),0,0,0,0,0,0)*10^-3 %Do with bot sol
80      % Mole frac CO2
81      x_CO2 = SCO2/(N_NF+SCO2);
82      %Mole frac NF
83      x_NF = 1-x_CO2;
84      myu_CNF05(t,p) = ((x_CO2*myu_CO2(t,p)*sqrt(MW_CO2)+x_NF*myu_NF05(
            t,p)*sqrt(MW_NF))/((x_CO2*sqrt(MW_CO2)+x_NF*sqrt(MW_NF))));
85
86      SCO2 = (1+0.07*(dens005gl(t,p)-rhoH2O(t,p))/(dens1gl(t,p)-rhoH2O(
            t,p)))*CO2sol(P(p),T(t),0,0,0,0,0,0)*10^-3 %Do with bot sol
87      % Mole frac CO2
88      x_CO2 = SCO2/(N_NF+SCO2);
89      %Mole frac NF
90      x_NF = 1-x_CO2;
91      myu_CNF005(t,p) = ((x_CO2*myu_CO2(t,p)*sqrt(MW_CO2)+x_NF*
            myu_NF005(t,p)*sqrt(MW_NF))/((x_CO2*sqrt(MW_CO2)+x_NF*sqrt(
            MW_NF))));
92
93      end
94  end
```

Appendix D

Tables: Experimentally found volume change

TABLE D.1: Relative volume change of *n*-decane with time, exposed to 1 g/l DIW-CNF *saturated* 25°C.

Time [min]	10 bar	20 bar	30 bar	40 bar	50 bar	60 bar	70 bar
0	1.0000	1.0000	1.0000	1.0000	1.0000	1.0000	1.0000
5	1.0121	1.0086	1.1054	1.1268	1.2187	1.2815	1.2270
10	1.0156	1.0186	1.1399	1.2122	1.3501	1.4200	1.3802
15	1.0171	1.0279	1.1598	1.2557	1.4680	1.5625	1.4990
20	1.0190	1.0364	1.1733	1.2883	1.5702	1.6826	1.6179
25	1.0194	1.0454	1.1838	1.3110	1.6662	1.7875	1.7211
30	1.0199	1.0537	1.1932	1.3337	1.7432	1.9006	1.8192
35	1.0207	1.0560	1.1991	1.3480	1.8024	2.0228	1.9169
40	1.0206	1.0611	1.2042	1.3605	1.8697	2.1224	2.0073
45	1.0207	1.0740	1.2084	1.3726	1.9165	2.2221	2.1075
50	1.0210	1.0800	1.2107	1.3850	1.9672	2.3183	2.1913
55	1.0212	1.0853	1.2131	1.3953	2.0072	2.4265	2.2868
60	1.0211	1.0892	1.2165	1.4043	2.0407	2.5136	2.3446
65	1.0211	1.0951	1.2189	1.4126	2.0833	2.6131	2.4025
70	1.0211	1.0996	1.2210	1.4205	2.1055	2.7072	2.4253
75	1.0211	1.1029	1.2244	1.4270	2.1292	2.7927	2.4253
80	1.0211	1.1071	1.2278	1.4334	2.1514	2.8810	2.4253
85	1.0211	1.1131	1.2284	1.4389	2.1796	2.9769	2.4253
90	1.0211	1.1177	1.2329	1.4448	2.2017	3.0641	2.4253
95	1.0211	1.1229	1.2363	1.4494	2.2144	3.1242	2.4253
100	1.0211	1.1270	1.2361	1.4538	2.2372	3.2151	2.4253
105	1.0211	1.1304	1.2377	1.4572	2.2507	3.3188	2.4253
110	1.0211	1.1361	1.2393	1.4600	2.2735	3.3862	2.4253
115	1.0211	1.1382	1.2409	1.4647	2.2830	3.4000	2.4253
120	1.0211	1.1434	1.2405	1.4658	2.3008	3.4319	2.4253
125	1.0211	1.1453	1.2429	1.4701	2.3200	3.4516	2.4253
130	1.0211	1.1471	1.2419	1.4712	2.3211	3.4516	2.4253
135	1.0211	1.1497	1.2446	1.4739	2.3334	3.4516	2.4253
140	1.0211	1.1519	1.2442	1.4738	2.3334	3.4516	2.4253
145	1.0211	1.1547	1.2446	1.4774	2.3334	3.4516	2.4253
150	1.0211	1.1554	1.2446	1.4803	2.3334	3.4516	2.4253
155	1.0211	1.1571	1.2446	1.4814	2.3334	3.4516	2.4253
160	1.0211	1.1587	1.2446	1.4849	2.3334	3.4516	2.4253
165	1.0211	1.1597	1.2446	1.4862	2.3334	3.4516	2.4253
170	1.0211	1.1617	1.2446	1.4880	2.3334	3.4516	2.4253
175	1.0211	1.1628	1.2446	1.4890	2.3334	3.4516	2.4253
180	1.0211	1.1627	1.2446	1.4901	2.3334	3.4516	2.4253
185	1.0211	1.1627	1.2446	1.4920	2.3334	3.4516	2.4253
190	1.0211	1.1627	1.2446	1.4915	2.3334	3.4516	2.4253
195	1.0211	1.1627	1.2446	1.4912	2.3334	3.4516	2.4253
200	1.0211	1.1627	1.2446	1.4918	2.3334	3.4516	2.4253
205	1.0211	1.1627	1.2446	1.4932	2.3334	3.4516	2.4253
210	1.0211	1.1627	1.2446	1.4942	2.3334	3.4516	2.4253
215	1.0211	1.1627	1.2446	1.4947	2.3334	3.4516	2.4253
220	1.0211	1.1627	1.2446	1.4947	2.3334	3.4516	2.4253
225	1.0211	1.1627	1.2446	1.4947	2.3334	3.4516	2.4253
230	1.0211	1.1627	1.2446	1.4947	2.3334	3.4516	2.4253
235	1.0211	1.1627	1.2446	1.4947	2.3334	3.4516	2.4253
240	1.0211	1.1627	1.2446	1.4947	2.3334	3.4516	2.4253
245	1.0211	1.1627	1.2446	1.4947	2.3334	3.4516	2.4253
250	1.0211	1.1627	1.2446	1.4947	2.3334	3.4516	2.4253
255	1.0211	1.1627	1.2446	1.4947	2.3334	3.4516	2.4253
260	1.0211	1.1627	1.2446	1.4947	2.3334	3.4516	2.4253
265	1.0211	1.1627	1.2446	1.4947	2.3334	3.4516	2.4253
270	1.0211	1.1627	1.2446	1.4947	2.3334	3.4516	2.4253
275	1.0211	1.1627	1.2446	1.4947	2.3334	3.4516	2.4253
280	1.0211	1.1627	1.2446	1.4947	2.3334	3.4516	2.4253
285	1.0211	1.1627	1.2446	1.4947	2.3334	3.4516	2.4253
290	1.0211	1.1627	1.2446	1.4947	2.3334	3.4516	2.4253
295	1.0211	1.1627	1.2446	1.4947	2.3334	3.4516	2.4253
300	1.0211	1.1627	1.2446	1.4947	2.3334	3.4516	2.4253
305	1.0211	1.1627	1.2446	1.4947	2.3334	3.4516	2.4253
310	1.0211	1.1627	1.2446	1.4947	2.3334	3.4516	2.4253
315	1.0211	1.1627	1.2446	1.4947	2.3334	3.4516	2.4253
320	1.0211	1.1627	1.2446	1.4947	2.3334	3.4516	2.4253
325	1.0211	1.1627	1.2446	1.4947	2.3334	3.4516	2.4253
330	1.0211	1.1627	1.2446	1.4947	2.3334	3.4516	2.4253
335	1.0211	1.1627	1.2446	1.4947	2.3334	3.4516	2.4253
340	1.0211	1.1627	1.2446	1.4947	2.3334	3.4516	2.4253
345	1.0211	1.1627	1.2446	1.4947	2.3334	3.4516	2.4253
350	1.0211	1.1627	1.2446	1.4947	2.3334	3.4516	2.4253
355	1.0211	1.1627	1.2446	1.4947	2.3334	3.4516	2.4253
360	1.0211	1.1627	1.2446	1.4947	2.3334	3.4516	2.4253
365	1.0211	1.1627	1.2446	1.4947	2.3334	3.4516	2.4253
370	1.0211	1.1627	1.2446	1.4947	2.3334	3.4516	2.4253
375	1.0211	1.1627	1.2446	1.4947	2.3334	3.4516	2.4253
380	1.0211	1.1627	1.2446	1.4947	2.3334	3.4516	2.4253
385	1.0211	1.1627	1.2446	1.4947	2.3334	3.4516	2.4253
390	1.0211	1.1627	1.2446	1.4947	2.3334	3.4516	2.4253
395	1.0211	1.1627	1.2446	1.4947	2.3334	3.4516	2.4253
400	1.0211	1.1627	1.2446	1.4947	2.3334	3.4516	2.4253

TABLE D.2: Relative volume change of *n*-decane with time, exposed to 1 g/l DIW-CNF *gradually saturated* 25°C.

Time [min]	10 bar	20 bar	30 bar	40 bar	50 bar	60 bar	70 bar
0	1.0000	1.0000	1.0000	1.0000	1.0000	1.0000	1.0000
5	1.0026	1.0100	1.0117	1.0131	1.0313	1.0196	0.9900
10	1.0059	1.0204	1.0209	1.0281	1.0553	1.0433	1.0215
15	1.0102	1.0308	1.0309	1.0403	1.0696	1.0647	1.0461
20	1.0130	1.0407	1.0425	1.0579	1.0984	1.0985	1.0686
25	1.0156	1.0485	1.0565	1.0747	1.1428	1.1251	1.0914
30	1.0187	1.0558	1.0655	1.0917	1.1720	1.1676	1.1277
35	1.0215	1.0627	1.0774	1.1070	1.2141	1.2017	1.1632
40	1.0232	1.0713	1.0895	1.1252	1.2443	1.2396	1.2028
45	1.0251	1.0781	1.0979	1.1396	1.2820	1.2755	1.2441
50	1.0266	1.0852	1.1108	1.1564	1.3172	1.3195	1.2792
55	1.0282	1.0902	1.1185	1.1716	1.3624	1.3649	1.3183
60	1.0299	1.0948	1.1294	1.1879	1.3889	1.4067	1.3606
65	1.0315	1.1003	1.1363	1.1980	1.4208	1.4430	1.3998
70	1.0336	1.1031	1.1449	1.2124	1.4562	1.4913	1.4180
75	1.0351	1.1064	1.1545	1.2257	1.5013	1.5253	1.4595
80	1.0369	1.1110	1.1583	1.2366	1.5331	1.5681	1.4980
85	1.0380	1.1165	1.1661	1.2498	1.5619	1.6105	1.5264
90	1.0396	1.1224	1.1726	1.2584	1.5926	1.6564	1.5678
95	1.0401	1.1281	1.1753	1.2723	1.6300	1.7135	1.5943
100	1.0420	1.1323	1.1826	1.2797	1.6625	1.7582	1.6328
105	1.0435	1.1352	1.1864	1.2829	1.6926	1.7975	1.6657
110	1.0436	1.1389	1.1910	1.2952	1.7294	1.8436	1.6898
115	1.0447	1.1436	1.1946	1.3021	1.7644	1.8860	1.7338
120	1.0463	1.1461	1.1961	1.3091	1.7985	1.9352	1.7645
125	1.0468	1.1490	1.1989	1.3164	1.8334	1.9959	1.7751
130	1.0480	1.1516	1.2044	1.3232	1.8690	2.0395	1.7954
135	1.0491	1.1543	1.2089	1.3282	1.8992	2.0864	1.8111
140	1.0501	1.1562	1.2088	1.3354	1.9258	2.1411	1.8111
145	1.0517	1.1575	1.2136	1.3398	1.9595	2.1937	1.8111
150	1.0522	1.1584	1.2163	1.3437	1.9901	2.2421	1.8111
155	1.0536	1.1596	1.2160	1.3482	2.0168	2.2916	1.8111
160	1.0544	1.1618	1.2191	1.3522	2.0474	2.3514	1.8111
165	1.0560	1.1630	1.2220	1.3534	2.0736	2.4175	1.8111
170	1.0564	1.1660	1.2256	1.3565	2.1032	2.4702	1.8111
175	1.0571	1.1669	1.2287	1.3531	2.1341	2.5142	1.8111
180	1.0578	1.1678	1.2297	1.3564	2.1551	2.5854	1.8111
185	1.0582	1.1689	1.2305	1.3603	2.1859	2.6436	1.8111
190	1.0581	1.1689	1.2320	1.3649	2.2133	2.6806	1.8111
195	1.0587	1.1689	1.2326	1.3677	2.2399	2.7567	1.8111
200	1.0588	1.1689	1.2343	1.3714	2.2637	2.8331	1.8111
205	1.0588	1.1689	1.2355	1.3731	2.2923	2.8559	1.8111
210	1.0588	1.1689	1.2383	1.3751	2.3156	2.9080	1.8111
215	1.0588	1.1689	1.2386	1.3781	2.3404	2.9334	1.8111
220	1.0588	1.1689	1.2400	1.3791	2.3660	2.9687	1.8111
225	1.0588	1.1689	1.2421	1.3806	2.3866	2.9744	1.8111
230	1.0588	1.1689	1.2429	1.3835	2.4102	2.9964	1.8111
235	1.0588	1.1689	1.2457	1.3862	2.4468	3.0187	1.8111
240	1.0588	1.1689	1.2447	1.3877	2.4657	3.0311	1.8111
245	1.0588	1.1689	1.2467	1.3878	2.4825	3.0311	1.8111
250	1.0588	1.1689	1.2484	1.3892	2.5050	3.0311	1.8111
255	1.0588	1.1689	1.2489	1.3912	2.5182	3.0311	1.8111
260	1.0588	1.1689	1.2497	1.3915	2.5484	3.0311	1.8111
265	1.0588	1.1689	1.2506	1.3919	2.5666	3.0311	1.8111
270	1.0588	1.1689	1.2531	1.3925	2.5666	3.0311	1.8111
275	1.0588	1.1689	1.2525	1.3919	2.5666	3.0311	1.8111
280	1.0588	1.1689	1.2527	1.3926	2.5666	3.0311	1.8111
285	1.0588	1.1689	1.2544	1.3923	2.5666	3.0311	1.8111
290	1.0588	1.1689	1.2548	1.3932	2.5666	3.0311	1.8111
295	1.0588	1.1689	1.2548	1.3925	2.5666	3.0311	1.8111
300	1.0588	1.1689	1.2571	1.3924	2.5666	3.0311	1.8111
305	1.0588	1.1689	1.2591	1.3926	2.5666	3.0311	1.8111
310	1.0588	1.1689	1.2603	1.3926	2.5666	3.0311	1.8111
315	1.0588	1.1689	1.2629	1.3926	2.5666	3.0311	1.8111
320	1.0588	1.1689	1.2617	1.3926	2.5666	3.0311	1.8111
325	1.0588	1.1689	1.2602	1.3926	2.5666	3.0311	1.8111
330	1.0588	1.1689	1.2619	1.3926	2.5666	3.0311	1.8111
335	1.0588	1.1689	1.2636	1.3926	2.5666	3.0311	1.8111
340	1.0588	1.1689	1.2653	1.3926	2.5666	3.0311	1.8111
345	1.0588	1.1689	1.2649	1.3926	2.5666	3.0311	1.8111
350	1.0588	1.1689	1.2653	1.3926	2.5666	3.0311	1.8111
355	1.0588	1.1689	1.2641	1.3926	2.5666	3.0311	1.8111
360	1.0588	1.1689	1.2668	1.3926	2.5666	3.0311	1.8111
365	1.0588	1.1689	1.2662	1.3926	2.5666	3.0311	1.8111
370	1.0588	1.1689	1.2688	1.3926	2.5666	3.0311	1.8111
375	1.0588	1.1689	1.2675	1.3926	2.5666	3.0311	1.8111
380	1.0588	1.1689	1.2699	1.3926	2.5666	3.0311	1.8111
385	1.0588	1.1689	1.2697	1.3926	2.5666	3.0311	1.8111
390	1.0588	1.1689	1.2709	1.3926	2.5666	3.0311	1.8111
395	1.0588	1.1689	1.2709	1.3926	2.5666	3.0311	1.8111
400	1.0588	1.1689	1.2722	1.3926	2.5666	3.0311	1.8111

TABLE D.3: Relative volume change of *n*-decane with time, exposed to 1 g/l DIW-CNF *saturated* 45°C.

Time [min]	20 bar	30 bar	50 bar	60 bar	70 bar	80 bar	90 bar
0	1.0000	1.0000	1.00000	1.0000	1.0000	1.0000	1.0000
5	1.0292	1.0377	1.11725	1.1748	1.1780	1.2721	1.3281
10	1.0382	1.0597	1.18290	1.2555	1.2779	1.4233	1.5318
15	1.0463	1.0700	1.21412	1.3128	1.3615	1.5431	1.7133
20	1.0501	1.0820	1.25011	1.3536	1.4221	1.6357	1.8417
25	1.0551	1.0946	1.27074	1.3862	1.4768	1.7199	1.8684
30	1.0585	1.1068	1.29390	1.4055	1.5233	1.7870	1.8684
35	1.0634	1.1144	1.30902	1.4281	1.5532	1.8443	1.8684
40	1.0686	1.1251	1.31546	1.4407	1.5820	1.8552	1.8684
45	1.0711	1.1339	1.32002	1.4541	1.6061	1.8552	1.8684
50	1.0755	1.1463	1.32671	1.4639	1.6320	1.8552	1.8684
55	1.0783	1.1549	1.33023	1.4808	1.6565	1.8552	1.8684
60	1.0830	1.1658	1.33571	1.4910	1.6779	1.8552	1.8684
65	1.0873	1.1764	1.33963	1.4946	1.6970	1.8552	1.8684
70	1.0914	1.1841	1.34118	1.4949	1.7159	1.8552	1.8684
75	1.0958	1.1932	1.34669	1.4949	1.7283	1.8552	1.8684
80	1.0992	1.2040	1.34936	1.4949	1.7357	1.8552	1.8684
85	1.1034	1.2090	1.34821	1.4949	1.7435	1.8552	1.8684
90	1.1031	1.2197	1.35133	1.4949	1.7621	1.8552	1.8684
95	1.1098	1.2295	1.35133	1.4949	1.7655	1.8552	1.8684
100	1.1118	1.2329	1.35133	1.4949	1.7752	1.8552	1.8684
105	1.1158	1.2471	1.35133	1.4949	1.7775	1.8552	1.8684
110	1.1170	1.2593	1.35133	1.4949	1.7775	1.8552	1.8684
115	1.1188	1.2678	1.35133	1.4949	1.7775	1.8552	1.8684
120	1.1225	1.2778	1.35133	1.4949	1.7775	1.8552	1.8684
125	1.1243	1.2817	1.35133	1.4949	1.7775	1.8552	1.8684
130	1.1275	1.2934	1.35133	1.4949	1.7775	1.8552	1.8684
135	1.1277	1.3024	1.35133	1.4949	1.7775	1.8552	1.8684
140	1.1321	1.3056	1.35133	1.4949	1.7775	1.8552	1.8684
145	1.1327	1.3093	1.35133	1.4949	1.7775	1.8552	1.8684
150	1.1327	1.3229	1.35133	1.4949	1.7775	1.8552	1.8684
155	1.1353	1.3276	1.35133	1.4949	1.7775	1.8552	1.8684
160	1.1360	1.3302	1.35133	1.4949	1.7775	1.8552	1.8684
165	1.1379	1.3369	1.35133	1.4949	1.7775	1.8552	1.8684
170	1.1391	1.3414	1.35133	1.4949	1.7775	1.8552	1.8684
175	1.1410	1.3503	1.35133	1.4949	1.7775	1.8552	1.8684
180	1.1426	1.3545	1.35133	1.4949	1.7775	1.8552	1.8684
185	1.1430	1.3597	1.35133	1.4949	1.7775	1.8552	1.8684
190	1.1431	1.3611	1.35133	1.4949	1.7775	1.8552	1.8684
195	1.1436	1.3658	1.35133	1.4949	1.7775	1.8552	1.8684
200	1.1436	1.3662	1.35133	1.4949	1.7775	1.8552	1.8684
205	1.1436	1.3662	1.35133	1.4949	1.7775	1.8552	1.8684
210	1.1436	1.3662	1.35133	1.4949	1.7775	1.8552	1.8684
215	1.1436	1.3662	1.35133	1.4949	1.7775	1.8552	1.8684
220	1.1436	1.3662	1.35133	1.4949	1.7775	1.8552	1.8684
225	1.1436	1.3662	1.35133	1.4949	1.7775	1.8552	1.8684
230	1.1436	1.3662	1.35133	1.4949	1.7775	1.8552	1.8684
235	1.1436	1.3662	1.35133	1.4949	1.7775	1.8552	1.8684
240	1.1436	1.3662	1.35133	1.4949	1.7775	1.8552	1.8684
245	1.1436	1.3662	1.35133	1.4949	1.7775	1.8552	1.8684
250	1.1436	1.3662	1.35133	1.4949	1.7775	1.8552	1.8684
255	1.1436	1.3662	1.35133	1.4949	1.7775	1.8552	1.8684
260	1.1436	1.3662	1.35133	1.4949	1.7775	1.8552	1.8684
265	1.1436	1.3662	1.35133	1.4949	1.7775	1.8552	1.8684
270	1.1436	1.3662	1.35133	1.4949	1.7775	1.8552	1.8684
275	1.1436	1.3662	1.35133	1.4949	1.7775	1.8552	1.8684
280	1.1436	1.3662	1.35133	1.4949	1.7775	1.8552	1.8684
285	1.1436	1.3662	1.35133	1.4949	1.7775	1.8552	1.8684
290	1.1436	1.3662	1.35133	1.4949	1.7775	1.8552	1.8684
295	1.1436	1.3662	1.35133	1.4949	1.7775	1.8552	1.8684
300	1.1436	1.3662	1.35133	1.4949	1.7775	1.8552	1.8684
305	1.1436	1.3662	1.35133	1.4949	1.7775	1.8552	1.8684
310	1.1436	1.3662	1.35133	1.4949	1.7775	1.8552	1.8684
315	1.1436	1.3662	1.35133	1.4949	1.7775	1.8552	1.8684
320	1.1436	1.3662	1.35133	1.4949	1.7775	1.8552	1.8684
325	1.1436	1.3662	1.35133	1.4949	1.7775	1.8552	1.8684
330	1.1436	1.3662	1.35133	1.4949	1.7775	1.8552	1.8684
335	1.1436	1.3662	1.35133	1.4949	1.7775	1.8552	1.8684
340	1.1436	1.3662	1.35133	1.4949	1.7775	1.8552	1.8684
345	1.1436	1.3662	1.35133	1.4949	1.7775	1.8552	1.8684
350	1.1436	1.3662	1.35133	1.4949	1.7775	1.8552	1.8684
355	1.1436	1.3662	1.35133	1.4949	1.7775	1.8552	1.8684
360	1.1436	1.3662	1.35133	1.4949	1.7775	1.8552	1.8684
365	1.1436	1.3662	1.35133	1.4949	1.7775	1.8552	1.8684
370	1.1436	1.3662	1.35133	1.4949	1.7775	1.8552	1.8684
375	1.1436	1.3662	1.35133	1.4949	1.7775	1.8552	1.8684
380	1.1436	1.3662	1.35133	1.4949	1.7775	1.8552	1.8684
385	1.1436	1.3662	1.35133	1.4949	1.7775	1.8552	1.8684
390	1.1436	1.3662	1.35133	1.4949	1.7775	1.8552	1.8684
395	1.1436	1.3662	1.35133	1.4949	1.7775	1.8552	1.8684
400	1.1436	1.3662	1.35133	1.4949	1.7775	1.8552	1.8684

TABLE D.4: Relative volume change of *n*-decane with time, exposed to 1 g/l DIW-CNF *gradually saturated* 45°C.

Time [min]	10 bar	30 bar	50 bar	60 bar	70 bar	80 bar	90 bar
0	1.0000	1.0000	1.0000	1.0000	1.0000	1.0000	1.0000
5	1.0045	1.0152	1.0334	1.0140	1.0024	1.0333	1.0153
10	1.0072	1.0267	1.0451	1.0348	1.0279	1.0819	1.0514
15	1.0110	1.0415	1.0631	1.0573	1.0555	1.1259	1.0943
20	1.0156	1.0506	1.0818	1.0836	1.0749	1.1721	1.1382
25	1.0152	1.0558	1.0977	1.1047	1.1097	1.2209	1.2035
30	1.0164	1.0669	1.1193	1.1330	1.1433	1.2736	1.2707
35	1.0206	1.0761	1.1414	1.1563	1.1803	1.3160	1.3344
40	1.0225	1.0843	1.1554	1.1916	1.2083	1.3692	1.3949
45	1.0234	1.0912	1.1759	1.2147	1.2423	1.4266	1.4423
50	1.0240	1.0982	1.1908	1.2343	1.2916	1.4830	1.5237
55	1.0264	1.1025	1.2087	1.2559	1.3152	1.5380	1.5830
60	1.0276	1.1078	1.2235	1.2792	1.3459	1.5802	1.6389
65	1.0294	1.1145	1.2348	1.2994	1.3730	1.6396	1.7038
70	1.0299	1.1171	1.2481	1.3161	1.4195	1.6922	1.7754
75	1.0335	1.1214	1.2594	1.3359	1.4456	1.7522	1.8318
80	1.0354	1.1243	1.2715	1.3540	1.4736	1.8095	1.9383
85	1.0346	1.1281	1.2841	1.3708	1.4949	1.8772	2.0126
90	1.0396	1.1368	1.2910	1.3869	1.5210	1.9290	2.1189
95	1.0418	1.1421	1.3098	1.3979	1.5424	2.0048	2.1617
100	1.0428	1.1466	1.3183	1.4174	1.5648	2.0444	2.1617
105	1.0443	1.1503	1.3243	1.4238	1.5882	2.0705	2.1617
110	1.0468	1.1548	1.3454	1.4430	1.6009	2.1005	2.1617
115	1.0456	1.1590	1.3543	1.4514	1.6144	2.0931	2.1617
120	1.0468	1.1624	1.3558	1.4716	1.6278	2.1064	2.1617
125	1.0481	1.1679	1.3631	1.4854	1.6458	2.1064	2.1617
130	1.0503	1.1710	1.3658	1.4972	1.6583	2.1064	2.1617
135	1.0485	1.1757	1.3741	1.5115	1.6647	2.1064	2.1617
140	1.0492	1.1806	1.3830	1.5191	1.6749	2.1064	2.1617
145	1.0510	1.1834	1.3847	1.5252	1.6798	2.1064	2.1617
150	1.0513	1.1839	1.3874	1.5337	1.6844	2.1064	2.1617
155	1.0529	1.1842	1.3924	1.5402	1.6844	2.1064	2.1617
160	1.0549	1.1842	1.3943	1.5471	1.6844	2.1064	2.1617
165	1.0547	1.1842	1.3943	1.5522	1.6844	2.1064	2.1617
170	1.0574	1.1842	1.3943	1.5556	1.6844	2.1064	2.1617
175	1.0568	1.1842	1.3943	1.5574	1.6844	2.1064	2.1617
180	1.0580	1.1842	1.3943	1.5574	1.6844	2.1064	2.1617
185	1.0581	1.1842	1.3943	1.5574	1.6844	2.1064	2.1617
190	1.0586	1.1842	1.3943	1.5574	1.6844	2.1064	2.1617
195	1.0589	1.1842	1.3943	1.5574	1.6844	2.1064	2.1617
200	1.0597	1.1842	1.3943	1.5574	1.6844	2.1064	2.1617
205	1.0603	1.1842	1.3943	1.5574	1.6844	2.1064	2.1617
210	1.0609	1.1842	1.3943	1.5574	1.6844	2.1064	2.1617
215	1.0625	1.1842	1.3943	1.5574	1.6844	2.1064	2.1617
220	1.0642	1.1842	1.3943	1.5574	1.6844	2.1064	2.1617
225	1.0650	1.1842	1.3943	1.5574	1.6844	2.1064	2.1617
230	1.0670	1.1842	1.3943	1.5574	1.6844	2.1064	2.1617
235	1.0689	1.1842	1.3943	1.5574	1.6844	2.1064	2.1617
240	1.0694	1.1842	1.3943	1.5574	1.6844	2.1064	2.1617
245	1.0698	1.1842	1.3943	1.5574	1.6844	2.1064	2.1617
250	1.0697	1.1842	1.3943	1.5574	1.6844	2.1064	2.1617
255	1.0710	1.1842	1.3943	1.5574	1.6844	2.1064	2.1617
260	1.0713	1.1842	1.3943	1.5574	1.6844	2.1064	2.1617
265	1.0722	1.1842	1.3943	1.5574	1.6844	2.1064	2.1617
270	1.0735	1.1842	1.3943	1.5574	1.6844	2.1064	2.1617
275	1.0742	1.1842	1.3943	1.5574	1.6844	2.1064	2.1617
280	1.0750	1.1842	1.3943	1.5574	1.6844	2.1064	2.1617
285	1.0746	1.1842	1.3943	1.5574	1.6844	2.1064	2.1617
290	1.0755	1.1842	1.3943	1.5574	1.6844	2.1064	2.1617
295	1.0771	1.1842	1.3943	1.5574	1.6844	2.1064	2.1617
300	1.0777	1.1842	1.3943	1.5574	1.6844	2.1064	2.1617
305	1.0792	1.1842	1.3943	1.5574	1.6844	2.1064	2.1617
310	1.0790	1.1842	1.3943	1.5574	1.6844	2.1064	2.1617
315	1.0797	1.1842	1.3943	1.5574	1.6844	2.1064	2.1617
320	1.0806	1.1842	1.3943	1.5574	1.6844	2.1064	2.1617
325	1.0802	1.1842	1.3943	1.5574	1.6844	2.1064	2.1617
330	1.0813	1.1842	1.3943	1.5574	1.6844	2.1064	2.1617
335	1.0827	1.1842	1.3943	1.5574	1.6844	2.1064	2.1617
340	1.0832	1.1842	1.3943	1.5574	1.6844	2.1064	2.1617
345	1.0834	1.1842	1.3943	1.5574	1.6844	2.1064	2.1617
350	1.0835	1.1842	1.3943	1.5574	1.6844	2.1064	2.1617
355	1.0840	1.1842	1.3943	1.5574	1.6844	2.1064	2.1617
360	1.0858	1.1842	1.3943	1.5574	1.6844	2.1064	2.1617
365	1.0870	1.1842	1.3943	1.5574	1.6844	2.1064	2.1617
370	1.0870	1.1842	1.3943	1.5574	1.6844	2.1064	2.1617
375	1.0869	1.1842	1.3943	1.5574	1.6844	2.1064	2.1617
380	1.0884	1.1842	1.3943	1.5574	1.6844	2.1064	2.1617
385	1.0886	1.1842	1.3943	1.5574	1.6844	2.1064	2.1617
390	1.0897	1.1842	1.3943	1.5574	1.6844	2.1064	2.1617
395	1.0901	1.1842	1.3943	1.5574	1.6844	2.1064	2.1617
400	1.0905	1.1842	1.3943	1.5574	1.6844	2.1064	2.1617

TABLE D.5: Relative volume change of *n*-decane with time, exposed to 0.5 g/l DIW-CNF *saturated* 25°C.

Time [min]	10 bar	20 bar	30 bar	40 bar	50 bar	60 bar	70 bar	80 bar	90 bar
0	1.0000	1.0000	1.0000	1.0000	1.0000	1.0000	1.0000	1.0000	1.0000
5	1.0383	1.0646	1.1153	1.1683	1.2277	1.2376	1.2503	1.2910	1.2624
10	1.0523	1.0865	1.1652	1.2649	1.3351	1.3773	1.3985	1.4692	1.4285
15	1.0551	1.0953	1.1872	1.3305	1.4225	1.4872	1.5164	1.6287	1.5656
20	1.0568	1.0990	1.2028	1.3849	1.4970	1.5823	1.6234	1.7730	1.6950
25	1.0570	1.1009	1.2138	1.4224	1.5518	1.6787	1.7180	1.9143	1.8175
30	1.0569	1.1027	1.2218	1.4524	1.6101	1.7650	1.8064	2.0438	1.9297
35	1.0570	1.1051	1.2293	1.4827	1.6576	1.8396	1.8935	2.1734	2.0427
40	1.0570	1.1067	1.2351	1.5088	1.7059	1.9060	1.9718	2.2910	2.1504
45	1.0570	1.1066	1.2390	1.5311	1.7467	1.9711	2.0516	2.4126	2.2541
50	1.0570	1.1071	1.2424	1.5496	1.7822	2.0361	2.1249	2.5221	2.3498
55	1.0570	1.1079	1.2465	1.5673	1.8247	2.0962	2.1991	2.6329	2.4567
60	1.0570	1.1080	1.2494	1.5841	1.8502	2.1617	2.2674	2.7372	2.5500
65	1.0570	1.1091	1.2496	1.5965	1.8824	2.2231	2.3346	2.8413	2.6481
70	1.0570	1.1088	1.2547	1.6090	1.9158	2.2786	2.3975	2.9546	2.7451
75	1.0570	1.1097	1.2554	1.6219	1.9447	2.3344	2.4556	3.0211	2.8416
80	1.0570	1.1096	1.2577	1.6350	1.9737	2.3896	2.5185	3.1278	2.9313
85	1.0570	1.1113	1.2588	1.6449	2.0009	2.4415	2.5801	3.2702	3.0515
90	1.0570	1.1109	1.2595	1.6534	2.0318	2.4959	2.6316	3.3989	3.1330
95	1.0570	1.1112	1.2606	1.6613	2.0595	2.5463	2.6996	3.4018	3.1330
100	1.0570	1.1116	1.2623	1.6712	2.0822	2.5990	2.7581	3.4018	3.1330
105	1.0570	1.1116	1.2622	1.6794	2.1000	2.6489	2.8149	3.4018	3.1330
110	1.0570	1.1116	1.2635	1.6878	2.1246	2.6998	2.8740	3.4018	3.1330
115	1.0570	1.1116	1.2662	1.6955	2.1538	2.7471	2.9312	3.4018	3.1330
120	1.0570	1.1116	1.2660	1.7052	2.1686	2.7915	2.9957	3.4018	3.1330
125	1.0570	1.1116	1.2660	1.7141	2.1846	2.8401	3.0474	3.4018	3.1330
130	1.0570	1.1116	1.2662	1.7191	2.2051	2.8817	3.0996	3.4018	3.1330
135	1.0570	1.1116	1.2666	1.7283	2.2291	2.9258	3.0996	3.4018	3.1330
140	1.0570	1.1116	1.2673	1.7334	2.2521	2.9767	3.0996	3.4018	3.1330
145	1.0570	1.1116	1.2673	1.7354	2.2623	3.0164	3.0996	3.4018	3.1330
150	1.0570	1.1116	1.2673	1.7378	2.2821	3.0625	3.0996	3.4018	3.1330
155	1.0570	1.1116	1.2673	1.7438	2.2925	3.1120	3.0996	3.4018	3.1330
160	1.0570	1.1116	1.2673	1.7490	2.3153	3.1604	3.0996	3.4018	3.1330
165	1.0570	1.1116	1.2673	1.7512	2.3326	3.1604	3.0996	3.4018	3.1330
170	1.0570	1.1116	1.2673	1.7568	2.3464	3.1604	3.0996	3.4018	3.1330
175	1.0570	1.1116	1.2673	1.7588	2.3652	3.1604	3.0996	3.4018	3.1330
180	1.0570	1.1116	1.2673	1.7626	2.3757	3.1604	3.0996	3.4018	3.1330
185	1.0570	1.1116	1.2673	1.7647	2.3822	3.1604	3.0996	3.4018	3.1330
190	1.0570	1.1116	1.2673	1.7676	2.4021	3.1604	3.0996	3.4018	3.1330
195	1.0570	1.1116	1.2673	1.7683	2.4112	3.1604	3.0996	3.4018	3.1330
200	1.0570	1.1116	1.2673	1.7667	2.4228	3.1604	3.0996	3.4018	3.1330
205	1.0570	1.1116	1.2673	1.7735	2.4354	3.1604	3.0996	3.4018	3.1330
210	1.0570	1.1116	1.2673	1.7771	2.4446	3.1604	3.0996	3.4018	3.1330
215	1.0570	1.1116	1.2673	1.7773	2.4684	3.1604	3.0996	3.4018	3.1330
220	1.0570	1.1116	1.2673	1.7776	2.4818	3.1604	3.0996	3.4018	3.1330
225	1.0570	1.1116	1.2673	1.7776	2.4864	3.1604	3.0996	3.4018	3.1330
230	1.0570	1.1116	1.2673	1.7776	2.5034	3.1604	3.0996	3.4018	3.1330
235	1.0570	1.1116	1.2673	1.7776	2.5096	3.1604	3.0996	3.4018	3.1330
240	1.0570	1.1116	1.2673	1.7776	2.5209	3.1604	3.0996	3.4018	3.1330
245	1.0570	1.1116	1.2673	1.7776	2.5335	3.1604	3.0996	3.4018	3.1330
250	1.0570	1.1116	1.2673	1.7776	2.5446	3.1604	3.0996	3.4018	3.1330
255	1.0570	1.1116	1.2673	1.7776	2.5581	3.1604	3.0996	3.4018	3.1330
260	1.0570	1.1116	1.2673	1.7776	2.5672	3.1604	3.0996	3.4018	3.1330
265	1.0570	1.1116	1.2673	1.7776	2.5626	3.1604	3.0996	3.4018	3.1330
270	1.0570	1.1116	1.2673	1.7776	2.5849	3.1604	3.0996	3.4018	3.1330
275	1.0570	1.1116	1.2673	1.7776	2.5914	3.1604	3.0996	3.4018	3.1330
280	1.0570	1.1116	1.2673	1.7776	2.6015	3.1604	3.0996	3.4018	3.1330
285	1.0570	1.1116	1.2673	1.7776	2.6093	3.1604	3.0996	3.4018	3.1330
290	1.0570	1.1116	1.2673	1.7776	2.6209	3.1604	3.0996	3.4018	3.1330
295	1.0570	1.1116	1.2673	1.7776	2.6295	3.1604	3.0996	3.4018	3.1330
300	1.0570	1.1116	1.2673	1.7776	2.6366	3.1604	3.0996	3.4018	3.1330
305	1.0570	1.1116	1.2673	1.7776	2.6448	3.1604	3.0996	3.4018	3.1330
310	1.0570	1.1116	1.2673	1.7776	2.6533	3.1604	3.0996	3.4018	3.1330
315	1.0570	1.1116	1.2673	1.7776	2.6626	3.1604	3.0996	3.4018	3.1330
320	1.0570	1.1116	1.2673	1.7776	2.6675	3.1604	3.0996	3.4018	3.1330
325	1.0570	1.1116	1.2673	1.7776	2.6762	3.1604	3.0996	3.4018	3.1330
330	1.0570	1.1116	1.2673	1.7776	2.6862	3.1604	3.0996	3.4018	3.1330
335	1.0570	1.1116	1.2673	1.7776	2.6958	3.1604	3.0996	3.4018	3.1330
340	1.0570	1.1116	1.2673	1.7776	2.6990	3.1604	3.0996	3.4018	3.1330
345	1.0570	1.1116	1.2673	1.7776	2.7047	3.1604	3.0996	3.4018	3.1330
350	1.0570	1.1116	1.2673	1.7776	2.7047	3.1604	3.0996	3.4018	3.1330
355	1.0570	1.1116	1.2673	1.7776	2.7204	3.1604	3.0996	3.4018	3.1330
360	1.0570	1.1116	1.2673	1.7776	2.7302	3.1604	3.0996	3.4018	3.1330
365	1.0570	1.1116	1.2673	1.7776	2.7356	3.1604	3.0996	3.4018	3.1330
370	1.0570	1.1116	1.2673	1.7776	2.7320	3.1604	3.0996	3.4018	3.1330
375	1.0570	1.1116	1.2673	1.7776	2.7478	3.1604	3.0996	3.4018	3.1330
380	1.0570	1.1116	1.2673	1.7776	2.7555	3.1604	3.0996	3.4018	3.1330
385	1.0570	1.1116	1.2673	1.7776	2.7614	3.1604	3.0996	3.4018	3.1330
390	1.0570	1.1116	1.2673	1.7776	2.7676	3.1604	3.0996	3.4018	3.1330
395	1.0570	1.1116	1.2673	1.7776	2.7676	3.1604	3.0996	3.4018	3.1330
400	1.0570	1.1116	1.2673	1.7776	2.7676	3.1604	3.0996	3.4018	3.1330

TABLE D.6: Relative volume change of *n*-decane with time, exposed to 0.5 g/l DIW-CNF *gradually saturated* 25°C.

Time [min]	10 bar	30 bar	40 bar	50 bar	60 bar	70 bar	80 bar	90 bar
0	1.0000	1.0000	1.0000	1.0000	1.0000	1.0000	1.0000	1.0000
5	1.0071	0.9604	1.0228	1.0280	1.0171	1.0249	1.0341	1.0422
10	1.0078	0.9637	1.0368	1.0523	1.0442	1.0474	1.0529	1.0708
15	1.0127	0.9693	1.0582	1.0806	1.0696	1.0736	1.0852	1.0972
20	1.0151	0.9743	1.0710	1.1028	1.0933	1.0964	1.1158	1.1265
25	1.0176	0.9811	1.0884	1.1276	1.1217	1.1362	1.1582	1.1717
30	1.0180	0.9868	1.1042	1.1563	1.1467	1.1657	1.1911	1.2193
35	1.0206	0.9946	1.1204	1.1866	1.1722	1.1998	1.2324	1.2582
40	1.0228	0.9987	1.1442	1.2141	1.2096	1.2348	1.2757	1.3061
45	1.0260	1.0047	1.1628	1.2426	1.2418	1.2738	1.3158	1.3543
50	1.0262	1.0111	1.1812	1.2714	1.2680	1.3150	1.3615	1.4131
55	1.0283	1.0175	1.1994	1.3022	1.2958	1.3509	1.4058	1.4599
60	1.0280	1.0219	1.2172	1.3369	1.3206	1.3863	1.4527	1.5359
65	1.0300	1.0281	1.2332	1.3622	1.3440	1.4277	1.4967	1.5893
70	1.0316	1.0348	1.2550	1.3953	1.3708	1.4690	1.5465	1.6549
75	1.0323	1.0393	1.2728	1.4261	1.3953	1.5051	1.5902	1.7213
80	1.0322	1.0451	1.2878	1.4554	1.4198	1.5402	1.6440	1.7935
85	1.0344	1.0501	1.3029	1.4825	1.4418	1.5811	1.6876	1.8665
90	1.0350	1.0563	1.3219	1.5155	1.4697	1.6155	1.7438	1.9431
95	1.0353	1.0622	1.3332	1.5443	1.4972	1.6509	1.8039	2.0299
100	1.0368	1.0670	1.3485	1.5704	1.5246	1.6854	1.8594	2.1003
105	1.0388	1.0697	1.3644	1.6024	1.5523	1.7190	1.9076	2.1896
110	1.0416	1.0752	1.3768	1.6285	1.5805	1.7539	1.9711	2.2782
115	1.0403	1.0804	1.3915	1.6560	1.6063	1.7857	2.0265	2.3588
120	1.0417	1.0843	1.4052	1.6818	1.6327	1.8180	2.0935	2.4514
125	1.0412	1.0887	1.4176	1.7094	1.6605	1.8540	2.1587	2.5403
130	1.0446	1.0922	1.4276	1.7372	1.6846	1.8904	2.2169	2.6385
135	1.0429	1.0955	1.4413	1.7654	1.7091	1.9178	2.2815	2.7283
140	1.0452	1.0977	1.4532	1.7930	1.7335	1.9447	2.3403	2.8225
145	1.0467	1.1012	1.4644	1.8173	1.7578	1.9748	2.4072	2.9214
150	1.0468	1.1046	1.4749	1.8399	1.7818	2.0048	2.4757	3.0223
155	1.0461	1.1082	1.4909	1.8633	1.8043	2.0300	2.5435	3.1236
160	1.0470	1.1116	1.5016	1.8885	1.8307	2.0616	2.6135	3.2192
165	1.0463	1.1137	1.5097	1.9076	1.8582	2.1010	2.6874	3.3261
170	1.0465	1.1155	1.5190	1.9327	1.8766	2.1177	2.7592	3.4332
175	1.0465	1.1184	1.5311	1.9585	1.8997	2.1492	2.8395	3.5372
180	1.0465	1.1206	1.5416	1.9791	1.9245	2.1681	2.9202	3.6633
185	1.0465	1.1242	1.5486	2.0013	1.9384	2.2076	2.9966	3.7916
190	1.0465	1.1255	1.5590	2.0259	1.9683	2.2396	3.0913	3.8932
195	1.0465	1.1282	1.5709	2.0477	1.9842	2.2725	3.1276	4.0026
200	1.0465	1.1309	1.5768	2.0693	2.0089	2.2725	3.2165	4.1170
205	1.0465	1.1332	1.5857	2.0895	2.0126	2.2725	3.2611	4.2690
210	1.0465	1.1347	1.5941	2.1093	2.0466	2.2725	3.2611	4.4121
215	1.0465	1.1353	1.6013	2.1315	2.0476	2.2725	3.2611	4.5207
220	1.0465	1.1370	1.6079	2.1465	2.0580	2.2725	3.2611	4.5777
225	1.0465	1.1389	1.6155	2.1618	2.0580	2.2725	3.2611	4.5997
230	1.0465	1.1411	1.6241	2.1821	2.0580	2.2725	3.2611	4.5997
235	1.0465	1.1421	1.6326	2.2005	2.0580	2.2725	3.2611	4.5997
240	1.0465	1.1436	1.6386	2.2187	2.0580	2.2725	3.2611	4.5997
245	1.0465	1.1442	1.6404	2.2343	2.0580	2.2725	3.2611	4.5997
250	1.0465	1.1454	1.6508	2.2505	2.0580	2.2725	3.2611	4.5997
255	1.0465	1.1464	1.6541	2.2658	2.0580	2.2725	3.2611	4.5997
260	1.0465	1.1479	1.6624	2.2858	2.0580	2.2725	3.2611	4.5997
265	1.0465	1.1492	1.6675	2.2992	2.0580	2.2725	3.2611	4.5997
270	1.0465	1.1502	1.6726	2.3152	2.0580	2.2725	3.2611	4.5997
275	1.0465	1.1521	1.6751	2.3311	2.0580	2.2725	3.2611	4.5997
280	1.0465	1.1527	1.6751	2.3488	2.0580	2.2725	3.2611	4.5997
285	1.0465	1.1526	1.6751	2.3610	2.0580	2.2725	3.2611	4.5997
290	1.0465	1.1543	1.6751	2.3769	2.0580	2.2725	3.2611	4.5997
295	1.0465	1.1564	1.6751	2.3928	2.0580	2.2725	3.2611	4.5997
300	1.0465	1.1576	1.6751	2.4071	2.0580	2.2725	3.2611	4.5997
305	1.0465	1.1584	1.6751	2.4228	2.0580	2.2725	3.2611	4.5997
310	1.0465	1.1595	1.6751	2.4373	2.0580	2.2725	3.2611	4.5997
315	1.0465	1.1603	1.6751	2.4513	2.0580	2.2725	3.2611	4.5997
320	1.0465	1.1616	1.6751	2.4729	2.0580	2.2725	3.2611	4.5997
325	1.0465	1.1606	1.6751	2.4847	2.0580	2.2725	3.2611	4.5997
330	1.0465	1.1627	1.6751	2.5017	2.0580	2.2725	3.2611	4.5997
335	1.0465	1.1629	1.6751	2.5150	2.0580	2.2725	3.2611	4.5997
340	1.0465	1.1645	1.6751	2.5288	2.0580	2.2725	3.2611	4.5997
345	1.0465	1.1657	1.6751	2.5449	2.0580	2.2725	3.2611	4.5997
350	1.0465	1.1662	1.6751	2.5537	2.0580	2.2725	3.2611	4.5997
355	1.0465	1.1677	1.6751	2.5672	2.0580	2.2725	3.2611	4.5997
360	1.0465	1.1675	1.6751	2.5777	2.0580	2.2725	3.2611	4.5997
365	1.0465	1.1662	1.6751	2.5940	2.0580	2.2725	3.2611	4.5997
370	1.0465	1.1691	1.6751	2.6015	2.0580	2.2725	3.2611	4.5997
375	1.0465	1.1694	1.6751	2.6015	2.0580	2.2725	3.2611	4.5997
380	1.0465	1.1692	1.6751	2.6015	2.0580	2.2725	3.2611	4.5997
385	1.0465	1.1694	1.6751	2.6015	2.0580	2.2725	3.2611	4.5997
390	1.0465	1.1694	1.6751	2.6015	2.0580	2.2725	3.2611	4.5997
395	1.0465	1.1694	1.6751	2.6015	2.0580	2.2725	3.2611	4.5997
400	1.0465	1.1694	1.6751	2.6015	2.0580	2.2725	3.2611	4.5997

TABLE D.7: Relative volume change of n-decane with time, exposed to 0.5 g/l DIW-CNF *saturated* 45°C.

Time [min	10 bar	20 bar	30 bar	40 bar	50 bar	60 bar	70 bar	80 bar	90 bar
0	1.0000	1.0000	1.0000	1.0000	1.0000	1.0000	1.0000	1.0000	1.0000
5	1.0250	1.0498	1.0962	1.1177	1.1646	1.2086	1.2412	1.2920	1.3471
10	1.0306	1.0597	1.1245	1.1573	1.2327	1.3048	1.3674	1.4740	1.6006
15	1.0323	1.0618	1.1337	1.1781	1.2729	1.3774	1.4434	1.6279	1.8204
20	1.0333	1.0625	1.1405	1.1915	1.3018	1.4219	1.5158	1.7435	2.0035
25	1.0339	1.0628	1.1442	1.2000	1.3166	1.4567	1.5609	1.8574	2.1853
30	1.0344	1.0635	1.1468	1.2045	1.3359	1.4935	1.6057	1.9508	2.3803
35	1.0354	1.0638	1.1490	1.2078	1.3511	1.5111	1.6399	2.0141	2.4401
40	1.0361	1.0644	1.1506	1.2105	1.3600	1.5339	1.6736	2.0141	2.4401
45	1.0372	1.0650	1.1530	1.2138	1.3686	1.5491	1.7009	2.0141	2.4401
50	1.0381	1.0661	1.1525	1.2167	1.3769	1.5624	1.7309	2.0141	2.4401
55	1.0388	1.0659	1.1539	1.2198	1.3838	1.5778	1.7536	2.0141	2.4401
60	1.0399	1.0664	1.1532	1.2201	1.3871	1.5894	1.7766	2.0141	2.4401
65	1.0409	1.0667	1.1542	1.2215	1.3909	1.5963	1.7957	2.0141	2.4401
70	1.0419	1.0670	1.1552	1.2212	1.3959	1.6069	1.8126	2.0141	2.4401
75	1.0429	1.0671	1.1559	1.2233	1.3970	1.6132	1.8288	2.0141	2.4401
80	1.0439	1.0671	1.1559	1.2233	1.4019	1.6203	1.8475	2.0141	2.4401
85	1.0453	1.0683	1.1559	1.2233	1.4038	1.6279	1.8568	2.0141	2.4401
90	1.0469	1.0690	1.1559	1.2233	1.4048	1.6332	1.8705	2.0141	2.4401
95	1.0476	1.0699	1.1559	1.2233	1.4048	1.6384	1.8843	2.0141	2.4401
100	1.0474	1.0697	1.1559	1.2233	1.4048	1.6426	1.8957	2.0141	2.4401
105	1.0481	1.0704	1.1559	1.2233	1.4048	1.6479	1.9091	2.0141	2.4401
110	1.0482	1.0709	1.1559	1.2233	1.4048	1.6514	1.9158	2.0141	2.4401
115	1.0482	1.0714	1.1559	1.2233	1.4048	1.6571	1.9271	2.0141	2.4401
120	1.0482	1.0714	1.1559	1.2233	1.4048	1.6602	1.9367	2.0141	2.4401
125	1.0482	1.0720	1.1559	1.2233	1.4048	1.6641	1.9457	2.0141	2.4401
130	1.0482	1.0722	1.1559	1.2233	1.4048	1.6670	1.9539	2.0141	2.4401
135	1.0482	1.0725	1.1559	1.2233	1.4048	1.6721	1.9613	2.0141	2.4401
140	1.0482	1.0725	1.1559	1.2233	1.4048	1.6742	1.9679	2.0141	2.4401
145	1.0482	1.0725	1.1559	1.2233	1.4048	1.6773	1.9743	2.0141	2.4401
150	1.0482	1.0725	1.1559	1.2233	1.4048	1.6794	1.9743	2.0141	2.4401
155	1.0482	1.0725	1.1559	1.2233	1.4048	1.6851	1.9743	2.0141	2.4401
160	1.0482	1.0725	1.1559	1.2233	1.4048	1.6831	1.9743	2.0141	2.4401
165	1.0482	1.0725	1.1559	1.2233	1.4048	1.6872	1.9743	2.0141	2.4401
170	1.0482	1.0725	1.1559	1.2233	1.4048	1.6898	1.9743	2.0141	2.4401
175	1.0482	1.0725	1.1559	1.2233	1.4048	1.6925	1.9743	2.0141	2.4401
180	1.0482	1.0725	1.1559	1.2233	1.4048	1.6951	1.9743	2.0141	2.4401
185	1.0482	1.0725	1.1559	1.2233	1.4048	1.6959	1.9743	2.0141	2.4401
190	1.0482	1.0725	1.1559	1.2233	1.4048	1.7003	1.9743	2.0141	2.4401
195	1.0482	1.0725	1.1559	1.2233	1.4048	1.7020	1.9743	2.0141	2.4401
200	1.0482	1.0725	1.1559	1.2233	1.4048	1.7028	1.9743	2.0141	2.4401
205	1.0482	1.0725	1.1559	1.2233	1.4048	1.7050	1.9743	2.0141	2.4401
210	1.0482	1.0725	1.1559	1.2233	1.4048	1.7069	1.9743	2.0141	2.4401
215	1.0482	1.0725	1.1559	1.2233	1.4048	1.7114	1.9743	2.0141	2.4401
220	1.0482	1.0725	1.1559	1.2233	1.4048	1.7102	1.9743	2.0141	2.4401
225	1.0482	1.0725	1.1559	1.2233	1.4048	1.7149	1.9743	2.0141	2.4401
230	1.0482	1.0725	1.1559	1.2233	1.4048	1.7138	1.9743	2.0141	2.4401
235	1.0482	1.0725	1.1559	1.2233	1.4048	1.7164	1.9743	2.0141	2.4401
240	1.0482	1.0725	1.1559	1.2233	1.4048	1.7188	1.9743	2.0141	2.4401
245	1.0482	1.0725	1.1559	1.2233	1.4048	1.7206	1.9743	2.0141	2.4401
250	1.0482	1.0725	1.1559	1.2233	1.4048	1.7212	1.9743	2.0141	2.4401
255	1.0482	1.0725	1.1559	1.2233	1.4048	1.7226	1.9743	2.0141	2.4401
260	1.0482	1.0725	1.1559	1.2233	1.4048	1.7227	1.9743	2.0141	2.4401
265	1.0482	1.0725	1.1559	1.2233	1.4048	1.7270	1.9743	2.0141	2.4401
270	1.0482	1.0725	1.1559	1.2233	1.4048	1.7287	1.9743	2.0141	2.4401
275	1.0482	1.0725	1.1559	1.2233	1.4048	1.7300	1.9743	2.0141	2.4401
280	1.0482	1.0725	1.1559	1.2233	1.4048	1.7323	1.9743	2.0141	2.4401
285	1.0482	1.0725	1.1559	1.2233	1.4048	1.7332	1.9743	2.0141	2.4401
290	1.0482	1.0725	1.1559	1.2233	1.4048	1.7342	1.9743	2.0141	2.4401
295	1.0482	1.0725	1.1559	1.2233	1.4048	1.7332	1.9743	2.0141	2.4401
300	1.0482	1.0725	1.1559	1.2233	1.4048	1.7365	1.9743	2.0141	2.4401
305	1.0482	1.0725	1.1559	1.2233	1.4048	1.7389	1.9743	2.0141	2.4401
310	1.0482	1.0725	1.1559	1.2233	1.4048	1.7401	1.9743	2.0141	2.4401
315	1.0482	1.0725	1.1559	1.2233	1.4048	1.7415	1.9743	2.0141	2.4401
320	1.0482	1.0725	1.1559	1.2233	1.4048	1.7425	1.9743	2.0141	2.4401
325	1.0482	1.0725	1.1559	1.2233	1.4048	1.7419	1.9743	2.0141	2.4401
330	1.0482	1.0725	1.1559	1.2233	1.4048	1.7449	1.9743	2.0141	2.4401
335	1.0482	1.0725	1.1559	1.2233	1.4048	1.7446	1.9743	2.0141	2.4401
340	1.0482	1.0725	1.1559	1.2233	1.4048	1.7470	1.9743	2.0141	2.4401
345	1.0482	1.0725	1.1559	1.2233	1.4048	1.7467	1.9743	2.0141	2.4401
350	1.0482	1.0725	1.1559	1.2233	1.4048	1.7489	1.9743	2.0141	2.4401
355	1.0482	1.0725	1.1559	1.2233	1.4048	1.7493	1.9743	2.0141	2.4401
360	1.0482	1.0725	1.1559	1.2233	1.4048	1.7520	1.9743	2.0141	2.4401
365	1.0482	1.0725	1.1559	1.2233	1.4048	1.7496	1.9743	2.0141	2.4401
370	1.0482	1.0725	1.1559	1.2233	1.4048	1.7521	1.9743	2.0141	2.4401
375	1.0482	1.0725	1.1559	1.2233	1.4048	1.7539	1.9743	2.0141	2.4401
380	1.0482	1.0725	1.1559	1.2233	1.4048	1.7556	1.9743	2.0141	2.4401
385	1.0482	1.0725	1.1559	1.2233	1.4048	1.7562	1.9743	2.0141	2.4401
390	1.0482	1.0725	1.1559	1.2233	1.4048	1.7574	1.9743	2.0141	2.4401
395	1.0482	1.0725	1.1559	1.2233	1.4048	1.7582	1.9743	2.0141	2.4401
400	1.0482	1.0725	1.1559	1.2233	1.4048	1.7582	1.9743	2.0141	2.4401

TABLE D.8: Relative volume change of *n*-decane with time, exposed to 0.5 g/l DIW-CNF *gradually saturated* 45°C.

	10 bar	20 bar	30 bar	40 bar	50 bar	60 bar	70 bar	80 bar	90 bar
0	1.0000	1.0000	1.0000	1.0000	1.0000	1.0000	1.0000	1.0000	1.0000
5	1.0064	1.0108	1.0154	1.0200	1.0306	1.0230	1.0332	1.0323	1.0902
10	1.0120	1.0221	1.0304	1.0376	1.0534	1.0518	1.0682	1.0701	1.2146
15	1.0176	1.0317	1.0419	1.0542	1.0782	1.0779	1.0974	1.1132	1.3592
20	1.0221	1.0380	1.0541	1.0727	1.1019	1.1114	1.1412	1.1731	1.5332
25	1.0263	1.0420	1.0644	1.0863	1.1280	1.1403	1.1670	1.2189	1.7124
30	1.0303	1.0495	1.0749	1.1034	1.1516	1.1732	1.2083	1.2763	1.9217
35	1.0322	1.0534	1.0841	1.1178	1.1722	1.2032	1.2489	1.3333	2.1335
40	1.0344	1.0575	1.0912	1.1292	1.1962	1.2303	1.2860	1.3939	2.3403
45	1.0376	1.0614	1.0983	1.1393	1.2148	1.2600	1.3219	1.4471	2.5819
50	1.0401	1.0656	1.1050	1.1507	1.2328	1.2871	1.3590	1.5159	2.5819
55	1.0416	1.0707	1.1099	1.1592	1.2507	1.3052	1.3926	1.5793	2.5819
60	1.0441	1.0736	1.1154	1.1690	1.2666	1.3386	1.4181	1.6453	2.5819
65	1.0446	1.0756	1.1197	1.1772	1.2796	1.3632	1.4553	1.7038	2.5819
70	1.0455	1.0775	1.1234	1.1834	1.2921	1.3839	1.4846	1.7728	2.5819
75	1.0466	1.0786	1.1275	1.1863	1.3047	1.4044	1.5200	1.8368	2.5819
80	1.0474	1.0786	1.1303	1.1921	1.3155	1.4302	1.5509	1.9038	2.5819
85	1.0470	1.0809	1.1323	1.1968	1.3269	1.4472	1.5755	1.9591	2.5819
90	1.0486	1.0822	1.1345	1.2013	1.3342	1.4682	1.5978	2.0298	2.5819
95	1.0500	1.0841	1.1364	1.2041	1.3462	1.4846	1.6292	2.0912	2.5819
100	1.0507	1.0874	1.1379	1.2059	1.3531	1.5043	1.6504	2.1594	2.5819
105	1.0537	1.0878	1.1395	1.2083	1.3620	1.5198	1.6733	2.2162	2.5819
110	1.0548	1.0896	1.1417	1.2105	1.3699	1.5311	1.6935	2.2927	2.5819
115	1.0562	1.0899	1.1429	1.2128	1.3766	1.5464	1.7140	2.3408	2.5819
120	1.0590	1.0911	1.1456	1.2163	1.3843	1.5576	1.7330	2.3660	2.5819
125	1.0598	1.0923	1.1462	1.2176	1.3926	1.5761	1.7581	2.3660	2.5819
130	1.0598	1.0939	1.1473	1.2202	1.3983	1.5868	1.7702	2.3660	2.5819
135	1.0598	1.0935	1.1489	1.2234	1.4042	1.6015	1.7878	2.3660	2.5819
140	1.0598	1.0962	1.1505	1.2259	1.4090	1.6106	1.8033	2.3660	2.5819
145	1.0598	1.0968	1.1515	1.2282	1.4153	1.6215	1.8192	2.3660	2.5819
150	1.0598	1.0975	1.1527	1.2289	1.4211	1.6295	1.8345	2.3660	2.5819
155	1.0598	1.0988	1.1533	1.2321	1.4254	1.6402	1.8345	2.3660	2.5819
160	1.0598	1.0995	1.1533	1.2317	1.4294	1.6467	1.8345	2.3660	2.5819
165	1.0598	1.0999	1.1533	1.2329	1.4318	1.6556	1.8345	2.3660	2.5819
170	1.0598	1.1009	1.1533	1.2332	1.4363	1.6608	1.8345	2.3660	2.5819
175	1.0598	1.1020	1.1533	1.2357	1.4388	1.6689	1.8345	2.3660	2.5819
180	1.0598	1.1033	1.1533	1.2367	1.4407	1.6816	1.8345	2.3660	2.5819
185	1.0598	1.1031	1.1533	1.2373	1.4472	1.6855	1.8345	2.3660	2.5819
190	1.0598	1.1030	1.1533	1.2387	1.4464	1.6928	1.8345	2.3660	2.5819
195	1.0598	1.1043	1.1533	1.2408	1.4502	1.6969	1.8345	2.3660	2.5819
200	1.0598	1.1039	1.1533	1.2408	1.4552	1.7003	1.8345	2.3660	2.5819
205	1.0598	1.1039	1.1533	1.2419	1.4612	1.7092	1.8345	2.3660	2.5819
210	1.0598	1.1039	1.1533	1.2420	1.4655	1.7131	1.8345	2.3660	2.5819
215	1.0598	1.1039	1.1533	1.2436	1.4651	1.7131	1.8345	2.3660	2.5819
220	1.0598	1.1039	1.1533	1.2443	1.4684	1.7131	1.8345	2.3660	2.5819
225	1.0598	1.1039	1.1533	1.2464	1.4713	1.7131	1.8345	2.3660	2.5819
230	1.0598	1.1039	1.1533	1.2452	1.4735	1.7131	1.8345	2.3660	2.5819
235	1.0598	1.1039	1.1533	1.2473	1.4747	1.7131	1.8345	2.3660	2.5819
240	1.0598	1.1039	1.1533	1.2490	1.4760	1.7131	1.8345	2.3660	2.5819
245	1.0598	1.1039	1.1533	1.2495	1.4792	1.7131	1.8345	2.3660	2.5819
250	1.0598	1.1039	1.1533	1.2504	1.4803	1.7131	1.8345	2.3660	2.5819
255	1.0598	1.1039	1.1533	1.2525	1.4803	1.7131	1.8345	2.3660	2.5819
260	1.0598	1.1039	1.1533	1.2531	1.4803	1.7131	1.8345	2.3660	2.5819
265	1.0598	1.1039	1.1533	1.2541	1.4803	1.7131	1.8345	2.3660	2.5819
270	1.0598	1.1039	1.1533	1.2552	1.4803	1.7131	1.8345	2.3660	2.5819
275	1.0598	1.1039	1.1533	1.2556	1.4803	1.7131	1.8345	2.3660	2.5819
280	1.0598	1.1039	1.1533	1.2577	1.4803	1.7131	1.8345	2.3660	2.5819
285	1.0598	1.1039	1.1533	1.2581	1.4803	1.7131	1.8345	2.3660	2.5819
290	1.0598	1.1039	1.1533	1.2589	1.4803	1.7131	1.8345	2.3660	2.5819
295	1.0598	1.1039	1.1533	1.2603	1.4803	1.7131	1.8345	2.3660	2.5819
300	1.0598	1.1039	1.1533	1.2599	1.4803	1.7131	1.8345	2.3660	2.5819
305	1.0598	1.1039	1.1533	1.2605	1.4803	1.7131	1.8345	2.3660	2.5819
310	1.0598	1.1039	1.1533	1.2617	1.4803	1.7131	1.8345	2.3660	2.5819
315	1.0598	1.1039	1.1533	1.2616	1.4803	1.7131	1.8345	2.3660	2.5819
320	1.0598	1.1039	1.1533	1.2617	1.4803	1.7131	1.8345	2.3660	2.5819
325	1.0598	1.1039	1.1533	1.2623	1.4803	1.7131	1.8345	2.3660	2.5819
330	1.0598	1.1039	1.1533	1.2624	1.4803	1.7131	1.8345	2.3660	2.5819
335	1.0598	1.1039	1.1533	1.2631	1.4803	1.7131	1.8345	2.3660	2.5819
340	1.0598	1.1039	1.1533	1.2651	1.4803	1.7131	1.8345	2.3660	2.5819
345	1.0598	1.1039	1.1533	1.2653	1.4803	1.7131	1.8345	2.3660	2.5819
350	1.0598	1.1039	1.1533	1.2642	1.4803	1.7131	1.8345	2.3660	2.5819
355	1.0598	1.1039	1.1533	1.2662	1.4803	1.7131	1.8345	2.3660	2.5819
360	1.0598	1.1039	1.1533	1.2677	1.4803	1.7131	1.8345	2.3660	2.5819
365	1.0598	1.1039	1.1533	1.2688	1.4803	1.7131	1.8345	2.3660	2.5819
370	1.0598	1.1039	1.1533	1.2677	1.4803	1.7131	1.8345	2.3660	2.5819
375	1.0598	1.1039	1.1533	1.2703	1.4803	1.7131	1.8345	2.3660	2.5819
380	1.0598	1.1039	1.1533	1.2705	1.4803	1.7131	1.8345	2.3660	2.5819
385	1.0598	1.1039	1.1533	1.2710	1.4803	1.7131	1.8345	2.3660	2.5819
390	1.0598	1.1039	1.1533	1.2715	1.4803	1.7131	1.8345	2.3660	2.5819
395	1.0598	1.1039	1.1533	1.2735	1.4803	1.7131	1.8345	2.3660	2.5819
400	1.0598	1.1039	1.1533	1.2735	1.4803	1.7131	1.8345	2.3660	2.5819

TABLE D.9: Relative volume change of *n*-decane with time, exposed to 0.05 g/l DIW-CNF *saturated* 25°C.

Time [min]	10 bar	20 bar	30 bar	40 bar	50 bar	60 bar	70 bar	80 bar	90 bar
0	1.0000	1.0000	1.0000	1.0000	1.0000	1.0000	1.0000	1.0000	1.0000
5	1.0294	1.0725	1.1268	1.1544	1.1941	1.2217	1.2342	1.2390	1.2727
10	1.0349	1.0901	1.1697	1.2180	1.3128	1.3377	1.3723	1.3808	1.4393
15	1.0381	1.0986	1.1983	1.2499	1.3979	1.4377	1.4728	1.5007	1.5947
20	1.0390	1.1028	1.2175	1.2825	1.4647	1.5226	1.5696	1.6071	1.7363
25	1.0408	1.1049	1.2290	1.3041	1.5200	1.5966	1.6536	1.7182	1.8682
30	1.0415	1.1059	1.2391	1.3225	1.5696	1.6672	1.7408	1.8221	1.9907
35	1.0429	1.1076	1.2474	1.3371	1.6124	1.7415	1.8026	1.9196	2.1234
40	1.0437	1.1084	1.2527	1.3509	1.6513	1.8102	1.8739	2.0132	2.2432
45	1.0449	1.1084	1.2576	1.3618	1.6918	1.8718	1.9361	2.1012	2.3569
50	1.0458	1.1085	1.2620	1.3712	1.7130	1.9329	1.9947	2.1897	2.4656
55	1.0464	1.1084	1.2651	1.3796	1.7396	1.9905	2.0451	2.2764	2.5745
60	1.0477	1.1088	1.2680	1.3873	1.7683	2.0426	2.0887	2.3589	2.6848
65	1.0476	1.1088	1.2686	1.3941	1.7882	2.0959	2.1302	2.4482	2.7955
70	1.0489	1.1088	1.2722	1.4007	1.8159	2.1408	2.1896	2.5377	2.8993
75	1.0499	1.1088	1.2735	1.4051	1.8325	2.1983	2.2240	2.6142	3.0084
80	1.0503	1.1088	1.2761	1.4102	1.8474	2.2401	2.2617	2.7041	3.1218
85	1.0511	1.1088	1.2792	1.4151	1.8687	2.2928	2.3127	2.7858	3.2384
90	1.0523	1.1088	1.2806	1.4196	1.8818	2.3395	2.3533	2.8459	3.3081
95	1.0531	1.1088	1.2814	1.4243	1.8919	2.3884	2.3859	2.8459	3.3081
100	1.0533	1.1088	1.2807	1.4283	1.9118	2.4329	2.4090	2.8459	3.3081
105	1.0538	1.1088	1.2825	1.4321	1.9206	2.4734	2.4446	2.8459	3.3081
110	1.0538	1.1088	1.2831	1.4362	1.9345	2.5243	2.4431	2.8459	3.3081
115	1.0545	1.1088	1.2831	1.4390	1.9445	2.5605	2.4544	2.8459	3.3081
120	1.0542	1.1088	1.2866	1.4407	1.9600	2.6208	2.4670	2.8459	3.3081
125	1.0546	1.1088	1.2887	1.4451	1.9625	2.6694	2.4699	2.8459	3.3081
130	1.0546	1.1088	1.2873	1.4475	1.9790	2.6993	2.4699	2.8459	3.3081
135	1.0546	1.1088	1.2890	1.4505	1.9839	2.7237	2.4699	2.8459	3.3081
140	1.0546	1.1088	1.2894	1.4521	1.9957	2.7668	2.4699	2.8459	3.3081
145	1.0546	1.1088	1.2908	1.4531	2.0062	2.8108	2.4699	2.8459	3.3081
150	1.0546	1.1088	1.2899	1.4539	2.0184	2.8318	2.4699	2.8459	3.3081
155	1.0546	1.1088	1.2933	1.4572	2.0253	2.8508	2.4699	2.8459	3.3081
160	1.0546	1.1088	1.2938	1.4585	2.0236	2.8596	2.4699	2.8459	3.3081
165	1.0546	1.1088	1.2942	1.4607	2.0312	2.8804	2.4699	2.8459	3.3081
170	1.0546	1.1088	1.2922	1.4628	2.0490	2.8843	2.4699	2.8459	3.3081
175	1.0546	1.1088	1.2937	1.4626	2.0547	2.8843	2.4699	2.8459	3.3081
180	1.0546	1.1088	1.2937	1.4649	2.0562	2.8843	2.4699	2.8459	3.3081
185	1.0546	1.1088	1.2937	1.4655	2.0592	2.8843	2.4699	2.8459	3.3081
190	1.0546	1.1088	1.2937	1.4668	2.0614	2.8843	2.4699	2.8459	3.3081
195	1.0546	1.1088	1.2937	1.4692	2.0621	2.8843	2.4699	2.8459	3.3081
200	1.0546	1.1088	1.2937	1.4697	2.0621	2.8843	2.4699	2.8459	3.3081
205	1.0546	1.1088	1.2937	1.4711	2.0621	2.8843	2.4699	2.8459	3.3081
210	1.0546	1.1088	1.2937	1.4714	2.0621	2.8843	2.4699	2.8459	3.3081
215	1.0546	1.1088	1.2937	1.4730	2.0621	2.8843	2.4699	2.8459	3.3081
220	1.0546	1.1088	1.2937	1.4741	2.0621	2.8843	2.4699	2.8459	3.3081
225	1.0546	1.1088	1.2937	1.4757	2.0621	2.8843	2.4699	2.8459	3.3081
230	1.0546	1.1088	1.2937	1.4771	2.0621	2.8843	2.4699	2.8459	3.3081
235	1.0546	1.1088	1.2937	1.4785	2.0621	2.8843	2.4699	2.8459	3.3081
240	1.0546	1.1088	1.2937	1.4783	2.0621	2.8843	2.4699	2.8459	3.3081
245	1.0546	1.1088	1.2937	1.4809	2.0621	2.8843	2.4699	2.8459	3.3081
250	1.0546	1.1088	1.2937	1.4812	2.0621	2.8843	2.4699	2.8459	3.3081
255	1.0546	1.1088	1.2937	1.4832	2.0621	2.8843	2.4699	2.8459	3.3081
260	1.0546	1.1088	1.2937	1.4841	2.0621	2.8843	2.4699	2.8459	3.3081
265	1.0546	1.1088	1.2937	1.4845	2.0621	2.8843	2.4699	2.8459	3.3081
270	1.0546	1.1088	1.2937	1.4856	2.0621	2.8843	2.4699	2.8459	3.3081
275	1.0546	1.1088	1.2937	1.4862	2.0621	2.8843	2.4699	2.8459	3.3081
280	1.0546	1.1088	1.2937	1.4882	2.0621	2.8843	2.4699	2.8459	3.3081
285	1.0546	1.1088	1.2937	1.4886	2.0621	2.8843	2.4699	2.8459	3.3081
290	1.0546	1.1088	1.2937	1.4887	2.0621	2.8843	2.4699	2.8459	3.3081
295	1.0546	1.1088	1.2937	1.4895	2.0621	2.8843	2.4699	2.8459	3.3081
300	1.0546	1.1088	1.2937	1.4895	2.0621	2.8843	2.4699	2.8459	3.3081
305	1.0546	1.1088	1.2937	1.4895	2.0621	2.8843	2.4699	2.8459	3.3081
310	1.0546	1.1088	1.2937	1.4895	2.0621	2.8843	2.4699	2.8459	3.3081
315	1.0546	1.1088	1.2937	1.4895	2.0621	2.8843	2.4699	2.8459	3.3081
320	1.0546	1.1088	1.2937	1.4895	2.0621	2.8843	2.4699	2.8459	3.3081
325	1.0546	1.1088	1.2937	1.4895	2.0621	2.8843	2.4699	2.8459	3.3081
330	1.0546	1.1088	1.2937	1.4895	2.0621	2.8843	2.4699	2.8459	3.3081
335	1.0546	1.1088	1.2937	1.4895	2.0621	2.8843	2.4699	2.8459	3.3081
340	1.0546	1.1088	1.2937	1.4895	2.0621	2.8843	2.4699	2.8459	3.3081
345	1.0546	1.1088	1.2937	1.4895	2.0621	2.8843	2.4699	2.8459	3.3081
350	1.0546	1.1088	1.2937	1.4895	2.0621	2.8843	2.4699	2.8459	3.3081
355	1.0546	1.1088	1.2937	1.4895	2.0621	2.8843	2.4699	2.8459	3.3081
360	1.0546	1.1088	1.2937	1.4895	2.0621	2.8843	2.4699	2.8459	3.3081
365	1.0546	1.1088	1.2937	1.4895	2.0621	2.8843	2.4699	2.8459	3.3081
370	1.0546	1.1088	1.2937	1.4895	2.0621	2.8843	2.4699	2.8459	3.3081
375	1.0546	1.1088	1.2937	1.4895	2.0621	2.8843	2.4699	2.8459	3.3081
380	1.0546	1.1088	1.2937	1.4895	2.0621	2.8843	2.4699	2.8459	3.3081
385	1.0546	1.1088	1.2937	1.4895	2.0621	2.8843	2.4699	2.8459	3.3081
390	1.0546	1.1088	1.2937	1.4895	2.0621	2.8843	2.4699	2.8459	3.3081
395	1.0546	1.1088	1.2937	1.4895	2.0621	2.8843	2.4699	2.8459	3.3081
400	1.0546	1.1088	1.2937	1.4895	2.0621	2.8843	2.4699	2.8459	3.3081

TABLE D.10: Relative volume change of *n*-decane with time, exposed to 0.05 g/l DIW-CNF *gradually saturated* 25°C.

Time [min]	10 bar	20 bar	30 bar	40 bar	50 bar	60 bar	70 bar	80 bar	90 bar
0	1.0000	1.0000	1.0000	1.0000	1.0000	1.0000	1.0000	1.0000	1.0000
5	1.0046	1.0070	1.0096	1.0175	1.0176	1.0000	1.0180	1.0159	1.0213
10	1.0116	1.0132	1.0256	1.0343	1.0438	1.0339	1.0410	1.0405	1.0384
15	1.0176	1.0212	1.0364	1.0448	1.0612	1.0571	1.0650	1.0643	1.0601
20	1.0231	1.0313	1.0475	1.0686	1.0868	1.0901	1.0915	1.0964	1.0851
25	1.0296	1.0358	1.0577	1.0870	1.1102	1.1233	1.1217	1.1233	1.1251
30	1.0336	1.0429	1.0681	1.1046	1.1382	1.1647	1.1527	1.1551	1.1600
35	1.0373	1.0490	1.0800	1.1265	1.1681	1.2002	1.1895	1.1889	1.1916
40	1.0413	1.0539	1.0904	1.1480	1.2011	1.2501	1.2261	1.2284	1.2427
45	1.0481	1.0582	1.1010	1.1652	1.2323	1.2867	1.2606	1.2677	1.2845
50	1.0521	1.0642	1.1098	1.1843	1.2626	1.3420	1.3001	1.3125	1.3285
55	1.0550	1.0680	1.1180	1.2072	1.3002	1.3855	1.3369	1.3493	1.3786
60	1.0593	1.0741	1.1273	1.2249	1.3275	1.4254	1.3794	1.3936	1.4284
65	1.0640	1.0800	1.1377	1.2441	1.3558	1.4700	1.4188	1.4384	1.4836
70	1.0673	1.0844	1.1414	1.2607	1.3860	1.5185	1.4610	1.4838	1.5404
75	1.0712	1.0875	1.1496	1.2804	1.4156	1.5623	1.4987	1.5305	1.6004
80	1.0742	1.0909	1.1585	1.2976	1.4472	1.6024	1.5394	1.5749	1.6510
85	1.0774	1.0953	1.1630	1.3160	1.4743	1.6454	1.5743	1.6218	1.7195
90	1.0790	1.0982	1.1704	1.3292	1.5002	1.6920	1.6117	1.6694	1.7835
95	1.0812	1.1005	1.1747	1.3482	1.5260	1.7345	1.6462	1.7167	1.8497
100	1.0828	1.1040	1.1809	1.3621	1.5498	1.7815	1.6880	1.7742	1.9174
105	1.0848	1.1074	1.1862	1.3766	1.5673	1.8192	1.7260	1.8352	1.9876
110	1.0870	1.1096	1.1919	1.3912	1.5916	1.8624	1.7618	1.8926	2.0457
115	1.0883	1.1115	1.1950	1.4036	1.6132	1.9023	1.7958	1.9488	2.1273
120	1.0907	1.1143	1.2000	1.4172	1.6397	1.9422	1.8303	2.0089	2.2021
125	1.0919	1.1153	1.2025	1.4296	1.6624	1.9778	1.8645	2.0652	2.2788
130	1.0933	1.1185	1.2070	1.4425	1.6828	2.0159	1.8991	2.1247	2.3516
135	1.0933	1.1201	1.2128	1.4541	1.7039	2.0553	1.9314	2.1845	2.4125
140	1.0942	1.1224	1.2133	1.4639	1.7259	2.0922	1.9630	2.2434	2.4830
145	1.0954	1.1252	1.2177	1.4737	1.7447	2.1253	1.9919	2.3048	2.5610
150	1.0964	1.1255	1.2169	1.4850	1.7647	2.1597	2.0215	2.3627	2.6284
155	1.0972	1.1268	1.2219	1.4935	1.7815	2.1969	2.0517	2.4176	2.6944
160	1.0980	1.1289	1.2266	1.5051	1.8002	2.2368	2.0827	2.4753	2.7523
165	1.0980	1.1299	1.2320	1.5097	1.8168	2.2637	2.1116	2.5433	2.8567
170	1.0982	1.1301	1.2324	1.5205	1.8339	2.2993	2.1418	2.5940	2.8567
175	1.0989	1.1325	1.2354	1.5295	1.8490	2.3339	2.1646	2.6702	2.8567
180	1.0989	1.1333	1.2374	1.5391	1.8627	2.3396	2.1855	2.6702	2.8567
185	1.0989	1.1346	1.2391	1.5482	1.8770	2.3871	2.2282	2.6702	2.8567
190	1.0989	1.1360	1.2405	1.5539	1.8940	2.4258	2.2491	2.6702	2.8567
195	1.0989	1.1371	1.2457	1.5616	1.9083	2.4224	2.2748	2.6702	2.8567
200	1.0989	1.1390	1.2466	1.5683	1.9232	2.4224	2.2595	2.6702	2.8567
205	1.0989	1.1402	1.2484	1.5752	1.9384	2.4224	2.2595	2.6702	2.8567
210	1.0989	1.1408	1.2501	1.5821	1.9518	2.4224	2.2595	2.6702	2.8567
215	1.0989	1.1412	1.2518	1.5892	1.9626	2.4224	2.2595	2.6702	2.8567
220	1.0989	1.1411	1.2541	1.5938	1.9740	2.4224	2.2595	2.6702	2.8567
225	1.0989	1.1423	1.2547	1.6004	1.9863	2.4224	2.2595	2.6702	2.8567
230	1.0989	1.1427	1.2558	1.6070	1.9969	2.4224	2.2595	2.6702	2.8567
235	1.0989	1.1428	1.2584	1.6158	2.0127	2.4224	2.2595	2.6702	2.8567
240	1.0989	1.1441	1.2601	1.6187	2.0264	2.4224	2.2595	2.6702	2.8567
245	1.0989	1.1437	1.2620	1.6231	2.0326	2.4224	2.2595	2.6702	2.8567
250	1.0989	1.1452	1.2659	1.6301	2.0452	2.4224	2.2595	2.6702	2.8567
255	1.0989	1.1449	1.2654	1.6349	2.0540	2.4224	2.2595	2.6702	2.8567
260	1.0989	1.1463	1.2664	1.6393	2.0654	2.4224	2.2595	2.6702	2.8567
265	1.0989	1.1484	1.2664	1.6445	2.0741	2.4224	2.2595	2.6702	2.8567
270	1.0989	1.1484	1.2664	1.6505	2.0844	2.4224	2.2595	2.6702	2.8567
275	1.0989	1.1493	1.2664	1.6552	2.0968	2.4224	2.2595	2.6702	2.8567
280	1.0989	1.1491	1.2664	1.6590	2.1053	2.4224	2.2595	2.6702	2.8567
285	1.0989	1.1498	1.2664	1.6641	2.1115	2.4224	2.2595	2.6702	2.8567
290	1.0989	1.1507	1.2664	1.6690	2.1199	2.4224	2.2595	2.6702	2.8567
295	1.0989	1.1512	1.2664	1.6715	2.1286	2.4224	2.2595	2.6702	2.8567
300	1.0989	1.1525	1.2664	1.6778	2.1381	2.4224	2.2595	2.6702	2.8567
305	1.0989	1.1525	1.2664	1.6808	2.1465	2.4224	2.2595	2.6702	2.8567
310	1.0989	1.1528	1.2664	1.6861	2.1503	2.4224	2.2595	2.6702	2.8567
315	1.0989	1.1527	1.2664	1.6911	2.1632	2.4224	2.2595	2.6702	2.8567
320	1.0989	1.1530	1.2664	1.6939	2.1723	2.4224	2.2595	2.6702	2.8567
325	1.0989	1.1537	1.2664	1.6956	2.1789	2.4224	2.2595	2.6702	2.8567
330	1.0989	1.1544	1.2664	1.6994	2.1828	2.4224	2.2595	2.6702	2.8567
335	1.0989	1.1547	1.2664	1.7032	2.1937	2.4224	2.2595	2.6702	2.8567
340	1.0989	1.1551	1.2664	1.7082	2.1978	2.4224	2.2595	2.6702	2.8567
345	1.0989	1.1560	1.2664	1.7082	2.2084	2.4224	2.2595	2.6702	2.8567
350	1.0989	1.1554	1.2664	1.7082	2.2110	2.4224	2.2595	2.6702	2.8567
355	1.0989	1.1554	1.2664	1.7082	2.2110	2.4224	2.2595	2.6702	2.8567
360	1.0989	1.1554	1.2664	1.7082	2.2110	2.4224	2.2595	2.6702	2.8567
365	1.0989	1.1554	1.2664	1.7082	2.2110	2.4224	2.2595	2.6702	2.8567
370	1.0989	1.1554	1.2664	1.7082	2.2110	2.4224	2.2595	2.6702	2.8567
375	1.0989	1.1554	1.2664	1.7082	2.2110	2.4224	2.2595	2.6702	2.8567
380	1.0989	1.1554	1.2664	1.7082	2.2110	2.4224	2.2595	2.6702	2.8567
385	1.0989	1.1554	1.2664	1.7082	2.2110	2.4224	2.2595	2.6702	2.8567
390	1.0989	1.1554	1.2664	1.7082	2.2110	2.4224	2.2595	2.6702	2.8567
395	1.0989	1.1554	1.2664	1.7082	2.2110	2.4224	2.2595	2.6702	2.8567
400	1.0989	1.1554	1.2664	1.7082	2.2110	2.4224	2.2595	2.6702	2.8567

TABLE D.11: Relative volume change of *n*-decane with time, exposed to 0.05 g/l DIW-CNF *saturated* 45°C.

Time [min]	10 bar	20 bar	30 bar	40 bar	50 bar	60 bar	70 bar	80 bar	90 bar
0	1.0000	1.0000	1.0000	1.0000	1.0000	1.0000	1.0000	1.0000	1.0000
5	1.0216	1.0429	1.0776	1.1163	1.1403	1.1129	1.2164	1.2423	1.3320
10	1.0250	1.0516	1.0969	1.1681	1.1956	1.1720	1.3149	1.3560	1.5577
15	1.0258	1.0567	1.1051	1.1931	1.2335	1.2045	1.3870	1.4517	1.7383
20	1.0266	1.0574	1.1105	1.2053	1.2560	1.2388	1.4485	1.5312	1.9081
25	1.0268	1.0602	1.1121	1.2178	1.2726	1.2695	1.4966	1.5988	2.0636
30	1.0266	1.0605	1.1161	1.2184	1.2895	1.2970	1.5281	1.6503	2.2141
35	1.0266	1.0626	1.1169	1.2242	1.3026	1.3216	1.5628	1.6965	2.3490
40	1.0270	1.0634	1.1194	1.2275	1.3186	1.3429	1.5913	1.7170	2.3490
45	1.0270	1.0652	1.1187	1.2297	1.3294	1.3666	1.6154	1.7922	2.3490
50	1.0270	1.0658	1.1192	1.2311	1.3366	1.3842	1.6359	1.7922	2.3490
55	1.0270	1.0663	1.1215	1.2347	1.3455	1.4011	1.6600	1.7922	2.3490
60	1.0270	1.0689	1.1231	1.2375	1.3534	1.4233	1.6782	1.7922	2.3490
65	1.0270	1.0692	1.1254	1.2358	1.3616	1.4361	1.7006	1.7922	2.3490
70	1.0270	1.0699	1.1268	1.2377	1.3676	1.4536	1.7141	1.7922	2.3490
75	1.0270	1.0702	1.1286	1.2369	1.3702	1.4706	1.7338	1.7922	2.3490
80	1.0270	1.0723	1.1291	1.2427	1.3745	1.4895	1.7464	1.7922	2.3490
85	1.0270	1.0726	1.1316	1.2374	1.3796	1.5033	1.7600	1.7922	2.3490
90	1.0270	1.0727	1.1316	1.2402	1.3844	1.5180	1.7704	1.7922	2.3490
95	1.0270	1.0728	1.1332	1.2414	1.3885	1.5386	1.7794	1.7922	2.3490
100	1.0270	1.0747	1.1345	1.2421	1.3923	1.5514	1.7904	1.7922	2.3490
105	1.0270	1.0749	1.1348	1.2430	1.3956	1.5625	1.8004	1.7922	2.3490
110	1.0270	1.0759	1.1367	1.2409	1.3989	1.5761	1.8127	1.7922	2.3490
115	1.0270	1.0770	1.1360	1.2431	1.4023	1.5856	1.8230	1.7922	2.3490
120	1.0270	1.0764	1.1371	1.2420	1.4048	1.5970	1.8339	1.7922	2.3490
125	1.0270	1.0780	1.1383	1.2420	1.4089	1.6095	1.8359	1.7922	2.3490
130	1.0270	1.0779	1.1399	1.2420	1.4103	1.6185	1.8494	1.7922	2.3490
135	1.0270	1.0785	1.1411	1.2420	1.4139	1.6329	1.8519	1.7922	2.3490
140	1.0270	1.0785	1.1432	1.2420	1.4158	1.6420	1.8656	1.7922	2.3490
145	1.0270	1.0788	1.1429	1.2420	1.4176	1.6519	1.8685	1.7922	2.3490
150	1.0270	1.0795	1.1443	1.2420	1.4203	1.6558	1.8792	1.7922	2.3490
155	1.0270	1.0801	1.1432	1.2420	1.4224	1.6571	1.8821	1.7922	2.3490
160	1.0270	1.0801	1.1456	1.2420	1.4232	1.6571	1.8913	1.7922	2.3490
165	1.0270	1.0801	1.1461	1.2420	1.4258	1.6571	1.8994	1.7922	2.3490
170	1.0270	1.0801	1.1486	1.2420	1.4276	1.6571	1.9005	1.7922	2.3490
175	1.0270	1.0801	1.1486	1.2420	1.4272	1.6571	1.9106	1.7922	2.3490
180	1.0270	1.0801	1.1486	1.2420	1.4300	1.6571	1.9160	1.7922	2.3490
185	1.0270	1.0801	1.1486	1.2420	1.4312	1.6571	1.9230	1.7922	2.3490
190	1.0270	1.0801	1.1486	1.2420	1.4341	1.6571	1.9275	1.7922	2.3490
195	1.0270	1.0801	1.1486	1.2420	1.4363	1.6571	1.9324	1.7922	2.3490
200	1.0270	1.0801	1.1486	1.2420	1.4375	1.6571	1.9386	1.7922	2.3490
205	1.0270	1.0801	1.1486	1.2420	1.4375	1.6571	1.9506	1.7922	2.3490
210	1.0270	1.0801	1.1486	1.2420	1.4375	1.6571	1.9518	1.7922	2.3490
215	1.0270	1.0801	1.1486	1.2420	1.4375	1.6571	1.9592	1.7922	2.3490
220	1.0270	1.0801	1.1486	1.2420	1.4375	1.6571	1.9617	1.7922	2.3490
225	1.0270	1.0801	1.1486	1.2420	1.4375	1.6571	1.9660	1.7922	2.3490
230	1.0270	1.0801	1.1486	1.2420	1.4375	1.6571	1.9725	1.7922	2.3490
235	1.0270	1.0801	1.1486	1.2420	1.4375	1.6571	1.9759	1.7922	2.3490
240	1.0270	1.0801	1.1486	1.2420	1.4375	1.6571	1.9842	1.7922	2.3490
245	1.0270	1.0801	1.1486	1.2420	1.4375	1.6571	1.9895	1.7922	2.3490
250	1.0270	1.0801	1.1486	1.2420	1.4375	1.6571	1.9918	1.7922	2.3490
255	1.0270	1.0801	1.1486	1.2420	1.4375	1.6571	1.9962	1.7922	2.3490
260	1.0270	1.0801	1.1486	1.2420	1.4375	1.6571	2.0008	1.7922	2.3490
265	1.0270	1.0801	1.1486	1.2420	1.4375	1.6571	2.0100	1.7922	2.3490
270	1.0270	1.0801	1.1486	1.2420	1.4375	1.6571	2.0086	1.7922	2.3490
275	1.0270	1.0801	1.1486	1.2420	1.4375	1.6571	2.0202	1.7922	2.3490
280	1.0270	1.0801	1.1486	1.2420	1.4375	1.6571	2.0195	1.7922	2.3490
285	1.0270	1.0801	1.1486	1.2420	1.4375	1.6571	2.0219	1.7922	2.3490
290	1.0270	1.0801	1.1486	1.2420	1.4375	1.6571	2.0241	1.7922	2.3490
295	1.0270	1.0801	1.1486	1.2420	1.4375	1.6571	2.0319	1.7922	2.3490
300	1.0270	1.0801	1.1486	1.2420	1.4375	1.6571	2.0375	1.7922	2.3490
305	1.0270	1.0801	1.1486	1.2420	1.4375	1.6571	2.0451	1.7922	2.3490
310	1.0270	1.0801	1.1486	1.2420	1.4375	1.6571	2.0439	1.7922	2.3490
315	1.0270	1.0801	1.1486	1.2420	1.4375	1.6571	2.0482	1.7922	2.3490
320	1.0270	1.0801	1.1486	1.2420	1.4375	1.6571	2.0574	1.7922	2.3490
325	1.0270	1.0801	1.1486	1.2420	1.4375	1.6571	2.0552	1.7922	2.3490
330	1.0270	1.0801	1.1486	1.2420	1.4375	1.6571	2.0596	1.7922	2.3490
335	1.0270	1.0801	1.1486	1.2420	1.4375	1.6571	2.0657	1.7922	2.3490
340	1.0270	1.0801	1.1486	1.2420	1.4375	1.6571	2.0704	1.7922	2.3490
345	1.0270	1.0801	1.1486	1.2420	1.4375	1.6571	2.0690	1.7922	2.3490
350	1.0270	1.0801	1.1486	1.2420	1.4375	1.6571	2.0724	1.7922	2.3490
355	1.0270	1.0801	1.1486	1.2420	1.4375	1.6571	2.0763	1.7922	2.3490
360	1.0270	1.0801	1.1486	1.2420	1.4375	1.6571	2.0802	1.7922	2.3490
365	1.0270	1.0801	1.1486	1.2420	1.4375	1.6571	2.0830	1.7922	2.3490
370	1.0270	1.0801	1.1486	1.2420	1.4375	1.6571	2.0897	1.7922	2.3490
375	1.0270	1.0801	1.1486	1.2420	1.4375	1.6571	2.0905	1.7922	2.3490
380	1.0270	1.0801	1.1486	1.2420	1.4375	1.6571	2.0908	1.7922	2.3490
385	1.0270	1.0801	1.1486	1.2420	1.4375	1.6571	2.0897	1.7922	2.3490
390	1.0270	1.0801	1.1486	1.2420	1.4375	1.6571	2.0897	1.7922	2.3490
395	1.0270	1.0801	1.1486	1.2420	1.4375	1.6571	2.0897	1.7922	2.3490
400	1.0270	1.0801	1.1486	1.2420	1.4375	1.6571	2.0897	1.7922	2.3490

TABLE D.12: Relative volume change of *n*-decane with time, exposed to 0.05 g/l DIW-CNF *gradually saturated* 45°C.

Time [min]	10 bar	20 bar	30 bar	40 bar	50 bar	60 bar	70 bar	80 bar	90 bar
0	1.0000	1.0000	1.0000	1.0000	1.0000	1.0000	1.0000	1.0000	1.0000
5	1.0045	1.0342	1.0348	1.0315	1.0266	1.0452	1.0276	1.0228	1.0276
10	1.0075	1.0439	1.0488	1.0528	1.0515	1.0689	1.0570	1.0542	1.0672
15	1.0114	1.0488	1.0584	1.0664	1.0789	1.0938	1.0904	1.0920	1.1082
20	1.0135	1.0553	1.0686	1.0914	1.1073	1.1261	1.1291	1.1225	1.1532
25	1.0144	1.0577	1.0801	1.1077	1.1347	1.1543	1.1690	1.1611	1.2076
30	1.0166	1.0637	1.0883	1.1239	1.1545	1.1827	1.2057	1.1995	1.2558
35	1.0189	1.0691	1.0963	1.1336	1.1810	1.2131	1.2429	1.2301	1.3106
40	1.0197	1.0729	1.1072	1.1484	1.2049	1.2360	1.2746	1.2676	1.3703
45	1.0214	1.0745	1.1140	1.1634	1.2237	1.2651	1.3116	1.2960	1.4248
50	1.0224	1.0778	1.1200	1.1761	1.2480	1.2915	1.3536	1.3273	1.4938
55	1.0238	1.0786	1.1250	1.1860	1.2647	1.3128	1.3875	1.3559	1.5559
60	1.0248	1.0826	1.1305	1.1977	1.2830	1.3371	1.4237	1.3853	1.6248
65	1.0266	1.0845	1.1366	1.2058	1.3049	1.3601	1.4475	1.4129	1.6965
70	1.0273	1.0867	1.1408	1.2117	1.3166	1.3813	1.4795	1.4396	1.7607
75	1.0287	1.0880	1.1412	1.2209	1.3306	1.4024	1.5135	1.4664	1.8370
80	1.0291	1.0907	1.1472	1.2255	1.3442	1.4203	1.5421	1.4913	1.9139
85	1.0302	1.0918	1.1509	1.2342	1.3566	1.4367	1.5639	1.5169	2.0178
90	1.0306	1.0913	1.1504	1.2385	1.3664	1.4494	1.5923	1.5416	2.0528
95	1.0318	1.0930	1.1560	1.2448	1.3789	1.4704	1.6152	1.5657	2.0528
100	1.0317	1.0943	1.1560	1.2484	1.3872	1.4836	1.6404	1.5880	2.0528
105	1.0321	1.0965	1.1608	1.2548	1.3965	1.4968	1.6564	1.6134	2.0528
110	1.0329	1.0972	1.1625	1.2598	1.4057	1.5144	1.6794	1.6303	2.0528
115	1.0331	1.0985	1.1639	1.2641	1.4135	1.5272	1.7013	1.6467	2.0528
120	1.0334	1.1003	1.1657	1.2663	1.4226	1.5365	1.7107	1.6662	2.0528
125	1.0348	1.1013	1.1688	1.2675	1.4276	1.5530	1.7307	1.6798	2.0528
130	1.0344	1.1028	1.1701	1.2742	1.4341	1.5647	1.7494	1.6921	2.0528
135	1.0349	1.1028	1.1714	1.2783	1.4405	1.5747	1.7547	1.7035	2.0528
140	1.0350	1.1049	1.1728	1.2824	1.4461	1.5861	1.7740	1.7167	2.0528
145	1.0360	1.1050	1.1736	1.2799	1.4536	1.5946	1.7883	1.7266	2.0528
150	1.0361	1.1059	1.1752	1.2841	1.4590	1.6082	1.7984	1.7377	2.0528
155	1.0363	1.1065	1.1764	1.2851	1.4623	1.6200	1.7998	1.7477	2.0528
160	1.0369	1.1083	1.1792	1.2858	1.4674	1.6241	1.7998	1.7570	2.0528
165	1.0371	1.1081	1.1806	1.2890	1.4734	1.6319	1.7998	1.7647	2.0528
170	1.0376	1.1093	1.1808	1.2892	1.4781	1.6397	1.7998	1.7729	2.0528
175	1.0374	1.1097	1.1818	1.2892	1.4812	1.6452	1.7998	1.7797	2.0528
180	1.0380	1.1091	1.1852	1.2892	1.4812	1.6593	1.7998	1.7833	2.0528
185	1.0388	1.1104	1.1852	1.2892	1.4903	1.6627	1.7998	1.7936	2.0528
190	1.0395	1.1098	1.1856	1.2892	1.4888	1.6692	1.7998	1.7998	2.0528
195	1.0395	1.1112	1.1916	1.2892	1.4921	1.6758	1.7998	1.8044	2.0528
200	1.0395	1.1118	1.1921	1.2892	1.4983	1.6868	1.7998	1.8109	2.0528
205	1.0407	1.1121	1.1940	1.2892	1.4946	1.6932	1.7998	1.8190	2.0528
210	1.0407	1.1127	1.1946	1.2892	1.5024	1.6985	1.7998	1.8128	2.0528
215	1.0408	1.1132	1.1977	1.2892	1.5050	1.7039	1.7998	1.8256	2.0528
220	1.0410	1.1145	1.1985	1.2892	1.5095	1.7092	1.7998	1.8325	2.0528
225	1.0420	1.1152	1.1971	1.2892	1.5088	1.7144	1.7998	1.8376	2.0528
230	1.0418	1.1171	1.1973	1.2892	1.5159	1.7184	1.7998	1.8295	2.0528
235	1.0425	1.1170	1.1996	1.2892	1.5197	1.7244	1.7998	1.8295	2.0528
240	1.0429	1.1171	1.2000	1.2892	1.5156	1.7302	1.7998	1.8295	2.0528
245	1.0434	1.1178	1.2018	1.2892	1.5198	1.7354	1.7998	1.8295	2.0528
250	1.0436	1.1181	1.2013	1.2892	1.5258	1.7354	1.7998	1.8295	2.0528
255	1.0443	1.1181	1.2038	1.2892	1.5279	1.7354	1.7998	1.8295	2.0528
260	1.0440	1.1181	1.2051	1.2892	1.5300	1.7354	1.7998	1.8295	2.0528
265	1.0443	1.1181	1.2068	1.2892	1.5331	1.7354	1.7998	1.8295	2.0528
270	1.0444	1.1181	1.2104	1.2892	1.5363	1.7354	1.7998	1.8295	2.0528
275	1.0446	1.1181	1.2091	1.2892	1.5374	1.7354	1.7998	1.8295	2.0528
280	1.0449	1.1181	1.2123	1.2892	1.5402	1.7354	1.7998	1.8295	2.0528
285	1.0453	1.1181	1.2109	1.2892	1.5405	1.7354	1.7998	1.8295	2.0528
290	1.0451	1.1181	1.2132	1.2892	1.5431	1.7354	1.7998	1.8295	2.0528
295	1.0459	1.1181	1.2135	1.2892	1.5515	1.7354	1.7998	1.8295	2.0528
300	1.0466	1.1181	1.2161	1.2892	1.5485	1.7354	1.7998	1.8295	2.0528
305	1.0458	1.1181	1.2146	1.2892	1.5528	1.7354	1.7998	1.8295	2.0528
310	1.0465	1.1181	1.2146	1.2892	1.5534	1.7354	1.7998	1.8295	2.0528
315	1.0473	1.1181	1.2164	1.2892	1.5542	1.7354	1.7998	1.8295	2.0528
320	1.0472	1.1181	1.2174	1.2892	1.5553	1.7354	1.7998	1.8295	2.0528
325	1.0471	1.1181	1.2199	1.2892	1.5591	1.7354	1.7998	1.8295	2.0528
330	1.0478	1.1181	1.2196	1.2892	1.5609	1.7354	1.7998	1.8295	2.0528
335	1.0478	1.1181	1.2206	1.2892	1.5611	1.7354	1.7998	1.8295	2.0528
340	1.0480	1.1181	1.2200	1.2892	1.5572	1.7354	1.7998	1.8295	2.0528
345	1.0481	1.1181	1.2216	1.2892	1.5639	1.7354	1.7998	1.8295	2.0528
350	1.0482	1.1181	1.2234	1.2892	1.5606	1.7354	1.7998	1.8295	2.0528
355	1.0484	1.1181	1.2221	1.2892	1.5679	1.7354	1.7998	1.8295	2.0528
360	1.0487	1.1181	1.2263	1.2892	1.5686	1.7354	1.7998	1.8295	2.0528
365	1.0488	1.1181	1.2274	1.2892	1.5699	1.7354	1.7998	1.8295	2.0528
370	1.0489	1.1181	1.2284	1.2892	1.5718	1.7354	1.7998	1.8295	2.0528
375	1.0490	1.1181	1.2270	1.2892	1.5733	1.7354	1.7998	1.8295	2.0528
380	1.0485	1.1181	1.2271	1.2892	1.5748	1.7354	1.7998	1.8295	2.0528
385	1.0492	1.1181	1.2271	1.2892	1.5762	1.7354	1.7998	1.8295	2.0528
390	1.0492	1.1181	1.2271	1.2892	1.5783	1.7354	1.7998	1.8295	2.0528
395	1.0492	1.1181	1.2271	1.2892	1.5783	1.7354	1.7998	1.8295	2.0528
400	1.0492	1.1181	1.2271	1.2892	1.5783	1.7354	1.7998	1.8295	2.0528

TABLE D.13: Relative volume change of n-decane with time, exposed to 1 g/l SSW-CNF at 45°C.

	saturated					*gradually saturated*				
Time [min]	10 bar	30 bar	50 bar	70 bar	90 bar	10 bar	30 bar	50 bar	70 bar	90 bar
0	1.0000	1.0000	1.0000	1.0000	1.0000	1.0000	1.0000	1.0000	1.0000	1.0000
5	1.0145	1.0587	1.1082	1.1049	1.1794	0.9979	1.0110	1.0135	1.0284	1.0439
10	1.0160	1.0788	1.1416	1.1362	1.2848	0.9984	1.0196	1.0320	1.0492	1.0756
15	1.0166	1.0871	1.1658	1.1552	1.3641	0.9998	1.0292	1.0504	1.0680	1.0968
20	1.0166	1.0928	1.1765	1.1691	1.4111	1.0004	1.0390	1.0608	1.0837	1.1327
25	1.0167	1.0946	1.1844	1.1795	1.4552	1.0015	1.0469	1.0710	1.1020	1.1635
30	1.0167	1.0973	1.1899	1.1836	1.4903	1.0011	1.0540	1.0887	1.1199	1.1942
35	1.0167	1.0989	1.1946	1.1895	1.5290	1.0015	1.0619	1.1014	1.1351	1.2271
40	1.0167	1.1017	1.1972	1.1942	1.5535	1.0054	1.0681	1.1141	1.1474	1.2590
45	1.0167	1.1036	1.2022	1.1977	1.5817	1.0031	1.0737	1.1237	1.1573	1.2887
50	1.0167	1.1052	1.2031	1.2019	1.6026	1.0037	1.0809	1.1314	1.1701	1.3166
55	1.0167	1.1058	1.2072	1.2050	1.6264	1.0033	1.0863	1.1375	1.1817	1.3446
60	1.0167	1.1058	1.2091	1.2076	1.6414	1.0042	1.0916	1.1481	1.1919	1.3724
65	1.0167	1.1058	1.2108	1.2104	1.6600	1.0043	1.0955	1.1539	1.2025	1.3992
70	1.0167	1.1058	1.2153	1.2123	1.6768	1.0024	1.1002	1.1594	1.2065	1.4235
75	1.0167	1.1058	1.2145	1.2158	1.6989	1.0031	1.1050	1.1658	1.2178	1.4477
80	1.0167	1.1058	1.2164	1.2175	1.7112	1.0036	1.1074	1.1701	1.2191	1.4731
85	1.0167	1.1058	1.2170	1.2193	1.7226	1.0083	1.1109	1.1743	1.2248	1.4963
90	1.0167	1.1058	1.2195	1.2206	1.7365	1.0100	1.1135	1.1790	1.2341	1.5132
95	1.0167	1.1058	1.2203	1.2225	1.7519	1.0115	1.1166	1.1806	1.2353	1.5411
100	1.0167	1.1058	1.2232	1.2220	1.7605	1.0129	1.1225	1.1854	1.2413	1.5588
105	1.0167	1.1058	1.2243	1.2236	1.7687	1.0135	1.1251	1.1880	1.2436	1.5750
110	1.0167	1.1058	1.2246	1.2265	1.7824	1.0142	1.1270	1.1898	1.2486	1.5953
115	1.0167	1.1058	1.2263	1.2290	1.7872	1.0157	1.1301	1.1944	1.2519	1.6086
120	1.0167	1.1058	1.2259	1.2315	1.8041	1.0168	1.1321	1.1956	1.2547	1.6265
125	1.0167	1.1058	1.2284	1.2323	1.7953	1.0177	1.1331	1.1983	1.2576	1.6400
130	1.0167	1.1058	1.2288	1.2333	1.8057	1.0184	1.1351	1.2018	1.2601	1.6550
135	1.0167	1.1058	1.2300	1.2367	1.8166	1.0197	1.1372	1.2023	1.2611	1.6668
140	1.0167	1.1058	1.2306	1.2367	1.8282	1.0200	1.1382	1.2048	1.2631	1.6798
145	1.0167	1.1058	1.2318	1.2365	1.8299	1.0205	1.1406	1.2069	1.2656	1.6913
150	1.0167	1.1058	1.2355	1.2394	1.8438	1.0214	1.1413	1.2082	1.2705	1.7036
155	1.0167	1.1058	1.2380	1.2395	1.8436	1.0209	1.1441	1.2104	1.2712	1.7133
160	1.0167	1.1058	1.2362	1.2392	1.8419	1.0205	1.1449	1.2110	1.2723	1.7245
165	1.0167	1.1058	1.2397	1.2416	1.8413	1.0214	1.1472	1.2115	1.2746	1.7373
170	1.0167	1.1058	1.2375	1.2414	1.8402	1.0210	1.1502	1.2143	1.2785	1.7452
175	1.0167	1.1058	1.2381	1.2416	1.8451	1.0208	1.1507	1.2145	1.2807	1.7589
180	1.0167	1.1058	1.2387	1.2424	1.8451	1.0222	1.1522	1.2161	1.2796	1.7674
185	1.0167	1.1058	1.2384	1.2443	1.8451	1.0230	1.1549	1.2175	1.2821	1.7752
190	1.0167	1.1058	1.2408	1.2453	1.8451	1.0242	1.1570	1.2181	1.2850	1.7828
195	1.0167	1.1058	1.2409	1.2469	1.8451	1.0237	1.1572	1.2205	1.2861	1.7894
200	1.0167	1.1058	1.2418	1.2465	1.8451	1.0244	1.1579	1.2211	1.2877	1.7978
205	1.0167	1.1058	1.2422	1.2474	1.8451	1.0248	1.1588	1.2205	1.2883	1.8042
210	1.0167	1.1058	1.2422	1.2501	1.8451	1.0249	1.1597	1.2228	1.2908	1.8162
215	1.0167	1.1058	1.2422	1.2507	1.8451	1.0271	1.1606	1.2227	1.2916	1.8205
220	1.0167	1.1058	1.2422	1.2507	1.8451	1.0272	1.1611	1.2237	1.2937	1.8277
225	1.0167	1.1058	1.2422	1.2501	1.8451	1.0267	1.1607	1.2243	1.2970	1.8352
230	1.0167	1.1058	1.2422	1.2515	1.8451	1.0278	1.1625	1.2251	1.2973	1.8442
235	1.0167	1.1058	1.2422	1.2495	1.8451	1.0278	1.1645	1.2266	1.2983	1.8537
240	1.0167	1.1058	1.2422	1.2511	1.8451	1.0278	1.1651	1.2284	1.2988	1.8600
245	1.0167	1.1058	1.2422	1.2535	1.8451	1.0278	1.1646	1.2287	1.2991	1.8663
250	1.0167	1.1058	1.2422	1.2548	1.8451	1.0278	1.1664	1.2295	1.3021	1.8722
255	1.0167	1.1058	1.2422	1.2539	1.8451	1.0278	1.1682	1.2299	1.3043	1.8767
260	1.0167	1.1058	1.2422	1.2566	1.8451	1.0278	1.1690	1.2310	1.3060	1.8837
265	1.0167	1.1058	1.2422	1.2569	1.8451	1.0278	1.1668	1.2324	1.3051	1.8867
270	1.0167	1.1058	1.2422	1.2576	1.8451	1.0278	1.1691	1.2315	1.3059	1.8945
275	1.0167	1.1058	1.2422	1.2584	1.8451	1.0278	1.1698	1.2340	1.3096	1.9016
280	1.0167	1.1058	1.2422	1.2587	1.8451	1.0278	1.1699	1.2338	1.3126	1.9072
285	1.0167	1.1058	1.2422	1.2580	1.8451	1.0278	1.1721	1.2356	1.3132	1.9149
290	1.0167	1.1058	1.2422	1.2596	1.8451	1.0278	1.1736	1.2365	1.3127	1.9249
295	1.0167	1.1058	1.2422	1.2602	1.8451	1.0278	1.1738	1.2373	1.3139	1.9272
300	1.0167	1.1058	1.2422	1.2610	1.8451	1.0278	1.1772	1.2373	1.3148	1.9281
305	1.0167	1.1058	1.2422	1.2614	1.8451	1.0278	1.1771	1.2386	1.3143	1.9354
310	1.0167	1.1058	1.2422	1.2613	1.8451	1.0278	1.1777	1.2382	1.3143	1.9413
315	1.0167	1.1058	1.2422	1.2642	1.8451	1.0278	1.1779	1.2403	1.3143	1.9478
320	1.0167	1.1058	1.2422	1.2633	1.8451	1.0278	1.1786	1.2397	1.3143	1.9451
325	1.0167	1.1058	1.2422	1.2633	1.8451	1.0278	1.1806	1.2409	1.3143	1.9543
330	1.0167	1.1058	1.2422	1.2633	1.8451	1.0278	1.1802	1.2421	1.3143	1.9576
335	1.0167	1.1058	1.2422	1.2633	1.8451	1.0278	1.1806	1.2439	1.3143	1.9588
340	1.0167	1.1058	1.2422	1.2633	1.8451	1.0278	1.1827	1.2438	1.3143	1.9588
345	1.0167	1.1058	1.2422	1.2633	1.8451	1.0278	1.1830	1.2445	1.3143	1.9588
350	1.0167	1.1058	1.2422	1.2633	1.8451	1.0278	1.1821	1.2446	1.3143	1.9588
355	1.0167	1.1058	1.2422	1.2633	1.8451	1.0278	1.1836	1.2457	1.3143	1.9588
360	1.0167	1.1058	1.2422	1.2633	1.8451	1.0278	1.1833	1.2457	1.3143	1.9588
365	1.0167	1.1058	1.2422	1.2633	1.8451	1.0278	1.1832	1.2483	1.3143	1.9588
370	1.0167	1.1058	1.2422	1.2633	1.8451	1.0278	1.1829	1.2477	1.3143	1.9588
375	1.0167	1.1058	1.2422	1.2633	1.8451	1.0278	1.1829	1.2485	1.3143	1.9588
380	1.0167	1.1058	1.2422	1.2633	1.8451	1.0278	1.1829	1.2498	1.3143	1.9588
385	1.0167	1.1058	1.2422	1.2633	1.8451	1.0278	1.1829	1.2500	1.3143	1.9588
390	1.0167	1.1058	1.2422	1.2633	1.8451	1.0278	1.1829	1.2491	1.3143	1.9588
395	1.0167	1.1058	1.2422	1.2633	1.8451	1.0278	1.1829	1.2491	1.3143	1.9588
400	1.0167	1.1058	1.2422	1.2633	1.8451	1.0278	1.1829	1.2491	1.3143	1.9588

Appendix E

Tables: Interfacial Tension

TABLE E.1: Interfacial tension [mN/m] between *n*-decane and nanofluid with time, exposed to 1 g/l DIW-CNF *saturated* 25°C.

Time [min]	10 bar	20 bar	30 bar	40 bar	50 bar	60 bar	70 bar
0	39.29	52.50	65.87	71.78	42.87	50.85	42.27
10	32.57	45.65	53.99	55.50	60.84	62.21	35.69
20	31.46	44.09	50.59	52.55	70.54	67.18	33.71
30	30.78	43.50	49.17	51.67	71.77	67.09	34.11
40	30.39	42.82	49.10	50.47	73.44	66.35	33.83
50	29.85	42.44	48.26	49.89	74.25	65.31	33.83
60	29.53	42.21	47.53	49.36	74.25	65.12	33.83
70	29.33	42.21	47.24	49.03	74.25	63.74	33.83
80	29.01	41.84	47.40	48.32	74.25	63.70	33.83
90	28.89	41.55	46.67	48.34	74.25	63.70	33.83
100	28.81	41.04	46.49	47.76	74.25	63.70	33.83
110	28.64	40.90	46.44	47.47	74.25	63.70	33.83
120	28.45	40.96	46.50	47.23	74.25	63.70	33.83
130	28.44	41.07	46.08	47.04	74.25	63.70	33.83
140	28.15	40.94	46.03	46.72	74.25	63.70	33.83
150	28.07	40.94	46.76	46.67	74.25	63.70	33.83
160	28.07	40.94	46.76	46.67	74.25	63.70	33.83
170	28.07	40.94	46.76	46.67	74.25	63.70	33.83
180	28.07	40.94	46.76	46.67	74.25	63.70	33.83
190	28.07	40.94	46.76	46.67	74.25	63.70	33.83
200	28.07	40.94	46.76	46.67	74.25	63.70	33.83
210	28.07	40.94	46.76	46.67	74.25	63.70	33.83
220	28.07	40.94	46.76	46.67	74.25	63.70	33.83
230	28.07	40.94	46.76	46.67	74.25	63.70	33.83
240	28.07	40.94	46.76	46.67	74.25	63.70	33.83
250	28.07	40.94	46.76	46.67	74.25	63.70	33.83
260	28.07	40.94	46.76	46.67	74.25	63.70	33.83
270	28.07	40.94	46.76	46.67	74.25	63.70	33.83
280	28.07	40.94	46.76	46.67	74.25	63.70	33.83
290	28.07	40.94	46.76	46.67	74.25	63.70	33.83
300	28.07	40.94	46.76	46.67	74.25	63.70	33.83
310	28.07	40.94	46.76	46.67	74.25	63.70	33.83
320	28.07	40.94	46.76	46.67	74.25	63.70	33.83
330	28.07	40.94	46.76	46.67	74.25	63.70	33.83
340	28.07	40.94	46.76	46.67	74.25	63.70	33.83
350	28.07	40.94	46.76	46.67	74.25	63.70	33.83
360	28.07	40.94	46.76	46.67	74.25	63.70	33.83
370	28.07	40.94	46.76	46.67	74.25	63.70	33.83
380	28.07	40.94	46.76	46.67	74.25	63.70	33.83
390	28.07	40.94	46.76	46.67	74.25	63.70	33.83
400	28.07	40.94	46.76	46.67	74.25	63.70	33.83

TABLE E.2: Interfacial tension [mN/m] between *n*-decane and nanofluid with time, exposed to 1 g/l DIW-CNF *gradually saturated* 25°C.

Time [min]	10 bar	20 bar	30 bar	40 bar	50 bar	60 bar	70 bar
0	48.44	71.36	79.22	79.53	57.78	98.74	34.79
10	39.72	59.30	69.25	67.28	68.06	91.54	35.55
20	36.38	55.84	64.89	62.47	75.44	79.90	37.70
30	35.11	53.97	60.52	58.64	81.22	74.97	38.05
40	34.13	52.24	58.47	55.30	76.13	70.15	36.49
50	33.44	50.30	56.92	52.36	73.58	67.07	34.67
60	32.53	49.60	55.53	50.19	73.64	65.08	33.22
70	32.35	48.72	54.50	49.15	73.09	63.17	32.26
80	32.01	48.10	54.24	48.17	72.63	61.35	32.65
90	31.72	47.64	52.88	47.81	71.10	60.49	33.63
100	31.28	47.11	52.48	47.47	66.96	61.16	32.51
110	31.17	46.91	52.02	46.98	63.34	62.11	31.85
120	30.96	46.81	51.96	46.82	61.85	62.18	32.41
130	30.63	46.43	51.54	46.36	61.14	61.99	32.41
140	30.47	45.78	51.19	46.05	62.60	61.60	32.41
150	30.37	45.61	50.90	45.82	65.08	61.46	32.41
160	30.26	45.15	50.52	45.54	67.46	61.68	32.41
170	30.10	44.71	50.07	45.39	68.87	60.74	32.41
180	29.84	44.14	49.85	44.88	70.35	60.12	32.41
190	29.80	44.46	49.24	44.90	70.35	60.32	32.41
200	29.62	43.98	49.10	44.59	71.00	60.32	32.41
210	29.59	43.87	49.07	44.43	70.32	60.32	32.41
220	29.59	43.98	48.70	44.23	70.37	60.32	32.41
230	29.59	43.79	48.98	44.15	68.62	60.32	32.41
240	29.59	43.29	48.61	44.09	68.76	60.32	32.41
250	29.59	43.28	48.05	43.96	68.02	60.32	32.41
260	29.59	43.07	48.47	43.87	68.68	60.32	32.41
270	29.59	42.92	47.90	43.77	68.68	60.32	32.41
280	29.59	42.98	48.06	43.62	68.68	60.32	32.41
290	29.59	43.08	48.42	43.41	68.68	60.32	32.41
300	29.59	42.90	48.17	43.50	68.68	60.32	32.41
310	29.59	42.52	48.09	43.35	68.68	60.32	32.41
320	29.59	42.44	47.93	43.23	68.68	60.32	32.41
330	29.59	42.68	48.23	43.23	68.68	60.32	32.41
340	29.59	42.72	48.28	43.23	68.68	60.32	32.41
350	29.59	42.49	48.04	43.23	68.68	60.32	32.41
360	29.59	42.51	48.26	43.23	68.68	60.32	32.41
370	29.59	42.73	47.83	43.23	68.68	60.32	32.41
380	29.59	42.77	47.95	43.23	68.68	60.32	32.41
390	29.59	42.77	47.78	43.23	68.68	60.32	32.41
400	29.59	42.77	47.92	43.23	68.68	60.32	32.41

TABLE E.3: Interfacial tension [mN/m] between *n*-decane and nanofluid with time, exposed to 1 g/l DIW-CNF *saturated* 45°C.

Time [min]	10 bar	20 bar	30 bar	40 bar	50 bar	60 bar	70 bar	80 bar	90 bar
0	23.9	46.8	52.7	60.1	54.1	55.3	66.7	52.1	52.3
10	23.9	37.5	45.5	51.9	43.5	44.0	48.4	52.4	56.7
20	24.1	35.9	42.9	49.2	40.6	40.2	53.7	52.0	47.7
30	24.3	34.8	41.9	48.1	38.6	38.7	53.0	51.4	47.7
40	24.2	33.9	41.7	47.2	38.1	38.7	53.0	51.7	47.7
50	24.6	33.8	41.0	46.4	37.0	39.4	52.4	51.7	47.7
60	25.1	34.0	41.1	46.1	37.0	39.6	52.8	51.7	47.7
70	25.7	34.0	40.9	45.9	36.6	39.1	52.5	51.7	47.7
80	26.2	33.5	41.0	45.7	36.7	39.9	52.5	51.7	47.7
90	26.4	33.4	40.7	46.0	36.6	40.0	52.5	51.7	47.7
100	26.7	33.4	40.7	46.0	36.4	40.0	52.5	51.7	47.7
110	27.0	33.6	40.7	46.0	36.7	40.0	52.5	51.7	47.7
120	27.5	32.8	40.7	46.0	36.7	40.0	52.5	51.7	47.7
130	27.2	32.9	40.4	46.0	36.6	40.0	52.5	51.7	47.7
140	27.2	32.7	40.8	46.0	36.6	40.0	52.5	51.7	47.7
150	27.5	32.5	40.7	46.0	36.6	40.0	52.5	51.7	47.7
160	27.5	33.0	40.8	46.0	36.6	40.0	52.5	51.7	47.7
170	27.3	32.6	40.5	46.0	36.6	40.0	52.5	51.7	47.7
180	27.5	32.7	40.4	46.0	36.6	40.0	52.5	51.7	47.7
190	27.5	33.0	40.2	46.0	36.6	40.0	52.5	51.7	47.7
200	27.3	33.0	40.1	46.0	36.6	40.0	52.5	51.7	47.7
210	27.2	33.0	39.9	46.0	36.6	40.0	52.5	51.7	47.7
220	27.4	33.0	39.9	46.0	36.6	40.0	52.5	51.7	47.7
230	27.2	33.0	39.9	46.0	36.6	40.0	52.5	51.7	47.7
240	27.4	33.0	39.9	46.0	36.6	40.0	52.5	51.7	47.7
250	27.3	33.0	39.9	46.0	36.6	40.0	52.5	51.7	47.7
260	27.3	33.0	39.9	46.0	36.6	40.0	52.5	51.7	47.7
270	27.3	33.0	39.9	46.0	36.6	40.0	52.5	51.7	47.7
280	27.3	33.0	39.9	46.0	36.6	40.0	52.5	51.7	47.7
290	27.3	33.0	39.9	46.0	36.6	40.0	52.5	51.7	47.7
300	27.3	33.0	39.9	46.0	36.6	40.0	52.5	51.7	47.7
310	27.3	33.0	39.9	46.0	36.6	40.0	52.5	51.7	47.7
320	27.3	33.0	39.9	46.0	36.6	40.0	52.5	51.7	47.7
330	27.3	33.0	39.9	46.0	36.6	40.0	52.5	51.7	47.7
340	27.3	33.0	39.9	46.0	36.6	40.0	52.5	51.7	47.7
350	27.3	33.0	39.9	46.0	36.6	40.0	52.5	51.7	47.7
360	27.3	33.0	39.9	46.0	36.6	40.0	52.5	51.7	47.7
370	27.3	33.0	39.9	46.0	36.6	40.0	52.5	51.7	47.7
380	27.3	33.0	39.9	46.0	36.6	40.0	52.5	51.7	47.7
390	27.3	33.0	39.9	46.0	36.6	40.0	52.5	51.7	47.7
400	27.3	33.0	39.9	46.0	36.6	40.0	52.5	51.7	47.7

TABLE E.4: Interfacial tension [mN/m] between *n*-decane and nanofluid with time, exposed to 1 g/l DIW-CNF *gradually saturated* 45°C.

Time [min]	10 bar	30 bar	40 bar	50 bar	60 bar	70 bar	80 bar	90 bar
0	46.0	64.2	63.8	63.5	43.7	54.5	70.1	64.1
10	39.9	53.5	53.7	58.2	43.5	53.3	68.0	65.7
20	36.3	46.9	47.9	52.5	44.8	51.3	63.7	64.1
30	35.1	44.6	46.3	50.1	44.8	50.8	61.1	63.0
40	34.8	42.1	46.4	48.8	44.1	52.0	58.5	58.6
50	33.9	40.2	44.9	47.3	43.6	47.0	55.6	55.2
60	33.5	37.9	45.3	47.2	43.1	43.6	58.4	56.8
70	33.1	37.5	44.3	45.8	42.7	48.3	57.2	56.9
80	33.4	37.0	44.3	45.8	41.2	51.3	56.8	56.9
90	33.2	36.2	44.3	45.2	40.1	50.4	56.1	56.9
100	33.0	35.4	44.3	45.0	40.0	49.3	56.3	56.9
110	32.4	35.3	44.3	44.6	39.5	49.5	56.3	56.9
120	32.3	35.0	44.3	44.3	39.2	49.4	56.3	56.9
130	32.5	34.6	44.3	43.0	39.1	49.0	56.3	56.9
140	32.1	33.7	44.3	43.1	39.2	47.8	56.3	56.9
150	32.2	34.3	44.3	43.0	38.8	46.3	56.3	56.9
160	32.6	34.3	44.3	43.0	38.8	46.3	56.3	56.9
170	32.6	34.3	44.3	43.0	39.1	46.3	56.3	56.9
180	32.6	34.3	44.3	43.0	39.3	46.3	56.3	56.9
190	32.0	34.3	44.3	43.0	39.6	46.3	56.3	56.9
200	31.9	34.3	44.3	43.0	39.6	46.3	56.3	56.9
210	31.9	34.3	44.3	43.0	39.6	46.3	56.3	56.9
220	31.9	34.3	44.3	43.0	39.6	46.3	56.3	56.9
230	31.7	34.3	44.3	43.0	39.6	46.3	56.3	56.9
240	31.7	34.3	44.3	43.0	39.6	46.3	56.3	56.9
250	31.9	34.3	44.3	43.0	39.6	46.3	56.3	56.9
260	31.8	34.3	44.3	43.0	39.6	46.3	56.3	56.9
270	31.7	34.3	44.3	43.0	39.6	46.3	56.3	56.9
280	31.6	34.3	44.3	43.0	39.6	46.3	56.3	56.9
290	31.8	34.3	44.3	43.0	39.6	46.3	56.3	56.9
300	31.6	34.3	44.3	43.0	39.6	46.3	56.3	56.9
310	31.5	34.3	44.3	43.0	39.6	46.3	56.3	56.9
320	31.6	34.3	44.3	43.0	39.6	46.3	56.3	56.9
330	31.3	34.3	44.3	43.0	39.6	46.3	56.3	56.9
340	31.5	34.3	44.3	43.0	39.6	46.3	56.3	56.9
350	31.1	34.3	44.3	43.0	39.6	46.3	56.3	56.9
360	31.4	34.3	44.3	43.0	39.6	46.3	56.3	56.9
370	31.4	34.3	44.3	43.0	39.6	46.3	56.3	56.9
380	31.4	34.3	44.3	43.0	39.6	46.3	56.3	56.9
390	31.4	34.3	44.3	43.0	39.6	46.3	56.3	56.9
400	31.4	34.3	44.3	43.0	39.6	46.3	56.3	56.9

TABLE E.5: Interfacial tension [mN/m] between *n*-decane and nanofluid with time, exposed to 0.5 g/l DIW-CNF *saturated* 25°C.

Time [min]	10 bar	20	30 bar	40 bar	50 bar	60 bar	70 bar	80 bar	90 bar
0	27.6	47.9	69.7	72.5	85.4	82.4	35.3	32.3	30.6
10	24.7	37.9	55.9	64.5	75.3	75.4	31.4	28.0	25.3
20	24.7	36.3	51.0	61.7	73.0	67.6	29.0	26.5	23.4
30	24.8	35.7	48.8	60.8	71.0	70.4	30.5	27.8	23.7
40	24.8	35.0	47.5	60.0	69.1	72.3	30.5	27.6	23.2
50	24.8	34.8	46.7	59.1	68.6	70.9	30.3	27.3	22.9
60	24.8	34.4	46.4	58.7	69.3	70.1	30.0	27.5	22.7
70	24.9	34.2	46.1	58.1	70.1	69.2	30.0	27.5	22.7
80	24.9	34.0	45.8	57.8	70.6	69.3	30.0	27.5	22.6
90	24.9	33.9	45.6	57.4	70.6	69.2	29.9	27.5	22.6
100	24.9	33.8	45.6	57.1	70.5	69.0	29.8	27.5	22.6
110	24.9	33.6	45.6	56.8	70.0	68.9	29.8	27.5	22.6
120	24.9	33.5	45.7	56.8	69.5	68.9	29.8	27.5	22.6
130	24.9	33.1	45.7	56.6	69.2	68.9	29.8	27.5	22.6
140	24.9	33.4	45.0	56.3	69.3	68.9	29.8	27.5	22.6
150	24.9	33.4	44.8	56.0	68.8	68.9	29.8	27.5	22.6
160	24.9	33.4	44.6	56.0	69.0	68.9	29.8	27.5	22.6
170	24.9	33.4	44.9	55.7	68.6	68.9	29.8	27.5	22.6
180	24.9	33.4	44.6	55.5	68.6	68.9	29.8	27.5	22.6
190	24.9	33.4	44.5	55.4	68.6	68.9	29.8	27.5	22.6
200	24.9	33.4	44.4	55.5	68.4	68.9	29.8	27.5	22.6
210	24.9	33.4	44.7	55.3	68.6	68.9	29.8	27.5	22.6
220	24.9	33.4	44.6	55.3	68.6	68.9	29.8	27.5	22.6
230	24.9	33.4	44.6	55.1	68.3	68.9	29.8	27.5	22.6
240	24.9	33.4	44.6	55.0	68.5	68.9	29.8	27.5	22.6
250	24.9	33.4	44.6	55.1	68.3	68.9	29.8	27.5	22.6
260	24.9	33.4	44.6	55.1	68.2	68.9	29.8	27.5	22.6
270	24.9	33.4	44.6	55.0	68.4	68.9	29.8	27.5	22.6
280	24.9	33.4	44.6	55.0	68.1	68.9	29.8	27.5	22.6
290	24.9	33.4	44.6	55.0	68.2	68.9	29.8	27.5	22.6
300	24.9	33.4	44.6	55.0	67.8	68.9	29.8	27.5	22.6
310	24.9	33.4	44.6	55.0	67.9	68.9	29.8	27.5	22.6
320	24.9	33.4	44.6	55.0	68.1	68.9	29.8	27.5	22.6
330	24.9	33.4	44.6	55.0	68.0	68.9	29.8	27.5	22.6
340	24.9	33.4	44.6	55.0	68.1	68.9	29.8	27.5	22.6
350	24.9	33.4	44.6	55.0	68.0	68.9	29.8	27.5	22.6
360	24.9	33.4	44.6	55.0	67.8	68.9	29.8	27.5	22.6
370	24.9	33.4	44.6	55.0	67.7	68.9	29.8	27.5	22.6
380	24.9	33.4	44.6	55.0	67.6	68.9	29.8	27.5	22.6
390	24.9	33.4	44.6	55.0	67.6	68.9	29.8	27.5	22.6
400	24.9	33.4	44.6	55.0	67.6	68.9	29.8	27.5	22.6

TABLE E.6: Interfacial tension [mN/m] between *n*-decane and nanofluid with time, exposed to 0.5 g/l DIW-CNF *gradually saturated* 25°C.

Time [min]	10 bar	30 bar	40 bar	50 bar	60 bar	70 bar	80 bar	90 bar
0	46.7	53.6	66.7	72.3	93.0	46.1	35.7	20.3
10	40.6	50.0	64.8	76.3	76.1	40.5	33.4	21.1
20	39.0	50.8	61.3	77.8	68.5	36.3	32.6	21.4
30	37.7	49.4	59.7	78.7	64.3	34.2	31.4	22.2
40	36.8	49.0	58.0	78.2	61.6	33.4	30.1	23.0
50	36.2	48.2	56.9	76.0	60.2	32.1	28.6	22.8
60	35.8	47.2	55.4	74.8	59.9	31.1	28.1	21.5
70	35.6	46.5	53.4	73.6	59.1	31.0	27.7	21.4
80	35.3	45.4	52.2	73.2	58.1	29.9	26.8	20.8
90	35.3	45.5	51.3	72.6	56.8	28.6	26.4	20.4
100	35.1	45.5	50.3	72.0	55.7	28.1	27.0	20.2
110	34.8	44.7	49.6	71.1	56.6	29.6	27.5	21.2
120	35.0	44.9	50.0	70.3	58.0	29.6	27.4	21.9
130	34.8	44.0	49.5	69.5	57.7	29.3	27.1	21.7
140	34.9	43.5	49.7	68.5	57.6	29.4	26.9	21.5
150	34.7	42.8	49.4	67.3	57.3	29.4	26.8	21.5
160	34.7	42.6	48.9	66.2	57.0	29.6	26.8	21.4
170	34.7	41.9	48.4	65.9	56.7	29.5	26.9	21.4
180	34.4	41.9	48.5	65.6	57.0	29.5	26.9	21.5
190	34.4	41.9	48.4	66.2	56.7	29.5	26.9	21.5
200	34.4	41.6	48.0	67.2	56.7	29.5	26.9	21.5
210	34.4	41.0	48.2	67.9	56.7	29.5	26.9	21.5
220	34.4	41.1	48.0	68.3	56.7	29.5	26.9	21.5
230	34.4	41.2	48.0	68.6	56.7	29.5	26.9	21.5
240	34.4	40.5	47.8	68.5	56.7	29.5	26.9	21.5
250	34.4	40.5	48.0	68.5	56.7	29.5	26.9	21.5
260	34.4	40.8	48.0	68.2	56.7	29.5	26.9	21.5
270	34.4	40.3	48.0	68.1	56.7	29.5	26.9	21.5
280	34.4	40.2	48.0	67.6	56.7	29.5	26.9	21.5
290	34.4	39.8	48.0	67.8	56.7	29.5	26.9	21.5
300	34.4	39.9	48.0	67.5	56.7	29.5	26.9	21.5
310	34.4	39.8	48.0	67.3	56.7	29.5	26.9	21.5
320	34.4	39.6	48.0	67.1	56.7	29.5	26.9	21.5
330	34.4	39.5	48.0	67.2	56.7	29.5	26.9	21.5
340	34.4	39.6	48.0	66.9	56.7	29.5	26.9	21.5
350	34.4	39.2	48.0	67.0	56.7	29.5	26.9	21.5
360	34.4	39.2	48.0	66.8	56.7	29.5	26.9	21.5
370	34.4	38.7	48.0	67.0	56.7	29.5	26.9	21.5
380	34.4	38.7	48.0	67.0	56.7	29.5	26.9	21.5
390	34.4	38.7	48.0	67.0	56.7	29.5	26.9	21.5
400	34.4	38.7	48.0	67.0	56.7	29.5	26.9	21.5

TABLE E.7: Interfacial tension [mN/m] between *n*-decane and nanofluid with time, exposed to 0.5 g/l DIW-CNF *saturated* 45°C.

Time [min]	10 bar	20	30 bar	40 bar	50 bar	60 bar	70 bar	80 bar	90 bar
0	46.1	49.6	56.1	53.2	72.2	76.1	70.9	68.1	68.3
10	40.4	43.5	39.9	36.7	43.9	55.6	50.8	48.7	50.6
20	38.2	42.1	36.3	35.9	41.8	49.0	45.0	50.3	50.5
30	36.3	41.2	35.4	35.5	40.4	50.8	46.9	49.9	50.5
40	34.8	39.8	35.0	35.4	39.8	50.9	47.3	49.9	50.5
50	33.8	39.2	35.0	35.1	39.4	50.7	46.8	49.9	50.5
60	32.8	38.4	35.0	35.1	38.6	50.6	46.3	49.9	50.5
70	32.4	38.1	35.1	35.0	38.6	49.9	45.9	49.9	50.5
80	32.0	37.4	35.1	34.8	38.4	50.1	45.3	49.9	50.5
90	31.3	37.1	35.1	34.7	38.5	49.6	45.4	49.9	50.5
100	31.7	36.6	35.1	34.6	38.5	49.8	45.6	49.9	50.5
110	31.4	36.2	35.1	34.6	38.5	49.8	45.5	49.9	50.5
120	31.5	36.1	35.1	34.6	38.5	49.7	45.4	49.9	50.5
130	31.2	35.8	35.1	34.5	38.5	49.5	45.1	49.9	50.5
140	31.2	35.6	35.1	34.5	38.5	49.4	45.3	49.9	50.5
150	30.7	35.4	35.1	34.5	38.5	49.6	45.3	49.9	50.5
160	31.1	35.4	35.1	34.5	38.5	49.4	45.3	49.9	50.5
170	30.9	35.0	35.1	34.5	38.5	49.4	45.3	49.9	50.5
180	31.1	35.1	35.1	34.5	38.5	49.4	45.3	49.9	50.5
190	30.5	35.0	35.1	34.5	38.5	49.4	45.3	49.9	50.5
200	30.6	35.1	35.1	34.5	38.5	49.4	45.3	49.9	50.5
210	30.6	35.1	35.1	34.5	38.5	49.4	45.3	49.9	50.5
220	30.6	34.7	35.1	34.5	38.5	49.4	45.3	49.9	50.5
230	30.6	34.6	35.1	34.5	38.5	49.4	45.3	49.9	50.5
240	30.6	34.9	35.1	34.5	38.5	49.4	45.3	49.9	50.5
250	30.6	34.7	35.1	34.5	38.5	49.4	45.3	49.9	50.5
260	30.6	34.6	35.1	34.5	38.5	49.4	45.3	49.9	50.5
270	30.6	34.3	35.1	34.5	38.5	49.4	45.3	49.9	50.5
280	30.6	34.3	35.1	34.5	38.5	49.4	45.3	49.9	50.5
290	30.6	34.2	35.1	34.5	38.5	49.4	45.3	49.9	50.5
300	30.6	34.4	35.1	34.5	38.5	49.4	45.3	49.9	50.5
310	30.6	34.3	35.1	34.5	38.5	49.4	45.3	49.9	50.5
320	30.6	34.1	35.1	34.5	38.5	49.4	45.3	49.9	50.5
330	30.6	34.3	35.1	34.5	38.5	49.4	45.3	49.9	50.5
340	30.6	34.0	35.1	34.5	38.5	49.4	45.3	49.9	50.5
350	30.6	33.9	35.1	34.5	38.5	49.4	45.3	49.9	50.5
360	30.6	33.9	35.1	34.5	38.5	49.4	45.3	49.9	50.5
370	30.6	33.9	35.1	34.5	38.5	49.4	45.3	49.9	50.5
380	30.6	33.8	35.1	34.5	38.5	49.4	45.3	49.9	50.5
390	30.6	33.9	35.1	34.5	38.5	49.4	45.3	49.9	50.5
400	30.6	33.9	35.1	34.5	38.5	49.4	45.3	49.9	50.5

TABLE E.8: Interfacial tension [mN/m] between *n*-decane and nanofluid with time, exposed to 0.5 g/l DIW-CNF *gradually saturated* 45°C.

Time [min]	10 bar	20	30 bar	40 bar	50 bar	60 bar	70 bar	80 bar	90 bar
0	31.1	54.8	67.3	73.1	79.1	83.9	65.5	82.1	70.0
10	29.0	49.5	59.7	52.4	69.5	68.1	60.1	64.2	66.5
20	29.1	47.3	55.4	45.0	63.1	62.1	54.9	59.6	60.6
30	29.3	45.2	52.9	42.4	55.1	54.8	51.5	56.5	56.9
40	29.4	43.5	51.0	41.2	49.5	52.3	48.6	51.7	48.6
50	29.4	42.9	49.7	40.6	47.5	51.4	44.8	49.3	50.5
60	29.4	42.3	48.9	40.5	46.1	50.4	43.6	50.1	50.8
70	29.5	41.6	46.8	40.0	46.2	48.8	42.3	49.9	50.5
80	29.7	41.4	46.2	39.6	45.2	47.4	42.4	49.6	50.3
90	29.7	40.9	45.3	39.3	45.2	46.8	42.5	50.1	50.3
100	29.7	40.5	44.4	39.2	44.7	46.2	43.9	50.5	50.3
110	29.7	40.2	43.8	39.1	44.2	46.9	43.8	50.4	50.3
120	29.7	40.1	43.3	39.0	43.7	47.4	44.6	50.4	50.3
130	29.7	39.6	43.0	38.9	43.1	47.6	44.5	50.4	50.3
140	29.7	39.3	42.5	38.7	42.9	48.2	44.4	50.4	50.3
150	29.7	39.2	42.0	38.5	42.5	48.3	44.1	50.4	50.3
160	29.7	38.8	42.0	38.4	42.3	47.6	44.1	50.4	50.3
170	29.7	38.7	41.5	38.3	42.0	47.7	44.1	50.4	50.3
180	29.7	38.5	41.5	38.3	41.6	47.2	44.1	50.4	50.3
190	29.7	38.3	41.3	38.4	41.6	47.0	44.1	50.4	50.3
200	29.7	38.1	41.3	38.4	41.5	47.3	44.1	50.4	50.3
210	29.7	37.8	41.2	38.4	41.3	47.1	44.1	50.4	50.3
220	29.7	37.7	40.8	38.4	41.1	47.1	44.1	50.4	50.3
230	29.7	37.7	40.9	38.4	41.2	47.1	44.1	50.4	50.3
240	29.7	37.7	40.7	38.4	40.9	47.1	44.1	50.4	50.3
250	29.7	37.7	40.7	38.4	40.9	47.1	44.1	50.4	50.3
260	29.7	37.7	40.8	38.4	40.9	47.1	44.1	50.4	50.3
270	29.7	37.7	40.8	38.4	40.9	47.1	44.1	50.4	50.3
280	29.7	37.7	40.8	38.4	40.9	47.1	44.1	50.4	50.3
290	29.7	37.7	40.8	38.4	40.9	47.1	44.1	50.4	50.3
300	29.7	37.7	40.8	38.4	40.9	47.1	44.1	50.4	50.3
310	29.7	37.7	40.8	38.4	40.9	47.1	44.1	50.4	50.3
320	29.7	37.7	40.8	38.4	40.9	47.1	44.1	50.4	50.3
330	29.7	37.7	40.8	38.4	40.9	47.1	44.1	50.4	50.3
340	29.7	37.7	40.8	38.4	40.9	47.1	44.1	50.4	50.3
350	29.7	37.7	40.8	38.4	40.9	47.1	44.1	50.4	50.3
360	29.7	37.7	40.8	38.4	40.9	47.1	44.1	50.4	50.3
370	29.7	37.7	40.8	38.4	40.9	47.1	44.1	50.4	50.3
380	29.7	37.7	40.8	38.4	40.9	47.1	44.1	50.4	50.3
390	29.7	37.7	40.8	38.4	40.9	47.1	44.1	50.4	50.3
400	29.7	37.7	40.8	38.4	40.9	47.1	44.1	50.4	50.3

TABLE E.9: Interfacial tension [mN/m] between *n*-decane and nanofluid with time, exposed to 0.05 g/l DIW-CNF *saturated* 25°C.

Time [min]	10 bar	20	30 bar	40 bar	50 bar	60 bar	70 bar	80 bar	90 bar
0	42.7	49.1	60.6	80.2	91.1	113.0	44.2	43.9	37.3
10	38.2	43.0	53.7	60.6	66.7	83.5	36.2	32.1	31.2
20	36.2	41.6	52.0	58.8	61.4	78.5	33.2	28.6	28.7
30	35.3	40.9	50.0	57.8	58.1	76.6	33.2	28.9	30.2
40	34.6	40.1	48.3	57.2	60.0	76.5	33.3	28.5	29.6
50	34.8	39.8	46.8	56.5	60.5	75.4	32.4	28.5	29.5
60	34.4	39.5	47.5	56.0	58.9	74.6	32.0	28.5	29.3
70	34.4	39.0	47.0	55.6	58.4	74.3	31.9	28.5	29.4
80	34.1	39.0	47.3	55.3	57.8	74.3	31.9	28.5	29.4
90	33.8	38.8	46.4	54.9	57.7	74.0	31.9	28.5	29.4
100	33.8	38.7	45.9	54.6	57.6	74.0	31.9	28.5	29.4
110	33.7	38.5	46.0	54.5	57.6	74.0	31.9	28.5	29.4
120	33.6	38.3	45.1	54.1	57.7	74.0	31.9	28.5	29.4
130	33.5	38.3	45.2	54.1	57.8	74.0	31.9	28.5	29.4
140	33.2	38.1	44.8	53.9	57.8	74.0	31.9	28.5	29.4
150	33.3	38.0	44.2	53.8	57.8	74.0	31.9	28.5	29.4
160	33.1	37.4	44.5	53.6	57.8	74.0	31.9	28.5	29.4
170	33.1	37.4	44.1	53.4	57.8	74.0	31.9	28.5	29.4
180	33.2	37.7	43.9	53.3	57.8	74.0	31.9	28.5	29.4
190	33.1	37.5	43.8	53.2	57.8	74.0	31.9	28.5	29.4
200	33.1	37.5	44.2	53.2	57.8	74.0	31.9	28.5	29.4
210	32.9	37.7	44.1	53.0	57.8	74.0	31.9	28.5	29.4
220	32.9	37.5	43.9	53.0	57.8	74.0	31.9	28.5	29.4
230	33.1	37.4	43.6	53.0	57.8	74.0	31.9	28.5	29.4
240	32.9	37.6	44.0	53.0	57.8	74.0	31.9	28.5	29.4
250	32.9	37.4	43.6	52.7	57.8	74.0	31.9	28.5	29.4
260	32.9	37.2	43.8	52.8	57.8	74.0	31.9	28.5	29.4
270	32.9	37.2	43.7	52.6	57.8	74.0	31.9	28.5	29.4
280	32.9	37.2	43.5	52.6	57.8	74.0	31.9	28.5	29.4
290	32.9	37.2	43.4	52.6	57.8	74.0	31.9	28.5	29.4
300	32.9	37.2	43.6	52.5	57.8	74.0	31.9	28.5	29.4
310	32.9	37.2	43.3	52.5	57.8	74.0	31.9	28.5	29.4
320	32.9	37.2	43.5	52.5	57.8	74.0	31.9	28.5	29.4
330	32.9	37.2	43.6	52.5	57.8	74.0	31.9	28.5	29.4
340	32.9	37.2	43.6	52.5	57.8	74.0	31.9	28.5	29.4
350	32.9	37.2	43.6	52.5	57.8	74.0	31.9	28.5	29.4
360	32.9	37.2	43.6	52.5	57.8	74.0	31.9	28.5	29.4
370	32.9	37.2	43.6	52.5	57.8	74.0	31.9	28.5	29.4
380	32.9	37.2	43.6	52.5	57.8	74.0	31.9	28.5	29.4
390	32.9	37.2	43.6	52.5	57.8	74.0	31.9	28.5	29.4
400	32.9	37.2	43.6	52.5	57.8	74.0	31.9	28.5	29.4

TABLE E.10: Interfacial tension [mN/m] between *n*-decane and nanofluid with time, exposed to 0.05 g/l DIW-CNF *gradually saturated* 25°C.

Time [min]	10 bar	20	30 bar	40 bar	50 bar	60 bar	70 bar	80 bar	90 bar
0	49.3	57.3	69.5	107.1	103.6	105.1	49.0	50.5	46.6
10	46.6	51.1	63.6	83.7	91.4	85.7	43.8	42.0	40.3
20	45.7	50.1	58.9	75.4	82.7	80.2	39.3	38.4	37.1
30	44.9	49.4	56.0	71.1	76.4	80.5	37.5	36.5	35.9
40	43.5	48.5	52.9	69.7	69.2	77.3	35.2	34.5	34.7
50	42.5	47.3	51.8	68.0	63.9	73.1	34.3	32.6	33.8
60	41.7	46.2	50.5	68.4	62.7	71.6	33.9	31.6	32.5
70	41.0	45.3	48.9	66.3	62.1	70.6	33.6	30.1	31.4
80	40.7	44.7	48.1	63.3	61.5	68.9	33.3	29.3	30.5
90	40.1	43.4	47.6	61.3	61.6	67.0	32.5	28.6	29.2
100	40.2	43.0	46.8	60.5	61.0	69.8	32.3	27.6	28.8
110	39.9	42.5	46.5	59.3	59.5	71.7	33.0	27.9	29.7
120	39.4	42.3	46.3	58.5	58.3	69.7	33.2	28.5	30.3
130	39.2	41.7	45.5	58.0	57.6	70.0	33.1	28.4	29.9
140	38.9	41.8	45.1	56.9	56.8	68.9	32.9	28.2	30.3
150	38.7	41.4	44.8	56.4	58.3	69.7	32.8	28.0	29.7
160	38.8	41.8	44.5	56.1	58.5	69.7	32.9	28.0	29.7
170	39.0	40.9	44.3	55.6	59.7	69.7	32.9	27.9	29.7
180	38.6	41.0	44.3	54.7	60.8	69.7	32.9	27.9	29.7
190	38.3	40.5	43.6	54.7	60.1	69.7	32.9	27.9	29.7
200	38.1	40.6	43.7	54.4	60.3	69.7	32.9	27.9	29.7
210	37.9	40.6	43.6	54.2	59.3	69.7	32.9	27.9	29.7
220	38.0	40.5	43.1	54.2	59.0	69.7	32.9	27.9	29.7
230	37.8	41.1	43.1	53.6	58.9	69.7	32.9	27.9	29.7
240	37.8	40.0	42.8	53.5	59.0	69.7	32.9	27.9	29.7
250	37.7	40.4	42.8	53.5	58.7	69.7	32.9	27.9	29.7
260	37.7	40.4	42.7	53.7	58.3	69.7	32.9	27.9	29.7
270	37.7	40.4	42.7	53.7	58.3	69.7	32.9	27.9	29.7
280	37.8	40.4	42.7	53.7	58.5	69.7	32.9	27.9	29.7
290	37.8	40.4	42.7	53.7	58.5	69.7	32.9	27.9	29.7
300	37.8	40.4	42.7	53.7	58.5	69.7	32.9	27.9	29.7
310	37.8	40.4	42.7	53.7	58.5	69.7	32.9	27.9	29.7
320	37.8	40.4	42.7	53.7	58.5	69.7	32.9	27.9	29.7
330	37.8	40.4	42.7	53.7	58.5	69.7	32.9	27.9	29.7
340	37.8	40.4	42.7	53.7	58.5	69.7	32.9	27.9	29.7
350	37.8	40.4	42.7	53.7	58.5	69.7	32.9	27.9	29.7
360	37.8	40.4	42.7	53.7	58.5	69.7	32.9	27.9	29.7
370	37.8	40.4	42.7	53.7	58.5	69.7	32.9	27.9	29.7
380	37.8	40.4	42.7	53.7	58.5	69.7	32.9	27.9	29.7
390	37.8	40.4	42.7	53.7	58.5	69.7	32.9	27.9	29.7
400	37.8	40.4	42.7	53.7	58.5	69.7	32.9	27.9	29.7

TABLE E.11: Interfacial tension [mN/m] between *n*-decane and nanofluid with time, exposed to 0.05 g/l DIW-CNF *saturated* 45°C.

Time [min]	10 bar	20	30 bar	40 bar	50 bar	60 bar	70 bar	80 bar	90 bar
0	38.0	46.6	50.4	58.4	62.2	78.7	74.2	80.9	82.5
10	23.7	39.2	39.1	39.9	43.4	61.6	64.9	55.1	54.9
20	22.9	35.5	37.6	38.3	41.1	59.2	57.7	55.3	54.3
30	22.4	34.9	36.8	37.2	39.9	56.7	60.4	53.1	54.3
40	22.1	34.8	36.3	37.3	39.2	55.1	60.9	53.1	54.3
50	21.9	35.0	36.0	36.6	39.0	54.1	60.2	53.1	54.3
60	22.0	34.0	35.7	36.4	38.6	53.0	59.5	53.1	54.3
70	21.7	33.7	35.6	36.3	38.3	51.8	58.8	53.1	54.3
80	21.6	34.1	35.5	35.9	38.1	52.8	58.2	53.1	54.3
90	21.6	34.1	35.1	36.3	38.0	53.0	58.7	53.1	54.3
100	21.6	33.1	35.1	36.2	38.0	53.7	58.2	53.1	54.3
110	21.6	33.4	35.0	36.2	37.9	54.5	58.1	53.1	54.3
120	21.6	32.6	34.9	36.2	38.0	54.2	57.9	53.1	54.3
130	21.6	32.9	34.9	36.2	37.9	54.2	57.8	53.1	54.3
140	21.6	32.9	34.9	36.2	37.9	54.5	57.8	53.1	54.3
150	21.6	33.2	34.9	36.2	37.9	54.1	57.8	53.1	54.3
160	21.6	33.2	34.9	36.2	37.8	54.1	57.8	53.1	54.3
170	21.6	33.2	34.9	36.2	37.8	54.1	57.8	53.1	54.3
180	21.6	33.2	34.9	36.2	37.8	54.1	57.8	53.1	54.3
190	21.6	33.2	34.9	36.2	37.8	54.1	57.8	53.1	54.3
200	21.6	33.2	34.9	36.2	37.8	54.1	57.8	53.1	54.3
210	21.6	33.2	34.9	36.2	37.8	54.1	57.8	53.1	54.3
220	21.6	33.2	34.9	36.2	37.8	54.1	57.8	53.1	54.3
230	21.6	33.2	34.9	36.2	37.8	54.1	57.8	53.1	54.3
240	21.6	33.2	34.9	36.2	37.8	54.1	57.8	53.1	54.3
250	21.6	33.2	34.9	36.2	37.8	54.1	57.8	53.1	54.3
260	21.6	33.2	34.9	36.2	37.8	54.1	57.8	53.1	54.3
270	21.6	33.2	34.9	36.2	37.8	54.1	57.8	53.1	54.3
280	21.6	33.2	34.9	36.2	37.8	54.1	57.8	53.1	54.3
290	21.6	33.2	34.9	36.2	37.8	54.1	57.8	53.1	54.3
300	21.6	33.2	34.9	36.2	37.8	54.1	57.8	53.1	54.3
310	21.6	33.2	34.9	36.2	37.8	54.1	57.8	53.1	54.3
320	21.6	33.2	34.9	36.2	37.8	54.1	57.8	53.1	54.3
330	21.6	33.2	34.9	36.2	37.8	54.1	57.8	53.1	54.3
340	21.6	33.2	34.9	36.2	37.8	54.1	57.8	53.1	54.3
350	21.6	33.2	34.9	36.2	37.8	54.1	57.8	53.1	54.3
360	21.6	33.2	34.9	36.2	37.8	54.1	57.8	53.1	54.3
370	21.6	33.2	34.9	36.2	37.8	54.1	57.8	53.1	54.3
380	21.6	33.2	34.9	36.2	37.8	54.1	57.8	53.1	54.3
390	21.6	33.2	34.9	36.2	37.8	54.1	57.8	53.1	54.3
400	21.6	33.2	34.9	36.2	37.8	54.1	57.8	53.1	54.3

TABLE E.12: Interfacial tension [mN/m] between *n*-decane and nanofluid with time, exposed to 0.05 g/l DIW-CNF *gradually saturated* 45°C.

Time [min]	10 bar	20	30 bar	40 bar	50 bar	60 bar	70 bar	80 bar	90 bar
0	22.6	62.2	50.7	73.8	82.5	90.9	71.2	89.1	91.9
10	22.5	51.5	46.8	65.3	67.0	72.0	63.2	74.1	74.8
20	22.5	47.2	44.8	56.8	60.7	65.3	61.4	65.7	65.4
30	22.3	43.1	43.5	54.2	57.0	61.3	59.8	61.5	61.5
40	22.2	39.6	41.3	51.7	55.6	58.9	57.3	59.8	58.5
50	22.5	38.1	39.7	50.1	53.9	58.1	53.9	58.2	55.9
60	22.5	37.6	40.0	48.7	53.2	57.1	50.7	56.4	56.2
70	23.0	37.2	38.7	47.2	52.6	56.7	50.2	54.5	54.1
80	22.5	36.8	38.4	45.7	51.4	55.5	51.8	53.5	53.8
90	22.8	37.0	38.6	44.6	51.0	55.0	53.1	55.1	53.8
100	22.8	36.8	38.7	44.8	50.0	54.1	54.2	56.4	53.8
110	22.6	36.1	37.9	44.5	49.2	54.3	55.4	56.7	53.8
120	22.6	35.2	38.1	44.1	48.8	53.7	55.1	56.1	53.8
130	22.6	36.5	38.3	43.8	48.6	54.4	54.7	55.8	53.8
140	22.6	36.1	37.6	43.4	48.5	54.7	53.9	55.3	53.8
150	22.6	36.1	37.9	42.9	48.6	54.6	53.9	54.9	53.8
160	22.6	36.1	37.3	43.3	48.3	54.6	53.9	54.9	53.8
170	22.6	36.1	37.3	43.2	48.4	54.6	53.9	54.9	53.8
180	22.6	36.1	37.3	43.2	47.5	54.6	53.9	54.9	53.8
190	22.6	36.1	37.3	43.2	47.5	54.6	53.9	54.9	53.8
200	22.6	36.1	37.3	43.2	47.6	54.6	53.9	54.9	53.8
210	22.6	36.1	37.3	43.2	47.5	54.6	53.9	54.9	53.8
220	22.6	36.1	37.3	43.2	47.5	54.6	53.9	54.9	53.8
230	22.6	36.1	37.3	43.2	47.5	54.6	53.9	54.9	53.8
240	22.6	36.1	37.3	43.2	47.5	54.6	53.9	54.9	53.8
250	22.6	36.1	37.3	43.2	47.5	54.6	53.9	54.9	53.8
260	22.6	36.1	37.3	43.2	47.5	54.6	53.9	54.9	53.8
270	22.6	36.1	37.3	43.2	47.5	54.6	53.9	54.9	53.8
280	22.6	36.1	37.3	43.2	47.5	54.6	53.9	54.9	53.8
290	22.6	36.1	37.3	43.2	47.5	54.6	53.9	54.9	53.8
300	22.6	36.1	37.3	43.2	47.5	54.6	53.9	54.9	53.8
310	22.6	36.1	37.3	43.2	47.5	54.6	53.9	54.9	53.8
320	22.6	36.1	37.3	43.2	47.5	54.6	53.9	54.9	53.8
330	22.6	36.1	37.3	43.2	47.5	54.6	53.9	54.9	53.8
340	22.6	36.1	37.3	43.2	47.5	54.6	53.9	54.9	53.8
350	22.6	36.1	37.3	43.2	47.5	54.6	53.9	54.9	53.8
360	22.6	36.1	37.3	43.2	47.5	54.6	53.9	54.9	53.8
370	22.6	36.1	37.3	43.2	47.5	54.6	53.9	54.9	53.8
380	22.6	36.1	37.3	43.2	47.5	54.6	53.9	54.9	53.8
390	22.6	36.1	37.3	43.2	47.5	54.6	53.9	54.9	53.8
400	22.6	36.1	37.3	43.2	47.5	54.6	53.9	54.9	53.8

TABLE E.13: Interfacial tension [mN/m] between *n*-decane and nanofluid with time, exposed to 1 g/l SSW-CNF *saturated* 45°C.

Time [min]	10 bar	30 bar	50 bar	70 bar	90 bar
0	29.6	34.9	52.3	48.4	60.3
10	29.0	27.7	39.2	38.9	50.7
20	28.6	26.7	37.0	37.6	48.3
30	28.4	26.3	36.3	37.0	48.0
40	28.5	26.0	36.0	36.2	46.5
50	28.5	25.9	35.7	36.0	46.3
60	29.0	25.8	35.7	36.0	45.9
70	29.1	25.7	35.7	35.6	45.7
80	29.0	25.6	35.7	35.6	44.9
90	29.3	25.4	35.7	35.5	44.6
100	29.3	25.4	35.7	35.5	44.6
110	29.3	25.3	35.7	35.5	44.6
120	29.3	25.3	35.7	35.5	44.6
130	29.3	25.3	35.7	35.5	44.6
140	29.3	25.3	35.7	35.5	44.6
150	29.3	25.3	35.7	35.5	44.6
160	29.3	25.2	35.7	35.5	44.6
170	29.3	25.2	35.7	35.5	44.6
180	29.3	25.2	35.7	35.5	44.6
190	29.3	25.2	35.7	35.5	44.6
200	29.3	25.2	35.7	35.5	44.6
210	29.3	25.2	35.7	35.5	44.6
220	29.3	25.3	35.7	35.5	44.6
230	29.3	25.3	35.7	35.5	44.6
240	29.3	25.3	35.7	35.5	44.6
250	29.3	25.3	35.7	35.5	44.6
260	29.3	25.3	35.7	35.5	44.6
270	29.3	25.3	35.7	35.5	44.6
280	29.3	25.3	35.7	35.5	44.6
290	29.3	25.3	35.7	35.5	44.6
300	29.3	25.3	35.7	35.5	44.6
310	29.3	25.3	35.7	35.5	44.6
320	29.3	25.3	35.7	35.5	44.6
330	29.3	25.3	35.7	35.5	44.6
340	29.3	25.3	35.7	35.5	44.6
350	29.3	25.3	35.7	35.5	44.6
360	29.3	25.3	35.7	35.5	44.6
370	29.3	25.3	35.7	35.5	44.6
380	29.3	25.3	35.7	35.5	44.6
390	29.3	25.3	35.7	35.5	44.6
400	29.3	25.3	35.7	35.5	44.6

TABLE E.14: Interfacial tension [mN/m] between *n*-decane and nanofluid with time, exposed to 1 g/l SSW-CNF *gradually saturated* 45°C.

Time [min]	10 bar	30 bar	50 bar	70 bar	90 bar
0	36.7	55.8	65.4	38.8	44.5
10	25.5	47.5	53.8	43.0	50.6
20	23.0	39.4	47.9	44.6	55.0
30	22.3	34.9	45.0	44.5	55.7
40	21.6	33.2	43.4	43.3	54.0
50	21.6	32.0	42.7	42.7	51.4
60	21.6	31.4	41.6	42.5	49.5
70	21.6	30.8	41.0	41.9	49.0
80	21.6	30.4	40.3	41.3	49.0
90	21.6	30.1	39.8	41.0	48.7
100	21.6	29.9	39.6	40.6	47.9
110	21.6	29.6	39.1	40.3	47.6
120	21.6	29.5	38.8	40.0	46.8
130	21.6	29.3	38.6	39.9	46.9
140	21.6	29.0	38.1	39.8	46.2
150	21.6	29.0	38.1	39.6	46.0
160	21.6	28.8	37.7	39.1	45.7
170	21.6	28.7	37.7	39.1	45.2
180	21.6	28.6	37.6	39.0	45.0
190	21.6	28.6	37.5	38.9	45.1
200	21.6	28.5	37.4	38.7	44.7
210	21.6	28.6	37.3	38.7	44.5
220	21.6	28.5	37.2	38.5	44.5
230	21.6	28.3	37.1	38.5	44.5
240	21.6	28.5	36.9	38.3	44.5
250	21.6	28.5	36.9	38.2	44.5
260	21.6	28.5	36.8	38.2	44.5
270	21.6	28.5	36.8	38.1	44.5
280	21.6	28.5	36.7	38.2	44.5
290	21.6	28.5	36.5	38.0	44.5
300	21.6	28.5	36.5	38.0	44.5
310	21.6	28.5	36.4	37.9	44.5
320	21.6	28.5	36.4	38.0	44.5
330	21.6	28.5	36.4	38.0	44.5
340	21.6	28.5	36.4	38.0	44.5
350	21.6	28.5	36.4	38.0	44.5
360	21.6	28.5	36.4	38.0	44.5
370	21.6	28.5	36.4	38.0	44.5
380	21.6	28.5	36.4	38.0	44.5
390	21.6	28.5	36.4	38.0	44.5
400	21.6	28.5	36.4	38.0	44.5

TABLE E.15: Equilibrium IFT [mN/m] at 25°C , *saturated*

P [bar]	0.05 g/l	0.5 g/l	1 g/l
10	32.93	24.95	28.07
20	37.16	33.37	40.94
30	43.55	44.60	46.76
40	52.53	55.00	46.67
50	57.83	67.62	74.25
60	74.00	68.94	63.70
70	31.94	29.84	33.83
80	28.53	27.50	-
90	29.35	22.59	-

TABLE E.16: Equilibrium IFT [mN/m] at 25°C , *gradually saturated*

P [bar]	0.05 g/l	0.5 g/l	1 g/l
10	37.79	34.36	29.59
20	40.42	-	42.77
30	42.70	38.69	47.92
40	53.70	48.03	43.23
50	58.52	67.04	68.68
60	69.67	56.75	60.32
70	32.88	29.55	32.41
80	27.91	26.91	-
90	29.67	21.49	-

TABLE E.17: Equilibrium IFT [mN/m] at 45°C , *saturated*

P [bar]	0.05 g/l	0.5 g/l	1 g/l
10	21.62	30.63	27.30
20	33.22	33.94	33.04
30	34.95	35.06	39.92
40	36.17	34.46	46.01
50	37.82	38.47	36.64
60	54.15	49.43	39.98
70	57.77	45.26	52.54
80	53.09	49.91	51.67
90	54.34	50.48	47.66

TABLE E.18: Equilibrium IFT [mN/m] at 45°C , *gradually saturated*

P [bar]	0.05 g/l	0.5 g/l	1 g/l
10	22.61	29.69	31.43
20	36.07	37.69	-
30	37.31	40.83	34.30
40	43.17	38.41	44.26
50	47.47	40.95	42.99
60	54.56	47.14	39.63
70	53.93	44.14	46.28
80	54.92	50.40	56.34
90	53.82	50.32	56.92

TABLE E.19: Equilibrium IFT [mN/m] at 45°C for 1 g/l SSW-based NF (*saturated* and gradually saturated)

P [bar]	*saturated*l	*gradually saturated*
10	29.32	21.61
30	25.27	28.51
50	35.70	36.40
70	35.51	37.98
90	44.62	44.54

Appendix F

Tables: Mole fraction - Viscosity - Density

TABLE F.1: Experimentally obtained properties of CO_2 saturated *n*-decane drop in 1 g/l DIW-CNF at 25 °C . Experimental conditions: *saturated*.

P [bar]	Mole frac.	Viscosity [cP]	Density [g/ml]
10	0.00175	0.85652	0.71263
20	0.02793	0.85423	0.63174
30	0.06503	0.84585	0.59818
40	0.16987	0.79921	0.51904
50	0.43656	0.63314	0.38803
60	0.67388	0.43285	0.34722
70	0.82388	0.29986	0.73845

TABLE F.2: Experimentally obtained properties of CO_2 saturated *n*-decane drop in 1 g/l DIW-CNF at 25 °C . Experimental conditions: *gradually saturated*.

P [bar]	Mole frac.	Viscosity [cP]	Density [g/ml]
10	0.00487	0.85505	0.68790
20	0.02897	0.85373	0.62860
30	0.06756	0.84456	0.59384
40	0.13972	0.81607	0.55023
50	0.47652	0.60230	0.36470
60	0.63126	0.47471	0.36895
70	0.72694	0.40755	0.73690

TABLE F.3: Experimentally obtained properties of CO_2 saturated *n*-decane drop in 1 g/l DIW-CNF at 45 °C . Experimental conditions: *saturated*.

P [bar]	Mole frac.	Viscosity [cP]	Density [g/ml]
10	-	0.65475	0.71779
20	0.02313	0.65475	0.62775
30	0.08697	0.63814	0.53771
40	-	0.63323	0.54766
50	0.14719	0.62832	0.55761
60	0.24034	0.59366	0.52597
70	0.39108	0.52297	0.48353
80	0.48143	0.47606	0.49808
90	0.56869	0.42562	0.54153

TABLE F.4: Experimentally obtained properties of CO_2 saturated *n*-decane drop in 1 g/l DIW-CNF at 45 °C . Experimental conditions: *gradually saturated*.

P [bar]	Mole frac.	Viscosity [cP]	Density [g/ml]
10	0.00708	0.65272	0.65415
20	-	0.65340	0.63283
30	0.04573	0.65408	0.61151
40	-	0.63796	0.57764
50	0.16227	0.62184	0.54377
60	0.26271	0.58298	0.51055
70	0.36115	0.53938	0.50014
80	0.54569	0.43468	0.46742
90	0.63817	0.37560	0.51386

TABLE F.5: Experimentally obtained properties of CO_2 saturated *n*-decane drop in 0.5 g/l DIW-CNF at 25 °C . Experimental conditions: *saturated*.

P [bar]	Mole frac.	Viscosity [cP]	Density [g/ml]
10	0.00472	0.85512	0.68905
20	0.01933	0.85840	0.65897
30	0.07064	0.84299	0.58862
40	0.24337	0.75597	0.45129
50	0.50668	0.57810	0.34775
60	0.64550	0.46097	0.36165
70	0.87328	0.23918	0.73945
80	0.89167	0.22160	0.76372
90	0.88262	0.23859	0.77851

TABLE F.6: Experimentally obtained properties of CO_2 saturated *n*-decane drop in 0.5 g/l DIW-CNF at 25 °C . Experimental conditions: *gradually saturated*.

P [bar]	Mole frac.	Viscosity [cP]	Density [g/ml]
10	0.00382	0.85555	0.69602
20	-	0.85551	0.66428
30	0.04595	0.85547	0.63253
40	0.21830	0.77107	0.47319
50	0.48202	0.59795	0.36157
60	0.47137	0.61388	0.45328
70	0.80683	0.31986	0.73815
80	0.88570	0.22941	0.76316
90	0.92695	0.17866	0.78525

TABLE F.7: Experimentally obtained properties of CO_2 saturated *n*-decane drop in 0.5 g/l DIW-CNF at 45 °C . Experimental conditions: *saturated*.

P [bar]	Mole frac.	Viscosity [cP]	Density [g/ml]
10	0.00378	0.65390	0.67989
20	0.01180	0.65889	0.66701
30	0.03896	0.65664	0.62511
40	0.07581	0.65012	0.59889
50	0.16586	0.62029	0.54054
60	0.32645	0.55121	0.46842
70	0.44592	0.49151	0.45360
80	0.52402	0.44898	0.47780
90	0.68617	0.33846	0.49373

TABLE F.8: Experimentally obtained properties of CO_2 saturated *n*-decane drop in 0.5 g/l DIW-CNF at 45 °C . Experimental conditions: *gradually saturated*.

P [bar]	Mole frac.	Viscosity [cP]	Density [g/ml]
10	0.00469	0.65358	0.67261
20	0.01684	0.65705	0.64904
30	0.03835	0.65688	0.62637
40	0.09131	0.64397	0.57848
50	0.19091	0.60928	0.51850
60	0.31313	0.55802	0.47701
70	0.40805	0.51343	0.47420
80	0.59726	0.39915	0.44258
90	0.70604	0.32241	0.48515

TABLE F.9: Experimentally obtained properties of CO_2 saturated *n*-decane drop in 0.05 g/l DIW-CNF at 25 °C . Experimental conditions: *saturated*.

P [bar]	Mole frac.	Viscosity [cP]	Density [g/ml]
10	0.00452	0.85522	0.69060
20	0.01886	0.86885	0.66050
30	0.07706	0.83970	0.57794
40	0.16839	0.80005	0.52052
50	0.38164	0.67337	0.42181
60	0.61363	0.49139	0.37802
70	0.82831	0.29459	0.73854
80	0.86350	0.25790	0.76119
90	0.89055	0.22816	0.77963

TABLE F.10: Experimentally obtained properties of CO_2 saturated *n*-decane drop in 0.05 g/l DIW-CNF at 25 °C . Experimental conditions: *gradually saturated*.

P [bar]	Mole frac.	Viscosity [cP]	Density [g/ml]
10	0.00816	0.85350	0.66350
20	0.02671	0.85483	0.63550
30	0.07040	0.84311	0.58901
40	0.22656	0.76614	0.46585
50	0.41304	0.65066	0.40224
60	0.54522	0.55284	0.41376
70	0.80522	0.32172	0.73812
80	0.85128	0.27320	0.76018
90	0.86746	0.25820	0.77647

TABLE F.11: Experimentally obtained properties of CO_2 saturated *n*-decane drop in 0.05 g/l DIW-CNF at 45 °C . Experimental conditions: *saturated*.

P [bar]	Mole frac.	Viscosity [cP]	Density [g/ml]
10	0.00212	0.65450	0.69356
20	0.01303	0.65845	0.66257
30	0.03721	0.65731	0.62872
40	0.08164	0.64782	0.59110
50	0.17692	0.61546	0.53069
60	0.29579	0.56675	0.48836
70	0.47373	0.47481	0.43866
80	0.46237	0.48777	0.50711
90	0.67194	0.34971	0.49979

TABLE F.12: Experimentally obtained properties of CO_2 saturated *n*-decane drop in 0.05 g/l DIW-CNF at 45 °C . Experimental conditions: *gradually saturated*.

P [bar]	Mole frac.	Viscosity [cP]	Density [g/ml]
10	0.00386	0.65388	0.67925
20	0.01910	0.65623	0.64126
30	0.05577	0.65026	0.59217
40	0.09605	0.64206	0.57241
50	0.22125	0.59559	0.49305
60	0.31979	0.55463	0.47270
70	0.39784	0.51920	0.47981
80	0.47383	0.48076	0.50168
90	0.61515	0.39265	0.52321

TABLE F.13: Experimentally obtained properties of CO_2 saturated *n*-decane drop in 1 g/l SSW-CNF at 45 °C . Experimental conditions: *saturated*.

P [bar]	Mole frac.	Viscosity [cP]	Density [g/ml]
10	0.00131	0.65478	0.70041
30	0.02677	0.66121	0.65083
50	0.10631	0.64542	0.59707
70	0.17862	0.62918	0.60579
90	0.56201	0.43021	0.54411

TABLE F.14: Experimentally obtained properties of CO_2 saturated *n*-decane drop in 1 g/l SSW-CNF at 45 °C . Experimental conditions: *gradually saturated*.

P [bar]	Mole frac.	Viscosity [cP]	Density [g/ml]
10	0.002184	0.65447	0.69303
30	0.045424	0.65420	0.61212
50	0.109014	0.64431	0.59437
70	0.206106	0.61668	0.58938
90	0.592783	0.40875	0.53212

TABLE F.15: CO_2 density [g/ml] and viscosity [cP] at 25°C and 45°C

P [bar]	ρ_{CO_2}@25°C	ρ_{CO_2}@45°C	μ_{CO_2}@25°C	μ_{CO_2}@45°C
10	0.01872	0.01735	0.01503	0.01598
20	0.03977	0.03634	0.01520	0.01613
30	0.06409	0.05741	0.01548	0.01636
40	0.09335	0.08120	0.01593	0.01669
50	0.13127	0.10869	0.01670	0.01718
60	0.19061	0.14161	0.01832	0.01791
70	0.74303	0.18320	0.06160	0.01905
80	0.77664	0.24105	0.06679	0.02105
90	0.79965	0.33751	0.07065	0.02548

TABLE F.16: CO_2 density [g/ml] and viscosity [cP] at 25°C and 45°C

P [bar]	ρ_{CO_2}@25°C	ρ_{CO_2}@45°C	μ_{CO_2}@25°C	μ_{CO_2}@45°C
10	0.72725	0.71180	0.85734	0.65525
20	0.72805	0.71270	0.86764	0.66316
30	0.72884	0.71359	0.87797	0.67108
40	0.72963	0.71447	0.88835	0.67902
50	0.73040	0.71533	0.89877	0.68698
60	0.73117	0.71619	0.90923	0.69496
70	0.73193	0.71704	0.91974	0.70297
80	0.73268	0.71788	0.93028	0.71099
90	0.73342	0.71871	0.94087	0.71904

Appendix G

Tables: Diffusion Coefficients

TABLE G.1: Diffusion Coefficients of CO_2 from *saturated* CNF at 25°C

P [bar]	0.05 g/l CNF	0.5g/l CNF	1 g/l CNF
10	5.230	3.850	3.610
20	3.988	3.256	2.690
30	2.080	1.530	1.352
40	1.283	0.876	0.815
50	0.780	0.624	0.603
60	0.607	0.580	0.523
70	0.932	0.711	0.696
80	1.116	0.972	0.925
90	1.256	1.114	1.102

TABLE G.2: Diffusion Coefficients of CO_2 from *gradually saturated* CNF at 25°C

P [bar]	0.05 g/l CNF	0.5g/l CNF	1 g/l CNF
10	0.4485	0.4865	0.5612
20	0.4016	0.4416	0.4665
30	0.3140	0.3243	0.4192
40	0.2898	0.2967	0.3716
50	0.3071	0.3108	0.3940
60	0.3240	0.3230	0.4321
70	0.3726	0.3312	0.4582
80	0.4220	0.3520	-
90	0.4970	0.4970	-

TABLE G.3: Diffusion Coefficients of CO_2 from *saturated* CNF at 45°C

P [bar]	0.05 g/l CNF	0.5g/l CNF	1 g/l CNF
10	7.9920	8.5830	7.2590
20	4.8120	6.1260	4.1230
30	3.3260	5.0600	3.0400
40	2.6350	3.5460	2.1540
50	1.2760	2.2830	1.1100
60	1.0050	1.6353	0.9568
70	0.8244	0.9456	1.0250
80	2.2010	2.2910	1.9900
90	3.3100	3.3230	3.2400

TABLE G.4: Diffusion Coefficients of CO_2 from *gradually saturated* CNF at 45°C

P [bar]	0.05 g/l CNF	0.5g/l CNF	1 g/l CNF
10	0.7970	0.8193	0.7789
20	0.6693	0.6968	0.6520
30	0.5727	0.5594	0.5560
40	0.5589	0.5012	0.4912
50	0.4623	0.4140	0.4260
60	0.3657	0.4071	0.3965
70	0.4968	0.4554	0.4360
80	0.5623	0.6901	0.5360
90	0.7038	0.7860	0.7210